



UNIL | Université de Lausanne

Unicentre

CH-1015 Lausanne

<http://serval.unil.ch>

---

Year : 2021

## Characterization of pharmacological modulators and study of ASIC activation with cysteine-based cross-linking

Vaithia Natha Subramanian Anand

Vaithia Natha Subramanian Anand, 2021, Characterization of pharmacological modulators and study of ASIC activation with cysteine-based cross-linking

Originally published at : Thesis, University of Lausanne

Posted at the University of Lausanne Open Archive <http://serval.unil.ch>

Document URN : urn:nbn:ch:serval-BIB\_1910F37FB68D8

### **Droits d'auteur**

L'Université de Lausanne attire expressément l'attention des utilisateurs sur le fait que tous les documents publiés dans l'Archive SERVAL sont protégés par le droit d'auteur, conformément à la loi fédérale sur le droit d'auteur et les droits voisins (LDA). A ce titre, il est indispensable d'obtenir le consentement préalable de l'auteur et/ou de l'éditeur avant toute utilisation d'une oeuvre ou d'une partie d'une oeuvre ne relevant pas d'une utilisation à des fins personnelles au sens de la LDA (art. 19, al. 1 lettre a). A défaut, tout contrevenant s'expose aux sanctions prévues par cette loi. Nous déclinons toute responsabilité en la matière.

### **Copyright**

The University of Lausanne expressly draws the attention of users to the fact that all documents published in the SERVAL Archive are protected by copyright in accordance with federal law on copyright and similar rights (LDA). Accordingly it is indispensable to obtain prior consent from the author and/or publisher before any use of a work or part of a work for purposes other than personal use within the meaning of LDA (art. 19, para. 1 letter a). Failure to do so will expose offenders to the sanctions laid down by this law. We accept no liability in this respect.



**UNIL** | Université de Lausanne

Faculté de biologie  
et de médecine

**Département of Biomédicale Sciences**

Characterization of pharmacological modulators  
and study of ASIC activation with  
cysteine-based cross-linking

Thèse de doctorat ès sciences de la vie (PhD)

Présentée à la

Faculté de biologie et de  
**médecine de l'Université de**  
Lausanne

par

**Anand VAI THIA NATHA SUBRAMANIAN**

Master of Science in Molecular Biotechnology,  
University of Skövde, Sweden

Jury

Prof. Romano REGAZZI, Président  
Dr. Stephan KELLENBERGER, Directeur de thèse  
Dr. Roland SCHÖNHERR, Expert  
Prof. Hugues ABRIEL, Expert

Lausanne (2021)

# Imprimatur

Vu le rapport présenté par le jury d'examen, composé de

|                                 |          |       |         |                     |
|---------------------------------|----------|-------|---------|---------------------|
| <b>Président·e</b>              | Monsieur | Prof. | Romano  | <b>Regazzi</b>      |
| <b>Directeur·trice de thèse</b> | Monsieur | Dr    | Stephan | <b>Kellenberger</b> |
| <b>Expert·e·s</b>               | Monsieur | Dr    | Roland  | <b>Schönherr</b>    |
|                                 | Monsieur | Prof. | Hugues  | <b>Abriel</b>       |

le Conseil de Faculté autorise l'impression de la thèse de

**Monsieur Anand Vaithia Natha Subramanian**

Master of Science, Université de Skövde, Suède

intitulée

**Characterization of pharmacological modulators  
and study of ASIC activation with cysteine-based  
cross-linking**

Date de l'examen : 18 février 2021

Date d'émission de l'imprimatur : Lausanne, le 24 février 2021

pour le Doyen  
de la Faculté de biologie et de médecine



Prof. Niko GELDNER  
Directeur de l'Ecole Doctorale

# Table of Contents

|   |           |
|---|-----------|
| <b>ACKNOWLEDGEMENT</b> .....  | <b>5</b>  |
| <b>ABSTRACT</b> .....   | <b>6</b>  |
| <b>RÉSUMÉ</b> .....   | <b>7</b>  |
| <b>ABBREVIATIONS</b> .....  | <b>9</b>  |
| <b>1. INTRODUCTION</b> .....  | <b>10</b> |
| 1.1. ACID-SENSING ION CHANNELS .....  | 10        |
| 1.1.1. EXPRESSION PATTERN OF ASICs .....  | 11        |
| 1.1.2. BIOPHYSICAL PROPERTIES OF ASICs .....  | 12        |
| 1.1.3. PHYSIOLOGICAL AND PATHOLOGICAL ROLES OF ASICs .....                                    | 14        |
| 1.1.3.1. ROLES OF ASICs IN THE CNS .....  | 14        |
| 1.1.3.1.1. ACIDOSIS-ASSOCIATED ASIC ACTIVATION .....  | 14        |
| 1.1.3.1.2. SYNAPTIC PLASTICITY AND SPATIAL MEMORY .....                                       | 15        |
| 1.1.3.1.3. FEAR CONDITIONING .....  | 16        |
| 1.1.3.1.4. ACIDOSIS-INDUCED NEURODEGENERATION .....   | 18        |
| 1.1.3.1.5. EPILEPSY .....   | 19        |
| 1.1.3.2. ROLES OF ASICs IN THE PNS .....  | 19        |
| 1.1.3.2.1. NOCICEPTION .....  | 19        |
| 1.1.3.2.2. MECHANOTRANSDUCTION .....  | 21        |
| 1.1.4. STRUCTURE OF ASIC .....  | 22        |
| 1.1.4.1. GENERAL TOPOLOGY .....   | 22        |
| 1.1.4.2. CRYSTAL STRUCTURE OF ASIC1 .....   | 22        |
| 1.1.4.3. STATE-DEPENDENT CONFORMATIONAL CHANGES IN ASIC1A .....                               | 24        |
| 1.1.5. PHARMACOLOGY OF ASICs .....  | 25        |
| 1.1.5.1. SYNTHETIC COMPOUNDS .....  | 25        |
| 1.1.5.2. ENDOGENOUS MODULATORS .....  | 27        |
| 1.1.5.3. ANIMAL TOXINS .....  | 28        |
| 1.2. TECHNICAL INTRODUCTION TO CROSS-LINKING APPROACHES IN PROTEINS .....                     | 29        |
| 1.2.1. OPTICAL CONTROL OF ION CHANNELS USING THIOL-SPECIFIC OPTICAL TWEEZERS .....            | 29        |
| 1.2.2. BISMETHANESULFONATE-BASED CROSS-LINKING .....  | 31        |
| <b>2. SCIENTIFIC INTRODUCTION TO THESIS PROJECTS</b> .....                                    | <b>34</b> |
| <b>3. HYPOTHESES</b> .....  | <b>34</b> |
| <b>4. AIMS</b> .....  | <b>35</b> |
| <b>5. RESULTS</b> .....   | <b>35</b> |
| 5.1. PROJECT 1 - ASSESSMENT OF ASIC1A AND ASIC3 ACTIVITY BY GMQ AND ITS DERIVATIVES .....     | 36        |
| 5.1.1. MY CONTRIBUTION TO THE ARTICLE .....   | 36        |
| 5.2. PROJECT 2 - INVESTIGATION ON THE DIFFERENCES BETWEEN WT ASIC1A AND ITS RARE MUTANT ..... | 54        |
| 5.2.1. MY CONTRIBUTION TO THE ARTICLE .....   | 55        |

|           |   |            |
|-----------|---|------------|
| 5.3.      | PROJECT 3: INVESTIGATION OF THE ACTIVATION MECHANISM OF HUMAN ASIC1A CHANNEL BY USING CROSS-LINKERS ..... | 71         |
| 5.3.1.    | MY CONTRIBUTION TO THE ARTICLE .....  | 72         |
| <b>6.</b> | <b><u>DISCUSSION.....</u></b>   | <b>115</b> |
| 6.1.      | MODULATORY EFFECT BY NON-PROTON LIGAND GMQ AND ITS DERIVATIVES ON ASIC1A.....                             | 115        |
| 6.1.1.    | BLOCKING AND GATING EFFECT BY GMQ DERIVATIVES ON ASIC1A AND ASIC3 .....                                   | 116        |
| 6.1.2.    | GATING AND BLOCKING EFFECT BY GMQ DERIVATIVES ON HETEROMERIC CHANNELS .....                               | 117        |
| 6.2.      | DIFFERENCE IN THE BIOPHYSICAL PROPERTIES BETWEEN WT (G212) AND MUTANT (D212) ASIC1A .....                 | 118        |
| 6.3.      | ANALYSIS ON THE STRUCTURE-FUNCTION RELATIONSHIP OF ASIC1A CHANNEL ACTIVATION.....                         | 120        |
| 6.3.1.    | LIGHT-INDUCED CHANNEL ACTIVATION IN ASIC1A.....   | 120        |
| 6.3.2.    | LIGHT-INDUCED SHIFT IN THE PH DEPENDENCE OF ACTIVATION .....  | 121        |
| 6.3.3.    | SHIFT IN PH DEPENDENCE OF ACTIVATION BY MTS CROSS-LINKERS .....   | 122        |
| <b>7.</b> | <b><u>CONCLUSION AND PERSPECTIVES.....</u></b>  | <b>126</b> |
| <b>8.</b> | <b><u>REFERENCES .....</u></b>  | <b>127</b> |

## ACKNOWLEDGEMENT

First, I would like to thank Dr. Stephan Kellenberger to offer me a PhD position in his group and pursue different projects on my research interest. It was a great journey in this 5 year of research work in his lab and for the continuous support and guidance through different projects. The projects were by itself challenging and stimulating the curiosity. In the project, I did not only illuminate the ASIC channel, but 5 years of research experience in his laboratory has illuminated my research career and life. It was a wonderful time to learn a systematic approach and execution and to also learn a lot more about science. It was a great pleasure to be in his lab and get guided under various circumstances. His continuous support has provided me with a good end to my PhD experiences.

I would like to also thank the lab members Omar, Sabrina, Zhong, Olivier, Nicolas, Ophélie, Sophie and Ivan. It was of great help from all my lab members in providing feedback and support needed during the projects. Because of them, several wonderful moments were possible. Even during a hard time of COVID-19, support by Ivan to obtain *Xenopus* oocytes was highly appreciable that led me to finish my project on time.

I want to also thank the members of the department who had directly or indirectly provided me with their support. A special thanks to Prof. Laurent Schild, Prof. Olivier Staub, Dr. Marie-Christine, Prof. Edith Hummler, and Dr. Miguel van Bemmelen for motivating my research interest. I would also like to thank Dr. Dimitri Frisov and Dr. Dario Diviani for providing inputs during my progress report. A special thanks also to my committee members for timely feedback, ideas, and suggestions on the progress of my project.

My thanks do not end here, and I want to thank my parents, family members and friends for the moral support and encouragement during hard times. A special thanks to my wife Deepika Anand, who stood with me throughout the wonderful journey.

## ABSTRACT

Acid-sensing ion channels (ASICs) are proton-gated, voltage-insensitive Na<sup>+</sup> channels that are localized in the central and the peripheral nervous system participating in a range of physiological and pathological functions such as pain sensation, learning and memory, fear, and neurodegeneration after stroke. ASICs form homo- or heterotrimeric channels. ASIC structures of the closed, toxin-bound open and the desensitized state have been solved. Despite the available high-resolution ASIC structures, it is not known exactly how protons activate ASICs. Using experimental approaches, the structure-function relationship of ASIC activity was investigated here in three sub-projects. 1) 2-guanidine-4-methylquinazoline (GMQ) is a known pharmacological modulator of ASIC1a and ASIC3. New derivatives of GMQ were studied. Several quinazoline and quinoline derivatives produced a modulatory effect on ASIC activity in a sub-type specific manner. Guanidinopyridines strongly inhibited the peak current at pH5 in ASIC1a and ASIC3 with ~20-fold better potency than GMQ. Interestingly, 2-guanidino-quinolines and -pyridines produced in ASIC1a a potentiation at low, and an inhibition at high concentrations. 2) Comparison of the rare mutation D212 in hASIC1a that was used in many laboratories as wild type, with the real wild type human ASIC1a-G212 showed slower current decay kinetics, higher current amplitude per surface-expressed channel, increased surface expression of the channel, and a stronger dependence of the current decay kinetics on the extracellular anion in hASIC1a-G212. 3) To test the effect of distance constraints on channel function, the optical tweezer 4,4'-bis(maleimido)azobenzene (BMA) and bis-methane-thiosulfonate (MTS) cross-linkers were used. In hASIC1a-I428C to which BMA was tethered, light-dependent activation by 440nm light was observed, however without the formation of a cross-link. A modulatory effect by BMA upon 360nm light illumination was found in three double mutants of the extracellular domain. In a second approach, MTS cross-linkers of different lengths were used. In comparison to control condition, treatment with MTS-17-MTS produced an acidic-shift of the pH dependence of activation in hASIC1a-D237C/I312C, and an alkaline or a small acidic-shift in the single mutants, hASIC1a-I312C and -D237C. Further validation of cross-linking is required in D237C/I312C. Our findings provide structural insights into ASIC1a activity.

## RÉSUMÉ

Les canaux ioniques sensibles à l'acide (ASIC) sont des canaux à sodium, proton-dépendants et insensibles au voltage, localisés dans le système nerveux central et périphérique. Ils participent à une gamme de fonctions physiologiques et pathologiques telles que la sensation de douleur, l'apprentissage et la mémoire, la peur et sont impliqués dans la neurodégénérescence après un AVC. Les ASIC forment des canaux homo- ou hétérotrimériques. La structure du poulet ASIC1a a été résolue à l'état fermé, dans l'état ouvert lié à la toxine, et désensibilisé et pour l'ASIC1a humaine (hASIC1a) dans l'état fermé. Malgré les structures ASIC haute résolution disponibles, on ne sait pas exactement comment les protons activent les ASIC. À l'aide d'approches expérimentales, la relation structure-fonction de l'activité ASIC1a a été étudiée. Dans ce contexte 1) la 2-guanidine-4-méthylquinazoline (GMQ) est un modulateur pharmacologique connu des ASIC1a et ASIC3, et ses dérivés quiazoline et quinoléine ont produit un effet modulateur à 1 mM sur l'activité ASIC par sous-type de manière spécifique. Les guanidinopyridines ont fortement inhibé le courant de pointe à pH 5 dans ASIC1a et ASIC3 avec une puissance ~20 fois supérieure à celle du GMQ. Fait intéressant, les 2guanidino-quinoléines et -pyridines ont produit un effet d'inhibition ou de potentialisation dépendant de la concentration sur le sous-type ASIC et dans les ASIC1a/2a et ASIC3/2a hétéromères, seuls quelques composés, y compris le GMQ, ont produit un petit effet modulateur sur l'activité, 2) Une comparaison de la mutation rare D212 dans hASIC1a qui a été utilisée dans de nombreux laboratoires comme type sauvage, avec le vrai type sauvage hASIC1a-G212 a montré une cinétique de décroissance du courant plus lente, une amplitude de courant plus élevée par canal exprimé en surface, une expression de surface accrue du canal, et cinétique de désintégration actuelle dépendante de l'anion extracellulaire dans hASIC1a-G212, et 3) en utilisant l'approche de réticulation et pour trouver une paire de résidus impliqués dans les changements de conformation lors de l'activation d'ASIC1a, les deux pinces optiques 4,4'-bis (maléimido) azobenzène (BMA) et des agents de réticulation bis-méthane-thiosulfonate (MTS) ont été appliqués. Dans hASIC1a-I428C attaché à BMA, une activation dépendante de la lumière sous une lumière de 440 nm a été observée sans la formation de la réticulation. Un effet modulateur par BMA sur une illumination lumineuse de 360 nm a été trouvé dans les mutants hASIC1a-D237C/E315C, -D237C/E355C et -K246C/D347C. Dans une seconde approche, des réticulant MTS de différentes longueurs ont été utilisés. Par rapport à la condition témoin, le traitement avec MTS-17-MTS a produit un changement acide de la dépendance au pH dans hASIC1a-D237C/I312C, et un changement alcalin ou petit acide chez les mutants simples, hASIC1a-I312C et -D237C. Une validation supplémentaire de la réticulation est requise dans D237C/I312C. Nos résultats fournissent de

nouvelles informations structurelles sur l'activité ASIC1a.

## **Caractérisation des modulateurs pharmacologiques et étude de l'activation ASIC avec réticulation à base de cystéine**

Une cellule est considérée comme un bloc l'unité de base de tout organisme vivant, et elle est composée de composants intracellulaires séparés des cellules voisines par la membrane plasmique et travaille 24 heures sur 24 pour maintenir différentes fonctions comme le support structurel, produire de l'énergie, permettre le transport passif et actif de divers ions et molécules, la gestion des réactions métaboliques et la respiration. Pour l'important échange d'ions mentionné ci-dessus, la cellule a recouru à des protéines traversant la membrane cellulaire et qui possèdent un pore sélectif permettant le passage des ions : les « canaux ioniques ». Ces canaux ioniques contrôlent divers processus biologiques comme la fonction cardiaque, la contraction des muscles squelettiques et lisses, le transport épithélial, etc. Le canal ionique peut être activé par un ligand, une tension électrique et mécaniquement. Dans notre recherche, nous travaillons avec des canaux ioniques sensibles à l'acide (ASIC) qui sont activés par acidification extracellulaire et localisés dans les neurones. Lorsqu'ils sont activés, ils sont parfois fermés ou ouverts, le passage d'ions qu'ils entraînent active les neurones. Ils sont impliqués dans diverses conditions physiopathologiques comme la douleur, les démangeaisons, l'apprentissage et la mémoire, l'épilepsie, les accidents vasculaires cérébraux, la maladie d'Alzheimer etc. On ne sait pas comment l'acidification extracellulaire peut activer le canal et quels sont les changements conformationnels associés dans ces domaines ? En mettant l'accent sur l'identification du mécanisme d'activation du canal, j'ai trouvé que 1) certaines petites molécules dérivées d'une molécule existante appelée 2-guanidine-4-méthylquinazoline (GMQ) peuvent moduler l'activité ASIC, 2) ont caractérisé une mutation rare dans l'ASIC1a humaine clone, ayant des propriétés légèrement modifiées par rapport à l'ASIC1a humain de type sauvage réel, 3) Les composés de liaison croisée, à savoir le 4,4'-bis (maléimido) azobenzène (BMA), est un composé qui peut se fixer à ses deux extrémités à un résidu cystéine modifié dans l'ASIC1a et exercer une force mécanique sur les domaines en étendant ou en pliant son forme par application d'une longueur d'onde spécifique de la lumière. Les composés à base de bis-méthane-thiosulfonate (MTS) sont de différentes longueurs qui peuvent également se fixer aux deux extrémités au résidu de cystéine modifié sans changer de forme. Les deux composés ont affecté l'activation de l'ASIC1a. Une enquête plus approfondie est nécessaire pour conclure les changements de conformation dans les domaines identifiés pendant l'activation du canal. Dans l'ensemble, plusieurs aspects associés à la relation structure-fonction de l'activité ASIC1a ont été identifiés. À l'avenir, les études présentées dans cette thèse seront utiles pour concevoir des molécules thérapeutiques en mesure

d'inhiber ou d'activer le canal.

## ABBREVIATIONS

ASICs - Acid-sensing ion channels

ENaC - Epithelial Na<sup>+</sup> Channel

DEG – Degenerin

DRG - Dorsal Root Ganglion

PNS - Peripheral Nervous System

CNS - Central Nervous System

TM -Transmembrane

NSAIDs - Non-Steroid Anti-Inflammatory Drugs

PcTx1- Psalmotoxin

GMQ -N-(4-Methyl-2-quinazolinyl)-guanidine hydrochloride

FaNaC - FMRFamide peptide-activated sodium channel

MitTx - Micrurus tener toxin

BMA - 4, 4'-Bis (maleimido) azobenzene

ATP - Adenosine triphosphate

MEA-TMA - Maleimide ethylene azobenzene trimethyl ammonium derivative

MAM - 4,4'-bis(maleimido-glycine) azobenzene

CHO – Chinese hamster ovary

GFP – Green fluorescent protein

LED – Light emitting diode

LTP – Long-term potentiation

MES - 2-Morpholinoethanesulfonic Acid

HEPES - (4-(2-hydroxyethyl)-1-piperazineethanesulfonic acid)

HEK – Human embryonic cell

EGTA - (ethylene glycol-bis (β-aminoethyl ether)-N, N, N', N'-tetraacetic acid)

LTP – Long term potentiation

LTD- Long term depression

NMDA- N-methyl-D-aspartate receptor

WT- Wild type

KO- Knockout

ExAC – Exome Aggregation Consortium

rASIC1a- rat ASIC1a

hASIC1a – human ASIC1a

mASIC1a – mouse ASIC1a

LRET - Luminescence Resonance Energy Transfer

## 1. Introduction

Ion channels are proteins that span across the cell membrane of animal and plant cells, those conduct ions and have various important physiological and pathological roles. Ion channels are classified based on their ion selectivity and mechanism of activation. Based on the ion selectivity, they are classified as chloride, potassium, sodium, calcium, proton and non-selective cation channels, while based on mechanism of activation they are classified into three superfamilies: voltage-gated, ligand-gated and mechano-sensitive ion channels. They are widely expressed in different cell types and are of crucial physiological importance. They play a principal role in regulating cellular excitability. This thesis work is based on a class of ligand-gated ion channels called Acid-sensing ion channels (ASICs).

### 1.1. Acid-sensing ion channels

In 1980, it was shown for the first time that protons increased the excitability of the cultured neuron<sup>3</sup>. In the late 1990s, ASICs were cloned from human<sup>4,5</sup>, rat<sup>6-8</sup> and mouse<sup>9</sup>. In those studies that cloned ASICs, it was not known that these channels can be activated by protons<sup>3,10,11</sup>. By 1997, ASIC was first shown to produce acid-induced inward current upon extracellular acidification<sup>12-14</sup> and shown to be a voltage-insensitive Na<sup>+</sup>-channel. ASICs belong to the ENaC/DEG (Epithelial Na<sup>+</sup> Channel/Degenerin) superfamily of ion channels. A phylogenetic tree of the ENaC/DEG family is represented in Figure 1. The ENaC/DEG superfamily of ion channel comprises 60 different proteins that form channels, which are either constitutively active, gated by mechanical stress or gated by ligands. ENaC is an epithelial sodium channel that forms constitutively active, Na<sup>+</sup> conducting, and voltage insensitive channel in different tissues and organ. There are four main subunits  $\alpha$ -,  $\beta$ -,  $\gamma$ -and  $\delta$ -ENaC<sup>15</sup>. ASIC share ~25% sequence homology with ENaC. Degenerin (DEG), in contrast, is a mechanosensitive channel of *C. elegans* involved in the stretch and touch sensation<sup>1</sup>. ASICs are encoded by four different genes ASIC1-4 (ACCN1-4) encoding six different subunits ASIC1a (BNaC2)<sup>4,7</sup>, ASIC1b (ASIC1 $\beta$ )<sup>16,17</sup>, ASIC2a (MDEG1/BNaC1)<sup>5,8</sup>, ASIC2b (MDEG2)<sup>9</sup>, ASIC3 (DRASIC)<sup>6,18</sup>, and ASIC4

(BNaC4)<sup>19,20</sup>. In humans, ASIC3 has three different subunits namely ASIC3a, 3b and 3c<sup>18,21</sup>.

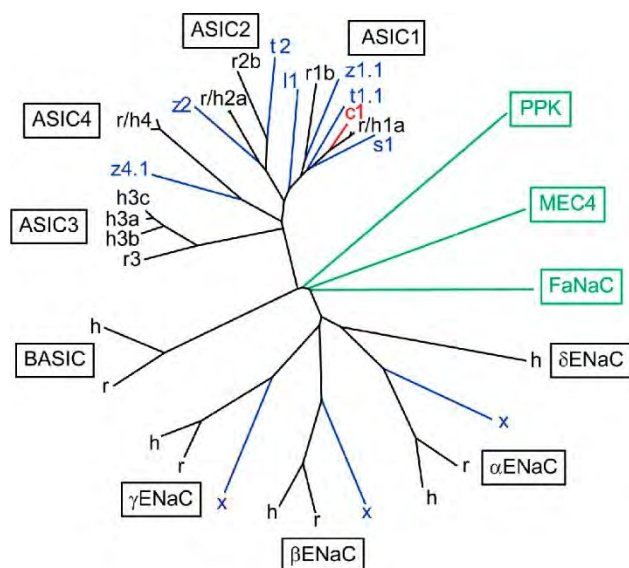


**Figure 1.** Phylogenetic tree from genes of PPK- Pickpocket, DEG MEC4-Mechanosensitive channel of *C.elegans*, FaNaC- peptide gated channel of *H.aspersa*, ENaC- Epithelial Na<sup>+</sup> channel, ASIC-Acid-sensing ion channel and BASIC- Bile acid-sensing ion channel subfamilies. The genes pick-pocket (PPK) from *Drosophila*, DEG MEC4 from *C.elegans*, and the peptide-gated FaNaC of *H.aspera* and are shown in green. Clustal W algorithm was used to align the protein expression. Single letter corresponds to the species, h-human, c-chicken, r-rat, s-shark, t-toad fish, l-lamprey, x-xenopus, z-zebra fish. Adapted figure<sup>1</sup>.

ASICs are widely expressed among chordates and vertebrates and are highly conserved<sup>22</sup>. A functional ASIC channel is formed by the assembly of three individual subunits forming the pore. It can exist either as a homotrimeric or heterotrimeric channel. Each homomeric or heteromeric channel has its unique property of pH-sensitivity and kinetics. A functional homomeric channel is formed by ASIC1a, ASIC1b, ASIC2a and ASIC3, while ASIC2b and ASIC4 do not form a functional channel. All ASICs, except ASIC4, can form functional heteromers<sup>23</sup>. The trimeric assembly of ASIC has been observed in several crystal structures of ASIC1<sup>24-29</sup>, in a stoichiometry study of ASIC1a/ASIC2a assembly<sup>30</sup> and by atomic force microscopy (AFM). Interestingly, ASIC was also found to form heteromeric assembly with ENaC<sup>31</sup>.

### 1.1.1. Expression pattern of ASICs

ASICs are expressed in both the central nervous system (CNS) and peripheral nervous system (PNS) (Table 1). In rodents, only ASIC1a, ASIC2a, ASIC2b and ASIC4 are expressed in CNS<sup>4,7,32</sup>, while in humans, in addition to ASIC1a, ASIC2a, ASIC2b and ASIC4, very low expression of ASIC3 was detected<sup>33</sup>. High expression of ASIC1a, ASIC2a, ASIC2b and ASIC4 mRNA expression is found in the cultured hippocampus, hypothalamus, cerebellum, cortical region, olfactory bulb, habenula, dorsal raphe and basolateral amygdala, striatum, nucleus accumbens, amygdala and cerebral cortex<sup>34,35</sup>. Transfection of epitope-tagged ASIC1a in

cultured hippocampal neurons shows the distribution in cell bodies and dendrites<sup>36</sup>, and studies also reported the localization of ASIC1a at the post-synaptic terminal<sup>35,36</sup>, together with post-synaptic proteins like PICK1<sup>37</sup>, CaMKII<sup>38</sup>, PSD-95<sup>36</sup> and AKAP150<sup>39</sup>. The less pH-sensitive ASIC2a also interacts with neuronal synaptic scaffolding protein PSD-95<sup>40,41</sup>. In the PNS, all ASIC subunits are expressed, except ASIC4<sup>42-44</sup>. ASIC subunits are expressed in sensory neurons of dorsal root ganglion (DRG) and are localized in the axon growth cone, cell bodies and nerve terminals<sup>45</sup>. Increasing evidence show ASIC expression in non-neuronal cells, like astrocyte<sup>46</sup>, monocytes, arthritic chondrocytes, osteoblasts, osteoclasts<sup>47</sup> and muscle cells<sup>48</sup>.

### 1.1.2. Biophysical properties of ASICs

The biophysical properties of a channel comprise their permeability to ions, voltage or ligand dependence, and associated kinetics. To study the biophysical properties, the ASICs are expressed in vitro in *Xenopus* oocytes or cell lines, e.g. COS7, HEK293 and CHO for electrophysiological characterization. ASICs can exist in three different functional states, namely closed, open and desensitized (Figure 2A). Upon extracellular acidification, ASICs undergo rapid transient activation, followed by desensitization. Activation of the channel occurs rapidly (ms) in all functional ASICs, and the desensitization kinetics depends on subunit composition<sup>23</sup>. ASICs remain closed at physiological pH7.4 and open upon extracellular acidification to  $\leq$  pH6.8 (C-O transition). They undergo steady-state desensitization (SSD) upon persistent exposure to mild acidic pH6.9-7.2 that can desensitize the channel activity directly from closed to desensitized state without opening (C-D transition). In some ASIC subtype like ASIC2a and ASIC3, the desensitization is not complete, and a sustained current is observed. As an example, a typical current trace of the activation followed by desensitization of human ASIC1a from a

patch-clamp recording is shown (Figure 2A).

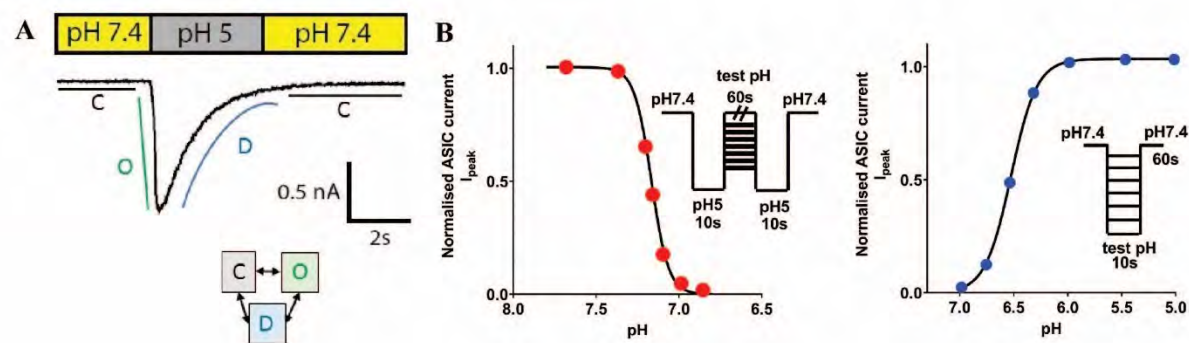


**Figure 2. Schematic illustration of current trace and pH dependence curves.** **A.** The current trace of ASIC1a from whole-cell patch-clamp experiment at -60mV on CHO cells expressing ASIC1a. Green line represents the channel activation, blue line for desensitization during prolonged acidification and black line for the return towards resting state. Underneath, the boxes labelled with C (Closed), O (Open) and D (Desensitize) stand for the different functional states. **B.** Stead-state desensitization (SSD) curve (left) and activation curve (right) of ASIC1a. Steady-state desensitization is a state of ASIC1a, where it enters the desensitized state when exposed to pH less than pH7.4 and pH greater than the pH required for minimal activation of the channel for a few seconds. For obtaining SSD curve (left), a control was performed by applying conditioning pH7.4 for 60s and channel activation by pH5 for 10s. Following each control application, different conditioning pH, from pH7.8 to pH6.8 was applied for 60s and the channel was activated by pH5 for 10s. The peak currents obtained from different conditioning pHs were normalized to peak current obtained from the control condition. The normalized peak currents were plotted as a function of the conditioning pHs and fitted to obtain the SSD curve. For the activation curve (right), the channel was exposed to extracellular conditioning pH7.4 for 60s, followed by activation with different test pHs (pH6.8 to pH5) for 10s. Conditioning with pH7.4 was applied between each activation for 60s. The normalized values of the peak current were obtained from different pH condition for activation and it is plotted using the Hill equation to obtain the activation curve.

The sensitivity of the channel to the  $H^+$  is defined by the pH dependence. The pH-dependence differs based on the subunit composition. The channel activity for activation is defined by pH dependence of activation (Figure 2B, right) and the half-maximal activation is defined by  $pH_{50}$  (half-maximal activation). Whereas, desensitization of the channel is defined by steady-state desensitization (Figure 2B, left) and half-maximal desensitization is defined  $pHD_{50}$  (half-maximal steady-state desensitization). Half-maximal activation is obtained by fitting the normalized values of activation from experiments to Hill equation,  $I = I_{max} / (1 + (10^{-pH_{50}} / 10^{-pH})^{nH})$ , where  $I_{max}$  is the maximal peak current amplitude and  $nH$  is the Hill coefficient. An analogous equation is used for fitting the SSD values. Table 1 shows the  $pH_{50}$  and  $pHD_{50}$  values of homomeric ASICs.

| ASIC subtypes | pH <sub>50</sub> activation | pHD <sub>50</sub> SSD | Localisation |
|---------------|-----------------------------|-----------------------|--------------|
| ASIC1a        | 6.6 – 6.2                   | ~7.2                  | CNS, PNS     |
| ASIC1b        | 6.3 – 5.9                   | ~6.7                  | PNS          |
| ASIC2a        | 4.9 – 4.0                   | ~5.6                  | CNS, PNS     |
| ASIC2b        | NA                          | NA                    | CNS, PNS     |
| ASIC3         | 7.7 – 6.4                   | ~7.1                  | PNS          |
| ASIC4         | NA                          | NA                    | CNS          |

**Table 1.** pH<sub>50</sub> of ASIC activation and desensitisation. The values are represented based on different articles. pH<sub>50</sub> - Half-maximal activation of the channel, pHD<sub>50</sub> - Half-maximal steady-state desensitisation, NA - Not applicable. Table adapted<sup>2</sup>.

The cloned ASICs were shown to be Na<sup>+</sup>-selective<sup>49-51</sup>. Selectivity for Na<sup>+</sup> over K<sup>+</sup>, P<sub>Na<sup>+</sup></sub>/P<sub>K<sup>+</sup></sub>, is ≤10-folds and for ASIC1a homotrimers, which are permeable to the Ca<sup>2+</sup> ion has P<sub>Na<sup>+</sup></sub>/P<sub>Ca<sup>2+</sup></sub> ≥15<sup>16</sup>. Other than Na<sup>+</sup> and Ca<sup>2+</sup>, ASIC is also permeable to H<sup>+</sup>, however, the magnitude is negligible, and it causes tachyphylaxis in homomeric ASIC1a. Tachyphylaxis is a phenomenon that leads to rapid diminishing of the response of the channel to successive doses of agonist. It is believed that H<sup>+</sup> permeates through the channels that lead to a long-lived inactive state. The tachyphylaxis of ASIC1a activity depends on extracellular pH and Ca<sup>2+</sup> ion concentration, intracellular pH, duration of acidic stimulation<sup>52</sup>.

### 1.1.3. Physiological and pathological roles of ASICs

#### 1.1.3.1. Roles of ASICs in the CNS

##### 1.1.3.1.1. Acidosis-associated ASIC activation

Maintenance of the body fluid pH in the range between pH7.35-7.45 is an important parameter for normal functioning and several buffering systems play important role in the exchange of H<sup>+</sup> between cellular components<sup>53</sup>. For example, lactic acid produced from glucose and glycogen breakdown in skeletal muscles, pyruvic acid as an intermediate metabolite of glycolytic system, and beta-hydroxybutyric acid, a ketone body as a result of fatty acid metabolism. Compared to the extracellular pH, intracellular pH is slightly acidic in most living organisms. In the CNS, maintenance of the pH homeostasis is a key requirement for proper neurotransmissions. The pH in the CNS is 0.1-0.2 units more acidic than that of the body fluids.

In the CNS, ASIC1a, -2a, and -2b are prominently expressed and among this ASIC1a is more pH-sensitive. Slow changes in the extracellular pH from pH7.4 to pH7.2-6.9 can desensitize the ASICs, while more rapid acidic pH change should activate ASIC1a. However, the time scale of pH change in the synaptic terminals depends on the situation, like rapid acidification (in ms or less) during vesicle release, followed by slower alkalosis (~20-200 ms) and slower acidosis (in minutes). pH changes not only activate ASICs, but also other ion channels like two-pore K<sup>+</sup> (K2P) channel, P2X receptors, BK channel, and TRPV channels<sup>2</sup>. The V-H<sup>+</sup>-ATPases shuttles protons into synaptic vesicles and lowers their pH to ~5.5<sup>54</sup>. The proton gradient results in neurotransmitter uptake by synaptic vesicles. The fusion of synaptic vesicle with the to pre-synaptic membrane releases the neurotransmitter, causing acidification of the synaptic cleft occurs (in a millisecond or less). This led to the activation of ASIC1a localized at the post-synapse. After acidification, the local environment undergoes slower alkalization. Since changes in extracellular pH regulate ASICs activity, ASICs are considered as a potent pH sensor regulating various physiological processes. *Ex vivo* studies showed that 1) A drop in the extracellular pH of mouse CNS neurons produced acid-induced action potentials by ASIC1a expressing neurons, and ASICs are involved in seizure inhibition<sup>55</sup>, 2) Presynaptic stimulation in the lateral amygdala produces excitatory post-synaptic ASIC1a current<sup>56</sup>, 3) Genetic disruption of ASIC1a results in the absence of acid-induced current (pH6.0-5.0) in hippocampal, cortical and amygdala neurons<sup>35,36,57</sup>.

#### **1.1.3.1.2. Synaptic plasticity and spatial memory**

The expression of ASIC1a is prominent in the regions of the CNS with high synaptic density. The activation of postsynaptic ASIC1a by extracellular acidification through presynaptic vesicular release in a controlled microdomain is shown to influence the synaptic plasticity. Studies using pH-sensitive fluorescence indicators have shown presynaptic stimulation leading to acidification of the synaptic cleft and light-induced activation of proton pumps causing extracellular acidification<sup>58,59</sup>. Initially, a study showed that loss of ASIC1a in the mice

hippocampus impaired the long-term potentiation (LTP), spatial learning and eye-blinking condition which defines the underlying role of ASIC1a in synaptic plasticity. The mice were generated by embryonic deletion of ASIC1. The loss of postsynaptic ASIC1a in hippocampus impaired the high frequency stimulated long-term potentiation due to reduced excitatory potentials and NMDA receptor activation<sup>36</sup>. Presynaptic stimulation transiently reduced extracellular pH in the amygdala and ASIC present in lateral amygdala pyramidal neurons were activated, generating postsynaptic ASIC current and LTP<sup>56</sup>. The contrary, another study showed ASIC1a was not required for hippocampal long-term potentiation (LTP) and spatial memory<sup>60</sup>. This effect was observed in the ASIC1a KO mice generated from selective deletion and breeding of transgenic mice ASIC1a<sup>flox/flox</sup> and Nestin-cre. The difference in the LTP effect might originate through the strategy used for deletion of ASIC1a. In hippocampal neurons, the magnitude of LTD induced by application of mGlu1 receptor agonist (S)-3,5-Dihydroxyphenylglycine (DHPG) or by paired-pulse low-frequency stimulation (PP-LFS) was mediated by ASIC1a and the LTD was inhibited by PcTx1, suggesting the role of ASIC1a in mGlu receptor-mediated LTD<sup>61</sup>. Involvement of ASICs in synaptic transmission was evaluated from hippocampal neurons from WT and ASIC knockout (KO) mice, where the probability of neurotransmitter release was higher in neurons from KO mice, suggesting the influence of ASIC1a in glutamatergic synaptic transmission through presynaptic mechanism<sup>62</sup>. In medial nucleus of the trapezoid body (MTNB), drop of extracellular pH induced postsynaptic ASIC current and it was inhibited by PcTx1 and ASIC1a KO mice. Independent of glutamergic current, action potential was still elicited by extracellular acidification. During high-frequency stimulation (HTS), lack of ASIC1a resulted enhanced short-term depression (STD) of glutamergic EPSCs<sup>63</sup>. Thus, ASIC1a has a role in improving synaptic signaling.

#### **1.1.3.1.3. Fear conditioning**

ASIC1a is widely expressed in the CNS and several studies have shown the role of ASIC1a

in fear-related behavior. Higher expression of ASIC1a was found in amygdala neurons and elicited greater current density than hippocampal neurons and disrupting the ASIC1a gene eliminated the H<sup>+</sup>-induced current. Effect of ASIC1a on amygdala-dependent behavior showed ASIC1a KO mice displayed a deficit in cue and context fear conditioning<sup>35</sup>. Targeting the ASIC1a reduced innate fear and altered the neuronal activity. Disrupting the ASIC1a in mice resulted in reduced fear in the open field test and with predator odor trimethylthiazoline (TMT). Similarly, intracerebroventricular administration of PcTx1 reduced TMT-evoked freezing in wild-type mice and not in the ASIC1a KO mice, suggesting ASIC1a mediated fear conditioning. The fear circuit activity was assessed with an expression of the c-fos gene as fear circuit marker. The results showed loss of ASIC1a reduced the TMT-evoked fear-related behaviour and led to a loss of c-fos expression in the amygdala and dorsal periaqueductal gray<sup>64</sup>. Fear memory was also assessed by restoring the ASIC1a using viral vector-mediated gene transfer in basolateral amygdala of ASIC1a KO mice and exposure of the mice to TMT odor. Together, these experiments identified the re-expression of ASIC1a in the basolateral amygdala was enough to rescue the conditioned fear memory, but not the unconditioned fear response. However, ASIC1a might also play a role in unconditioned fear response, as ASIC1a is also expressed abundantly in the bed nucleus of the stria terminalis (BNST) which is involved in unconditioned fear response<sup>65</sup>. In a different approach, human ASIC1a was overexpressed in mice using synapsin 1 promoter. hASIC1a interacted with endogenous mouse ASIC1a and distributed in the synaptosome. The amygdala showed prominent expression ASIC1a and overexpressing it enhanced the fear conditioning<sup>66</sup>. All these studies suggest the role of ASIC1a in fear conditioning and anxiety development. The fear learning and activity-induced LTP in the basolateral amygdala were reduced in ASIC1a KO mice, in which ASIC1a was selectively deleted in GABAergic cells<sup>67</sup>. Thus, the region of basolateral amygdala drives the fear switch and reward responsive behavior by influencing spatial memory.

#### 1.1.3.1.4. Acidosis-induced neurodegeneration

Neurodegeneration is a progressive loss of the structure and function of neurons, resulting in loss of neuronal activity. A common feature of neurological conditions such as ischemic stroke, epilepsy, trauma is a drop in the tissue extracellular pH. Inflammation and metabolic stress may also result in a drop in the extracellular pH. Reduced blood flow in the brain during a stroke, can reduce the oxygen supply leading to anaerobic respiration utilizing glucose to produce lactate, in turn inducing subsequent acidosis. Some studies provide the evidence for homomeric ASIC1a conducting  $\text{Ca}^{2+}$  and acidosis-induced neuronal injury<sup>57,68</sup>. Using an *in vivo* ischemic animal model, where ischemia was induced by middle artery occlusion (MCAO) and the role of ASIC1 blockade in neuroprotection was established. Blockade of ASIC1a by amiloride or PcTx1 or using ASIC1 KO in mice showed a reduction in infarct volume of the brain. These studies suggested the blockade of ASIC1a can provide additional protection when NMDA receptors were also blocked<sup>57,69</sup>. While the above-mentioned studies performed experiments with transient MCAO model, neuroprotection was also demonstrated after permanent MCAO<sup>69</sup>. Alteration of the brain tissue pH after ischemia was measured continuously in the ipsilateral and contralateral parietal cortex of mice after MCA suture removal. The pH values dropped to pH6.5 after MCAO. The acidosis was attenuated by i.c.v administration of  $\text{NaHCO}_3$  or blocking of ASIC1a by i.c.v or i.n administration of PcTx1 reduced the infarct volume, and additional protection was obtained by blocking NMDA receptors with memantine<sup>69</sup>. In a related study from rat cortical neurons, ASIC1a was inhibited using either amiloride or PcTx1, in a combination setting of ischemia and acidosis resulting in decrease of intracellular  $\text{Ca}^{2+}$  elevation. However, at very low pH, PcTx1 and amiloride failed to block elevated steady-state  $\text{Ca}^{2+}$  levels in response to ischemia with acidosis. Also, the sustained current component activated in response to combined ischemia and acidosis was not inhibited by ASIC1a inhibitors. This suggests that elevated calcium levels due to acidosis was in part due to proton dependent activation of ASIC1a<sup>70</sup>. Yi-Zhi Wang et al suggested neuronal necroptosis through ASIC1a. Acidic stimulation recruits the serine/threonine

kinase receptor interaction protein 1 (RIP1) to the ASIC1a c-terminus, causing RIP1 phosphorylation and subsequent neuronal death. Deletion of the ASIC1a gene prevented the phosphorylation of RIP1 and brain damage caused by increased acidity due to stroke<sup>71</sup>. A comprehensive review by Wemmie J.A. et al provides detailed information on ASIC associated neurological diseases<sup>44</sup>.

#### **1.1.3.1.5. Epilepsy**

ASICs were investigated for their role in status epilepticus (SE), a condition in which neuronal overexcitation leads to acidosis. Rats were treated with pilocarpine, a cholinergic agent to induce SE. Reduction in the mRNA expression of ASIC1a and ASIC2b were observed in CA1-2 of the hippocampus, which might blunt the pH-dependent responsiveness<sup>34</sup>. Inhalation of 10% CO<sub>2</sub> after the onset of tonic-clonic seizures induced hypercarbic acidosis *in vivo* mouse model stopped epileptic activity and inhibited seizures. Acidosis activated inhibitory interneurons and shortened the seizure duration<sup>55</sup>. Under glucose hypometabolism, ASIC2a overexpression was observed in an epileptic model of rat hippocampal slices<sup>72</sup>. A high concentration of amiloride administered in an animal model has also been shown to inhibit pilocarpine-induced seizures via ASICs<sup>73,74</sup>. It has been postulated that the hydrophilic nature of amiloride may prevent it from crossing the blood-brain barrier contradicting the seizure termination through ASIC inhibition by amiloride. Though amiloride reaches the brain, they are known to block ENaC and sodium-hydrogen exchanger (NHE) other than ASICs. Thus, seizure inhibition may occur also through Na<sup>+</sup>/H<sup>+</sup> exchanger, but anti-epileptic mechanism was shown associated with deactivation of ASIC1a and ASIC3 instead of NHE in rats<sup>73</sup>. Also, the role of amiloride in enhancing the anticonvulsant effect of an antiepileptic drug in mice has been demonstrated<sup>75,76</sup>.

#### **1.1.3.2. Roles of ASICs in the PNS**

##### **1.1.3.2.1. Nociception**

Nociception involves the transmission of neuronal signals induced by nociceptive stimuli

to the CNS. It is useful as a warning system to avoid excessive damage. The different stimuli, either chemical or physical, can activate different molecular mechanisms involving activation of different types of receptors<sup>77</sup>. To study the pain signaling, ASIC3 knockout mice was generated by Chen. C et al. Mutant mice displayed normal health and responded to sensory stimuli, however they displayed reduced latency to the onset of pain response with moderate to high-intensity stimuli<sup>78</sup>. To avoid heteromultimerisation of ASIC subunit, a dominant-negative form of ASIC3 transgenic mice which was generated to inactivate all native neuronal ASIC currents by oligomerization. The transgenic mice displayed more sensitivity to mechanical pain and chemical stimuli<sup>79</sup>. The two studies showed rather an anti-nociceptive effect of ASIC3. Several studies have shown the role of ASICs in nociception<sup>80-83</sup>. While a specific knockdown of ASIC3 using intrathecal administration of siRNA in rats produced analgesic effects against primary inflammation-induced hyperalgesia<sup>84</sup>. Similarly, injection of MitTx in mice activated ASIC1a channel on capsaicin-sensitive nerve fibers and evoked ASIC1a dependent pain-related behaviour<sup>85</sup>. Intraplanar injection of mambalgin-1 in mice evoked peripheral analgesic effects through ASIC1b<sup>86</sup>. The same research group showed mambalgin-1 inhibiting ASIC1a and ASIC1b in neuropathic and inflammatory pain<sup>87</sup>. Peripheral ASIC1b and ASIC3 were inhibited by diminazene and APETx2 to elicit an antihyperalgesic effect in rats injected previously with Freund's complete adjuvant (FCA) in the paw<sup>88</sup>. In rats, subcutaneous injection of moderate pH7 or in combination with hypertonicity and arachidonic acid (AA) increased the excitability of ASIC3-expressing neuron and induced action potential firing, which was totally inhibited by APETx2, producing analgesic effect against primary inflammation<sup>84</sup>. In the study, in which GMQ was identified as a non-proton activator of ASIC3, it was shown that injection of GMQ in mouse paw elicited pain-related behaviour<sup>89</sup>. Exposure of the DRG neurons to acidic pH-induced action potentials and subsequent application of either diclofenac, salicylic acid, or flurbiprofen diminished the number of action potential<sup>42</sup>. Similarly, the endogenous molecules lysophosphatidylcholine (LPC) and AA were shown to activate hASIC3 without extracellular

acidification<sup>90</sup>. These findings suggest the potent role of ASICs in peripheral pain perception.

In the CNS, intrathecal and intracerebroventricular (ICV) injection of PcTx1 in ASIC1a expressing mice showed an antinociceptive effect in tail immersion and hot plate test. The involvement of ASIC1a was also confirmed by intrathecal injection of ASIC1a-antisense in wild-type mice and it decreased the thermal nociception<sup>91</sup>. The brain-derived neurotrophic factor (BDNF) promotes ASIC1a expression and activity via the downstream phosphoinositide 3-kinase (PIK3)-protein kinase B (PKB/Akt) cascade. BDNF was found to sensitizes ASIC1a function by enhancing its surface expression Both WT and ASIC1<sup>-/-</sup> mice developed mechanical hyperalgesia, however, mechanical hyperalgesia was sustained in WT mice, suggesting ASIC1a role<sup>92</sup>.

#### **1.1.3.2.2. Mechanotransduction**

Mechanotransduction is a conversion of the mechanical force to electrical signals. The molecular topology of ASIC resembles the mechanosensitive channel MEC-4 and MEC-10 from *C.elegans*. Among ASICs, the role of ASIC1a is less addressed in the cutaneous mechanosensation. Activation of ASIC1a in mice by MitTx resulted in pain-related behavior in hind paw<sup>85</sup>. The role of ASIC1a in visceral and not in cutaneous mechanosensation was supported by a study performed on gastroesophageal and cutaneous afferent fibres in mice<sup>93</sup>. Moving on to ASIC2, it was shown that ASIC2 deficient mice developed hypertension and impaired mechanosensation<sup>94</sup>. Knockout of ASIC2 decreased the sensitivity to rapid-adapting (RA) and slow-adapting (SA) mechanoreceptor<sup>95</sup>. ASIC3 KO mice are very sensitive to mechanical pressure<sup>78</sup>. A triple knockout of ASIC1a, ASIC2 and ASIC3 in mice enhanced the cutaneous mechanosensation<sup>96</sup>. There are several other studies from different organs elucidating the role of ASIC in mechanosensation, which is well described in the review<sup>97</sup>.

### 1.1.4. Structure of ASIC

#### 1.1.4.1. General topology

ASIC subunits are composed of 500 to 560 amino acid residues. Until 2007, the membrane topology of ASIC was described based on secondary-structure predictions and biochemical analysis. The first crystal structure of ASIC obtained from chicken revealed three individual subunits assembled to form the channel. ASIC subunits consist of a large extracellular domain linked to the 2 $\alpha$ -helices, the transmembrane domains (TM1 and TM2) per subunit, and intracellular C- and N-terminal domains. The extracellular domain of each subunit is compared to a clenched hand holding a ball, where the domains are named as a finger, thumb, palm,  $\beta$ -ball, wrist, and transmembrane domain (TM) forming the pore. The interface between thumb,  $\beta$ -ball and finger contains many negatively charged amino acids, and this region is collectively called acidic pocket. In terms of sequence similarity, cASIC1 shares 90% homology with hASIC1a, mASIC1a and rASIC1a. The percentage of sequence homology between different ASIC subunits are shown in Table 1 of the appendix.

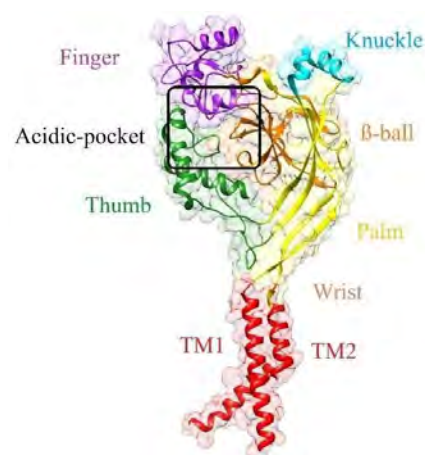


**Figure 3. Crystal structure of ASIC subunit in the closed state.** Chicken ASIC1a (PDB: 5WKU) single subunit represented with a domain organization.

#### 1.1.4.2. Crystal structure of ASIC1

ASIC was very first crystallized from chicken ASIC1 (PDB ID:2QTS) at low pH5-6 in 2007 and it was obtained from a non-functional form with N- and C-terminals truncated<sup>29</sup>. By 2009, crystallized cASIC1 (PDB ID: 4NYK) was obtained at low pH6.5<sup>28</sup>. The first ASIC1a structure (2QTS) was obtained from a non-functional channel having truncated C-terminal, while later (4NYK) was determined from a functional channel with truncated-terminal in the desensitized state and a closed pore. In 2012, the crystal structure of cASIC1 in complex with Psalmotoxin

(PcTx1), a toxin from the spider, was obtained at 3.0Å, low pH5.5, with truncated C- and N-terminals resulting in a non-functional form (PDB ID: 3S3X)<sup>19</sup>. PcTx1 increases ligand affinity of ASIC1a and it is a gating modifier, as it shifts the pH dependence of activation and desensitization to alkaline values<sup>26,98</sup>. In the same year, two different crystal structures of cASIC1 in complex with PcTx1 were resolved at 2.8Å, low pH5.5 (PDB ID: 4FZ0) and 3.3 Å, high pH7.25 (PDB ID: 4FZ1)<sup>20</sup>. The structure at high pH7.25 had a large pore diameter of ~10Å and the channel in the presence of 1µM produced a non-selective current at pH7.25, while the structure obtained at low pH5.5 had a uniform lining of the pore with hydrophobic residue and the channel resulted in Na<sup>+</sup>-selective and amiloride-sensitive current when activated by pH5.5 with 100nM PcTx1. With these structures, it was hypothesized that the channel opens through an expansion of the extracellular vestibule and amino acid rearrangements in the subunit interface. Likewise, cASIC1 was crystallized with a toxin named MitTx, from black mamba snake at 3.6 Å in the open state (PDB ID: 4NTW)<sup>18</sup>. The TM2 domain was identified with a bend at GAS motifs. Having the toxin-bound open state and desensitized state crystal structures, the closed state crystal structure of cASIC1 at 3.7Å became available in 2018<sup>17</sup>. This is the only known crystal structure in the closed state (PDB ID: 5WKV, with Ca<sup>2+</sup> and PDB ID: 5WKU, with Ba<sup>2+</sup>) (Figure 3). These crystal structures have provided information on state-dependent conformations, yet conformational changes during channel activation remain elusive. This year, two more crystal structures were added to pre-existing structures. Yoder.N and Gouaux.E developed cryo-EM cASIC1a structure both in high and low pH. The structure in resting and desensitized channels reveal re-entrant loop at N-terminal that contains highly conserved ‘His-Gly’ motif. It implicated the importance of re-entrant loop lining the ion permeation pathway in gating and ion-selectivity<sup>44</sup>. For the very first time, a human ASIC1a cryo-EM structure and hASIC1a-Mamba1 complex at a resolution of 3.56Å and 3.90Å. It was shown that mamba1 binds to hASIC1a in a closed state

and reduces the proton sensitivity by trapping the channel in a closed state. Comparison of closed state structures of cASIC1a and hASIC1a revealed minor deviation between the structures<sup>45</sup>.

### 1.1.4.3. State-dependent conformational changes in ASIC1a

The conformation changes of ASIC1a domains is state-dependent. In the closed state, the channel adopts a conformation with the thumb domain facing away from the central axis and finger domain, thereby holding the acidic pocket in an extended conformation, and a closed pore<sup>24</sup>. Upon activation, a structural rearrangement has been postulated at the  $\alpha 4$  and  $\alpha 5$  of the thumb helices, where  $\alpha 5$  makes a lateral pivot towards palm domain of neighboring subunit. This rearrangement of the thumb domain brings the residues of acidic pocket closer upon protonation of the acidic residues for the formation of carboxyl-carboxylate pairing to stabilize the interface between thumb, finger and palm domains. Upon the collapse of acidic pocket and stable subunit interface formation, two different  $\beta$ -strands of the palm domain,  $\beta 1$  and  $\beta 12$  undergo a small angular twist leading to an outward displacement of the TM1 and TM2 domains. These structural rearrangements lead to expansion of the pore and  $\text{Na}^+$  ions entry.

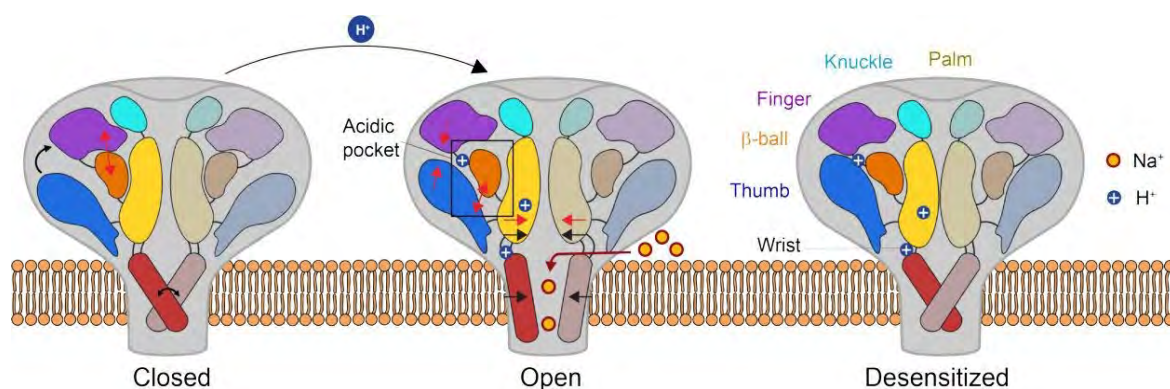


**Figure 4. Theoretical conformational changes during ASIC activity.** Conformational changes predicted from different experimental approaches and crystal structure. Cartoon representation of two of the three subunit of ASIC1a in closed, open and desensitized state. In closed state, acidic pocket resides with an extended conformation of thumb facing away from the  $\beta$ -ball and finger domain. Transmembrane domain in the closed state adapts constrained conformation and shuts the gate for passage of  $\text{Na}^+$ . Protonation events (middle) marked with + symbol, brings thumb domain closer to  $\beta$ -ball and finger domain, and allows the passage of  $\text{Na}^+$  ions through expanded transmembrane domain. During channel desensitization (right), substantial rearrangements in the acidic pocket, and relaxation of palm and transmembrane domain like in closed state occurs. Black arrow- conformational changes observed from crystal structure and red arrow- Evidence of conformation changes observed from voltage-clamp fluorometry. Figure from Vullo S and Kellenberger S, 2019<sup>46</sup>.

When the channel is persistently exposed to acidification, it results in the channel desensitization

due to the relaxation of the lower palm towards the central vertical axis and lateral displacement of TM domains, thereby adopting a closed pore. During desensitization state, L415 and N416 in the  $\beta$ 11-  $\beta$ 12 linker rotate 180°, thereby uncouples the upper ECD from the lower channel domains<sup>17</sup>. A recent functional study found a residue Q276, located in the middle of  $\beta$ 9 strand works together with the rotation of L415 and N416, and compression of  $\beta$ 11-  $\beta$ 12 linker by locking them to achieve steady-state desensitization under low-pH. Substitution of these three residues results in incomplete or no desensitization<sup>99</sup>. The desensitized state adapts the relaxed conformation of the wrist and TM domains like the closed state and a collapsed acidic pocket like in the open state conformation<sup>100</sup>. A recent functional study also showed that mutating all the negatively charged residues in acidic pocket still produced transient currents upon extracellular acidification. This suggests that pH sensing occurs in the acidic pocket that collapses during channel activation but not the driving force for channel activation. Activation of the channel depends on the protonation of multiple residues in different domains. Mutations in the acidic pocket produced an acidic shift in the pH<sub>50</sub> of activation, an alkaline shift in the pH<sub>D50</sub> and decrease in the Hill coefficient of activation, but not SSD, thereby involved in fine-tuning of pH dependence<sup>51</sup>. Although, the conformational changes are explained with the help of crystal structures and functional studies<sup>51,99,101</sup>, the mechanism of channel activation upon protonation is yet unknown. A hypothetical scheme of channel activation and desensitization by extracellular acidification is shown in figure 4.

### **1.1.5. Pharmacology of ASICs**

The pharmacology of ASICs comprises of a wide range of compounds, ranging from small synthetic to natural molecules, endogenous peptides, animal toxins and ions.

#### **1.1.5.1. Synthetic compounds**

Amiloride is a clinically used diuretic for the treatment of hypertension and heart failure. It is a well-known inhibitor of ENaC with an IC<sub>50</sub> of 0.1-0.3 $\mu$ M and it blocks non-selectively ASICs,

and exchangers like  $\text{Na}^+/\text{H}^+$  and  $\text{Na}^+/\text{Ca}^{2+}$ <sup>102</sup>. The  $\text{IC}_{50}$  of ASIC inhibition ranges from 5-100 $\mu\text{M}$  depending on the ASIC subunit composition<sup>103</sup>. Amidine A-317567 is a small molecule having similar potency as amiloride with an  $\text{IC}_{50}$  of 2-30 $\mu\text{M}$ ; its efficacy has been proven both *in vitro* and in *in vivo* pain models<sup>104</sup>. A few drugs of the non-steroid anti-inflammatory drugs (NSAIDs) class like salicylic acid, ibuprofen, flurbiprofen, aspirin, diclofenac, are also known to produce a significant inhibitory effect on ASIC activation ( $\text{IC}_{50}$  92-350  $\mu\text{M}$ )<sup>42</sup>. Antiparasitic drugs like diminazene ( $\text{IC}_{50}$  ~0.2-0.8 $\mu\text{M}$ ), hydroxystilbamidine ( $\text{IC}_{50}$ ~1.5 $\mu\text{M}$ ), and pentamidine ( $\text{IC}_{50}$ ~40 $\mu\text{M}$ )<sup>105</sup> are also potent inhibitors of ASICs. Amiloride binds to the pore entry of ASIC1a and ASIC3<sup>106</sup>, while diminazene involves both allosteric modulation and pore block in ASIC1a<sup>107</sup>. The modulatory effect by diminazene is caused by binding to Glu residue at 79 and 418 (mouse ASIC1a numbering) of lower palm domain that undergoes structural rearrangement during channel opening. Diminazene is also shown to inhibit ASIC subtypes like ASIC1b, -2a, and -3 via open-channel inhibition<sup>88</sup>. A novel small molecule named NS383 was identified as to inhibit ASIC1a and -3 in pH-dependent manner ( $\geq \text{pH}6.5$ ) at a sub-micromolar concentration ( $\text{IC}_{50}$ ~0.61-2.2  $\mu\text{M}$ )<sup>108</sup>. 2-guanidine-4-methyl quinazoline (GMQ) is a small molecule containing a guanidium group and a heterocyclic ring. It was shown as the first non-proton ligand to activate ASIC3 at physiological pH 7.4<sup>89</sup>, and later as a modulator of ASICs<sup>106</sup>. However, GMQ does not activate ASIC1a, ASIC1b or ASIC2a at physiological pH 7.4. At a concentration of 1mM, GMQ potentiates the sustained current of ASIC3. This is due to the shift in the pH-dependence of activation to alkaline values and of the pH-dependence of desensitization to acidic values. GMQ at high concentration inhibits ASIC current by pore block. Binding of GMQ to pore region, where amiloride is known to bind was confirmed by mutagenesis and other residues in the pore region of ASIC1a were also proposed to be involved<sup>106</sup>. Endogenous compounds like the arginine metabolite agmatine and can exert similar effect like GMQ on ASIC3<sup>89,109</sup>. GMQ and amiloride

shift the pH-dependence of activation and desensitization in a similar manner for ASIC1a and ASIC3, and pharmacological modulation depends on the extracellular domain<sup>110</sup>.

### 1.1.5.2. Endogenous modulators

Divalent metal ions ( $\text{Ca}^{2+}$ ,  $\text{Zn}^{2+}$ ,  $\text{Mg}^{2+}$ ) are endogenous modulators of ASICs. They exert different roles in the modulation of the ASICs.  $\text{Ca}^{2+}$  and  $\text{Mg}^{2+}$  exert an acidic shift of the pH dependence of activation and desensitization. In contrast,  $\text{Zn}^{2+}$  inhibits ASIC1a, ASIC1b and ASIC3 current<sup>111</sup> and potentiates ASIC2 current<sup>112</sup>.

ASICs are also a target of neuropeptides. The FMRFamide-gated  $\text{Na}^+$  channel (FaNaC), a molluscan ion channel and the Hydra-RFamide gated  $\text{Na}^+$  channel (HyNaC) are FMRFamide peptide-activated channels that belong to ENaC/Deg superfamily of ion channels<sup>113</sup>. The FMRFamide peptide is not endogenously synthesised in mammals and its mode of action occurs mostly through G-protein coupled receptors. In fact, mammals do synthesize five similar peptides called FMRFamide-like peptides (RFRP), neuropeptide FF (NPFF), prolactin-releasing peptide (PrRP), Kisspeptin and pyroglutamylated RF-amide peptide. RFamide peptides potentiate the  $\text{H}^+$ -induced current, slow the desensitization and induce a sustained current in homomeric ASIC1a and ASIC3 ( $\text{EC}_{50} \sim 10\text{-}50\mu\text{M}$ ), and not in ASIC2a<sup>114</sup>. The resulting sustained current is due to the shift in steady-state desensitization of the channel to acidic values. A few peptides structurally similar to FMRFamide, such as neuropeptide FF and SF also exhibit similar effects on ASIC1 and ASIC3<sup>114</sup>. It was shown that the RFamide binds to the region of extracellular palm domain of ASIC1a contributing to conformational changes and slowing of desensitization<sup>115</sup>. The FMRFamide-related peptides slow the desensitization time course of ASIC1a and ASIC3<sup>116</sup>, and induce sustained current and acidic shift in the pH dependence of desensitization<sup>117</sup>. Two endogenous opioid neuropeptides, dynorphin A and big dynorphin enhance ASIC1a activity ( $\text{EC}_{50} \sim 30\text{nm}$ ). Big dynorphin also enhances ASIC1b activity<sup>118</sup>. A recent study suggests that big

dynorphin binds to the acidic pocket of ASIC1a<sup>119</sup>.

### 1.1.5.3. Animal toxins

Apparently, many compounds have different roles in altering the ASIC activity. Interestingly, toxins act either as inhibitor/activator or modulator of ASIC activity. Psalmotoxin (PcTx1), a peptide of 40 amino acids obtained from the South American tarantula *Psalmopoeus cambridgei*<sup>120</sup>, the most potent hASIC1a specific inhibitor (IC<sub>50</sub> ~1nM). PcTx1 is a 40 amino acid cysteine-rich peptide containing three disulphide bridges whose structure was resolved by NMR<sup>121</sup>. PcTx1 inhibits ASIC1a by binding to the acidic pocket. PcTx1 is a gating modifier as it shifts the steady-state desensitization curve towards alkaline values, which results in the channel desensitization at  $\leq$  pH 7.4<sup>98</sup>. One PcTx1 peptide binds deeply to the acidic pocket of each ASIC1a subunit. The peptide contains hydrophobic and charged residues on the surface. The hydrophobic patch of PcTx1 envelope around the  $\alpha$ 5 helix of ASIC1a and the basic cluster of PcTx1 interacts deeply into the acidic pocket<sup>25,27</sup>.

MitTx- $\alpha/\beta$  a pain-inducing toxin obtained from the Texas coral snake *Micrurus tener*, activates ASIC1a and ASIC1b at pH7.4 (EC<sub>50</sub>~9-30 nM), ASIC3 (EC<sub>50</sub>  $\leq$  800nM) and weakly activates ASIC2a<sup>85</sup>. MitTx consists of  $\alpha$  and  $\beta$ -subunits, non-covalently associated and requires both subunit association for its activity. Like PcTx1, one molecule of MitTx binds to each subunit of ASIC1a by interaction with wrist, palm and thumb domain. The interaction site of  $\beta$  subunit of MitTx overlaps with PcTx1. The Phe14 of MitTx- $\alpha$  hook into lower thumb subunit interaction interface and Lys16 into the wrist. The interaction was shown with the crystal structure of cASIC1 in complex with MitTx<sup>25</sup>.

Mambalgin 1-3, is a 57-amino acid peptide, isolated from African black mamba *Dendroaspis polylepis* venom. Mambalgins do not have sequence similarity to PcTx1 and MitTx. It inhibits homomeric ASIC1a and heteromeric ASIC1a/2a and ASIC1a/2b (IC<sub>50</sub> ~55-246nM). Mambalgin-1 is a gating modifier which binds to the closed state of the channel and induces

strong acidic shift to the pH dependence of activation<sup>86</sup>. Mambalgin2, which differ from Mambalgin1 only by one residue was shown to bind to the upper palm domain, palm domain of adjacent subunit and  $\beta$ -ball domain of ASIC1a<sup>122</sup>, which is close to PcTx1 binding site.

APETx2 is 42 amino-acid toxin from sea anemone *Anthopleura elegantissima* and it inhibits homomeric and heteromeric ASIC3 ( $IC_{50} \sim 63 \text{ nM} - 2 \mu\text{M}$ )<sup>123</sup>. APETx2 rapidly and reversibly inhibits ASIC3 peak and sustained current at pH7.0. APETx2 binding site on ASICs is not yet identified, however it has been suggested to bind as like PcTx1 to the acidic pocket<sup>98</sup>.

## 1.2. Technical introduction to cross-linking approaches in proteins

In my thesis, the hASIC1a channel activation mechanism was assessed using two different approaches. The section 1.2.1 describes the usage of an optical tweezer-based cross-linking approach and section 1.2.2 is about using monovalent and bivalent methane sulfonate compounds.

### 1.2.1. Optical control of ion channels using thiol-specific optical tweezers

Different types of optical approaches are available to study ion channels including photochemical, genetic and hybrid approaches. Photochemical approaches comprise the use of caged compounds, photo-switchable ligands, and photo-affinity labels<sup>58,59,124-126</sup>.

In my thesis work, 4,4'-Bis(maleimido)azobenzene (BMA), an azobenzene-based optical tweezer was used to determine the structure-function relationship of ASIC1a channel activation. Depending on the wavelength of light applied, BMA can adopt the *cis*- or *trans*-conformation. Compounds of this type contain, either one or two functional sulfhydryl-modifying groups that will attach to introduced cysteine residues in the channel via covalent bond(s). A molecule with one sulfhydryl-reacting group, could be used to attach a functional group, the orientation of which could then be controlled by light. Some molecules contain two cysteine-binding functional groups, one on each end, and can form a cross-link. Photo-isomerization of azobenzene to *trans*-*cis* isomerization is proposed to consist of rotation, inversion, concerted inversion or inversion-assisted rotation of central azo bond<sup>127</sup>. Azobenzene-containing compounds like azobenzene-

trimethyl ammonium derivative (MEA-TMA)<sup>128</sup>, quaternary ammonium–azobenzene–quaternary ammonium (QAQ)<sup>129</sup>, 4,4'-bis(maleimido-glycine) azobenzene (MAM)<sup>130</sup>, and 4,4'-Bis(maleimido)azobenzene (BMA)<sup>131</sup> have been used to previously to study ion channels.

In MEA-TMA, MEA binds covalently to engineered cysteine residues. TMA is a cation moiety, which can be used to block channels in a voltage-dependent manner. A cysteine residue was engineered in the conduction pathway of P2X2 channel to place MEA-TMA close to the channel pore<sup>128</sup>. After attachment of the molecule, the light was used to change the orientation of the TMA group and to thereby block the channel or remove the block. This molecule was used to study the role of P2X receptor in neuronal activity<sup>128</sup>. QAQ is another photoisomerizable molecule having a central azobenzene moiety coupled on both sides with quaternary ammonium groups. When QAQ is delivered intracellular, it reversibly blocks most of the Na<sup>+</sup>, Ca<sup>2+</sup> and K<sup>+</sup> current in *trans* configuration and the blockade can be released in the *cis* configuration. Structurally, QAQ resembles lidocaine and its derivative QX-314 that act as a local anaesthetic by blocking Na<sup>+</sup> channels<sup>129,132</sup>. This molecule was used for understanding signaling mechanisms in acute and chronic pain<sup>129</sup>. MAM is a semi-rigid photo-switchable azobenzene that was used to cross-link engineered cysteines in P2X2 receptor to elucidate the pore opening mechanism<sup>130</sup>. BMA is a cross-linking molecule like MAM having shorter functional arms. Upon illumination with 360nm and 440nm light, BMA can adapt its conformation to *cis* and *trans* state, respectively (Figure 5). The absorption spectrum of BMA consists of a strong near UV band ( $\epsilon \sim 22000 \text{ L mol}^{-1} \text{ cm}^{-1}$ ) and a weaker band in the visible region ( $\epsilon \sim 400 \text{ L mol}^{-1} \text{ cm}^{-1}$ ). A thermal isomerization step that occurs in fractions of ps is well described by Bandara et al<sup>127</sup>. The end-to-end distance of the molecule is 22Å in the *trans*-state and 13Å in the *cis* state. Browne L. E et al used BMA to tether with engineered cysteines in the transmembrane domain of rP2X2, rP2X3 and hASIC1a. Application of 440nm light produced a current in rP2X2-P329C rP2X2, rP2X3-P320C, hASIC1a-I428C and -G430C<sup>131</sup>. The residues I428 and G430 are in TM2

domain of hASIC1a. The light-induced current in both mutants had 15% of maximal current induced by pH5. But it was not tested whether cross-linking by BMA produced light-induced current.

Therefore, BMA was used in my thesis to extend the optical tweezer approach on the hASIC1a channel activation mechanism. For this strategy, cysteine mutations were engineered in different domains of the hASIC1a, and a specific wavelength of light was applied on the cysteine mutants tethered with BMA to exert mechanical force to open the channel. First, it was tested whether BMA attached to different parts can open the channel, and in the second series of experiments, the modulatory effect of BMA upon application of 440nm and 360nm light was tested. The current ratio at  $I_{pH6.x}/I_{pH5}$  and peak current at  $I_{pH5}$  were measured under the standard condition and were later observed for changes by application of light. Cross-linking at transmembrane domain residues by BMA was tested using western blot analysis and no cross-linking by BMA was observed.

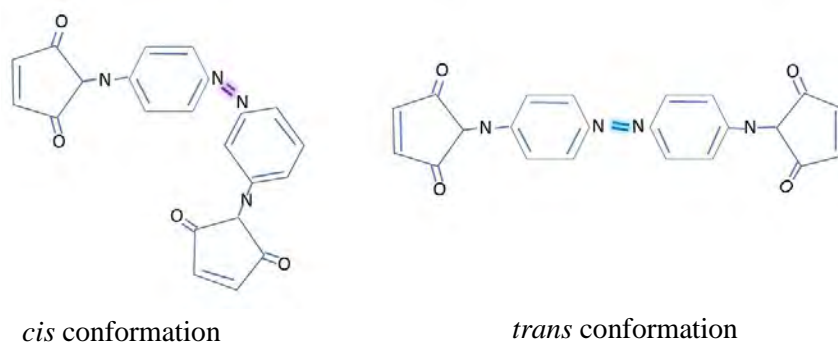


**Figure 5. Structure of BMA.** BMA in *cis* (left) and *trans* conformation (right) obtained upon application of 360nm and 440nm wavelength of light.

### 1.2.2. Bismethanesulfonate-based cross-linking

As an alternative approach to photoisomerizable BMA molecule, whose length can be modified by application of light, different lengths of bismethanesulfonate-based (MTS) cross-linking compounds were applied. The length of MTS cross-linkers cannot be modified like BMA and it attaches on its both ends to cysteine residue through covalent sulfhydryl bond. MTS cross-linking reagents are alkylthiosulfonates that favorably and rapidly form covalent bonds with

cysteine residues under mild conditions. The disulfide bond is reversible only under the exposure to reducing agents such as  $\beta$ -mercaptoethanol, dithiothreitol (DTT) or tris(2-carboxyethyl) phosphine (TCEP). The rate constant of disulfide bond formation is on the order of  $10^5 \text{ M}^{-1} \text{ sec}^{-1}$  which facilitates rapid covalent bond formation with cysteine residues in the protein. MTS reagents can be classified either as charged, neutral, spin-labelled, fluorescently labelled, biotin-labelled, photoreactive labelled compounds and cross-linkers. However, mostly monovalent, and cross-linkers MTS reagents are used to study ion channel structure-function relationship.

1. Charged or monovalent MTS reagents, like MTSEA, MTSET and MTSES are used in many structure-function relationship studies in diverse ion channels<sup>115,133-135</sup>. In a study, cysteine mutations were introduced at the N-terminus and in the transmembrane helices of ASIC1a. The engineered cysteine residues were then modified by application of MTSET, resulting in channel inhibition, suggesting that the mutated residues are part of pore<sup>134</sup>. A highly conserved region of the extracellular part of ASIC1a that forms a contact region between the finger, the adjacent  $\beta$ -ball and the upper palm domain was found important for channel function as application of MTSET, MTS-TAE and MTS-TBAE reduced current amplitudes in a state-dependent manner, suggesting conformation changes during channel inactivation<sup>136</sup>. To map the proton binding site, MTSET was applied to acidic pocket and lower palm cysteine mutants and shown to reduce the proton affinity for activation<sup>137</sup>. Conformational changes in the lower palm of ASIC1a were assessed using MTSET, highlighting the contribution of the lower palm to desensitization<sup>115,138</sup>. Other than ASICs, MTS reagents were also used in studies with ENaC<sup>139</sup>, voltage-gated  $K_v1.3$ <sup>140</sup>, and voltage-gated  $Na_v1.5$ <sup>141</sup>.



## 2. Scientific introduction to thesis projects

Since the cloning of ASICs, much progress has been made to understand the physiological and pathological roles of ASICs. A lot of emphases are put on to understand the conformation changes in the structure associated with the channel activation mechanism. Determining the crystal structures of ASIC1a from closed, toxin-bound open and desensitized states has contributed some insight on putative proton binding sites, the key residues involved in ASIC gating. While the structure-function relationship studies on ASICs have provided more information on conformational changes occurring at different domains during ASIC activity, the channel activation mechanism is yet unclear. To better understand the structure-function relationship of ASIC1a activity, we wanted to address three different aspects in ASIC as follows

- 1) As there is no potent and selective small-molecule available, that can inhibit ASIC activity, we tested derivatives of GMQ, where GMQ is a known modulator of ASIC activity,
- 2) A hASIC1a clone containing a mutation to Asp of Gly212 was used over years as WT in many laboratories. However, this mutation occurs at a low frequency of  $8.26 \times 10^{-6}$  according to Exome Aggregation Consortium (ExAC). The ASIC1a containing Asp at 212 is located on the  $\beta$ -ball domain at a subunit interface, facing the thumb domain of a neighboring subunit. We then tested the biophysical and pharmacological properties of the channel between WT (G212) and the rare mutant (D212),
- 3) Using cross-linking optical tweezer BMA and MTS-based compounds, pair of residues were identified in hASIC1a involved in the channel activation by introducing structural constrain.

## 3. Hypotheses

1. GMQ derivatives could provide better potency and subunit-dependent selectivity.
2. Through the identification of functional differences between ASIC1a WT (G212) and mutant (D212), the results from previous studies in the background of ASIC1a-D212 can be interpreted correctly.
3. By applying cross-linking approach and as consequence, introducing structural constraints between two residues, the domain or residues involved in the channel activation or modulation can be determined.

#### **4. Aims**

To test the hypotheses mentioned above, the aims of my thesis work are as follows:

1. Identify potent GMQ derivatives with subunit-dependent selectivity and understand their structure-function relationship.
2. Identify any functional differences of the biophysical and pharmacological properties between hASIC1a WT and the rare hASIC1a-G212D mutant.
3. Identify cross-linked residues by BMA involved in the channel activation by applying mechanical force by light to activate the channel. Secondly, to apply cross-linking MTS reagents to hASIC1a containing engineered cysteine residues, to introduce structural constraints to identify residues involved in the channel activation.

#### **5. Results**

## 5.1. Project 1 - Assessment of ASIC1a and ASIC3 activity by GMQ and its derivatives

**Article:** Heteroarylguanidines as Allosteric Modulators of ASIC1a and ASIC3 Channels

**Authors:** Omar Alijevic, Hassan Hammoud, Anand Vaithia, Viktor Trendafilov, Maud Bollenbach, Martine Schmitt, Frédéric Bihel and Stephan Kellenberger

In this project, 2-Guanidine-4-methyl quinazoline (GMQ) and its derivatives having the guanidium group of GMQ as scaffold were evaluated for their efficacy on homotrimeric hASIC1a and rASIC3, and on heteromeric ASIC1a/2a and ASIC3/2a. Based on the experimental assessment, derivatives containing quinazoline and quinoline induced an alkaline shift of the pH dependence of activation in ASIC3 and an acidic shift in ASIC1a similar to GMQ. In contrast, 2-guanidinopyridines shifted the pH dependence of both ASIC1a and ASIC3 to acidic values. Compounds of this group had a higher potency for ASIC1a and ASIC3 inhibition than the parent compound. Interestingly, a biphasic effect was identified when guanidino-quinolines and -pyridines were used in ASIC1a. These compounds at higher concentration ( $IC_{50} > 100 \mu M$ ) inhibited ASIC1a and ASIC3 currents, and at low concentration ( $EC_{50} \approx 10 \mu M$ ) potentiated ASIC1a, but not ASIC3. In ASIC1a/2a heteromers, only very few compounds induced a shift in the pH dependence of activation, while many compounds showed increased tendency of  $I_{cpd}/I_{ctrl}$  ratio at pH5.8 over  $I_{pH4.0}$ . Only few compounds decreased the maximal peak amplitude. Almost none of the compounds produced a potentiation of heteromeric currents. Thus, heteromeric ASICs containing ASIC2a can possibly disrupt the binding pocket for many GMQ derivatives, thereby decreasing their efficacy to blocking effect.

### 5.1.1. My contribution to the article

This project was initially started by Dr. Omar Alijevic, a former PhD student in the lab.

After joining the group, I took over this project and performed many experiments with GMQ derivatives to assess the gating and blocking effect on hASIC1a and rASIC3. Additionally, I had made experiments requested by the reviewer on heteromeric ASIC1a/2a and ASIC3/2a. I had established a protocol to identify the expression of heteromeric ASIC1a/2a and ASIC3/2a and assessed the effect of GMQ derivatives on them. Apart from doing the experiments, I had analyzed the data, contributed to making figures, and to the writing of the manuscript.

## Heteroarylguanidines as Allosteric Modulators of ASIC1a and ASIC3 Channels

Omar Alijevic,<sup>†</sup> Hassan Hammoud,<sup>‡</sup> Anand Vaithia,<sup>†</sup> Viktor Trendafilov,<sup>‡</sup> Maud Bollenbach,<sup>‡</sup> Martine Schmitt,<sup>‡</sup> Frédéric Bihel,<sup>\*,‡</sup> and Stephan Kellenberger<sup>\*,†,‡</sup>

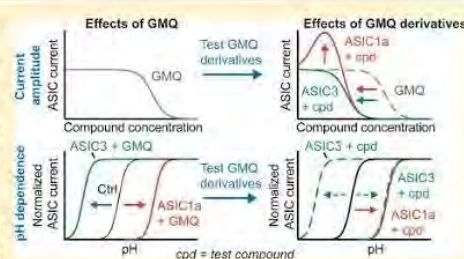
<sup>†</sup>Department of Pharmacology and Toxicology, University of Lausanne, 1011 Lausanne, Switzerland

<sup>‡</sup>Faculty of Pharmacy, University of Strasbourg, 67401 Illkirch Cedex, France

### Supporting Information

**ABSTRACT:** Acid-sensing ion channels (ASICs) are neuronal Na<sup>+</sup>-selective ion channels that open in response to extracellular acidification. They are involved in pain, fear, learning, and neurodegeneration after ischemic stroke. 2-Guanidine-4-methylquinazoline (GMQ) was recently discovered as the first nonproton activator of ASIC3. GMQ is of interest as a gating modifier and pore blocker of ASICs. It has however a low potency, and exerts opposite effects on ASIC1a and ASIC3. To further explore the molecular mechanisms of GMQ action, we have used the guanidinium moiety of GMQ as a scaffold and tested the effects of different GMQ derivatives on the ASIC pH dependence and maximal current. We report that GMQ derivatives containing quinazoline and quinoline induced, as GMQ, an alkaline shift of the pH dependence of activation in ASIC3 and an acidic shift in ASIC1a. Another group of 2-guanidinopyridines shifted the pH dependence of both ASIC1a and ASIC3 to more acidic values. Several compounds induced an alkaline shift of the pH dependence of ASIC1a/2a and ASIC2a/3 heteromers. Compared to GMQ, guanidinopyridines showed a 20-fold decrease in the IC<sub>50</sub> for ASIC1a and ASIC3 current inhibition at pH 5. Strikingly, 2-guanidino-quinolines and -pyridines showed a concentration-dependent biphasic effect that resulted at higher concentrations in ASIC1a and ASIC3 inhibition (IC<sub>50</sub> > 100 μM), while causing at lower concentration a potentiation of ASIC1a, but not ASIC3 currents (EC<sub>50</sub> ≈ 10 μM). In conclusion, we describe a new family of small molecules as ASIC ligands and identify an ASIC subtype-specific potentiation by a subgroup of these compounds.

**KEYWORDS:** Acid-sensing ion channel, channel regulation, structure–activity relationship, compound testing



### INTRODUCTION

Acid-sensing ion channels (ASICs) are Na<sup>+</sup>-selective ion channels that are activated by a rapid drop in extracellular pH.<sup>1,2</sup> They form a subfamily of the ENaC/degenerin channel superfamily, to which besides ASICs the epithelial Na<sup>+</sup> channel ENaC, the *Caenorhabditis elegans* degenerins, and the mollusk channel FaNaC belong.<sup>1</sup> ENaC plays a role in transepithelial Na<sup>+</sup> transport, the degenerins are part of a mechanotransduction complex, while FaNaC is a peptide-gated neuronal ion channel. ASICs are mostly found in the nervous system, and their activation induces a membrane depolarization of the neurons in which they are expressed, affecting thereby neuronal signaling.<sup>3,4</sup> The subunits ASIC1a, -1b, -2a, -2b, and -3 can assemble into homo- or heterotrimeric channels.<sup>5,6</sup> Biophysical properties of the ASICs, such as pH dependence and current kinetics, depend on the subunit composition, and it has been shown that ASIC1a is especially important in the central nervous system, while ASIC3 appears to be the most important ASIC subunit in the peripheral nervous system.<sup>1,7</sup> Studies with ASIC knockout mice provided evidence for roles of ASICs in learning, fear behavior, neurodegeneration after ischemic stroke, mechanosensation and pain sensation.<sup>1,7–14</sup> ASICs are

therefore attractive potential targets for analgesic and anxiolytic drugs and for the pharmacological treatment of stroke. Positive allosteric modulators of ASICs may improve learning. The prototype ASIC inhibitor amiloride is used as a K<sup>+</sup>-sparing diuretic due to its high affinity inhibition of ENaC.<sup>15,16</sup> On ASICs, amiloride has however a low potency (IC<sub>50</sub> of 10–100 μM, compared to 100 nM on ENaC<sup>1</sup>). Amiloride concentrations required to inhibit ASIC currents affect also other transporters and ion channels.<sup>17</sup> In spite of efforts of several laboratories and drug companies, it seems that so far no clearly superior small molecule ASIC inhibitors have been discovered.<sup>1,7,18–22</sup> In contrast, several toxins inhibit ASIC currents with nanomolar affinity.<sup>23</sup>

For many years, protons were the only known activators of ASICs. In the search for other ASIC activators, a large number of ASIC modulators has been identified.<sup>1,7</sup> Such modulators, which are, for example, divalent and polyvalent ions, small molecules, and peptides, change in most cases the ASIC pH

Received: December 29, 2017

Accepted: March 22, 2018

Published: March 22, 2018

dependence.<sup>1,7</sup> Recently, the molecule 2-guanidine-4-methylquinazoline (GMQ) was shown to activate ASIC3 at physiological pH7.4 and to induce pain in an ASIC3-dependent manner, when injected into the paw of a mouse.<sup>24</sup> Our laboratory has subsequently shown that GMQ induces ASIC3 activation by changes in its pH dependence that create a window current at pH7.4. The GMQ-induced changes in ASIC3 pH dependence are different from the gating modulation by GMQ observed in other ASIC subtypes.<sup>25</sup> GMQ can activate the ENaC/degenerin family member FaNaC, but has no effect on ENaC currents.<sup>26</sup> It has also been shown that the endogenous arginine metabolites agmatine and arcaine exert similar effects on ASIC3 currents<sup>27</sup> as does GMQ. It is therefore possible that GMQ-like substances may be endogenous modulators of ASICs. GMQ contains, like amiloride, a guanidinium group. Interestingly, it was observed that GMQ inhibits ASICs by a pore block in addition to its effects on gating,<sup>25</sup> and that at high concentrations, amiloride can affect the ASIC3 gating in a similar way as does GMQ.<sup>28,29</sup> It would be interesting to better understand the molecular mechanisms of GMQ action and to use GMQ as a pharmacological tool in animal and cellular studies. Currently, the use of GMQ is limited by its low potency, with EC<sub>50</sub> and IC<sub>50</sub> values of the order of 2 mM.<sup>24,25</sup> The discovery of GMQ opened however the way for the design of new chemical entities modulating the dependence of ASIC activity on pH.

The aim of the present study was to find GMQ analogues with improved affinity, and to understand the structure–activity relationship of GMQ-like compounds on ASICs. Among the derivatives tested, we identified groups with distinct effects on ASIC pH dependence. Most of the compounds showed also a strong inhibition of the maximal peak current of ASIC1a, but less of ASIC3. In ASIC1a/2a and ASIC2a/3 heteromers, the maximal current inhibition by these compounds was less pronounced, and shifts in pH dependence, if they occurred, were similar to those observed with ASIC3. Several compounds exerted a biphasic action on ASIC1a, inducing potentiation at concentrations of 10–80  $\mu$ M, and inhibition at  $\geq 100$   $\mu$ M.

## RESULTS AND DISCUSSION

**Compound Library and Testing Protocol.** ASIC activation by acidification leads only to a transient channel opening, because these channels desensitize rapidly (within hundreds of ms to s) after activation.<sup>1</sup> ASICs can exist in three different functional states, closed, open and desensitized. The pH dependence of activation (Figure 1a), the transition from the closed to the open state, determines the current induced by a solution change from pH7.4 to a given acidic pH. The pH that induces half of the maximal current amplitude (pH<sub>50</sub>) is 6.5–6.7 for ASIC1a and ASIC3.<sup>30,31</sup> When ASICs are exposed for tens of seconds to a pH that is more acidic than pH 7.4, but not sufficiently acidic to open them, they can enter the desensitized state without apparent opening, in a process called steady-state desensitization (SSD). The midpoint of SSD (pHD<sub>50</sub>) is  $\sim 7.2$  for ASIC1a and  $\sim 7.1$  for ASIC3.<sup>1</sup> The pH dependence of SSD determines the availability of the channels for opening at a given basal pH. It was previously shown that GMQ shifts the pH dependence of activation of ASIC1a to more acidic, and that of ASIC3 to more alkaline values, as illustrated schematically in Figure 1a.<sup>25,29</sup> Due to an additional acidic shift of the pH dependence of SSD in ASIC3, GMQ induces a sustained (i.e., a non- or partially desensitizing) current at pH  $\geq 6$  in this ASIC subtype.<sup>25</sup> In addition, GMQ

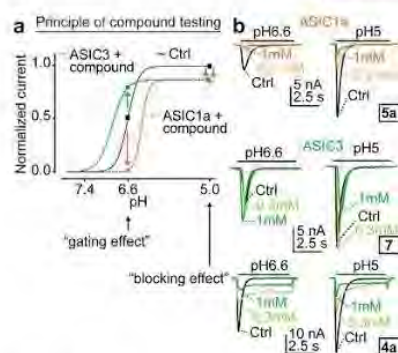


**Figure 1.** Principle of compound testing. (a) Hypothetical pH dependence of activation is shown for ASIC1a and ASIC3 in the absence of a test compound (solid black line), and in the presence of a compound with similar properties as GMQ on ASIC3 (green dashed line) and ASIC1a (orange dashed line), showing the change in pH dependence and maximal current amplitude. The arrows indicate the changes in current amplitude measured at pH 6.6 (“gating effect”) and pH 5 (“blocking effect”). (b) Traces of a representative experiment with compound 5a on ASIC1a (top) and compounds 7 (center) and 4a (bottom) on ASIC3 at concentrations of 0.3 and 1 mM. ASICs were expressed in CHO cells, and their currents were measured with whole-cell patch-clamp.

decreases the maximal current amplitude induced by acidification to pH 5 due to its pore-blocking effect (Figure 1a).<sup>25</sup> To characterize the effects of GMQ derivatives, the current response was measured at pH 6.6 to detect effects on pH dependence (“gating effect”), and at pH 5, where the current is maximal, to quantify the pore block (“blocking effect”), as illustrated in Figure 1a with the hypothetical pH dependence curves of ASIC1a and ASIC3 in the absence or presence of a GMQ derivative. Experiments were carried out with CHO cell lines stably expressing human ASIC1a<sup>32</sup> or rat ASIC3,<sup>30</sup> at compound concentrations of 0.3 and 1 mM. Typical current traces obtained under such conditions in the absence and presence of the GMQ derivatives 5a in ASIC1a and 7, as well as 4a in ASIC3, are shown in Figure 1b. A sustained current was induced by compound 4a (Figure 1b, bottom panel; the compounds used in this study are shown in Figure 2). The ASIC3 current increase at pH 6.6 in the presence of compound 7 (Figure 1b, middle panel) indicates an alkaline shift in pH dependence. An inhibition of the pH 5-induced current was observed with all three compounds shown in Figure 1b.

The initial analysis of the structure–activity relationship of GMQ by Yu et al.<sup>24</sup> was limited to the 2-guanidino-4-methylquinazoline scaffold, since 2-guanidino-benzimidazole, -benzothiazole, and -benzoxazole were found to modulate ASIC3 poorly or not at all. In the present study, we modified the quinazoline scaffold of GMQ (Figure 2). In a first series (cluster #1), we conserved the bicyclic system of GMQ, but we replaced the benzene ring by a cyclohexene ring (1) to evaluate the influence of the aromatic ring on activity. We also synthesized quinoxaline (2) and quinoline (3a, b) bicycles as GMQ analogues, in order to evaluate the role of the methyl group at position 4, but more importantly because the removal of the nitrogen atom at position 3 of GMQ limits the formation of an H-bond interaction with guanidine to the nitrogen atom at position 1. In a second series, we disconnected both rings to generate the 6-, 5-, and 4-phenyl-2-guanidinopyridines, forming

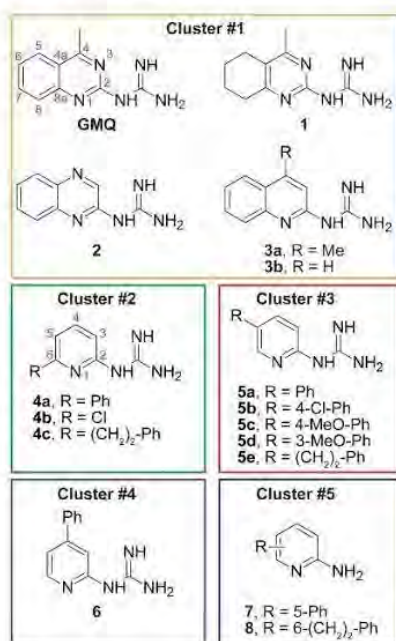


**Figure 2.** GMQ derivatives tested. Structures of the different compounds tested in this study are shown, and the clusters are identified.

clusters #2 (4a–c), #3 (5a–e), and #4 (6), respectively. Finally, we investigated the loss of the guanidine moiety with the 2-aminopyridines 7 and 8 (cluster #5).

**Blocking Effect of GMQ and Its Derivatives on ASIC1a at pH 5.** At pH 5 and a concentration of 1 mM, GMQ inhibited the maximal current of ASIC1a ( $I_{\text{GMQ}}/I_{\text{ctrl}} = 0.68 \pm 0.06$  at pH 5;  $n = 7$ ,  $p < 0.01$ ; Figure 3a, filled bars). Compound 1 showed no significant inhibition ( $I_{\text{cpd}}/I_{\text{ctrl}} = 0.81 \pm 0.10$ ,  $p > 0.05$ ), while quinoxaline 2, as well as the quinoline 3b, showed a similar modest inhibition as GMQ. Quinoline 3a, however, produced a stronger inhibition than GMQ ( $I_{\text{cpd}}/I_{\text{ctrl}} = 0.26 \pm 0.13$ ,  $p < 0.01$  vs GMQ). This suggests that the nitrogen atom at position 3 of GMQ alters the blocking effect on ASIC1a. Interestingly, all the guanidinopyridine analogues (clusters #2, #3, and #4) showed a blocking effect on ASIC1a that was similar or even greater than that by GMQ. While the presence of an aryl group at position 6 of the pyridine did not change the blocking effect (4a–c), aryl groups at position 3 (5b–c) or 4 (6) led to efficient pore blockers with  $I_{\text{cpd}}/I_{\text{ctrl}}$  ratios of  $0.24 \pm 0.08$  ( $p < 0.01$ ),  $0.16 \pm 0.11$  ( $p < 0.0001$ ), and  $0.22 \pm 0.02$  ( $p < 0.001$ ), respectively. Finally, the two compounds lacking the guanidine moiety, 5-phenyl-2-aminopyridine (7) and 6-phenethyl-2-aminopyridine (8), showed a moderate inhibition quite similar to the one by GMQ.

**Gating Effect of GMQ and Its Derivatives on ASIC1a at pH 6.6.** The  $\text{pH}_{50}$  of ASIC1a and ASIC3 activation is  $\sim 6.5$  and  $\sim 6.7$ , respectively.<sup>1,7,25</sup> Modulatory effects of test compounds on the ASIC pH dependence were measured at pH 6.6 (Figure 3a, open bars). Because pH 6.6 is within the steep range of the pH–current relationship (Figure 1a), the pH 6.6-induced current is very sensitive to changes in pH dependence. GMQ at 1 mM abolished the pH 6.6-induced current of ASIC1a (“gating effect”,  $I_{\text{GMQ}}/I_{\text{ctrl}} = 0.03 \pm 0.01$ ), while reducing the

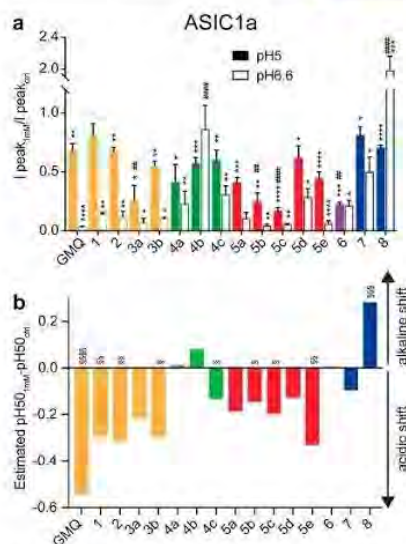


**Figure 3.** Functional analysis of GMQ derivatives on ASIC1a. (a) Bar graph indicating the peak current amplitudes induced with pH 5 (filled bars) or pH 6.6 (open bars), in the presence of 1 mM test compound, normalized to the current amplitude measured at the same pH in the absence of the compound. (b) Shift of the pH dependence of activation by different compounds, estimated from comparison of the  $I_{\text{cpd}}/I_{\text{ctrl}}$  ratios at pH 6.6 and pH 5 (see Methods). Significance indications are  $p < 0.05$ , 0.01, 0.001, and 0.0001, respectively for 1, 2, 3, or 4 symbols; in (a), \*inhibition at pH 5 or change in amplitude at pH 6.6; †effect of compound different from GMQ effect; in (b), ‡difference between the  $I_{\text{cpd}}/I_{\text{ctrl}}$  ratio at pH 5 and pH 6.6 for a given compound ( $n = 3–10$ ).

pH 5-induced peak amplitude (“blocking effect”) by  $\sim 30\%$ . With compounds that induce an inhibition of the maximal current amplitude (filled bars in Figure 3a), an  $I_{\text{cpd}}/I_{\text{ctrl}}$  ratio at pH 6.6 (open bars) that is smaller than the corresponding ratio at pH 5 indicates an acidic shift of the pH dependence due to the tested compound, while an  $I_{\text{cpd}}/I_{\text{ctrl}}$  ratio at pH 6.6 higher than that at pH 5 indicates an alkaline shift. Based on these ratios at pH 5 and pH 6.6, and under the assumption that the compounds did not change the steepness of the pH–current relationship, we estimated the shift of  $\text{pH}_{50}$  ( $\Delta\text{pH}_{50}$ ) for the activation curve of each compound in comparison with the control condition (Figure 3b, ( $\Delta\text{pH}_{50} > 0$ : alkaline shift;  $\Delta\text{pH}_{50} < 0$ : acidic shift; see Methods). Figure 3b indicates thus the estimated shifts in pH dependence induced by the different compounds.

GMQ and its analogues, except for 4a,b, 6, and 7, produced  $I_{\text{cpd}}/I_{\text{ctrl}}$  ratios at pH 6.6 that were significantly different from the  $I_{\text{cpd}}/I_{\text{ctrl}}$  ratio measured at pH 5.0. Based on this comparison we can conclude that these compounds significantly shift the ASIC1a pH dependence. GMQ analogues from cluster #1 (yellow bars in Figure 3, bicycles 1, 2, 3a, 3b), as well as cluster #3 (red bars, 5-substituted pyridines 5a–e) have thus a qualitatively similar profile as GMQ, inducing an acidic shift of the  $\text{pH}_{50}$ . Of the 6- and 4-substituted pyridines from cluster #2 (green bars) and #4 (purple bar), respectively, only 4c induced a modest shift in  $\text{pH}_{50}$ , similarly as compounds from cluster #1 (1–3). The aminopyridine 8 (cluster #5) was the only compound to produce an alkaline shift in ASIC1a.

C

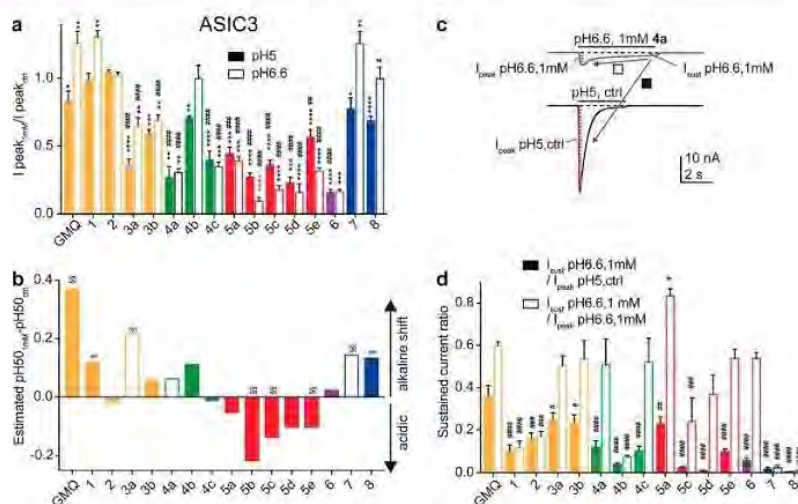


**Figure 4.** Functional analysis of GMQ derivatives on ASIC3. (a) Bar graph indicating the peak current amplitudes induced with pH 5 (filled bars) or pH 6.6 (open bars), in the presence of 1 mM test compound, normalized to the current amplitude measured at the same pH in the absence of the compound. (b) Shift of the pH dependence of activation by different compounds, estimated from comparison of the  $I_{\text{cpd}}/I_{\text{ctrl}}$  ratios at pH 6.6 and pH 5 (see Methods). The open bars represent values calculated in a different way (Methods). (c) Representative current traces of ASIC3 obtained either by pH 6.6 together with 1 mM of the compound 4a (top), or by a control application of pH 5.0 (bottom) from the same cell, to illustrate the two ways of  $I_{\text{sust}}$  normalization. The dotted red vertical lines represent the different amplitudes. The arrows indicate the ratio represented in (d) by the open bars ( $I_{\text{sust}} \text{ pH } 6.6, 1 \text{ mM} / I_{\text{peak}} \text{ pH } 6.6, 1 \text{ mM}$ ) and the filled bars ( $I_{\text{sust}} \text{ pH } 6.6, 1 \text{ mM} / I_{\text{peak}} \text{ pH } 5.0, \text{ ctrl}$ ). (d) Bar graph plotting the sustained current amplitude induced with 1 mM test compound at pH 6.6, normalized either to the peak current induced by pH 5 in absence of the compound (filled bars) or the pH 6.6-induced peak current in the presence of the compound (open bars; “shape”). Compounds 5b and 5d at 1 mM destabilized the recording when applied for >5 s. Therefore, the sustained current could not be measured in the presence of 5b and 5d. Significance indications are  $p < 0.05$ , 0.01, 0.001, and 0.0001, respectively for 1, 2, 3, or 4 symbols, in panel (a), \*inhibition at pH 5 or change in amplitude at pH 6.6; †effect of compound different from GMQ effect; in (b), ‡difference between the  $I_{\text{cpd}}/I_{\text{ctrl}}$  ratio at pH 5 and pH 6.6 for a given compound; in (d), ‡ $I_{\text{sust}}/I_{\text{peak}}$  ratio different from that of GMQ;  $n = 3-10$ .

**Blocking Effect of GMQ and Its Derivatives on ASIC3 at pH 5.** At pH 5 and a compound concentration of 1 mM, GMQ only slightly decreased the maximal peak current of ASIC3 ( $I_{\text{GMQ}}/I_{\text{ctrl}} = 0.83 \pm 0.07$ ,  $n = 8$ ; Figure 4a). Indeed, it had previously been shown that higher GMQ concentrations are needed to efficiently inhibit the pH 5-induced ASIC3 current ( $\text{IC}_{50} = 6.74 \pm 0.83 \text{ mM}$ ).<sup>25</sup> Compounds 1 and 2 showed no inhibitory activity at 1 mM ( $p > 0.05$ ), whereas both quinolines (3a and 3b) showed a significant blocking effect with  $I_{\text{cpd}}/I_{\text{ctrl}}$  ratios of  $0.37 \pm 0.03$  and  $0.59 \pm 0.03$ , respectively ( $p < 0.0001$  and  $< 0.001$ ,  $n = 4$ ). This result indicates that the substitution of the nitrogen atom at position 3 of GMQ alters the blocking effect on ASIC3, while the methyl group at position 4 has no influence. Interestingly, all the guanidinopyridines from clusters #2, #3, and #4, led to efficient inhibition of ASIC3 at 1 mM with  $I_{\text{cpd}}/I_{\text{ctrl}}$  ratios ranging from  $0.16 \pm 0.02$  (6,  $n = 5$ ) to  $0.44 \pm 0.05$  (5a,  $n = 5$ ). In contrast, the presence of a phenethyl group at position 5 led to less efficient pore block (5e vs 5d  $p < 0.05$ ). Finally, the compounds 7 and 8, lacking a guanidine moiety (cluster #5), showed only a modest blocking.

**Blocking Effects of GMQ Derivatives.** The inhibition experiments at pH 5 show that at 1 mM, GMQ and its derivatives belonging to cluster #1 were mostly poor inhibitors of both channels. The quinolines 3a and 3b showed stronger inhibition than GMQ on ASIC3, and 3a on ASIC1a, illustrating the contribution of the nitrogen atom at position 3. In addition, most of the guanidinopyridines (clusters #2–4) led to a substantial inhibition of both channels. Interestingly, this

inhibition seems to be independent of the position of the substituents on the pyridine ring, or of the  $\text{pK}_a$  of the molecules (Table S1). Finally, 2-aminopyridines (cluster #5) were poor inhibitors of both channels.

**Gating Effect of GMQ and Its Derivatives on ASIC3 at pH 6.6.** At pH 6.6 and a concentration of 1 mM, GMQ increased the ASIC3 current ( $I_{\text{GMQ}}/I_{\text{ctrl}} = 1.26 \pm 0.09$  at pH 6.6), consistent with a shift of the activation curve to a more alkaline value (Figure 4a). As for ASIC1a, an estimate of the shift in  $\text{pH}_{50}$  induced by each of these compounds, based on the peak current ratios at pH 5 and 6.6, is presented in Figure 4b ( $\Delta\text{pH}_{50} > 0$ : alkaline shift;  $\Delta\text{pH}_{50} < 0$ : acidic shift). Bicyclic analogues from cluster #1, except quinoxaline 2, tend to shift the  $\text{pH}_{50}$  to alkaline values on ASIC3, in an opposite manner to their shifts on ASIC1a. All 5-substituted guanidinopyridines (5a–e) showed a tendency of, or a significant acidic  $\text{pH}_{50}$  shift (5b, 5c, 5e), with  $\Delta\text{pH}_{50}$  values ranging from  $-0.05$  to  $-0.22$ . In contrast to compounds of cluster #1, compounds of cluster #3 induced an acidic  $\text{pH}_{50}$  shift (or a tendency of) in both channels. Finally, both 2-aminopyridines (7 and 8) induced an alkaline  $\text{pH}_{50}$  shift.

**Gating Effects of GMQ Derivatives.** Whereas the position of the substitution on the pyridine ring was not crucial for the inhibitory effect at pH 5, it was clearly important for the shift in pH dependence. Depending on the position of the aryl group on the pyridine ring, we observed no shift (clusters #2 and #4), an alkaline shift in ASIC3 and an acidic shift in ASIC1a (cluster #1), or a shift to more acidic values in both ASIC subtypes (cluster #3). This dependence of the gating effect on the

position of the aryl group suggests that the position of the aromatic group on the guanidinopyridine may be critical for the interaction with the modulatory GMQ binding site. Finally, the 2-aminopyridine **8** was the only tested compound to induce an alkaline shift in ASIC1a.

**Do GMQ Derivatives Induce a Sustained ASIC3 Current?** GMQ is known to generate a sustained current in ASIC3 with maximal amplitudes in the pH range 6.5–7.<sup>35</sup> We evaluated the capability of GMQ derivatives to generate a similar effect. The sustained current amplitude, measured at pH 6.6 in the presence of 1 mM of the compound, was normalized in two ways (Figure 4c). First, this sustained current was normalized to the maximal acid-induced current in the absence of the compound, as  $I_{\text{sust}}(\text{pH}6.6, \text{cpd})/I_{\text{peak}}(\text{pH}5, \text{ctrl})$  ratio (Figure 4d, filled bars). As an indication of the shape of the current, the  $I_{\text{sust}}(\text{pH}6.6, \text{cpd})/I_{\text{peak}}(\text{pH}6.6, \text{cpd})$  ratio, which compares the amplitude of the sustained current with the amplitude of the peak current induced by the test compound at pH 6.6, is provided as open bars in Figure 4d. For GMQ, these two ratios were similar ( $0.36 \pm 0.05$  vs  $0.60 \pm 0.02$ ), since the pH 6.6-induced peak amplitude in the presence of 1 mM GMQ is only slightly smaller than the pH 5-induced peak current amplitude under control conditions. In the absence of any compound, no sustained current was measured at pH 6.6, and both ratios were  $0.01 \pm 0.01$  ( $n = 16$ ). In most derivatives tested, the shape of the current was conserved with regard to GMQ, as indicated by similar  $I_{\text{sust}}(\text{pH}6.6, \text{cpd})/I_{\text{peak}}(\text{pH}6.6, \text{cpd})$  ratios (open bars). Only the 2-aminopyridines **7** and **8** from cluster #5 did not induce any sustained current. The  $I_{\text{sust}}(\text{pH}6.6, \text{cpd})/I_{\text{peak}}(\text{pH}5, \text{ctrl})$  ratios (filled bars in Figure 4d) were however considerably smaller than what had been observed with GMQ. The difference in the two ratios is essentially due to the strong current block observed with most GMQ derivatives other than guanidino-quinazolines (Figure 4a). A substantial  $I_{\text{sust}}(\text{pH}6.6, \text{cpd})/I_{\text{peak}}(\text{pH}5, \text{ctrl})$  ratio was only observed with the monocycle 2-guanidino-5-phenylpyridine **5a** and with some compounds of cluster #1. Together, this suggests that the mechanism underlying the formation of this sustained current is very sensitive to the chemical structure of the modulator, and is also affected by the inherent inhibitory effect of the modulator. In the presence of GMQ, the activation and SSD curves of ASIC3 cross each other at a pH of ~6.8–7.0. The pH dependence of the sustained ASIC3 current amplitude under these conditions forms a bell-shaped curve that has its maximum at the crossing of these two curves, consistent with it being a window current.<sup>25,29</sup> Analysis of the amplitude of the sustained ASIC3 current in the presence of selected GMQ derivatives at several pH conditions shows maximal sustained current amplitudes at pH 7 or 6.6 (Figure S1), further supporting that these compounds also induce a window current in ASIC3, as does GMQ. There was no indication of sustained ASIC1a currents in the presence of GMQ derivatives, in agreement with previous observations with GMQ.<sup>25,29</sup>

**Concentration Dependence of ASIC Current Inhibition at pH 5 by GMQ Derivatives.** All experiments described above were carried out at two compound concentrations, 1 and 0.3 mM, as documented for the pH 5-induced current in Table S2. Comparison of the effects at the two concentrations suggested an increased potency relative to GMQ of some of the test compounds. To confirm the predicted change in  $IC_{50}$  of current inhibition at pH 5 of some of the GMQ derivatives, inhibition curves were recorded for the 5-phenylpyridine **5a** and its two derivatives **5b** and **5c**, on ASIC1a and ASIC3 (Figure 5). This showed that in both

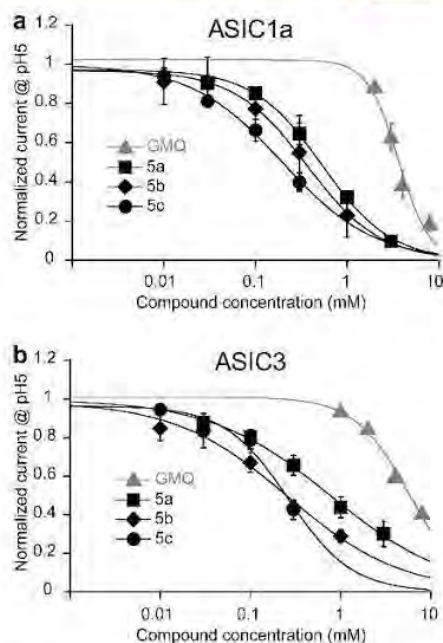


**Figure 5.** Inhibition curves by selected compounds. The indicated compounds were included at different concentrations in the stimulation solution of pH 5. Current amplitudes measured with compound were normalized to the amplitude obtained in the absence of the modulator. Data are from three to six experiments per compound, shown for ASIC1a (a) and ASIC3 (b). Inhibition curves were fitted to a Hill equation, and  $IC_{50}$  values are presented in the text.

ASIC1a and ASIC3, these three compounds inhibit currents at lower concentrations than does GMQ.  $IC_{50}$  values were  $3.3 \pm 0.8$  mM (ASIC1a) and  $7.4 \pm 1.1$  mM (ASIC3) for GMQ,  $0.53 \pm 0.07$  and  $0.58 \pm 0.11$  mM for **5a**,  $0.47 \pm 0.28$  and  $0.23 \pm 0.08$  mM for **5b**, and  $0.19 \pm 0.01$  and  $0.27 \pm 0.04$  mM for **5c** ( $n = 3–6$ ). This up to 20-fold increase in potency relative to GMQ was significant for **5c** in ASIC1a, and for **5b** and **5c** in ASIC3 ( $p < 0.01$ ).

**Modulation of Heteromeric ASIC Currents by GMQ Derivatives.** In the central nervous system, functional ASICs are mostly ASIC1a homomers, ASIC1a/2a heteromers and ASIC1a/2b heteromers, while in the peripheral nervous system most functional ASICs are heteromers of various compositions.<sup>1,7,33</sup> To expand our analysis, we determined the effect of selected compounds at a concentration of 1 mM on two different ASIC heteromers, ASIC1a/2a, representative of a central nervous system ASIC, and ASIC2a/3, representative of a peripheral nervous system ASIC. Heteromeric ASICs adapt a flexible stoichiometry that depends on the subunit availability, as shown for ASIC1a/2a.<sup>5</sup> The inclusion of ASIC2a subunits shifts the  $pH_{50}$  to more acidic values, in the range of pH 5.5 to pH 6 for both ASIC1a/2a and ASIC2a/3.<sup>34,35</sup> Measurements addressing the shift in pH dependence (“gating effect”) were therefore carried out at pH 5.8, while testing for effects on the maximal current amplitude (“blocking effect”) was done at pH 4. An  $I_{p15.8}/I_{p14.0}$  ratio close to ~0.5 served as an indication that the investigated currents were indeed mediated by heteromeric channels (Table S3). In ASIC1a/2a, only about half of the tested compounds induced amplitude changes that were significantly different between pH 5.8 and pH 4 and

indicated thus a shift of the pH dependence (Figure 6a). With GMQ, 4a and 6, the  $I_{cpd}/I_{ctrl}$  ratio was greater at pH 5.8 than at

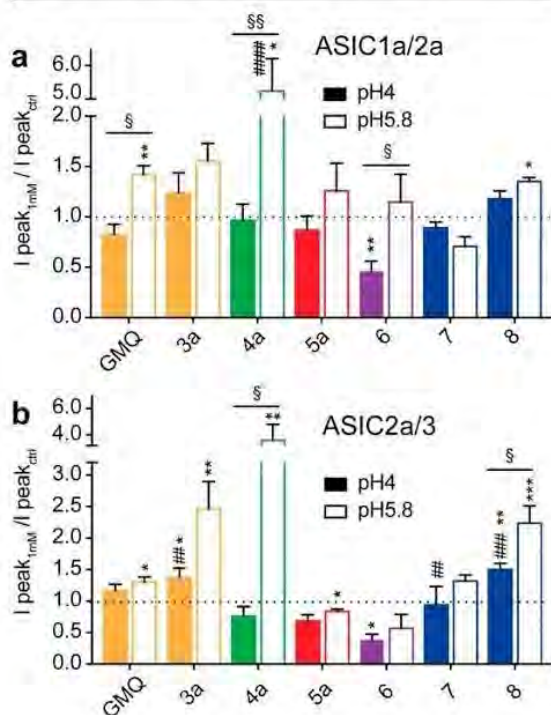


**Figure 6.** Functional analysis of GMQ derivatives on ASIC1a/2a and ASIC2a/3. (a, b) Bar graphs indicating the peak current amplitudes induced with pH4 (filled bars) or pH 5.8 (open bars), in the presence of 1 mM test compound, normalized to the current amplitude measured at the same pH in the absence of the compound, for ASIC1a/2a heteromers (a) and ASIC2a/3 heteromers (b). Significance indications are  $p < 0.05$ , 0.01, 0.001, and 0.0001, respectively for 1, 2, 3, or 4 symbols; \*change in amplitude by the compound at pH4 or 5.8; #effect of compound different from GMQ effect; §difference between the  $I_{cpd}/I_{ctrl}$  ratio at pH 4 and pH 5.8 for a given compound ( $n = 3-7$ ).

pH 4, indicating therefore an alkaline shift of the pH dependence of activation, opposed to what we had observed with ASIC1a homomers. The absence of shifts in pH dependence by many, and the predicted alkaline shift by GMQ, 4a and 6 in the ASIC1a/2a heteromers may be explained by the previously documented opposite GMQ-induced shifts of the activation pH dependence in ASIC1a and ASIC2a.<sup>25</sup> In ASIC2a/3 heteromers, several compounds showed a tendency of increased  $I_{cpd}/I_{ctrl}$  ratios at pH 5.8 over pH 4. These differences were however only significant for 4a and 8 (Figure 6b). We observed a high cell-to-cell variability of the  $I_{cpd}/I_{ctrl}$  and also a variability of the  $I_{pH\ 5.8}/I_{pH\ 4}$  ratio in the absence of any compound, which indicates differences of the ASIC2a:ASIC3 ratio of these heteromers. Interestingly, the potentiation of the pH 5.8-induced current by compounds 3a and 4a was greater in cells with a low  $I_{pH\ 5.8}/I_{pH\ 4}$  ratio, thus in cells with an important contribution of ASIC2a (Figure S2).

Only few compounds affected the  $I_{pH\ 4}$  amplitude in the heteromers, suggesting that the inclusion of ASIC2a may distort the GMQ binding site for blocking. Taken together,

heteromers with ASIC2a are generally less modulated by GMQ and its derivatives than the ASIC1a and ASIC3 homomers. Some compounds however exert strong effects on the heteromers. No acidic shifts in pH dependence were induced in the heteromers, showing that the response of heteromers to GMQ and its derivatives is closer to that of ASIC3 than ASIC1a.

**Potentiation of ASIC1a and ASIC Heteromer Currents by GMQ Derivatives at Low Concentrations.** Whereas most of the tested GMQ derivatives led to an inhibition of both ASIC1a and ASIC3 pH 5-induced currents at sub-millimolar concentrations, we observed that, at a lower concentration ( $<100\ \mu\text{M}$ ), compounds of several clusters induced an unexpected potentiation of the pH 6.6-induced ASIC1a current (Figure 7). The quinazoline GMQ did not potentiate ASIC1a

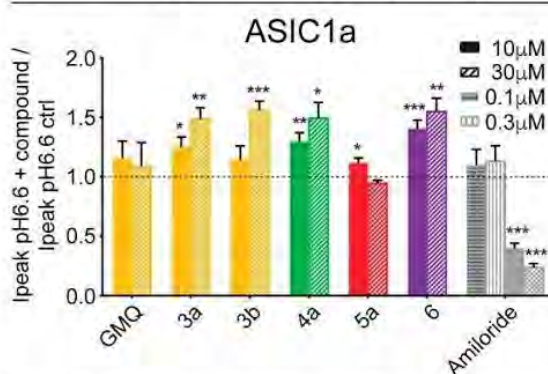


**Figure 7.** Potentiation of ASIC1a currents by selected GMQ derivatives. ASIC1a currents were induced by pH 6.6 with or without test compound. The indicated concentrations of the test compounds were included in the pH 6.6 solution. The current amplitude obtained in the presence of a test compound was normalized to the amplitude obtained in its absence. Data were obtained from three to seven cells per condition \* $p < 0.05$ , \*\* $p < 0.01$ , \*\*\* $p < 0.001$  between test and control condition, paired  $t$  test.

currents, whereas its quinoline analogues 3a and 3b showed a significant potentiation (of ~50%) of the current at 30  $\mu\text{M}$ . This potentiation effect was even observed at 10  $\mu\text{M}$  with the 4- and 6-phenylpyridines 6 and 4a, whereas the 5-phenylpyridine 5a induced only a very small potentiation at 10  $\mu\text{M}$  and none at 30  $\mu\text{M}$ . The ASIC inhibitor amiloride did not induce any potentiation at 10 and 30  $\mu\text{M}$ . A possible potentiation by amiloride might be hidden by its substantial pore block at this concentration.<sup>15,19</sup> At lower concentrations that do not inhibit ASIC1a, amiloride had however no effect on ASIC1a currents (Figure 7). No such effect was observed with any of the tested compounds at 10–30  $\mu\text{M}$  on ASIC3 (Figure S3a) or ASIC1a/2a (at pH 5.8, Figure S3b). In ASIC2a/3, GMQ induced at these concentrations a small inhibition, and 5a induced a strong potentiation (Figure S3c). A further analysis of the potentiation effects on ASIC1a was then carried out with compound 6. The  $EC_{50}$  for increasing the current amplitude was  $9.4 \pm 5.4\ \mu\text{M}$  (error of the fit,  $n = 3-8$ ), while the  $IC_{50}$  of inhibition was  $93.4 \pm 0.4\ \mu\text{M}$  ( $n = 4$ , Figure 8a). To test whether the current increase was due to a change in pH dependence, we measured the pH dependence of activation and of SSD of ASIC1a and ASIC3 in the absence and the presence of 30  $\mu\text{M}$  6. Compound 6 did not affect the  $pH_{50}$  values of activation or desensitization,

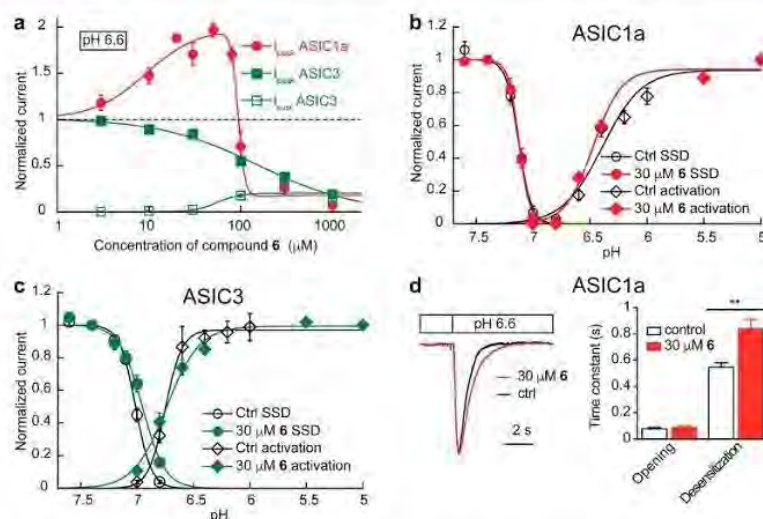


**Figure 8.** Analysis of ASIC1a current potentiation by compound 6. (a) ASIC currents were induced by acidification to pH 6.6 either under control conditions, or with increasing concentrations of compound 6 included in the pH 6.6 solution and were normalized to the pH 6.6-induced peak current amplitude in the absence of the compound. The concentration-dependent inhibition of ASIC3 currents (green, solid squares), the appearance of a sustained ASIC3 current (open green squares), and the biphasic effect on ASIC1a (red circles) are shown. The data were fitted to Hill equations; for ASIC1a, a combined equation was used. Fit parameters for ASIC1a are presented in the text. ASIC3 peak current inhibition  $IC_{50} = 153.7 \pm 20.4 \mu\text{M}$ ,  $n = 3-6$ ; ASIC3 sustained current  $EC_{50} = 55.2 \pm 29.5 \mu\text{M}$ ,  $n = 3-6$ . (b, c) Activation and steady-state desensitization curves obtained under control conditions (open symbols) and in the presence of  $30 \mu\text{M}$  compound 6 (filled, colored symbols), for ASIC1a (b) and ASIC3 (c). The fit parameters are shown in Table S4. (d) Left, representative current traces of ASIC1a induced by pH 6.6 in the absence or presence of  $30 \mu\text{M}$  6. The traces were normalized to allow comparison of the kinetics. Right, time constants of opening and desensitization (current decay) of pH 6.6-induced current in the absence (open bars) or presence (red) of  $30 \mu\text{M}$  6,  $n = 8$ .  $**p < 0.01$ .

it changed however the steepness of the pH dependence curves, rendering the ASIC1a activation curve steeper, and both curves of ASIC3 less steep (Figure 8b,c, Table S4). These changes can only partially explain the observed current increase in ASIC1a. We observed however also a slowing of the desensitization time course of ASIC1a (Figure 8d). This indicates that the transition into the desensitized state is slowed in the presence of  $30 \mu\text{M}$  compound 6, which will increase the current amplitude, and will contribute to the ASIC1a current potentiation. The kinetics of current appearance showed no apparent change in the presence of compound 6 (Figure 8d). In our whole-cell experiments, the kinetics of current appearance are however limited by the speed of perfusion change (Methods), which is slower than channel opening,<sup>36</sup> and we can therefore not draw conclusions about the opening kinetics.

Potentiating ASIC currents may be of interest in some instances, for example for increasing synaptic transmission or the induction of LTP.<sup>7</sup> For such applications, GMQ derivatives with only a small blocking effect, such as those of cluster #2, would be more suitable than compound 6.

The biphasic effect of GMQ on ASIC3,<sup>24,25</sup> and of these compounds on ASIC1a currents likely reflects binding to at least two binding sites, a modulatory and an inhibitory site, with different affinities, as previously suggested.<sup>25,37</sup> We have shown that the inhibition of ASIC1a and ASIC3 currents at pH 5 by GMQ was due to a pore block, since it decreased unitary current amplitudes and was affected by a mutation in the pore.<sup>25</sup> Based on molecular docking, site-directed mutagenesis and the measurement of GMQ-induced current at pH7.4, a detailed description of a GMQ binding site in the palm domain of ASIC3 has been provided,<sup>38</sup> which is therefore a strong

candidate for the "gating" binding site. A later analysis showed however that mutation of some residues suggested to be central for GMQ binding in the palm suppressed the GMQ-induced shift of the pH dependence of SSD, but not that of activation.<sup>25</sup> This suggested that either the individual mutations of palm residues cannot sufficiently disrupt GMQ binding, or that these mutations do not affect the GMQ binding itself, but rather the consequences of binding. The low apparent affinity of GMQ precludes a more precise analysis of its binding site. The GMQ derivatives with higher affinity than GMQ will allow studies that aim at identifying the precise GMQ binding site(s). This will help elucidate the activation mechanism of ASICs, and the development of more potent and specific ASIC modulators.

## METHODS

**Recombinant Expression of ASICs in Chinese Hamster Ovary (CHO) Cells.** CHO cell lines stably expressing human ASIC1a or rat ASIC3 had been established as indicated elsewhere,<sup>39</sup> based on the human ASIC1a clone of the Corey laboratory,<sup>32</sup> and the rat ASIC3 clone of the Lazdunski laboratory.<sup>40</sup> Heteromeric ASICs were expressed by transient cotransfection of the above-mentioned ASIC1a and ASIC3 cDNAs together with ASIC2a cDNA. The protein sequence of the human ASIC2a clone used here<sup>32</sup> is 99% identical with the rat ASIC2a clone. Transfections were carried out with ASIC clones in the peak8 expression vector (Edge Biosystems, Gaithersburg, MD), together with a green fluorescent protein construct, by using Roti-Fect (Carl Roth, Karlsruhe, Germany). The cDNA ratios for the transfections was 1:1 for ASIC1a/ASIC2a heteromers and 2:1 for ASIC2a/ASIC3 heteromers. The measured  $I_{pH5.8}/I_{pH4}$  ratios confirmed that the expressed channels were heteromeric (Table S3).

**Electrophysiology.** Electrophysiological measurements were carried out in the whole-cell patch-clamp mode at  $-60$  mV with an EPC9 or EPC10 amplifier (HEKA Electronics, Lambrecht, Germany)

and data acquisition was done with the Patchmaster software. Data were acquired at a sampling rate of 1 ms and filtered at 3 kHz. Pipettes were pulled from borosilicate glass (World Precision Instruments, Stevenage, UK). They had resistances of 2–5 M $\Omega$  when filled with the pipet solution. Series resistance compensation was set to 70–95%. The extracellular recording solution contained, in mM, NaCl 140, KCl 4, CaCl<sub>2</sub> 2, MgCl<sub>2</sub> 1, 4-morpholineethanesulfonic acid (MES) 10, HEPES 10, Glucose 10. The pH was adjusted to the desired value with NaOH. Conditioning solution (applied between acidifications) had a pH of 7.4. Fast solution changes were carried out with a MPRE8 perfusion head (Cell Micro-Controls, Norfolk, VA) and computer-controlled electrovalves from either Cell Micro-Controls or Biologic (Claix, France). The speed of the perfusion change at the cells was determined on the sustained component of the ASIC3 current at pH 7.0 by measuring the kinetics of the change in current amplitude when the perfusion solution was changed between the standard extracellular solution containing 140 mM Na<sup>+</sup> and a solution in which the Na<sup>+</sup> was replaced by the larger, ASIC-impermeable cation NMDG<sup>+</sup>. The (10% to 90%) rise time of the solution change was 210  $\pm$  20 ms,  $n$  = 6. The pipet solution contained, in mM, K-gluconate 90, KCl 10, NaCl 10, MgCl<sub>2</sub> 1, HEPES 60, EGTA 10, and its pH was adjusted to 7.3 with KOH. Data were analyzed with Fitmaster (HEKA). The compounds were included in the acidic extracellular solution (pH 6.6 and pH 5), and the pH of the solution was verified after addition of the compound, and adjusted if necessary.

**Analysis and Statistics.** Normalized activation curves (pH dependence of peak current amplitudes) were fitted to the Hill equation  $I = I_{max}/(1 + (10^{-pH_{50}}/10^{-pH})^{nH})$ , where  $I_{max}$  is the maximal current amplitude,  $pH_{50}$  is the value at which the current amplitude is half-maximal, and  $nH$  is the Hill coefficient. SSD curves were fitted to an analogous equation to obtain the  $pHD_{50}$  values. Data are presented as mean  $\pm$  SEM. To determine significance of differences in multiple comparisons we used two-way ANOVA followed by posthoc Tukey test. To determine whether the amplitude change by a given compound was significant, we used a paired  $t$  test (Graphpad Prism 7 and Microsoft Excel).

To estimate  $pH_{50}$  shifts from current ratios at pH 6.6, currents were expressed as a function of  $pH_{50}$  and  $nH$  by using the Hill equation, using  $nH$  values for the control situation previously measured in control conditions for each of the two subtypes, and the  $pH_{50}$  calculated for each condition from the measured current amplitudes induced by pH 6.6 and 5.0 in the absence of compound. The ratio  $I_{(compound,pH6.6)}/I_{(control,pH6.6)}$  was then calculated based on these equations, and  $pH_{50}(compound)$  was adjusted, while keeping  $nH$  unchanged, until the calculated  $I_{(compound,pH6.6)}/I_{(control,pH6.6)}$  ratio matched the experimental value of a given compound and ASIC subtype. The shift in  $pH_{50}$  was then calculated as  $pH_{50}(compound) - pH_{50}(control)$ . In three cases with ASIC3 (marked as open bars in Figure 4b), the measured  $I_{(compound,pH6.6)}/I_{(control,pH6.6)}$  ratio was greater than the theoretically possible value, most likely because the compound also induced a change in the Hill coefficient. For these cases, we plot in Figure 4b the  $\Delta pH_{50}$  corresponding to 95% of the maximal theoretical  $I_{(compound,pH6.6)}/I_{(control,pH6.6)}$  ratio.

**Substances.** The compounds were synthesized as described in the Supporting Information. GMQ was purchased from Sigma. Stock solutions of compounds were made in DMSO at 100 mM. Final concentrations of DMSO were maximally 1%.

## ■ ASSOCIATED CONTENT

### ● Supporting Information

The Supporting Information is available free of charge on the ACS Publications website at DOI: 10.1021/acschemneuro.7b00529.

Sustained current amplitudes of ASIC3 at various pH values, correlation of compound effects with relative subunit expression, and current ratios in cells expressing ASIC3 or heteromeric ASICs;  $pK_a$  values of compounds,

current ratios, and pH dependence parameters; methods describing in detail the compound synthesis (PDF)

## ■ AUTHOR INFORMATION

### Corresponding Authors

\*Concerning functional evaluation and ASICs. Mailing address: Department of Pharmacology and Toxicology, Rue du Bugnon 27, University of Lausanne, CH-1011 Lausanne, Switzerland. Phone ++4121 6925422. E-mail: stephan.kellenberger@unil.ch

\*Concerning medicinal chemistry. Mailing address: Faculty of Pharmacy, 74 Route du Rhin CS60024, University of Strasbourg, F-67401 Illkirch Cedex, France. Phone ++33 368854130. E-mail: fbihel@unistra.fr.

### ORCID

Frédéric Bihel: 0000-0002-4122-0929

Stephan Kellenberger: 0000-0003-1755-6198

### Author Contributions

O.A., V.T., and A.V. performed electrophysiological experiments and data analysis; H.H., M.B., and M.S. synthesized of the compounds; O.A., F.B., and S.K. designed the project, analyzed the data, prepared the figures, and wrote the manuscript.

### Funding

This work is supported by the Swiss National Science Foundation Grant 31003A\_172968 to S.K.

### Notes

The authors declare no competing financial interest.

## ■ ACKNOWLEDGMENTS

The authors thank Laurent Schild, Sabrina Vullo, Miguel van Bemmelen and Zhong Peng for their comments on a previous version of the manuscript, and for many discussions.

## ■ ABBREVIATIONS

ASIC, acid-sensing ion channel; CHO, Chinese hamster ovary; ENaC, epithelial Na<sup>+</sup> channel; GMQ, 2-guanidine-4-methylquinazoline;  $I_{cpd}$ , pH-induced current obtained in the presence of a compound;  $I_{ctrl}$ , pH-induced current obtained under control conditions;  $I_{GMQ}$ , pH-induced current in the presence of GMQ;  $I_{peak}$ , peak current;  $I_{ssst}$ , sustained current;  $nH$ , Hill coefficient;  $pH_{50}$ , pH of half-maximal activation;  $pHD_{50}$ , pH of half-maximal steady-state desensitization; SSD, steady-state desensitization.

## ■ REFERENCES

- (1) Kellenberger, S., and Schild, L. (2015) International Union of Basic and Clinical Pharmacology. XCL. Structure, Function, and Pharmacology of Acid-Sensing Ion Channels and the Epithelial Na<sup>+</sup> Channel. *Pharmacol. Rev.* 67, 1–35.
- (2) Yang, L., and Palmer, L. G. (2014) Ion conduction and selectivity in acid-sensing ion channel 1. *J. Gen. Physiol.* 144, 245–255.
- (3) Deval, E., Noel, J., Lay, N., Alloui, A., Diochot, S., Friend, V., Jodar, M., Lazdunski, M., and Lingueglia, E. (2008) ASIC3, a sensor of acidic and primary inflammatory pain. *EMBO J.* 27, 3047–3055.
- (4) Vukicevic, M., and Kellenberger, S. (2004) Modulatory effects of acid-sensing ion channels on action potential generation in hippocampal neurons. *Am. J. Physiol. Cell Physiol.* 287, C682–690.
- (5) Bartoi, T., Augustinowski, K., Pollechtner, G., Grunder, S., and Ulbrich, M. H. (2014) Acid-sensing ion channel (ASIC) 1a/2a heteromers have a flexible 2:1/1:2 stoichiometry. *Proc. Natl. Acad. Sci. U. S. A.* 111, 8281–8286.
- (6) Baconguis, L., Bohlen, C. J., Goehring, A., Julius, D., and Gouaux, E. (2014) X-ray structure of Acid-sensing ion channel 1-snake toxin

- complex reveals open state of a Na<sup>+</sup>-selective channel. *Cell* 156, 717–729.
- (7) Wemmie, J. A., Taugher, R. J., and Kreple, C. J. (2013) Acid-sensing ion channels in pain and disease. *Nat. Rev. Neurosci.* 14, 461–471.
- (8) Xiong, Z. G., Zhu, X. M., Chu, X. P., Minami, M., Hey, J., Wei, W. L., MacDonald, J. F., Wemmie, J. A., Price, M. P., Welsh, M. J., and Simon, R. P. (2004) Neuroprotection in ischemia: Blocking calcium-permeable acid-sensing ion channels. *Cell* 118, 687–698.
- (9) Kreple, C. J., Lu, Y., Taugher, R. J., Schwager-Gutman, A. L., Du, J., Stump, M., Wang, Y., Ghobbeh, A., Fan, R., Cosme, C. V., Sowers, L. P., Welsh, M. J., Radley, J. J., LaLumiere, R. T., and Wemmie, J. A. (2014) Acid-sensing ion channels contribute to synaptic transmission and inhibit cocaine-evoked plasticity. *Nat. Neurosci.* 17, 1083–1091.
- (10) Du, J., Reznikov, L. R., Price, M. P., Zha, X. M., Lu, Y., Moninger, T. O., Wemmie, J. A., and Welsh, M. J. (2014) Protons are a neurotransmitter that regulates synaptic plasticity in the lateral amygdala. *Proc. Natl. Acad. Sci. U. S. A.* 111, 8961–8966.
- (11) Ziemann, A. E., Allen, J. E., Dahdaleh, N. S., Drebot, II, Coryell, M. W., Wunsch, A. M., Lynch, C. M., Faraci, F. M., Howard, M. A., 3rd, Welsh, M. J., and Wemmie, J. A. (2009) The amygdala is a chemosensor that detects carbon dioxide and acidosis to elicit fear behavior. *Cell* 139, 1012–1021.
- (12) Chen, C. C., and Wong, C. W. (2013) Neurosensory mechanotransduction through acid-sensing ion channels. *Journal of cellular and molecular medicine* 17, 337–349.
- (13) Omerbasic, D., Schuhmacher, L. N., Bernal Sierra, Y. A., Smith, E. S., and Lewin, G. R. (2015) ASICs and mammalian mechanoreceptor function. *Neuropharmacology* 94, 80–86.
- (14) Liu, M. G., Li, H. S., Li, W. G., Wu, Y. J., Deng, S. N., Huang, C., Maximyuk, O., Sukach, V., Krystal, O., Zhu, M. X., and Xu, T. L. (2016) Acid-sensing ion channel 1a contributes to hippocampal LTP inducibility through multiple mechanisms. *Sci. Rep.* 6, 23350.
- (15) Schild, L., Schneeberger, E., Gautschi, L., and Firsov, D. (1997) Identification of amino acid residues in the alpha, beta, and gamma subunits of the epithelial sodium channel (ENaC) involved in amiloride block and ion permeation. *J. Gen. Physiol.* 109, 15–26.
- (16) Kellenberger, S., Gautschi, L., and Schild, L. (2003) Mutations in the epithelial Na<sup>+</sup> channel ENaC outer pore disrupt amiloride block by increasing its dissociation rate. *Mol. Pharmacol.* 64, 848–856.
- (17) Kleyman, T. R., and Cragoe, E. J. (1988) Amiloride and Its Analogs as Tools in the Study of Ion-Transport. *J. Membr. Biol.* 105, 1–21.
- (18) Baron, A., and Lingueglia, E. (2015) Pharmacology of acid-sensing ion channels - Physiological and therapeutic perspectives. *Neuropharmacology* 94, 19–35.
- (19) Schmidt, A., Rossetti, G., Jousen, S., and Grunder, S. (2017) Diminazene Is a Slow Pore Blocker of Acid-Sensing Ion Channel 1a (ASIC1a). *Mol. Pharmacol.* 92, 665.
- (20) Chen, X., Qiu, L., Li, M., Durnagel, S., Orser, B. A., Xiong, Z. G., and MacDonald, J. F. (2010) Diarylamidines: high potency inhibitors of acid-sensing ion channels. *Neuropharmacology* 58, 1045–1053.
- (21) Rash, L. D. (2017) Acid-Sensing Ion Channel Pharmacology, Past, Present, and Future. *Adv. Pharmacol.* 79, 35–66.
- (22) Lee, J. Y. P., Saez, N. J., Cristofori-Armstrong, B., Anangi, R., King, G. F., Smith, M. T., and Rash, L. D. (2017) Inhibition of acid-sensing ion channels by diminazene and APETx2 evoke partial and highly variable antihyperalgesia in a rat model of inflammatory pain. *Br. J. Pharmacol.*
- (23) Baron, A., Diochot, S., Salinas, M., Deval, E., Noel, J., and Lingueglia, E. (2013) Venom toxins in the exploration of molecular, physiological and pathophysiological functions of acid-sensing ion channels. *Toxicon* 75, 187–204.
- (24) Yu, Y., Chen, Z., Li, W. G., Cao, H., Feng, E. G., Yu, F., Liu, H., Jiang, H., and Xu, T. L. (2010) A nonproton ligand sensor in the acid-sensing ion channel. *Neuron* 68, 61–72.
- (25) Aljjevic, O., and Kellenberger, S. (2012) Subtype-specific modulation of acid-sensing ion channel (ASIC) function by 2-guanidine-4-methylquinazoline. *J. Biol. Chem.* 287, 36059–36070.
- (26) Yang, X. N., Niu, Y. Y., Liu, Y., Yang, Y., Wang, J., Cheng, X. Y., Liang, H., Wang, H. S., Hu, Y. M., Lu, X. Y., Zhu, M. X., Xu, T. L., Tian, Y., and Yu, Y. (2017) The nonproton ligand of acid-sensing ion channel 3 activates mollusk-specific FaNaC channels via a mechanism independent of the native FMRFamide peptide. *J. Biol. Chem.* 292, 21662–21675.
- (27) Li, W. G., Yu, Y., Zhang, Z. D., Cao, H., and Xu, T. L. (2010) ASIC3 channels integrate arginine and multiple inflammatory signals through the nonproton ligand sensing domain. *Mol. Pain* 6, 1744–8069-6-88.
- (28) Li, W. G., Yu, Y., Huang, C., Cao, H., and Xu, T. L. (2011) The nonproton ligand sensing domain is required for paradoxical stimulation of ASIC3 channels by amiloride. *J. Biol. Chem.* 286, 42635–42646.
- (29) Besson, T., Lingueglia, E., and Salinas, M. (2017) Pharmacological modulation of Acid-Sensing Ion Channels 1a and 3 by amiloride and 2-guanidine-4-methylquinazoline (GMQ). *Neuropharmacology* 125, 429–440.
- (30) Waldmann, R., Bassilana, F., Deweille, J., Champigny, G., Heurteaux, C., and Lazdunski, M. (1997) Molecular cloning of a non-inactivating proton-gated Na<sup>+</sup> channel specific for sensory neurons. *J. Biol. Chem.* 272, 20975–20978.
- (31) Waldmann, R., Champigny, G., Bassilana, F., Heurteaux, C., and Lazdunski, M. (1997) A proton-gated cation channel involved in acid-sensing. *Nature* 386, 173–177.
- (32) Garcia-Anoveros, J., Derfler, B., Nevillegolden, J., Hyman, B. T., and Corey, D. P. (1997) BNaC1 and BNaC2 constitute a new family of human neuronal sodium channels related to degenerins and epithelial sodium channels. *Proc. Natl. Acad. Sci. U. S. A.* 94, 1459–1464.
- (33) Benson, C. J., Xie, J. H., Wemmie, J. A., Price, M. P., Henss, J. M., Welsh, M. J., and Snyder, P. M. (2002) Heteromultimers of DEG/ENaC subunits form H<sup>+</sup>-gated channels in mouse sensory neurons. *Proc. Natl. Acad. Sci. U. S. A.* 99, 2338–2343.
- (34) Hesselager, M., Timmermann, D. B., and Ahring, P. K. (2004) pH dependency and desensitization kinetics of heterologously expressed combinations of acid-sensing ion channel subunits. *J. Biol. Chem.* 279, 11006–11015.
- (35) Joeres, N., Augustinowski, K., Neuhofer, A., Assmann, M., and Grunder, S. (2016) Functional and pharmacological characterization of two different ASIC1a/2a heteromers reveals their sensitivity to the spider toxin PcTx1. *Sci. Rep.* 6, 27647.
- (36) Bassler, E. L., Ngo-Anh, T. J., Geisler, H. S., Ruppertsberg, J. P., and Grunder, S. (2001) Molecular and functional characterization of acid-sensing ion channel (ASIC) 1b. *J. Biol. Chem.* 276, 33782–33787.
- (37) Smith, R. N., and Gonzales, E. B. (2014) Protons and Psalmotoxin-1 reveal nonproton ligand stimulatory sites in chicken acid-sensing ion channel: Implication for simultaneous modulation in ASICs. *Channels* 8, 49–61.
- (38) Yu, Y., Li, W. G., Chen, Z., Cao, H., Yang, H., Jiang, H., and Xu, T. L. (2011) Atomic level characterization of the nonproton ligand-sensing domain of ASIC3 channels. *J. Biol. Chem.* 286, 24996–25006.
- (39) Poirot, O., Berta, T., Decosterd, I., and Kellenberger, S. (2006) Distinct ASIC currents are expressed in rat putative nociceptors and are modulated by nerve injury. *J. Physiol.* 576, 215–234.

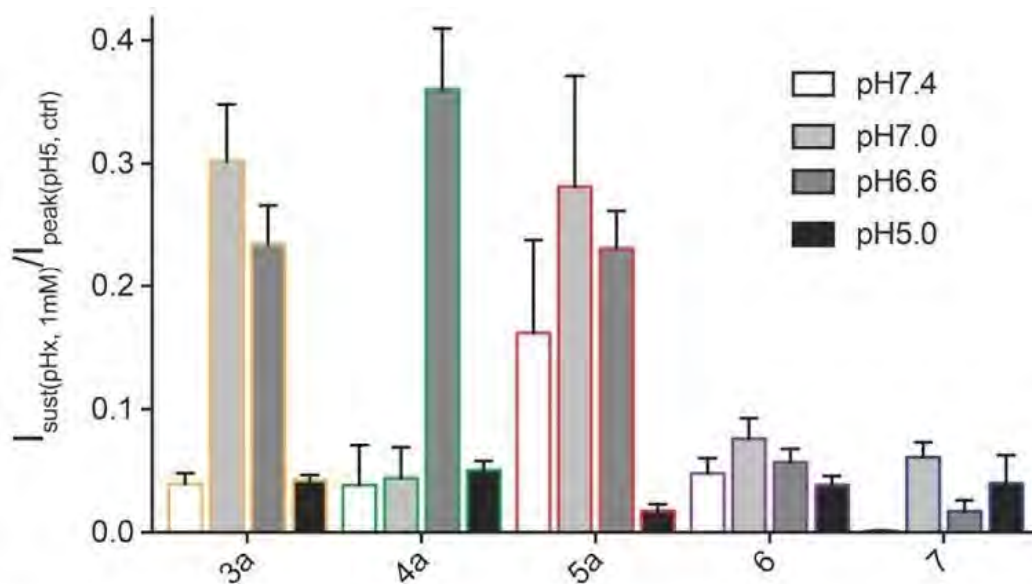


**Figure S1.** Sustained current amplitude induced in ASIC3 by GMQ derivatives. The sustained current amplitudes, obtained at the indicated pH in the presence of different compounds, were normalized to the pH5-induced peak current amplitude in the absence of compound measured in the same cell; n=3-10.

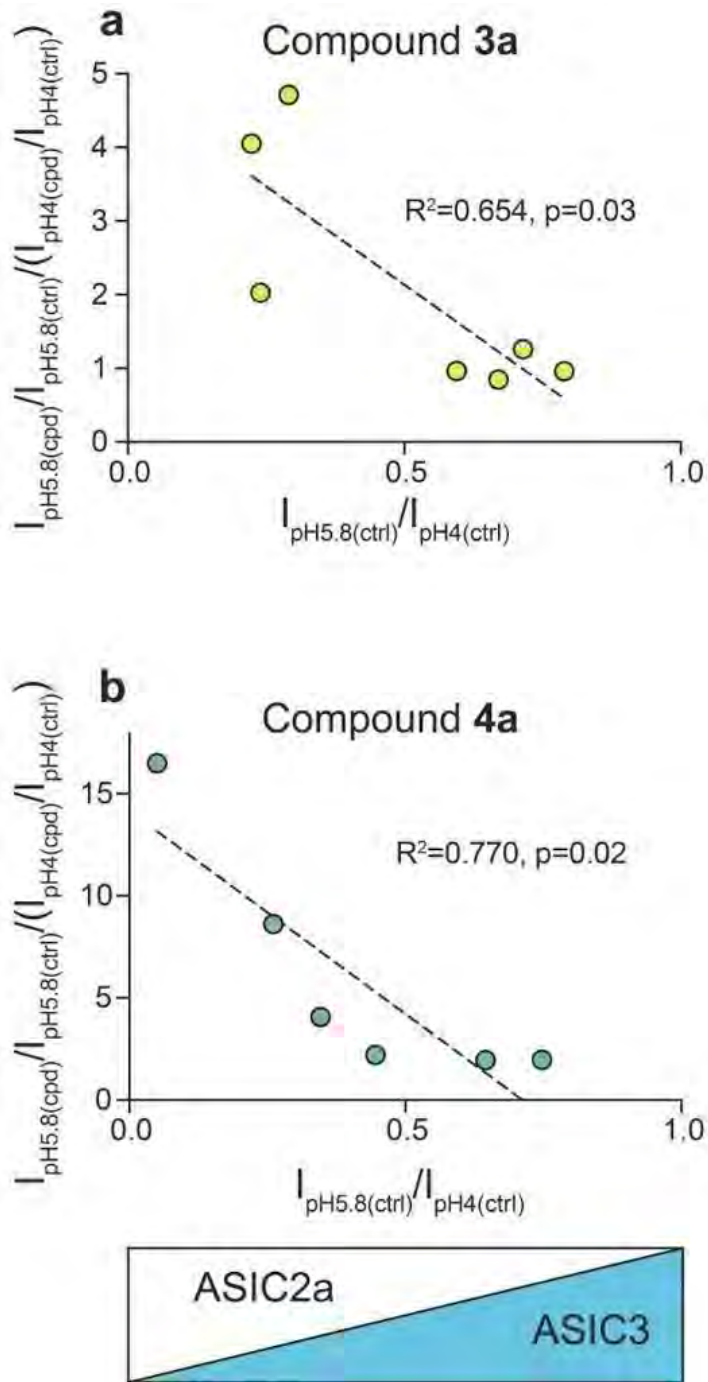


**Figure S2.** Dependence of “gating effect” on the relative subunit abundance in ASIC2a/3 heteromers. Data points represent individual experiments of **3a** (a) and **4a** (b) with ASIC2a/3 heteromers. The ratio of the “gating effect” / “blocking effect”,  $I_{\text{pH5.8(cpd)}}/I_{\text{pH5.8(ctrl)}} / (I_{\text{pH4(cpd)}}/I_{\text{pH4(ctrl)}})$  is plotted as a function of the  $I_{\text{pH5.8}}/I_{\text{pH4}}$  ratio measured in the absence of compound. The parameters  $R^2$  and  $p$  of the linear regression were determined in Graphpad Prism.

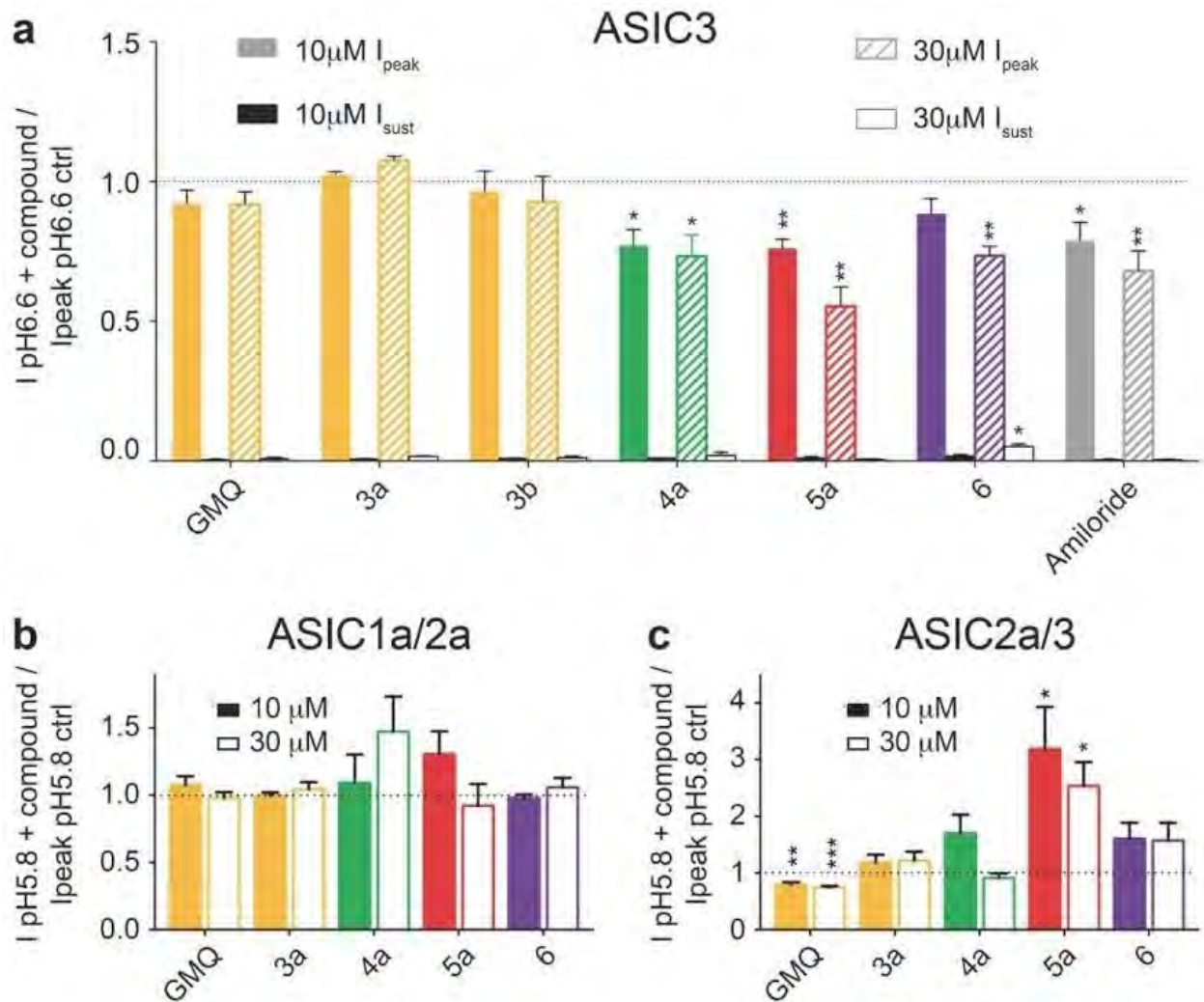


**Figure S3.** Effects of GMQ derivatives at micromolar concentrations. ASIC currents were induced by pH6.6 (ASIC3) or pH5.8 (ASIC1a/2a, ASIC2a/3) with or without test compound. The indicated concentrations of the test compounds were included in the acidic solution. The current amplitude obtained in the presence of a test compound was normalized to the amplitude obtained in its absence. Data were obtained from 3-7 cells per condition and are shown for ASIC3 (a), ASIC1a/2a (b) and ASIC2a/3 (c). \*,  $p < 0.05$ , \*\*,  $p < 0.01$ , \*\*\*,  $p < 0.001$  between test and control condition, paired t-test.

Table S1. pKa of GMQ and its derivatives

|           | pKa <sup>[a]</sup> |           | pKa <sup>[a]</sup> |
|-----------|--------------------|-----------|--------------------|
| GMQ       | 8.25               | <b>5a</b> | 9.05               |
|           |                    | <b>5b</b> | 8.70               |
| <b>1</b>  | 8.52               | <b>5c</b> | 8.83               |
| <b>2</b>  | 9.11               | <b>5d</b> | 8.76               |
| <b>3a</b> | 9.57               | <b>5e</b> | 8.73               |
| <b>3b</b> | 9.66               | <b>6</b>  | 9.13               |
| <b>4a</b> | 9.20               | <b>7</b>  | 6.33               |
| <b>4b</b> | 9.51               | <b>8</b>  | 7.38               |
| <b>4c</b> | 8.70               |           |                    |

[a] Calculator Plugins (Marvinsketch 14.8.18.0, 2014, <http://www.chemaxon.com>) were used for pKa prediction.

**Table S2. Current ratio at two different compound concentrations**

| Compound | ASIC1a  |        | n | ASIC3   |        | n  |
|----------|---|--------|---|---|--------|----|
|          | $I_{\text{pH5}}(1\text{mM})/I_{\text{pH5}}(0.3\text{mM})$ |        |   | $I_{\text{pH5}}(1\text{mM})/I_{\text{pH5}}(0.3\text{mM})$ |        |    |
| GMQ      | 0.75  | ± 0.04 | 7 | 0.87  | ± 0.03 | 7  |
| 1        | 0.94  | ± 0.03 | 4 | 0.98  | ± 0.03 | 3  |
| 2        | 0.79  | ± 0.03 | 4 | 0.92  | ± 0.03 | 4  |
| 3a       | 0.30  | ± 0.07 | 3 | 0.36  | ± 0.05 | 5  |
| 3b       | 0.63  | ± 0.02 | 3 | 0.80  | ± 0.03 | 4  |
| 4a       | 0.48  | ± 0.13 | 5 | 0.48  | ± 0.16 | 4  |
| 4b       | 0.78  | ± 0.04 | 7 | 0.78  | ± 0.01 | 3  |
| 4c       | 0.71  | ± 0.05 | 6 | 0.77  | ± 0.04 | 5  |
| 5a       | 0.55  | ± 0.04 | 4 | 0.77  | ± 0.05 | 6  |
| 5b       | 1.17  | ± 0.51 | 3 | 1.85  | ± 0.59 | 3  |
| 5c       | 0.31  | ± 0.10 | 4 | 0.79  | ± 0.08 | 6  |
| 5d       | 0.86  | ± 0.15 | 4 | 0.55  | ± 0.09 | 4  |
| 5e       | 0.66  | ± 0.08 | 7 | 0.78  | ± 0.07 | 5  |
| 6        | 0.40  | ± 0.02 | 3 | 0.53  | ± 0.04 | 5  |
| 7        | 0.77  | ± 0.09 | 7 | 0.76  | ± 0.06 | 10 |
| 8        | 0.82  | ± 0.04 | 7 | 1.07  | ± 0.09 | 7  |

Values < 1 indicate the degree by which the inhibition was lower with 0.3 as compared to 1 mM.

**Table S3.**  $I_{pH5.8}/I_{pH4}$  current ratio in the absence of compound

| Compound | ASIC1a/2a                         |        |    | ASIC2a/3                          |        |    |
|----------|-----------------------------------|--------|----|-----------------------------------|--------|----|
|          | $I_{pH5.8_{ctrl}}/I_{pH4_{ctrl}}$ |        | n  | $I_{pH5.8_{ctrl}}/I_{pH4_{ctrl}}$ |        | n  |
| GMQ      | 0.41                              | ± 0.05 | 12 | 0.51                              | ± 0.08 | 15 |
| 3a       | 0.41                              | ± 0.06 | 10 | 0.56                              | ± 0.07 | 11 |
| 4a       | 0.24                              | ± 0.05 | 11 | 0.38                              | ± 0.07 | 11 |
| 5a       | 0.28                              | ± 0.05 | 8  | 0.47                              | ± 0.09 | 8  |
| 6        | 0.31                              | ± 0.06 | 12 | 0.45                              | ± 0.09 | 6  |
| 7        | 0.39                              | ± 0.08 | 4  | 0.55                              | ± 0.20 | 3  |
| 8        | 0.38                              | ± 0.13 | 4  | 0.61                              | ± 0.09 | 6  |

The  $I_{pH5.8}/I_{pH4}$  current ratio in the absence of drug was measured in each experiment with ASIC1a/2a and ASIC2a/3, as a control of the functional expression of the heteromers. This ratio is indicated here for the experiments with the two types of heteromers, for the experiments in which the indicated compounds were tested.

**Table S4 pH dependence of ASIC1a and ASIC3 in absence and presence of compound 6**

| ASIC subtype / type of measurement | Parameter     | Control         | 30 $\mu$ M compound 6            |
|------------------------------------|---------------|-----------------|----------------------------------|
| <b>ASIC1a</b>                      |               |                 |                                  |
| Activation                         | pH50          | 6.39 $\pm$ 0.05 | 6.47 $\pm$ 0.00                  |
|                                    | nH activation | 2.51 $\pm$ 0.40 | 3.54 $\pm$ 0.14 <sup>*****</sup> |
| SSD                                | pHD50         | 7.13 $\pm$ 0.01 | 7.12 $\pm$ 0.00                  |
|                                    | nH SSD        | 7.84 $\pm$ 0.22 | 9.18 $\pm$ 0.61                  |
| <b>ASIC3</b>                       |               |                 |                                  |
| Activation                         | pH50          | 6.75 $\pm$ 0.02 | 6.74 $\pm$ 0.04                  |
|                                    | nH activation | 5.86 $\pm$ 0.36 | 2.99 $\pm$ 0.13 <sup>*****</sup> |
| SSD                                | pHD50         | 7.01 $\pm$ 0.00 | 6.95 $\pm$ 0.01                  |
|                                    | nH SSD        | 6.21 $\pm$ 0.69 | 4.33 $\pm$ 0.41 <sup>***</sup>   |

The fit parameters of the pH dependence measurements of Fig. 8b-c were determined in 3-5 experiments per condition. \*\*, p<0.01; \*\*\*, p<0.001; \*\*\*\*, p<0.0001, different from the corresponding value under control conditions.

## 5.2. Project 2 - Investigation on the differences between WT hASIC1a and its rare mutant

**Article:** Accelerated Current Decay Kinetics of a Rare Human Acid-Sensing ion Channel 1a Variant That Is Used in Many Studies as Wild Type

**Authors:** Anand Vaithia, Sabrina Vullo, Zhong Peng, Omar Alijevic and Stephan Kellenberger

In this project, our aim was to determine the difference between human ASIC1a WT (G212) and mutant (D212). The mutant ASIC1a-D212 occurs at a very low frequency of  $8.26 \times 10^{-6}$  according to ExAC and the WT contains Gly at 212 position. Human ASIC1a-D212 was used by many laboratories over years as WT. We found that the WT ASIC1a (hASIC1a-G212) had slower current decay kinetics, higher surface expression and current amplitudes, 2-fold decreased  $IC_{50}$  for Mambalgin1 and a smaller shift in the pH dependence of activation with 1mM GMQ compared to mutant hASIC1a-D212.  $Cl^-$  ions are known to modulate the ASIC1a function<sup>144</sup>. Since 212 is close to the  $Cl^-$  binding site<sup>145</sup>, we measured the maximal current amplitude, current kinetics and pH dependence of activation under the presence and absence of  $Cl^-$  ion. We found that current decay kinetics was significantly slower in hASIC1a-G212 under 140mM  $Cl^-$ /0mM  $SCN^-$  compared to 0mM  $Cl^-$ /140mM  $SCN^-$ . Similarly, under 140mM  $Cl^-$ /0mM  $SCN^-$  condition, the current decay kinetics was slower in hASIC1a-D212 but was ~4 fold smaller than hASIC1a-G212. Hence, the hASIC1a-G212 may not directly affect the  $Cl^-$  binding but it alters the current decay kinetics. Additionally, the previous experiments performed in the lab with hASIC1a-D212 construct were validated in the hASIC1a-G212 background and no difference was observed, suggesting the findings were conserved in both constructs.

### **5.2.1. My Contribution to the article**

I had performed experiments to measure the shift in pH dependence of activation in mouse and human constructs, surface expression, peak current amplitude, the kinetics of desensitization and recovery from desensitization, properties of heteromeric channels, the effects of toxin peptides and modulation by anion type. The article has 9 figures; I had performed the experiments shown in figures 2 to 6, except figure 3C, 3C and 5A.



# Accelerated Current Decay Kinetics of a Rare Human Acid-Sensing ion Channel 1a Variant That Is Used in Many Studies as Wild Type

Anand Vaithia<sup>†</sup>, Sabrina Vullo<sup>†</sup>, Zhong Peng, Omar Aljjevic and Stephan Kellenberger\*

Department of Pharmacology and Toxicology, University of Lausanne, Lausanne, Switzerland

## OPEN ACCESS

### Edited by:

Daniel F. Gilbert,  
University of Erlangen Nuremberg,  
Germany

### Reviewed by:

Angelo Karamidas,  
University of Queensland, Australia  
Ewan St. John Smith,  
University of Cambridge,  
United Kingdom

### \*Correspondence:

Stephan Kellenberger  
stephan.kellenberger@unil.ch

<sup>†</sup>These authors have contributed  
equally to this work

Received: 20 March 2019

Accepted: 08 May 2019

Published: 24 May 2019

### Citation:

Vaithia A, Vullo S, Peng Z, Aljjevic O  
and Kellenberger S  
(2019) Accelerated Current Decay  
Kinetics of a Rare Human  
Acid-Sensing Ion Channel 1a Variant  
That Is Used in Many Studies as  
Wild Type.  
*Front. Mol. Neurosci.* 12:133.  
doi: 10.3389/fnmol.2019.00133

Acid-sensing ion channels (ASICs) are neuronal Na<sup>+</sup>-permeable ion channels that are activated by extracellular acidification and are involved in fear sensing, learning, neurodegeneration after ischemia, and in pain sensation. We have recently found that the human ASIC1a (hASIC1a) wild type (WT) clone which has been used by many laboratories in recombinant expression studies contains a point mutation that occurs with a very low frequency in humans. Here, we compared the function and expression of ASIC1a WT and of this rare variant, in which the highly conserved residue Gly212 is substituted by Asp. Residue 212 is located at a subunit interface that undergoes changes during channel activity. We show that the modulation of channel function by commonly used ASIC inhibitors and modulators, and the pH dependence, are the same or only slightly different between hASIC1a-G212 and -D212. hASIC1a-G212 has however a higher current amplitude per surface-expressed channel and considerably slower current decay kinetics than hASIC1a-D212, and its current decay kinetics display a higher dependency on the type of anion present in the extracellular solution. We demonstrate for a number of channel mutants previously characterized in the hASIC1a-D212 background that they have very similar effects in the hASIC1a-G212 background. Taken together, we show that the variant hASIC1a-D212 that has been used as WT in many studies is, in fact, a mutant and that the properties of hASIC1a-D212 and hASIC1a-G212 are sufficiently close that the conclusions made in previous pharmacology and structure-function studies remain valid.

**Keywords:** ASIC, variant, mutation, kinetics, patch-clamp, voltage-clamp fluorometry

**Abbreviations:** ASIC, Acid-Sensing Ion Channel; cASIC1, chicken ASIC; cDNA, complementary deoxyribonucleic acid; CHO, Chinese hamster ovary; hASIC1a, human ASIC1a; GMQ, 2-Guanidine-4-methylquinazoline; Mamb1, Mambalgim1; mASIC1a, mouse ASIC1a; MD, Molecular dynamics; pH<sub>50</sub>, pH of half-maximal activation; pHD<sub>50</sub>, pH of half-maximal desensitization; PcTx1, Psalmotoxin1; SSD, Steady-state desensitization; VCF, voltage-clamp fluorometry; WT, wild-type.

## INTRODUCTION

A rare variant of the human acid-sensing ion channel 1a (hASIC1a) has been used as “wild type” (WT) in many functional studies involving recombinant expression of ASICs, including those carried out by our laboratory. Here, we investigate the differences between this variant, hASIC1a-D212, and the hASIC1a WT that has a Gly residue at position 212. ASICs are neuronal, Na<sup>+</sup>-conducting ion channels expressed in the central and peripheral nervous system (Wemmie et al., 2013; Yang and Palmer, 2014; Kellenberger and Schild, 2015). Their activation by extracellular acidification leads to neuronal depolarization (Deval et al., 2003; Vukicevic and Kellenberger, 2004). A sustained acidification leads to a transient ASIC current since these channels enter a non-conducting desensitized state rapidly after opening. ASICs contribute to fear sensation, neurodegeneration after ischemic stroke, to learning and to pain sensation (Wemmie et al., 2013; Kellenberger and Schild, 2015). Of the six different ASIC subunits, ASIC1a, ASIC1b, ASIC2a, ASIC2b and ASIC3 can form homo- or heterotrimeric channels (Jasti et al., 2007; Wemmie et al., 2013; Bartoi et al., 2014). The subunit composition determines the biophysical properties of the channel, such as pH dependence, current kinetics and presence or absence of a sustained current fraction (Wemmie et al., 2013; Grunder and Pusch, 2015; Kellenberger and Schild, 2015). Each ASIC subunit contains intracellular N- and C-termini, two transmembrane  $\alpha$  helices, and a large extracellular loop. Crystal structures of chicken ASIC1a (cASIC1a), whose sequence shares ~90% homology with hASIC1a, were obtained in conformations corresponding to the desensitized, the open and the closed state (Jasti et al., 2007; Gonzales et al., 2009; Bacongus and Gouaux, 2012; Dawson et al., 2012; Bacongus et al., 2014; Yoder et al., 2018). They show that the shape of a subunit is comparable to a hand, with the domains palm (yellow in Figure 1A),  $\beta$ -ball (orange), knuckle (cyan), finger (purple) and thumb (blue); the transmembrane domain would correspond to the forearm (Jasti et al., 2007). ASICs are the target of rather nonspecific small molecule inhibitors such as diminazene (Chen et al., 2010) and amiloride (Waldmann et al., 1997), of modulators such as 2-guanidine-4-methylquinazoline (GMQ; Yu et al., 2010) and of several high affinity toxins (Baron and Lingueglia, 2015; Rash, 2017).

We have recently realized that a hASIC1a clone, which is used by many laboratories in studies employing recombinant expression, contains a substitution by Asp of the conserved residue Gly212. A large proportion of published articles using hASIC1a was done with this clone (Supplementary Table S1). This clone [GenBank accession number U78181 (García-Añoveros et al., 1997)] is, however, a rare variant; in >99% of humans, the residue at position 212 is a Gly. It is not clear whether the presence of Asp at position 212 is due to a cloning artifact, or whether the individual from which the clone originates carried this mutation. According to the database of the Exome Aggregation Consortium<sup>1</sup> (Lek et al., 2016) the frequency

of Asp instead of Gly at position 212 is  $8.26 \times 10^{-6}$ . In the proximity of Gly212, there are two other Gly residues in ASIC1a, at positions 213 and 217 (Figure 1C). The Gly pair at positions 212 and 213 is highly conserved in ASICs (Supplementary Figure S1), and one of the two Gly residues is present in all mammalian Epithelial Na<sup>+</sup> channel (ENaC)/degenerin (DEG) family members. Since this region is otherwise not so well conserved among the superfamily, it is not possible to say whether Gly212 or Gly213 is conserved in the other mammalian ENaC/DEG subfamilies. Gly217, in contrast, is conserved in all ENaC/DEG family members. In the structural model of ASIC1a, Gly212 is located on the  $\beta$ -ball domain at a subunit interface, facing the thumb domain of a neighboring subunit, close to a proposed chloride binding site (Jasti et al., 2007; Figure 1B). In the present study, we compared the function and pharmacology of the WT hASIC1a-G212 and the mutant hASIC1a-D212 and found highly similar properties regarding many aspects. hASIC1a-G212 displayed, however, a higher current amplitude per surface-expressed channel, and slower desensitization kinetics.

## MATERIALS AND METHODS

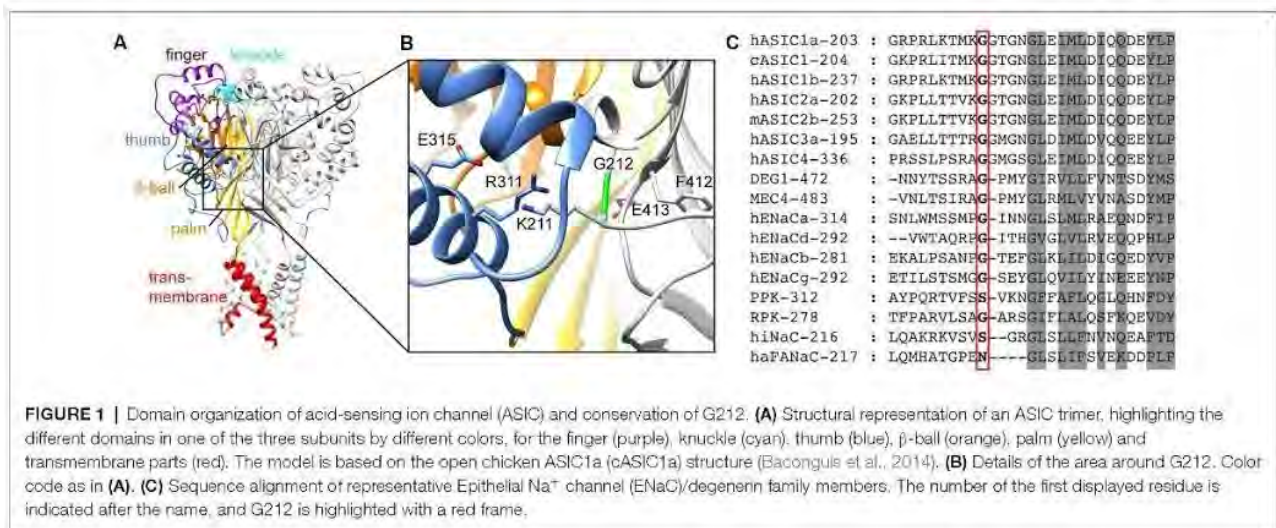
### Molecular Biology

For the expression in *Xenopus* oocytes, the hASIC1a sequence (García-Añoveros et al., 1997) was sub-cloned into a pSP65-derived vector containing 5' and 3' non-translated sequences of  $\beta$  globin to improve the stability and the expression in *Xenopus laevis* oocytes. For the expression in chinese hamster ovary (CHO) cells, the human and mouse ASIC1a sequences were sub-cloned into the peak8 vector (Edge Biosystems, Gaithersburg, MD, USA). Amino acid substitutions were generated by site-directed mutagenesis using KAPA HiFi HotStart PCR polymerase (KAPA Biosystems), using the Quikchange approach. Mutations were verified by sequencing (Synergen Biotech). *In vitro* transcription was performed using the mMESSAGING mMACHINE SP6 kit (Ambion/Life Technologies).

### Mammalian Cell Culture and Transfection

For the experiments with hASIC1a-D212 and mouse ASIC1a WT, CHO cells stably expressing these constructs were used (Poirot et al., 2004). For expression of hASIC1a-G212 and mASIC1a-G212D, CHO cells were transiently co-transfected with complementary deoxyribonucleic acid (cDNA) of EGFP together with the ASIC construct, by using Rotifect (CarlRoth). For expression of heteromeric ASICs, cDNA of hASIC1a-D212 and hASIC1a-G212 was transiently co-transfected with hASIC2a, EGFP and salmon sperm DNA into CHO cells. The ASIC1a/ASIC2a cDNA ratio for the transfections was 1:1. CHO cells were cultured in DMEM/Nutrient Mixture F-12 with GlutaMAX<sup>TM</sup> medium supplemented with 10% fetal bovine serum (FBS, ThermoFischer Scientific) and 1% Penicillin-Streptomycin (5,000 U/mL, ThermoFischer Scientific) and the cells were grown at 37°C under 5% CO<sub>2</sub> atmosphere. Stable cell lines were supplemented with puromycin (10  $\mu$ g/ml) to maintain the stable expression of ASICs.

<sup>1</sup>exac.broadinstitute.org



## Oocyte Handling and Injection

All experiments with *Xenopus laevis* oocytes were carried out in accordance with the Swiss federal law on animal welfare and had been approved by the committee on animal experimentation of the Canton de Vaud. After surgical removal, healthy stage V and VI oocytes of female *Xenopus* frogs were treated with collagenase for isolation and defolliculation. They were subsequently injected with 50 nl (0.02–0.8  $\mu\text{g}/\mu\text{l}$ ) of cRNA. After injection, they were kept at 19°C in Modified Barth's Solution (MBS) composed of (mM): 85 NaCl, 1 KCl, 2.4  $\text{NaHCO}_3$ , 0.33  $\text{Ca}(\text{NO}_3)_2$ , 0.82  $\text{MgSO}_4$ , 0.41  $\text{CaCl}_2$ , 10 HEPES and 4.08 NaOH. Experiments were performed 24 h to 48 h after injection.

## Electrophysiological Measurements

### Whole-Cell Patch-Clamp of Mammalian Cells

Whole-cell patch-clamp recordings were carried out in stable cell lines or after 48 h of transient transfection at  $-60$  mV with an EPC-9 amplifier (HEKA Electronics). The solution exchange was carried out using the MPRE8 perfusion head and electrovalves (Cell MicroControls). The sampling interval was set at 1 ms and the current filtering was set to 3 kHz. Patch pipettes (3–4  $\text{M}\Omega$ ) were pulled from borosilicate glass with filament (WPI Precision Instruments, UK) using the vertical dual-stage pipette puller PC10 (Narishige). Compensation of the series resistance was set to 70%–90%. The standard extracellular solution contained (in mM) 140 NaCl, 4 KCl, 2  $\text{CaCl}_2$ , 1  $\text{MgCl}_2$ , 10 MES, 10 HEPES, 10 Glucose, and pH was adjusted to 7.4 with NaOH. The intracellular solution contained (in mM) 90 K-Gluconate, 10 NaCl, 10 KCl, 60 HEPES, 10 EGTA, and the pH was adjusted to 7.3 with KOH. In the experiments with 100 nM extracellular  $\text{Ca}^{2+}$  concentration, 10–20 mM of a  $\text{Ca}^{2+}$  chelator (EGTA at pH >7.2, EDTA at pH  $\leq$ 7.2) was included and the total  $\text{Ca}^{2+}$  concentration was adjusted to obtain a free  $\text{Ca}^{2+}$  concentration of 100 nM according to Maxchelator (Bers et al., 2010). In the experiments with anion substitution, NaCl was replaced by NaSCN, and  $\text{K}^+$  was included as KOH,  $\text{Ca}^{2+}$  as Ca-Gluconate, and  $\text{Mg}^{2+}$  as  $\text{MgSO}_4$ . In these solutions,

the pH was adjusted to pH 6.0 with 10% acetic acid and to pH 7.4 with NaOH.

### Outside-Out Patches

For outside-out patches, the same solutions as for whole-cell measurements were used. Coverslips containing transfected CHO cells were maintained during recording with external solution of pH 7.4. Outside-out patches were excised with 4–6  $\text{M}\Omega$  borosilicate glass pipettes from transfected cells. The proton-evoked currents were recorded at  $-60$  mV, at a sampling rate of 50  $\mu\text{s}$  and low-pass-filtered at 2.9 kHz. Rapid pH changes (every 8 s) were carried out using a Piezo-controlled fast application system with a double-barrel application pipette that enables solution exchange (MXPZT-300L; Siskiyou, Grants Pass, OR, USA).

### Measurements From *Xenopus* Oocytes

Standard recording solutions contained (in mM) 110 NaCl, 2  $\text{CaCl}_2$ , and 10 HEPES for pH  $\geq$  6.8. For solutions with a pH < 6.8, HEPES was replaced by 10 mM MES. The pH was adjusted using NaOH or HCl. Whole-cell currents from *Xenopus* oocytes were recorded by two-electrode voltage clamp (TEV-200A; Dagan Corporation) at  $-60$  mV or as indicated, using Chartmaster software (HEKA Electronics) at a sampling rate of 1 ms and low-pass filtering at 2 kHz. Oocytes were placed in a RC-26Z recording chamber (Warner Instruments) and impaled with two glass electrodes filled with 1 M KCl, with a resistance of <0.5  $\text{M}\Omega$ . Oocytes were perfused at a rate of 5–15 mL/min. All experiments were performed at room temperature (20–25°C). To determine the pH dependence of the channel activation and steady-state desensitization (SSD), oocytes were exposed to a conditioning pH solution (generally pH 7.4 in activation protocols) and stimulated with an acidic pH for 5–10 s, or as indicated, once per minute.

### Voltage-Clamp Fluorometry

All voltage-clamp fluorometry (VCF) experiments were carried out on fluorophore-labeled cysteine mutants. Oocytes

were labeled in the dark with 5  $\mu$ M CF488- (Biotium) or AlexaFluor488 C-5 maleimide (Invitrogen) for 15 min at room temperature. VCF experiments were done in a RC-26Z recording chamber (Warner Instruments). The VCF setup was equipped with an Intensilight mercury lamp (C-HGFI; Nikon). A 40 $\times$  Nikon oil-immersion objective (CFI Plan Fluor; Nikon) was used to detect the fluorescence signal emitted by the labeled oocytes. The optical signal was measured by a photodiode (S1336-18BQ; Hamamatsu Photonics) coupled to the headstage of an amplifier (List EPC-7; HEKA). An offset device was used to adjust and measure the offset of the signal, allowing the measurement of the total fluorescence intensity. Changes in fluorescence intensity ( $\Delta F$ ) were normalized to the total fluorescence signal ( $F$ ).

## Electrophysiology Data Analysis and Statistics

Data were analyzed with the software FitMaster (HEKA Electronics) and with Origin PRO (OriginLab Corp., Northampton, MA, USA). pH response curves for H<sup>+</sup> activation were fitted with a Hill function:  $I = I_{\max}/(1 + (10^{-\text{pH}50}/10^{-\text{pH}})^{\text{nH}})$ , where  $I_{\max}$  is the maximal current amplitude, pH<sub>50</sub> is the pH inducing 50% of the maximal current amplitude, and nH is the Hill coefficient. SSD curves were fitted with an analogous equation. Time constants of desensitization were determined by fitting the decay time of current traces to a mono-exponential function. The results are presented as mean  $\pm$  SEM. They represent the mean of  $n$  independent experiments on different cells. Statistical analysis was performed with  $t$ -test where two conditions were compared, or with One-way ANOVA followed by Dunnett's or Tukey multiple comparisons test, or as indicated (Graphpad Prism 6).

## Surface Protein Biotinylation and Western Blot

These experiments were carried out as described elsewhere (Jiang et al., 2010). Briefly, cells were washed 48 h after transfection with PBS-CM (in mM, 137 NaCl, 2.7 KCl, 8 Na<sub>2</sub>HPO<sub>4</sub>, 2 KH<sub>2</sub>PO<sub>4</sub>, 0.1 CaCl<sub>2</sub>, 1 MgCl<sub>2</sub>) at pH7.4 and then washed twice with PBS-CM at pH8.0. All procedures were performed on ice. Cells were labeled with 1 mg/ml of EZ-Link<sup>TM</sup> Sulfo-NHS-SS-Biotin (Thermo Scientific) supplemented in PBS-CM at pH8.0 for 30 min. The biotinylation reaction was quenched by adding 10 ml of PBS-CM at pH7.4 containing 100 mM glycine for 10 min, followed by two washes with PBS-CM at pH7.4. Cell lysates were prepared by incubation for 15 min in cell lysis buffer containing 100 mM NaCl, 5 mM EDTA, 1% Triton X-100, 20 mM HEPES at pH7.4, supplemented with protease inhibitor cocktail. Cell lysates were clarified by centrifugation at 4°C for 20 min at 11,000 g. The total ASIC protein expression was determined by mixing 20  $\mu$ l of the supernatant with 5  $\mu$ l of 5 $\times$  sample loading buffer [1.5 M Sucrose, 10% SDS, 12.5mM EDTA, 312 mM Tris pH8.8, 0.25% (w/v) bromophenol blue, 125 mM DTT], followed by heating at 95°C for 10 min. These samples were then used for SDS-PAGE and western blot analysis. The remaining supernatant was mixed with 50  $\mu$ l neutravidin-agarose beads (Thermo Scientific) and incubated overnight at 4°C on a rotating wheel. Beads and supernatant were separated

by centrifugation at 1,000 g for 3 min and washed five times with PBS-CM at pH7.4 containing 1% Triton X-100. The supernatant was discarded and 50  $\mu$ l of 2 $\times$  sample loading buffer [20% glycerol, 6% SDS, 250 mM Tris-HCl at pH6.7, 0.1% (w/v) bromophenol blue, 50 mM DTT] was added to each sample, followed by heating at 95°C for 10 min. Protein samples of 20  $\mu$ l were separated on a 10% SDS-PAGE (running buffer: 27.5 mM Tris-base, 213 mM Glycine and 1% SDS) at 100V for 1.5 h. Samples were transferred to Protran<sup>TM</sup> 0.2  $\mu$ M nitrocellulose membranes (Amersham Biosciences) at 4°C, 100V for 2.5 h. After the transfer, the membrane was blocked by TBST (in mM, 137 NaCl, 2.7 KCl, 19 Tris base, 0.1% Tween 20) containing 5% BSA for 1 h. The membranes were exposed overnight at 4°C to anti-ASIC1 antibody (1:1,000, Alomone, Israel) in 1% BSA containing TBST buffer, washed three times, and were then exposed to Goat Anti-Rabbit IgG H&L horseradish peroxidase-linked secondary antibody (1:4,000, Abcam, Switzerland). To detect actin, the blots were exposed overnight at 4°C to Anti-Actin (1:1,000, Sigma Aldrich) in TBST buffer containing 1% BSA, washed three times and detected with Donkey anti-rabbit IgG horseradish peroxidase-linked secondary antibody (1:4,000, GE healthcare). Blots were exposed to secondary antibodies for 1 h at room temperature and washed three times. The signals were detected using the Fusion SOLO chemiluminescence system (Vilber Lourmat, Marne-la-Vallée, France) using SuperSignal<sup>TM</sup> West Femto Maximum Sensitivity Substrate (Thermo Scientific). Actin was detected from the cell lysate (Figure 2I), but not from the surface fraction (not shown). The band intensities were quantified by the linear analysis method of the software, with the area of measurement kept the same for all samples of the same blot. Background noise was subtracted prior to determining the intensity occupied by individual bands.

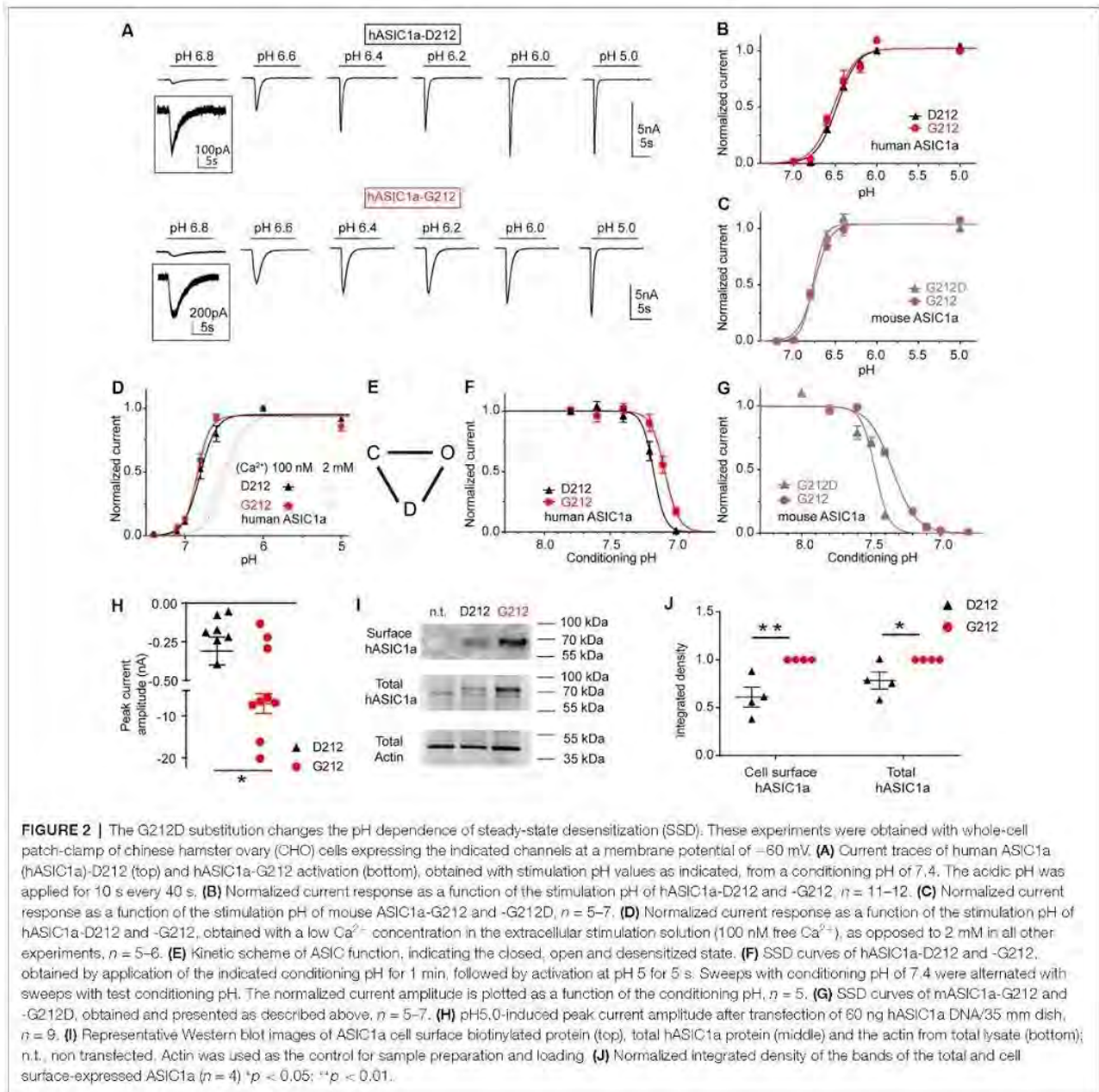
## Reagents

GMQ was purchased from Sigma, and a fresh GMQ stock solution in standard extracellular solution was prepared every day; dilutions were then made from the stock solution. Psalmotoxin1 was purchased from Smartox Biotechnology (France); solutions were made daily from a 214  $\mu$ M stock solution in water. Mambalgin1 was purchased from Peptides International (USA). Mambalgin solutions were made fresh daily from a 30  $\mu$ M stock solution in water. 0.05% BSA (final concentration) was included in solutions containing the toxins. Amiloride hydrochloride (Sigma Aldrich) was dissolved in the normal extracellular solution at pH6.0 at 1 mM and kept at 4°C. Solutions at different amiloride concentrations were freshly made on the days of the experiments.

## RESULTS

### Slower Current Decay Kinetics and Increased Current Amplitudes in hASIC1a-G212

HASIC1a-G212 and -D212 were expressed in CHO cells, and their function was assessed by whole-cell patch-clamp. The pH



dependence of activation was measured by activating ASICs by a short exposure to acidic solutions of different pH once every 40 s from a conditioning pH of 7.4 that was applied between the acidic stimulations. Typical current traces are shown in **Figure 2A**. The pH dependence of activation of the hASIC1a current is shown in **Figure 2B**. The pH of half-maximal activation ( $pH_{50}$ ) was not different, with  $pH_{50}$  of hASIC1a-D212 of  $6.47 \pm 0.02$  ( $n = 8$ ) and  $pH_{50}$  of hASIC1a-G212 of  $6.51 \pm 0.04$  ( $n = 6$ ;  $p = 0.74$ ). Similarly to the human clone, the mouse ASIC1a (mASIC1a) carries a Gly at the homologous position. The  $pH_{50}$  was not changed in mASIC1a by the G212D mutation ( $pH_{50} = 6.75 \pm 0.02$ ,  $n = 4$ )

compared to the  $pH_{50}$  of mASIC1a WT (G212,  $6.69 \pm 0.02$ ,  $n = 9$ ,  $p = 0.46$ , **Figure 2C**). These experiments were carried out at an extracellular  $Ca^{2+}$  concentration of 2 mM. Lowering the extracellular  $Ca^{2+}$  concentration in the stimulation solution is known to shift the pH curve of ASIC1a to more alkaline values, possibly because there is a competition between  $Ca^{2+}$  and protons (Babini et al., 2002). We confirm here such a shift in the pH dependence of activation for both, ASIC1a-G212 and -D212, when the extracellular  $Ca^{2+}$  concentration was lowered to 100 nM (**Figure 2D**;  $p < 0.001$ , the dotted lines indicate the respective pH dependence in the presence of 2 mM

extracellular  $\text{Ca}^{2+}$  from **Figure 2B** for comparison). The  $\text{pH}_{50}$  values were not different, with  $6.80 \pm 0.04$  (hASIC1a-D212,  $n = 5$ ) and  $6.85 \pm 0.02$  (hASIC1a-G212,  $n = 6$ ,  $p = 0.75$ ). The simplest kinetic scheme that can describe ASIC function, contains three states, the closed, open and desensitized state, as illustrated in **Figure 2E** (Blanchard and Kellenberger, 2011). When closed ASICs are exposed to a moderately acidic solution, they can enter the non-conducting desensitized state without apparent opening. This transition is called SSD. Changes in the pH dependence of SSD can affect the fraction of channels that are activated by an acidic pH. We have determined the pH dependence of SSD by exposing ASIC-expressing cells for 1 min to different conditioning pH values in the range of  $\text{pH}7.8$ – $6.8$ , each time followed by a short exposure to  $\text{pH}5.0$  to activate the channels. The  $\text{pH}5.0$ -induced current amplitude is plotted in **Figure 2F** as a function of the conditioning pH. This experiment showed a small acidic shift of the SSD pH dependence if Asp212 is replaced by Gly. The midpoint of the SSD pH dependence ( $\text{pH}_{D50}$ ) was  $7.17 \pm 0.01$  (hASIC1a-D212,  $n = 5$ ) and  $7.09 \pm 0.02$  (hASIC1a-G212,  $n = 5$ ,  $p < 0.05$ ). In mouse ASIC1a, these values were  $7.49 \pm 0.02$  (mASIC1a-G212D,  $n = 5$ , **Figure 2G**) and  $7.35 \pm 0.01$  (mASIC1a WT,  $n = 7$ ,  $p < 0.0001$ ), thus reproducing qualitatively the shift observed in hASIC1a.

We had observed that we needed to transfect cells with less cDNA coding for hASIC1a-G212 than with that coding for hASIC1a-D212 to obtain similar current amplitudes. When cells were transfected with the same amount of DNA, the current amplitudes were  $\sim 20$ -fold greater with G212 (**Figure 2H**,  $p < 0.05$ ). To distinguish whether this difference was due to an effect on the expression of the channel or on its function, we compared the total and the cell surface expression of ASIC1a-G212 and -D212 from Western blots (**Figures 2I,J**). This showed stronger bands of hASIC1a-G212 for the total and the cell surface expression (**Figure 2I**), and the quantification indicated that the surface-expressed hASIC1a-D212 protein amounted to  $\sim 60\%$  of the -G212 protein (**Figure 2J**,  $p < 0.01$ ). hASIC1a-G212 has, therefore, a  $\sim 10$ -fold higher ratio of the current/number of channels at the cell surface than hASIC1a-D212. Since the residue 212 is located quite far from the pore, it is unlikely that it influences the unitary conductance. Indeed, unitary current amplitudes of hASIC1a-D212 (Alijevic and Kellenberger, 2012), and rat ASIC1a which carries a Gly residue at the corresponding position (Zhang and Canessa, 2002) are highly similar. The slower open-desensitized transition in hASIC1a-G212, suggested by the slower current decay (**Figure 2A**), underlies some of the increase of macroscopic peak current amplitudes. The replacement of Asp212 by Gly increases likely in addition the fraction of membrane-resident channels that open upon acidification.

As mentioned above, a slower time course of the current decay in G212 was obvious from the current traces (**Figure 2A**). Analysis of the time constant of current decay by fitting this part of the current trace to a single exponential shows a clear slowing of the desensitization kinetics in the pH range  $6.6$ – $6.0$  when Asp212 was replaced by Gly (**Figure 3A**). At  $\text{pH}5.0$ , there

was no significant difference in the current decay kinetics. To measure the current kinetics at high temporal resolution, a series of experiments were carried out with a piezo-driven solution change system on excised outside-out patches from CHO cells expressing ASIC1a-D212 or -G212 (**Figures 3B–D**). Upon stimulation with  $\text{pH}5.0$ , the kinetics of current appearance, measured as (10%–90%) rise time, were not different between the two hASIC1a variants, with  $6.0 \pm 1.8$  ms (**Figures 3B,C**, hASIC1a-D212,  $n = 4$ ) and  $12.9 \pm 3.3$  ms (hASIC1a-G212,  $n = 6$ ,  $p < 0.05$ ). At the stimulation  $\text{pH}6.5$ , the current appearance was slower in hASIC1a-D212 ( $p < 0.001$ ). The kinetics of current decay was rapid in both, hASIC1a-G212 and -D212 at  $\text{pH}5.0$  (**Figure 3D**), with time constants of  $\sim 25$  ms. Since the current decay had two exponential components in some patches, and one in others, we express the time course of current decay as decay time (time to pass from 90% to 10% of the current amplitude). At  $\text{pH}5.0$ , the kinetics were similarly fast for both ASIC types, while at  $\text{pH}6.5$ , the current decay was slower in G212 ( $p < 0.01$ ). These observations suggest that in the pH range  $6.6$ – $6$ , the open-desensitized transition is slower in hASIC1a-G212 as compared to -D212. We wanted to know whether other transitions in and out of the desensitized state were also different between the two channels. To determine the kinetics of the closed-desensitized transition, channels were exposed for different durations to the conditioning pH 7.0, before activation of the non-desensitized channels by  $\text{pH}5.0$  (**Figure 3E**). These experiments showed that the closed-desensitized kinetics are slower in hASIC1a-G212 as compared to -D212 ( $p < 0.05$ ). The recovery from desensitization protocol (**Figure 3F**) showed, however, no difference between the two channel types ( $p > 0.05$ ). ASIC1a current responses are mostly transient, and only a very small sustained current persists at the end of a 5-s acidification. If a sustained current appears, it is due to channels that can exit the desensitized state and return, either directly or *via* the closed state, to the open state. A difference in the sustained current/peak current ( $I_{\text{sust}}/I_{\text{peak}}$ ) ratio would, therefore, indicate a difference in the rate leaving the desensitized state. The  $I_{\text{sust}}/I_{\text{peak}}$  ratio, measured under different pH conditions, showed no significant difference between hASIC1a-D212 and -G212 (**Figure 3G**). Taken together, the kinetic analysis indicates a slower entry to the desensitized state from the open and the closed state for hASIC1a-G212. The acidic shift of the pH dependence of SSD suggests that the desensitized state is energetically slightly less favorable in hASIC1a-G212 compared to -D212.

We have also tested whether the  $I_{\text{sust}}/I_{\text{peak}}$  ratio and the desensitization kinetics are different between heteromeric hASIC1a-D212/hASIC2a and hASIC1a-G212/hASIC2a channels. Heteromeric channels were obtained by co-transfection of hASIC1a and hASIC2a constructs.  $\text{IpH}5.8/\text{IpH}4.0$  current ratios of  $0.43 \pm 0.08$  (hASIC1a-D212/hASIC2a,  $n = 7$ ) and  $0.41 \pm 0.10$  (hASIC1a-G212/hASIC2a,  $n = 5$ ) indicated that mostly heteromeric channels were expressed (Joeres et al., 2016; Alijevic et al., 2018). Representative current traces are shown in **Figure 4A**. The  $I_{\text{sust}}/I_{\text{peak}}$  ratio was not different between the two types of heteromers (**Figure 4B**). Although there was a tendency towards

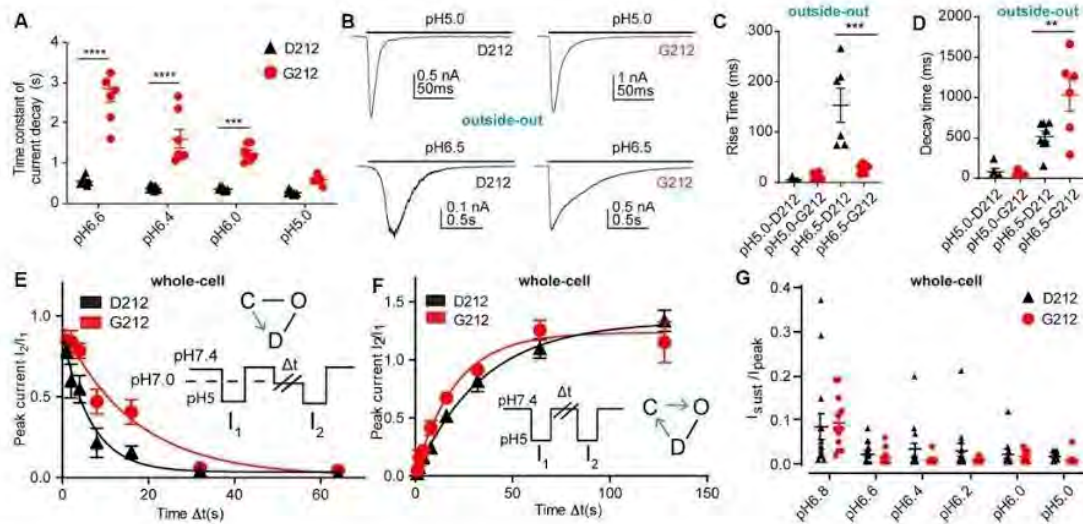


**FIGURE 3 |** Slower current decay kinetics in hASIC1a-G212. All data in this figure are from hASIC1a expressed in CHO cells, black symbols represent hASIC1a-D212, red symbols hASIC1a-G212; **(A–E–G)**, measured with whole-cell patch-clamp; **(B–D)**, measured from excised, outside-out patches. **(A)** Time constant of current decay, obtained from single exponential fits at the pH conditions indicated,  $n = 7–8$ . \*\*\*\* $p < 0.0001$ , \*\*\*\* $p < 0.0001$ , different between hASIC1a-D212 and -G212. **(B)** Representative traces showing ASIC1a currents from excised outside-out patches, induced by acidification to pH6.5 or pH5.0, by using an ultra-rapid perfusion system. **(C)** Rise time of current appearance (= time to pass from 10% to 90% of maximal peak amplitude),  $n = 5–6$ . **(D)** Current decay time,  $n = 5–8$ . \*\* $p < 0.01$ , \*\*\* $p < 0.001$ , determined with ANOVA, followed by Tukey post-test. **(E)** The kinetics of desensitization at pH7.0, without apparent opening (thus likely the closed—desensitized transition), was determined with the protocol illustrated in the inset. The duration of the exposure to pH7.4 was 40 s, that to pH5.0 5 s, while exposure to pH7.0 of different durations  $\Delta t$  was used. The current ratio  $I_2/I_1$  is plotted as a function of  $\Delta t$ . The solid lines represent single exponential fits, with  $\tau = 8.0 \pm 1.5$  s (hASIC1a-D212,  $n = 11$ ) and  $\tau = 17.4 \pm 3.5$  s (hASIC1a-G212,  $n = 11$ ,  $p > 0.05$ ). **(F)** The kinetics of recovery from desensitization was determined by the protocol shown in the inset. Two subsequent steps to pH5.0 were separated by an exposure of varying duration ( $\Delta t$ ) to pH7.4. After the second exposure, the cell was exposed for 40 s to pH7.4 before starting the next protocol. The current ratio  $I_2/I_1$  is plotted as a function of  $\Delta t$ . The solid lines represent single exponential fits to the kinetics of hASIC1a-D212 ( $\tau = 41.2 \pm 5.2$  s,  $n = 8$ ) and hASIC1a-G212 ( $\tau = 37.2 \pm 10.4$  s,  $n = 11$ ,  $p < 0.05$ ). **(G)** Sustained/peak current ratio of hASIC1a-D212 and -G212 at the indicated pH,  $n = 9–14$ . The sustained current was measured during the last second of the 10-s acidification. There was no significant difference between the  $I_{sust}/I_{peak}$  ratio of hASIC1a-D212 and -G212 at any pH measured (Two-way ANOVA, followed by Sidak post-test).

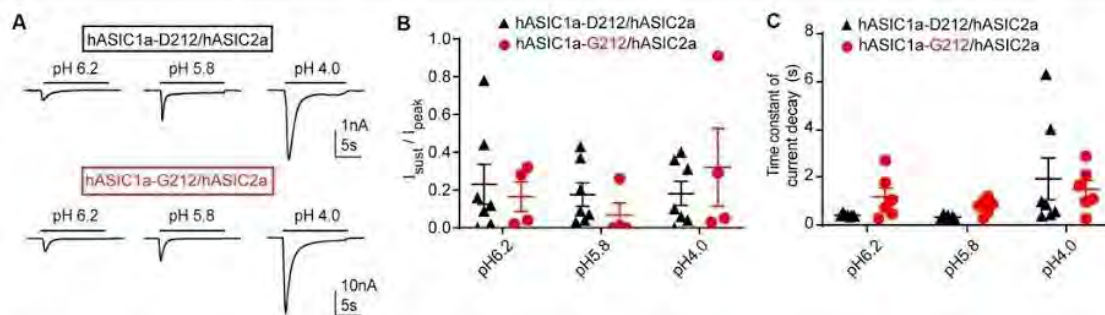


**FIGURE 4 |** Properties of ASIC1a/ASIC2a heteromers. The data are from CHO cells transfected with hASIC1a-D212/hASIC2a (black symbols) and hASIC1a-G212/hASIC2a (red symbols), measured with whole-cell patch-clamp. **(A)** Current traces of hASIC1a-D212/hASIC2a (top) and hASIC1a-G212/hASIC2a activation (bottom), obtained with stimulation pH values as indicated, from conditioning pH 7.4. The acidic pH was applied for 10 s with a sweep interval of 40 s. **(B)** Sustained/peak current ratio at the indicated stimulation pH,  $n = 4–7$ . The sustained current was measured during the last second of the 10-s acidification. There was no significant difference between the  $I_{sust}/I_{peak}$  ratio of the two channel types at any pH measured (Two-way ANOVA, followed by Sidak post-test). **(C)** Time constant of current decay, as obtained from single exponential fits, at the indicated pH,  $n = 6–7$ . There was no significant difference in the time constant of current decay between the two channel types at any pH measured (Two-way ANOVA, followed by Sidak post-test).

slower desensitization kinetics in hASIC1a-G212/hASIC2a as compared to hASIC1a-D212/hASIC2a at pH6.2 and 5.8, this difference was not statistically significant (**Figure 4C**).

Likely, the influence of the residue at position ASIC1a-212 on current kinetics was reduced by the additional presence of ASIC2a subunits.

## Small Differences in the Pharmacology and Modulation

In order to investigate possible differences in pharmacology, we measured the  $IC_{50}$  of the general ENaC/DEG channel inhibitor amiloride, as well as  $IC_{50}$  values of the two ASIC toxin inhibitors Psalmotoxin1 (PcTx1) and Mambalgin1 (Mamb1). Amiloride and PcTx1 did not distinguish between hASIC1a-D212 and -G212, as illustrated by  $IC_{50}$  values of  $1.91 \pm 0.03 \mu\text{M}$  (hASIC1a-D212) and  $1.54 \pm 0.41 \mu\text{M}$  (hASIC1a-G212) for amiloride (Figure 5A,  $n = 4-5$ ,  $p = 0.45$ ) and  $1.19 \pm 0.26 \text{ nM}$  (D212) and  $1.83 \pm 0.92 \text{ nM}$  (G212,  $n = 5-6$ ,  $p = 0.49$ ) for PcTx1 (Figure 5B). Mambalgin1 had a 2-fold higher  $IC_{50}$  in D212, with  $21.7 \pm 4.3 \text{ nM}$  (D212) and  $10.5 \pm 1.7 \text{ nM}$  (G212,  $n = 7$ ,  $p = 0.03$ ; Figure 5C). GMQ can activate ASIC3 at physiological pH7.4 (Yu et al., 2010). We have previously shown that GMQ induces in ASIC1a an acidic shift of the pH dependence of activation, in contrast to its effects on ASIC3 (Alijevic and Kellenberger, 2012). Figures 5D,E show that 1 mM GMQ induces a significant lowering of the  $pH_{50}$  in both hASIC1a-D212 [ $6.47 \pm 0.02$  (ctrl) and  $6.20 \pm 0.05$  (GMQ,  $n = 6-8$ ,  $p < 0.0001$ )] and hASIC1a-G212 [ $6.51 \pm 0.04$  (ctrl) and  $6.44 \pm 0.02$  (GMQ,  $n = 6-12$ ,  $p < 0.01$ )]. The

shift in pH dependence appears, however, to be substantially smaller in G212 as compared to D212. We have recently identified GMQ derivatives that also induced shifts in the pH dependence of ASIC channels (Alijevic et al., 2018). Two of these compounds, GMQ and 5-phenyl-2-guanidinopyridine were tested on hASIC1a-D212 and -G212. These compounds affected the pH dependence and the maximal current amplitude in the same way (Supplementary Figure S2).

## Altered Dependence of Current Kinetics on $Cl^-$ Concentration

Since residue 212 is located in the proximity of the site where a  $Cl^-$  ion was found in the desensitized and open ASIC structures (Jasti et al., 2007; Gonzales et al., 2009; Baconguis and Gouaux, 2012; Baconguis et al., 2014), and mutations of nearby residues were shown to affect the ASIC1a current decay kinetics (Kusama et al., 2010), we measured ASIC1a currents in solutions in which the extracellular  $Cl^-$  was in part or completely replaced by  $SCN^-$ . Figure 6A illustrates that the current amplitudes measured at pH6.0 decreased when the  $Cl^-$  concentration was reduced. Comparison of the two extreme conditions, by normalizing for each cell the  $I_{pH6.0}$  amplitude

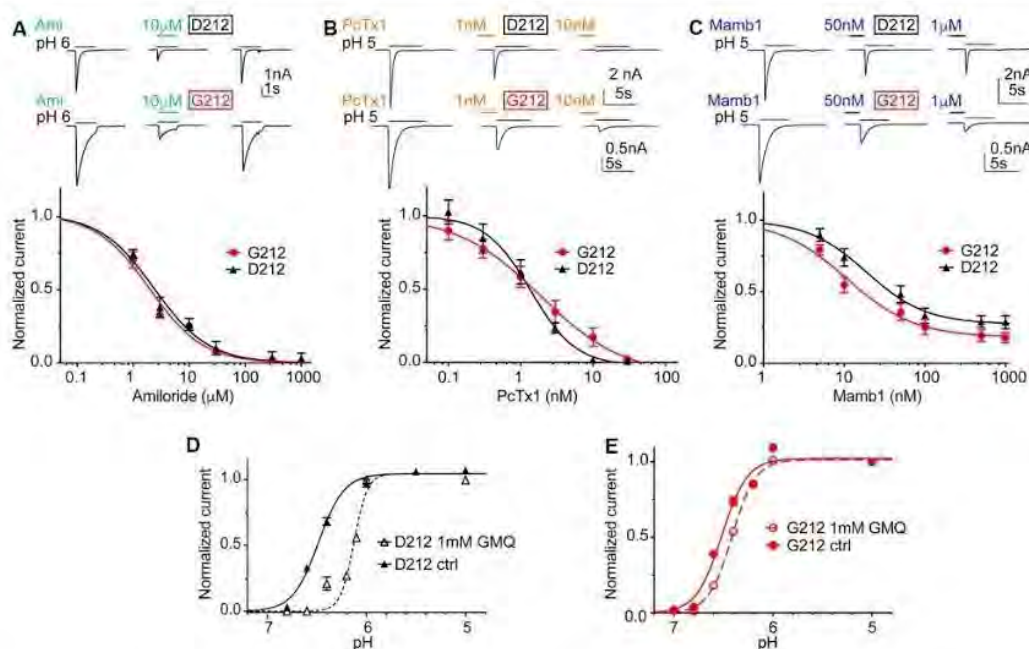
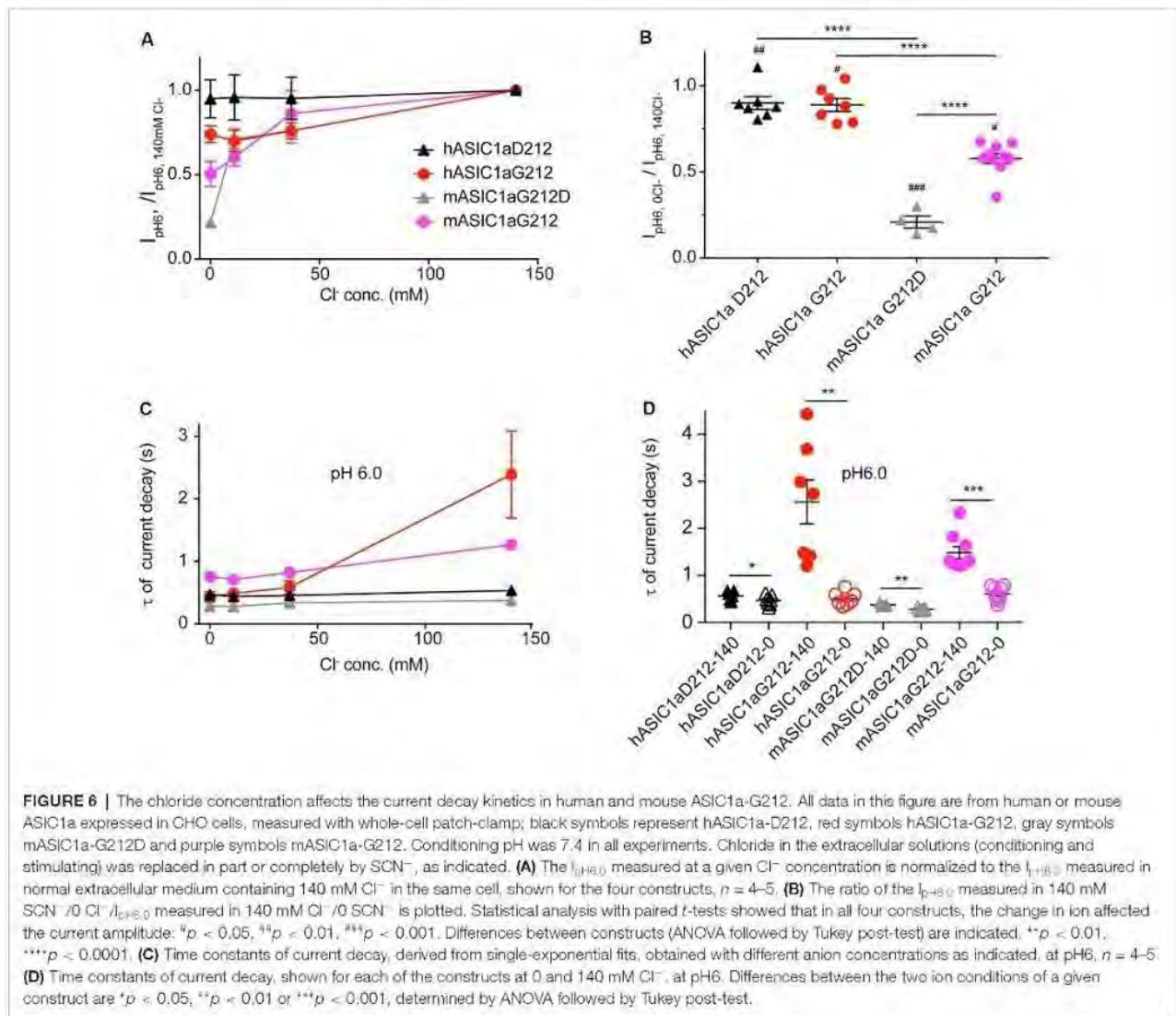


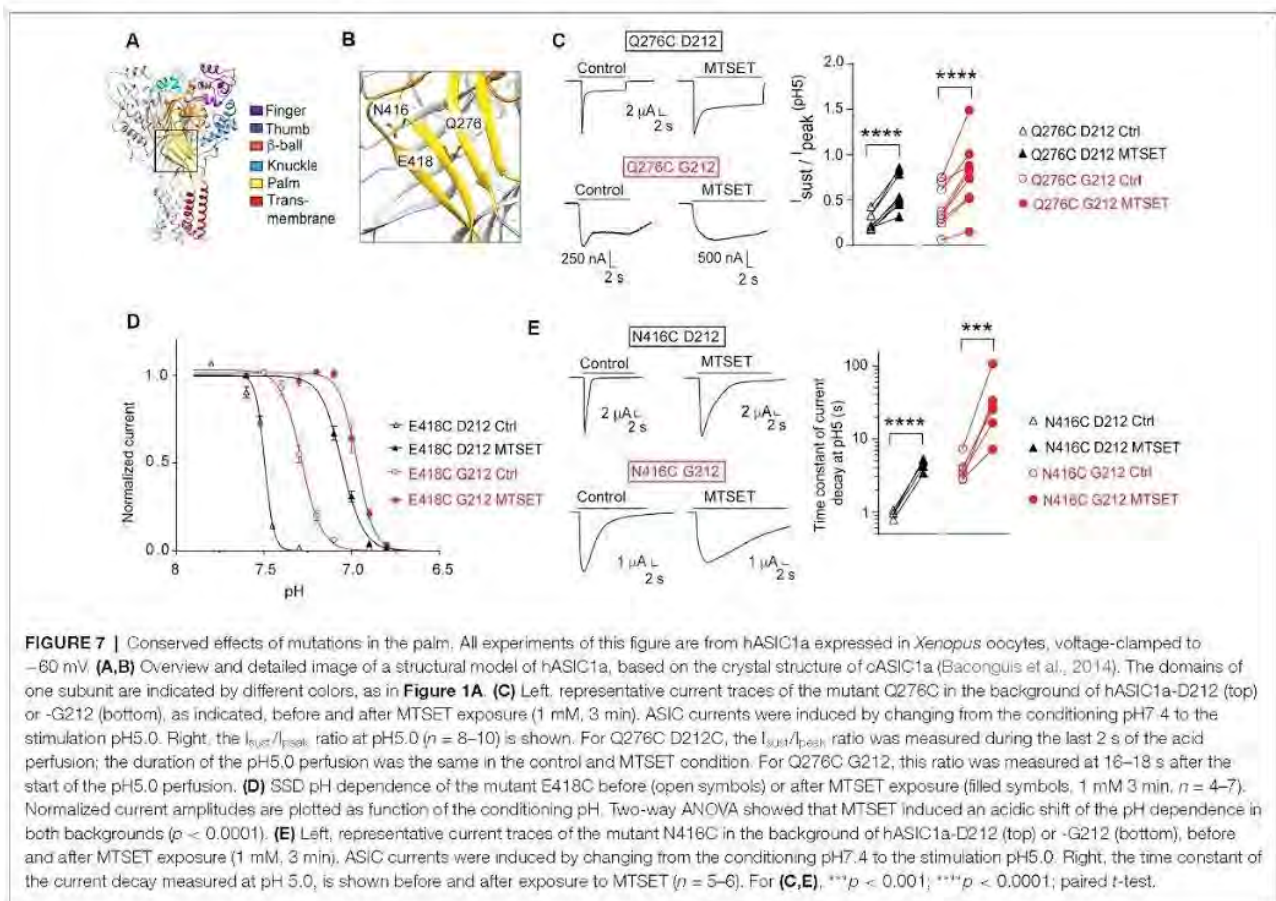
**FIGURE 5 |** Unchanged pharmacology in hASIC1a-D212. All data in this figure are from hASIC1a expressed in CHO cells, measured with whole-cell patch-clamp; black symbols represent hASIC1a-D212, red symbols hASIC1a-G212. Conditioning pH was 7.4 in all experiments, and lines are fits to a Hill equation. **(A)** Top, representative current traces of ASIC1a activated by pH6.0 for 3 s without inhibitor, in the presence of  $10 \mu\text{M}$  amiloride, and after washout of amiloride. Bottom, amiloride inhibition curve, plotting the current as a function of amiloride concentration, normalized to the response in the absence of amiloride,  $n = 4-5$ . **(B)** Top, representative current traces obtained under control conditions or after pre-administration of PcTx1 at the indicated concentrations. Bottom, PcTx1 inhibition curve,  $n = 6$ ; PcTx1 was pre-applied in the conditioning pH solution during 60 s, before activating ASICs with pH5.0 during 5 s. **(C)** Top, representative current traces obtained under control conditions or after pre-administration of Mambalgin1 at the indicated concentrations. Bottom, Mambalgin1 inhibition curve,  $n = 7-8$ ; Mambalgin1 was pre-applied in the conditioning pH solution during 60 s, before activating ASICs with pH5.0 during 5 s. **(D,E)** pH dependence of activation in the presence and absence of 1 mM 2-guanidine-4-methylquinazoline (GMQ) in the acidic solution, dotted lines and empty symbols represent the condition with GMQ. **(D)** D212,  $n = 10-11$ ,  $p < 0.0001$ . **(E)** G212,  $n = 11-12$ ,  $p < 0.01$ .

obtained at 0 mM  $\text{Cl}^-$ /140 mM  $\text{SCN}^-$  to that obtained with 140 mM  $\text{Cl}^-$ /0 mM  $\text{SCN}^-$ , shows that the current amplitudes were lower in the  $\text{Cl}^-$ -free condition, and that this current decrease was stronger in the mouse as compared to the human channels (Figure 6B). The reasons for this change in amplitude may involve changes in current kinetics and pH dependence. The current decay kinetics at pH6.0 were similarly rapid at 0, 11 and 37 mM  $\text{Cl}^-$  in all four ASIC1a constructs, and were slowed down for hASIC1a-G212 at 140 mM  $\text{Cl}^-$  (Figures 6C,D). In all these four channel variants, the current decay kinetics were different between the two extreme conditions (0 mM  $\text{Cl}^-$ /140 mM  $\text{SCN}^-$  compared to 140 mM  $\text{Cl}^-$ /0 mM  $\text{SCN}^-$ , Figure 6D). The ratio of the time constants between the two ionic conditions ( $\tau_{140\text{mMCl}^-} / \tau_{140\text{mMSCN}^-}$ ) was however small in mouse and hASIC1a carrying an Asp at position 212 and was significantly increased in hASIC1a-G212 ( $p < 0.01$ ).

## Confirmation in the hASIC1a-G212 Background of Results of Previous Mutagenesis Studies

Our laboratory has carried out several studies in the background of hASIC1a-D212 that analyzed the functional consequences of mutations in a number of channel domains. We have constructed here some key mutants in the background of hASIC1a-G212 and tested whether the effect of these mutations was conserved in the hASIC1a-G212 background. In a study addressing the conformational changes in the palm (Røy et al., 2013), we had investigated a large number of palm mutants. In these experiments we had shown among other observations that exposure to MTSET induced in Q276C an increase of the  $I_{\text{sust}}/I_{\text{peak}}$  ratio, in E418C an acidic shift of the pH dependence of SSD (see also Liechti et al., 2010), and in N416C a slowing of the kinetics of current decay. Figures 7A,B show the





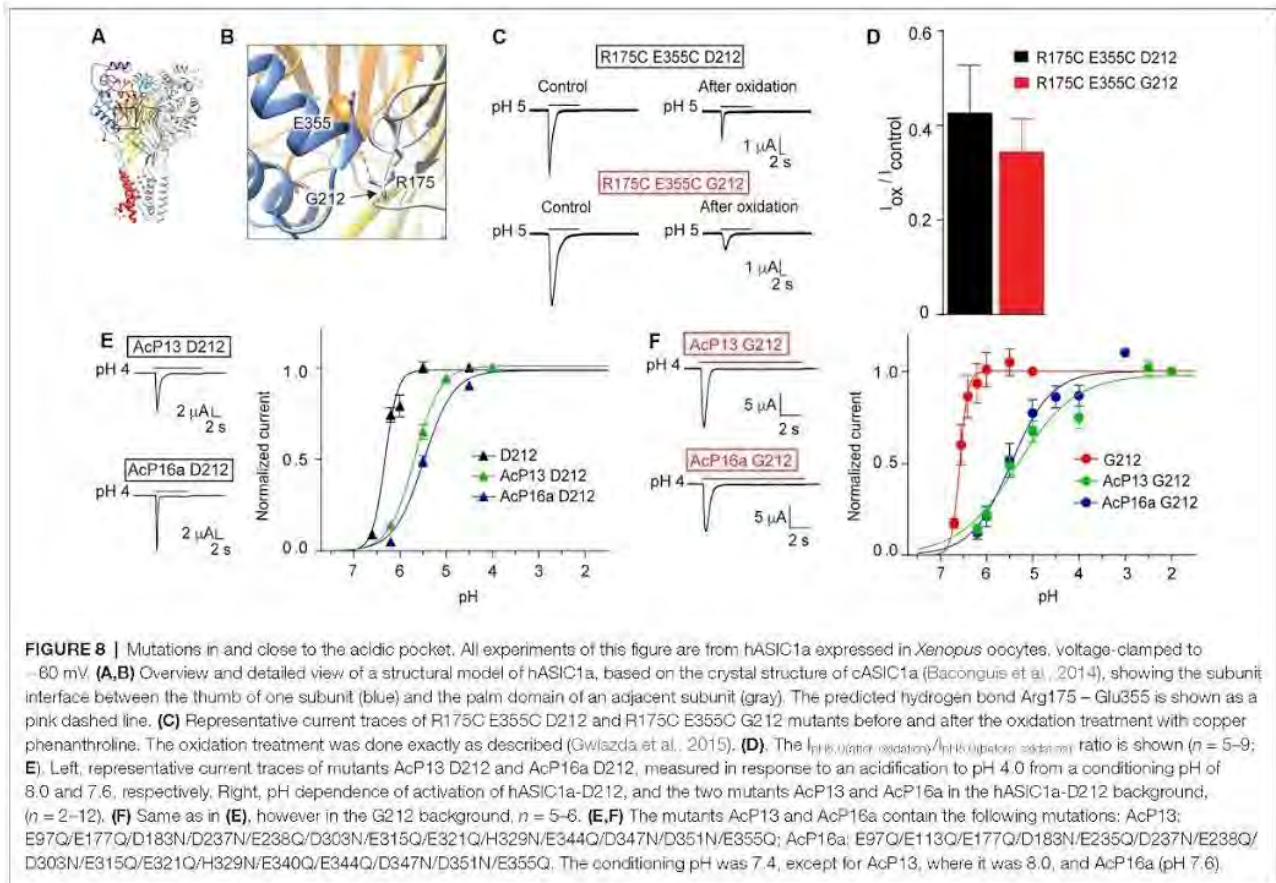
localization of these residues in the ASIC1a protein. When these three mutations were generated in hASIC1a-G212, the time course of current decay was as expected slower than in the original mutants made in hASIC1a-D212, as illustrated by the representative traces in **Figures 7C,E**. Exposure to MTSET induced however qualitatively the same effects as those observed in the original study, thus an increase of the  $I_{\text{sust}}/I_{\text{peak}}$  ratio of Q276C (**Figure 7C**), an acidic shift of the SSD pH dependence curve in E418C (**Figure 7D**), and a slowing of the current decay kinetics of N416C (**Figure 7E**).

In a study investigating ASIC1a intersubunit interactions, we had shown that among others, disulfide bond formation between E355C of one subunit and R175C of a neighboring subunit, forces the channel in a non-conducting state (Gwiazda et al., 2015). Glu355 and Arg175 are located in close proximity to residue 212 (**Figures 8A,B**). A key observation in this study was the current decrease after exposure to copper phenanthroline that promotes the formation of disulfide bonds. Here we show that the inhibition by copper phenanthroline is very similar in the R175C/E355C mutant made in the Gly212 background (**Figures 8C,D**).

In another study, we had shown that simultaneous neutralization of a high number of acidic residues in the acidic pocket induced an acidic shift of the pH dependence of

activation, but still allowed the activation of transient currents by extracellular acidification. We had concluded that the protonation events in the acidic pocket are not essential for ASIC activation, but have rather a modulatory role (Vullo et al., 2017). Here we have constructed two of these mutants, termed AcP13 (containing the mutations E97Q/E177Q/D183N/D237N/E238Q/D303N/E315Q/E321Q/H329N/E344Q/D347N/D351N/E355Q) and AcP16a (containing the mutations E97Q/E113Q/E177Q/D183N/E235Q/D237N/E238Q/D303N/E315Q/E321Q/H329N/E340Q/E344Q/D347N/D351N/E355Q) in the hASIC1a-G212 background. We show that these mutations in the Gly212 background produced current kinetics similar to those of the corresponding WT (**Figures 8E,F**), as had been observed in the original study. These mutations induced in both backgrounds an acidic shift of the pH dependence of activation (**Figures 8E,F**). These control experiments confirm that the effects of mutations investigated in these studies did not depend on the presence of a Gly or Asp residue at position 212.

In a very recent study, we have shown evidence for binding of the peptide Phe-Arg-Arg-Phe-amide, an ASIC modulator, to the palm of ASIC1a (Bargeton et al., 2019). This peptide generates a small sustained current in ASIC1a and induces an acidic shift of the pH dependence of SSD. The study was done in the background of D212. We have shown in the



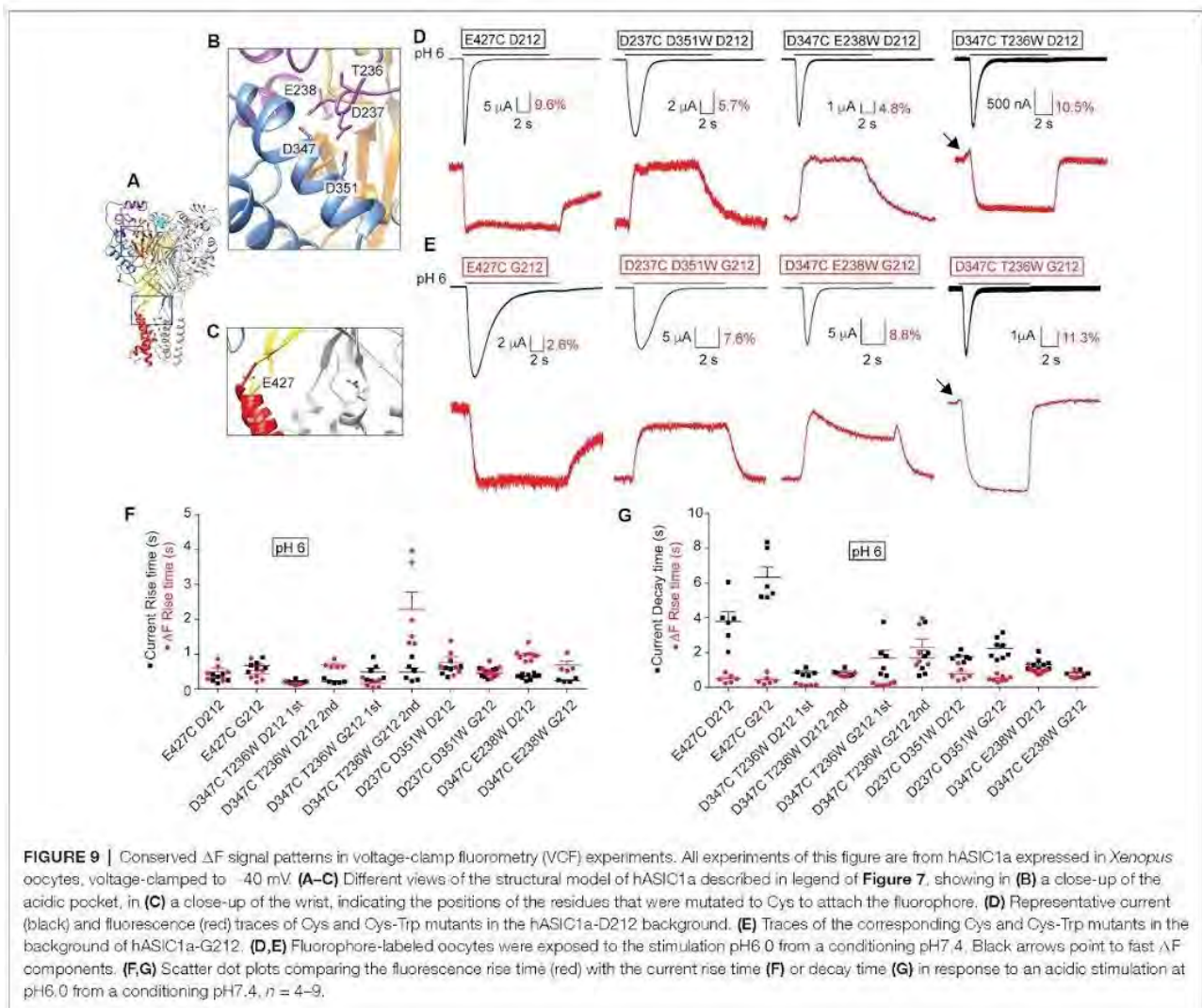
same study that this peptide induced a smaller shift of the pH dependence of SSD in hASIC1a-G212 as compared to hASIC1a-D212, but that the peptide-induced sustained current level was indistinguishable between hASIC1a-G212 and hASIC1a-D212 (Bargeton et al., 2019).

### Conservation of Voltage-Clamp Fluorometry Findings in the hASIC1a-G212 Background

We have previously used VCF to describe conformational changes in ASIC1a (Bonifacio et al., 2014; Vullo et al., 2017). In these studies, the fluorophore was attached to engineered Cys residues that had been placed in several different locations within the ASIC1a ectodomain (Figures 9A–C), and the ionic current and the fluorescence signal were simultaneously recorded, as illustrated in Figures 9D,E. One position, E427C in hASIC1a (Figure 9C), had previously been employed in mASIC1a (mASIC1a-E425C; Passero et al., 2009). The shape of the VCF signal with the fluorophore anchored at this position was highly similar in mASIC1a and in the hASIC1a-D212 (Passero et al., 2009; Bonifacio et al., 2014) and hASIC1a-G212 background (Figures 9D,E). We have determined the kinetics of the currents and fluorescence changes ( $\Delta F$ ) as rise or decay times (= time to pass from 10% to 90% of the total amplitude, or inverse).

The current rise time (black symbols) and  $\Delta F$  rise time (red) are plotted in Figure 9F, indicating for the E427C mutant in both backgrounds rapid current and  $\Delta F$  kinetics. In the G212 background, the kinetics of current appearance and decay of E427C were slower than in the D212 background [ $p < 0.01$  and  $p < 0.001$ , respectively (One-Way ANOVA followed by Tukey post-test)]. The  $\Delta F$  rise time was considerably faster than the current decay of E427C in both backgrounds (Figure 9G). To determine whether the relation between current and  $\Delta F$  kinetics in a given mutant is different between the D212 and G212 backgrounds, we have determined in each experiment the ratio of the current rise time/ $\Delta F$  rise time, and of the current decay time/ $\Delta F$  rise time. The comparison of these values showed that the relation between the current and  $\Delta F$  kinetics was not different between E427C D212 and E427C G212 (One-Way ANOVA, followed by Tukey post-test,  $p > 0.05$ ).

In our recent VCF study, we had combined the placement of a fluorophore via the introduction of a Cys residue with the insertion of a quenching group by a mutation to Trp nearby in the channel (Vullo et al., 2017). In this study, we had observed  $\Delta F$  with one or two components. We have now generated three of these mutations in the background of hASIC1a-G212. We show here that for these mutants the  $\Delta F$  pattern in both hASIC1a backgrounds is highly similar (Figures 9D,E). The quantitative analysis of the kinetics of these mutants is shown in



**Figures 9F,G.** A statistical comparison of the current/ $\Delta F$  kinetic ratios, carried out in the same way as described above for the E427C mutant, showed no significant effect of the residue at position 212 on the relation between current and  $\Delta F$  kinetics in any of these mutants.

## DISCUSSION

Several laboratories working with hASIC1a have used for many years, and are still using, a variant containing an Asp residue at the place of Gly212 as their WT clone. We found here the following differences in biophysical properties between hASIC1a-D212 and the WT hASIC1a-G212: (1) the midpoint of SSD is shifted by 0.08 pH units to more acidic values in hASIC1a-G212; (2) with the same amount of transfected DNA, hASIC1a-G212 shows  $\sim 20$ -fold higher current amplitudes, and a  $\sim 2$ -fold higher cell-surface expression than -D212; (3) the current decay kinetics are slower in

hASIC1a-G212 ( $\sim 5$ -fold at pH close to the  $pH_{1/2}$ , and  $\sim 2$ -fold at more acidic pH in whole-cell experiments). These kinetics depend on the extracellular  $Cl^-$  concentration in both channel types; the  $Cl^-$  dependence is however considerably stronger in hASIC1a-G212; and (4) the kinetics of the closed  $\rightarrow$  desensitized transition is 2-fold slower in hASIC1a-G212 as compared to -D212. Based on our observations, it is obvious that the hASIC1a-D212 clone needs to be replaced in future studies by the hASIC1a WT. Other parameters, such as the sustained current fraction and the kinetics of recovery from desensitization are not different between hASIC1a-G212 and -D212.

The higher current amplitude per amount of transfected DNA with hASIC1a-G212 should not have caused differences in the results in recombinant expression studies, since in such studies, the quantity of DNA is generally adjusted in order to obtain current amplitudes that are big enough to be detected, and small enough to allow a reliable measurement. The faster

kinetics of current decay in hASIC1a-D212 lead to a shorter window of activity than would be observed with -G212, and the small alkaline shift in the pH dependence of SSD can, under certain pH conditions, decrease the number of channels available for opening. The faster closed-desensitized transition in hASIC1a-D212 would add to this effect. Due to these differences, the functional impact of ASIC1a was somewhat underestimated in cellular studies with hASIC1a-D212.

One aim of the present work was to test whether results obtained with studies using hASIC1a-D212 as “WT” remain valid. With regard to modulation of ASIC1a function by compounds, we show here that the three tested inhibitors decrease currents of hASIC1a-D212 and -G212 in a concentration-dependent manner, with indistinguishable  $IC_{50}$  values between the two channel types in the case of amiloride and PcTx1, and with a 2-fold decreased  $IC_{50}$  value for hASIC1a-G212 in the case of Mambalgin1. GMQ leads to an acidic shift of the ASIC1a pH dependence (Alijevic and Kellenberger, 2012). This shift is observed in both ASIC1a types, it appears, however, to be smaller in hASIC1a-G212 as compared to -D212. An acidic shift of the activation pH dependence by GMQ was recently shown in rat ASIC1a, which contains a Gly at position 212 (Besson et al., 2017), further demonstrating that the existence of this shift does not depend on Asp212. The experiments with these different compounds show that qualitatively, the effects are the same in hASIC1a-G212 and -D212. Based on this analysis, we conclude that results obtained in pharmacological studies with most other compounds, or studies with modulators on hASIC1a-D212, are likely also valid if the binding site of the compound under investigation is not close to 212. There may however exist some differences in absolute  $IC_{50}$  values, as shown for Mambalgin1.

Many structure-function studies have been carried out with hASIC1a-D212. Since the pH dependence is only marginally different between hASIC1a-G212 and -D212, and the transient nature of  $H^+$ -induced currents is conserved in both hASIC1a types, we think that the presence of Asp212 should not much change the effects of other mutations. To test this interpretation, we have repeated key experiments of structure-function studies done in our laboratory in the past with hASIC1a-D212, this time with the mutants made in the Gly212 background. As expected, these mutants showed slower current decay kinetics when constructed in the hASIC1a-G212 background. The effects of the mutations observed in the hASIC1a-D212 background were however conserved in the -G212 background, indicating strongly that the conclusions of our original studies remain valid. In several studies, we had employed VCF to analyze conformational changes during channel activity (Bonifacio et al., 2014; Gwiazda et al., 2015; Vullo et al., 2017). We have now constructed four mutants used in these studies in the hASIC1a-G212 background, and have repeated the VCF experiments. We show that the pattern of the fluorescence signal and the relation between current and  $\Delta F$  kinetics are conserved, indicating that the conclusions made in the previous studies remain valid.

Given that the most striking effect of exchanging Asp and Gly at position 212 is the change in the kinetics of current

decay, we reasoned that this substitution should affect the transition from the open to the desensitized state. Gly212 is located in the  $\beta$ -ball, at a subunit interface in the proximity of the lower ends of the thumb  $\alpha$  helices  $\alpha 4$  and  $\alpha 5$ . Comparison of the crystal structures of cASIC1a in the closed, open and desensitized states indicates a substantial rearrangement of this interface in the transition from the closed to the open, but not from the open to the desensitized state (Gonzales et al., 2009; Bacongus et al., 2014; Yoder et al., 2018). Therefore, there is no obvious structural explanation for the difference in the current decay kinetics between hASIC1a-G212 and -D212.

A  $Cl^-$  binding site in close proximity of residue 212 was found in the open and desensitized but not in the closed ASIC1a structure (Jasti et al., 2007; Gonzales et al., 2009; Bacongus and Gouaux, 2012; Bacongus et al., 2014; Yoder and Gouaux, 2018; Yoder et al., 2018). It was shown that the chloride concentration affects the ASIC current decay kinetics (Kusama et al., 2010, 2013), and that mutations of the predicted  $Cl^-$  binding site disrupted the modulation of the current decay kinetics if introduced in ASIC1a (Kusama et al., 2010), and had a partial, or no effect if introduced into ASIC2a or ASIC3, respectively (Kusama et al., 2013). This indicates therefore that  $Cl^-$  likely binds to the proximity of position 212 to affect the current decay kinetics. We show here that the replacement of  $Cl^-$  by  $SCN^-$  accelerates the current decay kinetics in both, hASIC1a-D212 and -G212, but that this effect is significantly enhanced in hASIC1a-G212. Thus, the exchange of Gly and Asp at position 212 may not affect the binding of  $Cl^-$  itself, but rather its consequences on current decay kinetics. This is in line with the conclusion of the previous study, that both,  $SCN^-$  and  $Cl^-$  bind to the same binding site in ASIC1a, and that  $SCN^-$  even binds with higher affinity than  $Cl^-$ , but cannot induce a modulatory effect and therefore acts as a kind of competitive antagonist (Kusama et al., 2010).

In conclusion, we have compared the function of hASIC1a-D212, a mutant that has in many studies been used as the hASIC1a WT, with the WT hASIC1a-G212, and show that these two channels are similar in many functional aspects, including the biophysical properties, the pharmacology and the effect of mutations, but that hASIC1a-D212 has faster current decay kinetics than hASIC1a-G212.

## CONTRIBUTION TO THE FIELD STATEMENT

We have recently realized that the acid-sensing channel 1a (ASIC1a) construct that has been used as WT in studies by many laboratories is indeed a rare mutant. In the present study we have compared the functional and pharmacological properties of the mutant and the WT channel. We show that the mutant channel differs in its current kinetics and current expression from the WT. The effects of the tested pharmacological agents were however highly similar in both channel types. In the past, many structure-function studies have been carried out based on this mutant construct. We have therefore generated key mutations of previous studies in the WT background,

and have tested their effects. Our analysis shows that the effects of these mutations are conserved. Our study validates therefore the conclusions of the previous studies. Since an important part of the current understanding of the structure-function relationship and of the pharmacology of ASIC1a is based on studies using this mutant as “WT”, the validation of these studies is critical. Our results are therefore important for the field of ASIC and Epithelial Na<sup>+</sup> channel pharmacology and function, and for the structure-function relationship of these channels.

## DATA AVAILABILITY

All datasets generated for this study are included in the manuscript and/or the **Supplementary Files**.

## ETHICS STATEMENT

This study was carried out in accordance with the recommendations of Swiss federal law on animal welfare, controlled by the veterinary service of the canton de Vaud. The protocol was approved by the veterinary service of the canton de Vaud.

## REFERENCES

- Alijevic, O., Hammoud, H., Vaithia, A., Trendafilov, V., Bollenbach, M., Schmitt, M., et al. (2018). Heteroarylguanidines as allosteric modulators of ASIC1a and ASIC3 channels. *ACS Chem. Neurosci.* 9, 1357–1365. doi: 10.1021/acscchemneuro.7b00529
- Alijevic, O., and Kellenberger, S. (2012). Subtype-specific modulation of acid-sensing ion channel (ASIC) function by 2-guanidine-4-methylquinazoline. *J. Biol. Chem.* 287, 36059–36070. doi: 10.1074/jbc.M112.360487
- Babini, E., Paukert, M., Geisler, H. S., and Grunder, S. (2002). Alternative splicing and interaction with di- and polyvalent cations control the dynamic range of acid-sensing ion channel 1 (ASIC1). *J. Biol. Chem.* 277, 41597–41603. doi: 10.1074/jbc.M205877200
- Baconguis, L., Bohlen, C. I., Goehring, A., Julius, D., and Gouaux, E. (2014). X-ray structure of acid-sensing ion channel 1-snake toxin complex reveals open state of a Na<sup>+</sup>-selective channel. *Cell* 156, 717–729. doi: 10.1016/j.cell.2014.01.011
- Baconguis, L., and Gouaux, E. (2012). Structural plasticity and dynamic selectivity of acid-sensing ion channel-spider toxin complexes. *Nature* 489, 400–405. doi: 10.1038/nature11375
- Bargeton, B., Iwaszkiewicz, J., Bonifacio, G., Roy, S., Zoete, V., and Kellenberger, S. (2019). Mutations in the palm domain disrupt modulation of acid-sensing ion channel 1a currents by neuropeptides. *Sci. Rep.* 9:2599. doi: 10.1038/s41598-018-37426-5
- Baron, A., and Lingueglia, E. (2015). Pharmacology of acid-sensing ion channels—physiological and therapeutic perspectives. *Neuropharmacology* 94, 19–35. doi: 10.1016/j.neuropharm.2015.01.005
- Bartoi, T., Augustinowski, K., Polleitchner, G., Gründer, S., and Ulbrich, M. H. (2014). Acid-sensing ion channel (ASIC) 1a/2a heteromers have a flexible 2:1/1:2 stoichiometry. *Proc. Natl. Acad. Sci. U S A* 111, 8281–8286. doi: 10.1073/pnas.1324060111
- Bers, D. M., Patton, C. W., and Nuccitelli, R. (2010). A practical guide to the preparation of Ca<sup>2+</sup> buffers. *Methods Cell Biol.* 99, 1–26. doi: 10.1016/B978-0-12-374841-6.00001-3
- Besson, T., Lingueglia, E., and Salinas, M. (2017). Pharmacological modulation of acid-sensing ion channels 1a and 3 by amiloride and

## AUTHOR CONTRIBUTIONS

All authors designed together the project. AV, SV and ZP carried out the experiments. AV, SV, ZP, OA and SK wrote the manuscript.

## FUNDING

This research was supported by the Swiss National Science Foundation (Schweizerischer Nationalfonds zur Förderung der Wissenschaftlichen Forschung) grant 31003A\_172968 to SK.

## ACKNOWLEDGMENTS

We thank Nicolas Ambrosio for carrying out some experiments. We thank Miguel van Bemmelen, Olivier Staub, Olivier Bignucolo, Laurent Schild, Niklaus Johnner and Simon Bernèche for comments on the manuscript.

## SUPPLEMENTARY MATERIAL

The Supplementary Material for this article can be found online at: <https://www.frontiersin.org/articles/10.3389/fnmol.2019.00133/full#supplementary-material>

- 2-guanidine-4-methylquinazoline (GMQ). *Neuropharmacology* 125, 429–440. doi: 10.1016/j.neuropharm.2017.08.004
- Blanchard, M. G., and Kellenberger, S. (2011). Effect of a temperature increase in the non-noxious range on proton-evoked ASIC and TRPV1 activity. *Pflugers Arch.* 461, 123–139. doi: 10.1007/s00424-010-0884-3
- Bonifacio, G., Lelli, C. L., and Kellenberger, S. (2014). Protonation controls ASIC1a activity *via* coordinated movements in multiple domains. *J. Gen. Physiol.* 143, 105–118. doi: 10.1085/jgp.201311053
- Chen, X., Qiu, L., Li, M., Durrnagel, S., Orser, B. A., Xiong, Z. G., et al. (2010). Diarylamidines: high potency inhibitors of acid-sensing ion channels. *Neuropharmacology* 58, 1045–1053. doi: 10.1085/jgp.201311053
- Dawson, R. J., Benz, J., Stohler, P., Tetaz, T., Joseph, C., Huber, S., et al. (2012). Structure of the acid-sensing ion channel 1 in complex with the gating modifier Psalmotoxin 1. *Nat. Commun.* 3:936. doi: 10.1038/ncomms1917
- Deval, E., Baron, A., Lingueglia, E., Mazarguil, H., Zajac, J. M., and Lazdunski, M. (2003). Effects of neuropeptide SF and related peptides on acid sensing ion channel 3 and sensory neuron excitability. *Neuropharmacology* 44, 662–671. doi: 10.1016/s0028-3908(03)00047-9
- García-Añoveros, J., Derfler, B., Neville-Golden, J., Hyman, B. T., and Corey, D. P. (1997). BNaC1 and BNaC2 constitute a new family of human neuronal sodium channels related to degenerins and epithelial sodium channels. *Proc. Natl. Acad. Sci. U S A* 94, 1459–1464. doi: 10.1073/pnas.94.4.1459
- Gonzales, E. B., Kawate, T., and Gouaux, E. (2009). Pore architecture and ion sites in acid-sensing ion channels and P2X receptors. *Nature* 460, 599–604. doi: 10.1038/nature08218
- Grunder, S., and Pusch, M. (2015). Biophysical properties of acid-sensing ion channels (ASICs). *Neuropharmacology* 94, 9–18. doi: 10.1016/j.neuropharm.2014.12.016
- Gwiazda, K., Bonifacio, G., Vullo, S., and Kellenberger, S. (2015). Extracellular subunit interactions control transitions between functional states of acid-sensing ion channel 1a. *J. Biol. Chem.* 290, 17956–17966. doi: 10.1074/jbc.M115.641688
- Jasti, J., Furukawa, H., Gonzales, E. B., and Gouaux, E. (2007). Structure of acid-sensing ion channel 1 at 1.9 Å resolution and low pH. *Nature* 449, 316–323. doi: 10.1038/nature06163
- Jiang, R. T., Martz, A., Gonin, S., Taly, A., de Carvalho, L. P., and Grutter, T. (2010). A putative extracellular salt bridge at the subunit interface contributes

- to the ion channel function of the ATP-gated P2X2 receptor. *J. Biol. Chem.* 285, 15805–15815. doi: 10.1074/jbc.m110.101980
- Joeres, N., Augustinowski, K., Neuhoef, A., Assmann, M., and Grunder, S. (2016). Functional and pharmacological characterization of two different ASIC1a/2a heteromers reveals their sensitivity to the spider toxin PcTx1. *Sci. Rep.* 6:27647. doi: 10.1038/srep27647
- Kellenberger, S., and Schild, L. (2015). International union of basic and clinical pharmacology: XCl. Structure, function, and pharmacology of acid-sensing ion channels and the epithelial Na<sup>+</sup> channel. *Pharmacol. Rev.* 67, 1–35. doi: 10.1124/pr.114.009225
- Kusama, N., Gautam, M., Harding, A. M., Snyder, P. M., and Benson, C. J. (2013). Acid-sensing ion channels (ASICs) are differentially modulated by anions dependent on their subunit composition. *Am. J. Physiol. Cell Physiol.* 304, C89–C101. doi: 10.1152/ajpcell.00216.2012
- Kusama, N., Harding, A. M., and Benson, C. J. (2010). Extracellular chloride modulates the desensitization kinetics of acid-sensing ion channel 1a (ASIC1a). *J. Biol. Chem.* 285, 17425–17431. doi: 10.1074/jbc.m109.091561
- Lek, M., Karczewski, K. J., Minikel, E. V., Samocha, K. E., Banks, E., Fennell, T., et al. (2016). Analysis of protein-coding genetic variation in 60,706 humans. *Nature* 536, 285–291. doi: 10.1038/nature19057
- Liechti, L. A., Berneche, S., Bargeton, B., Iwaszkiewicz, J., Roy, S., Michielin, O., et al. (2010). A combined computational and functional approach identifies new residues involved in pH-dependent gating of ASIC1a. *J. Biol. Chem.* 285, 16315–16329. doi: 10.1074/jbc.m109.092015
- Passero, C. J., Okumura, S., and Carattino, M. D. (2009). Conformational changes associated with proton-dependent gating of ASIC1a. *J. Biol. Chem.* 284, 36473–36481. doi: 10.1074/jbc.m109.055418
- Poirot, O., Vukicevic, M., Boesch, A., and Kellenberger, S. (2004). Selective regulation of acid-sensing ion channel 1 by serine proteases. *J. Biol. Chem.* 279, 38448–38457. doi: 10.1074/jbc.m407381200
- Rash, L. D. (2017). Acid-sensing ion channel pharmacology, past, present, and future. *Adv. Pharmacol.* 79, 35–66. doi: 10.1016/bs.apha.2017.02.001
- Roy, S., Boiteux, C., Alijevic, O., Liang, C., Bernèche, S., and Kellenberger, S. (2013). Molecular determinants of desensitization in an ENaC/degnerin channel. *FASEB J.* 27, 5034–5045. doi: 10.1096/fj.13-230680
- Vukicevic, M., and Kellenberger, S. (2004). Modulatory effects of acid-sensing ion channels on action potential generation in hippocampal neurons. *Am. J. Physiol. Cell Physiol.* 287, C682–C690. doi: 10.1152/ajpcell.00127.2004
- Vullo, S., Bonifacio, G., Roy, S., Johnner, N., Berneche, S., and Kellenberger, S. (2017). Conformational dynamics and role of the acidic pocket in ASIC pH-dependent gating. *Proc. Natl. Acad. Sci. U S A* 114, 3768–3773. doi: 10.1073/pnas.1620560114
- Waldmann, R., Champigny, G., Bassilana, F., Heurteaux, C., and Lazdunski, M. (1997). A proton-gated cation channel involved in acid-sensing. *Nature* 386, 173–177. doi: 10.1038/386173a0
- Wemmie, J. A., Taugher, R. J., and Kreple, C. J. (2013). Acid-sensing ion channels in pain and disease. *Nat. Rev. Neurosci.* 14, 461–471. doi: 10.1038/nrn3529
- Yang, L., and Palmer, L. G. (2014). Ion conduction and selectivity in acid-sensing ion channel 1. *J. Gen. Physiol.* 144, 245–255. doi: 10.1085/jgp.201411220
- Yoder, N., and Gouaux, E. (2018). Divalent cation and chloride ion sites of chicken acid sensing ion channel 1a elucidated by x-ray crystallography. *PLoS One* 13:e0202134. doi: 10.1371/journal.pone.0202134
- Yoder, N., Yoshioka, C., and Gouaux, E. (2018). Gating mechanisms of acid-sensing ion channels. *Nature* 555, 397–401. doi: 10.1038/nature25782
- Yu, Y., Chen, Z., Li, W. G., Cao, H., Feng, E. G., Yu, F., et al. (2010). A nonproton ligand sensor in the acid-sensing ion channel. *Neuron* 68, 61–72. doi: 10.1016/j.neuron.2010.09.001
- Zhang, P., and Canessa, C. M. (2002). Single channel properties of rat acid-sensitive ion channel-1  $\alpha$ -, 2a, and -3 expressed in *Xenopus oocytes*. *J. Gen. Physiol.* 120, 553–566. doi: 10.1085/jgp.20028574

**Conflict of Interest Statement:** The authors declare that the research was conducted in the absence of any commercial or financial relationships that could be construed as a potential conflict of interest.

Copyright © 2019 Vaithia, Vullo, Peng, Alijevic and Kellenberger. This is an open-access article distributed under the terms of the Creative Commons Attribution License (CC BY). The use, distribution or reproduction in other forums is permitted, provided the original author(s) and the copyright owner(s) are credited and that the original publication in this journal is cited, in accordance with accepted academic practice. No use, distribution or reproduction is permitted which does not comply with these terms.

### 5.3. Project 3: Investigation of the activation mechanism of human ASIC1a channel by using cross-linkers

**Prepared manuscript for publication:** Probing conformational changes during activation of ASIC1a by an optical tweezer and methanethiosulfonate-based cross-linkers

**Authors:** Anand Vaithia and Stephan Kellenberger

Acid-sensing ion channels (ASICs) are proton-gated voltage-insensitive Na<sup>+</sup> channel, primarily activated by protons that initiate the conformational change towards the channel opening. A functional ASICs are formed by homo- or heterotrimeric assembly of ASIC subunits. ASICs contain a large extracellular domain composed of domains namely finger, knuckle,  $\beta$ -ball, thumb and palm connected to the intracellular domain through the transmembrane domain. Activation of ASIC by protons comprises of conformational changes that are not completely identified. It is believed that conformational changes occurring in the extracellular domains are passed to the transmembrane domain leading to ion flow into the pore. To further explore the activation mechanism, two cross-linking approaches were applied, the optical tweezer BMA and MTS reagents. In the first approach, by application of light on BMA tethered to ASIC1a mutants, it was found that I428C from TM2 domain can undergo light-dependent activation without the formation of cross-link with adjacent subunit. No other mutants from TM domain or extracellular domains produced light-dependent channel activation. Application of light produced a modulatory effect in some mutants of hASIC1a-E97C/D437C, -G430C, -D237C/E315C, -D237C/E355C and -K246C/D347C. In the second approach, using MTS cross-linkers, three mutants, hASIC1a-T236C/D351C, -D237C/I312C and -D237C/E315C showed stronger effects with cross-linker compared to monovalent MTS reagents. Uniquely, the effect on D327C/I312C by MTS-17-MTS could not be explained by the sum of the effects on the single mutant D237C and I312C, therefore suggesting a cross-linking may occur. Further analysis is required to assess the cross-linking to understand the structural aspect associated with channel function.

### **5.3.1. My contribution to the article**

In this project, I did all the molecular biology work necessary for the generation of various mutants for cell and oocyte expression system. For optical tweezer approach, I have developed the optical system assembly coupled to the patch-clamp setup to imitate the working conditions. In both approaches, all the experiments were performed by me. I have also contributed to making figures, data analysis and writing the final draft of the manuscript.

## **Probing conformational changes during activation of ASIC1a by an optical tweezer and methanethiosulfonate-based cross-linkers**

Anand Vaithia<sup>1</sup> and Stephan Kellenberger<sup>1\*</sup>

*<sup>1</sup>Department of Biomedical Sciences, University of Lausanne, Rue du Bugnon 27, 1011 Lausanne, Switzerland*

\* Corresponding author: Dr. Stephan Kellenberger, Department of Biomedical Sciences, University of Lausanne, Rue du Bugnon 27, CH-1011 Lausanne, Switzerland; [Stephan.kellenberger@unil.ch](mailto:Stephan.kellenberger@unil.ch); Phone : +41 21 692 5422, Fax: +41 21 692 5355.

### **ABSTRACT**

Acid-sensing ion channels (ASICs) are proton-gated, Na<sup>+</sup>-selective ion channels that are expressed in the central and peripheral nervous system. They are involved in various physiological and pathological processes such as neurodegeneration after stroke, pain sensation, fear behavior and learning. In this study we attempted to impose distance constraints between pairs of residues in different channel domains and to measure how this affected channel function, in order to obtain structural information on the activation mechanism. Optical tweezers such as 4'-Bis(maleimido)azobenzene (BMA) change their conformation depending on the wavelength of applied light. After exposure of channel mutants to BMA, an activation of the channel by light was observed with the previously reported mutant ASIC1a-I428C, but not for any other tested mutant of a series of mutants localized in proximity of the extracellular pore entry and in different parts of the extracellular domain. Western blot analysis indicated however that BMA did not cross-link two subunits in the I428C mutant, thus the observed activation was not due to a force exerted between the I428C residues of adjacent subunits. For some extracellular domain mutants, D237C/E315C, D237C/E355C and K246C/D347C, application of light modulated the pH dependence. In a second approach, methanethiosulfonate (MTS) cross-linker reagents of different lengths, when applied to ASIC1a Cys mutants,

changed the pH dependence of many of them. In three double mutants, D237C/I312C, T236C/D351C and D237C/E315C, the functional effect of cross-linkers was stronger than that of monovalent MTS reagents of similar size, suggesting that a cross-linking occurred. When cross-linkers were applied to these double mutants and to the corresponding single mutants, the effects on the single mutants considerably different between single and double mutants in one pair, D237C/I312C, suggesting therefore that the observed acidic shift in the pH dependence was due to a cross-link between the engineered Cys residues.

**Keywords:** ASIC1a, 4'-Bis(maleimido)azobenzene (BMA), MTS cross-linker, activation mechanism, optical tweezer

## INTRODUCTION

Acid-sensing ion channels (ASICs) are proton-gated voltage-independent Na<sup>+</sup>-selective ion channels that belong to Epithelial Na<sup>+</sup> Channel/Degenerin superfamily of ion channels. In rodents, 6 homologous ASIC subunits, ASIC1a, -1b, -2a, -2b, -3 and -4 have been identified. Homotrimeric or heterotrimeric assembly of ASIC subunits results in channels with different pH sensitivity, and activation and desensitization kinetics (Kellenberger and Schild 2002, Hesselager, Timmermann et al. 2004). ASIC1a, -2a, -2b and -4 are expressed in the CNS, and all ASICs except ASIC4 are expressed in the PNS (Wemmie, Taugher et al. 2013, Kellenberger and Schild 2015). ASICs are involved in various pathological and physiological functions, such as learning and memory, anxiety and fear (Wemmie, Taugher et al. 2013), neurodegeneration after ischemic stroke (Xiong, Zhu et al. 2004), seizure termination (Ziemann, Schnizler et al. 2008) and pain sensation (Price, McIlwrath et al. 2001, Deval, Noel et al. 2008). The channel exists in three different functional states, closed, open and desensitized (Wemmie, Taugher et al. 2013, Grunder and Pusch 2015, Kellenberger and Schild 2015). Extracellular acidification results in rapid ASIC activation, producing an inward current that is transient and decays when the channel enters the non-conducting desensitized state. High-resolution structures of chicken

ASIC1a in closed, toxin-opened and desensitized conformations (Jasti, Furukawa et al. 2007, Gonzales, Kawate et al. 2009, Dawson, Benz et al. 2012, Bacongus, Bohlen et al. 2014, Yoder, Yoshioka et al. 2018, Yoder and Gouaux 2020) and of human ASIC1a in the closed state (Sun, Liu et al. 2020) have been published and indicate that ASICs are trimers. The structure of a single ASIC subunit has been compared to the shape of a hand holding a small ball (**Figure 1A**), with the two transmembrane domains corresponding to the forearm (Jasti, Furukawa et al. 2007). The extracellular sub-domains were named accordingly as palm, finger, knuckle, thumb and  $\beta$ -ball. In each subunit, the finger, thumb and  $\beta$ -ball enclose together with the palm of a neighboring subunit a vestibule that is called acidic pocket because it contains several acidic amino acid residues. The wrist is a flexible region just above the pore entry. Structural comparison of the closed and open state indicates that during channel activation the acidic pocket collapses, the channel gate opens and the extracellular fenestrations are expanded (Yoder, Yoshioka et al. 2018). During desensitization, the lower palm domains collapse towards the central vertical axis and the transmembrane helices relax back to resting-like conformation leading to a closed pore (Gonzales, Kawate et al. 2009, Roy, Boiteux et al. 2013, Bacongus, Bohlen et al. 2014, Yoder, Yoshioka et al. 2018).

The structures have so far not identified the residues that are critical for channel activation. Several studies performed mutational analysis and identified residues of the extracellular domain that are likely involved in channel activation since their mutation resulted in a changed pH dependence (Smith, Zhang et al. 2007, Paukert, Chen et al. 2008, Li, Yang et al. 2010, Liechti, Berneche et al. 2010, Krauson, Rued et al. 2013, Schuhmacher, Srivats et al. 2015, Lynagh, Mikhaleva et al. 2018). The observation that simultaneous mutation of all acidic amino acid residues of the acidic pocket resulted in channels that were still activated by acidification, suggests that protonation of acidic pocket residues is not required for ASIC activation (Vullo, Bonifacio et al. 2017).

This study aimed at identifying conformational changes that are involved in ASIC1a activation. To this end, Cys mutants of human ASIC1a (hASIC1a) were exposed to two different types of cross-linkers. These single or double mutants had been designed to contain Cys residues at distances that matched the length of the cross-linkers. First, the optical tweezer, bis(maleimido)azobenzene (BMA), that can be switched by light of different wavelengths between an extended (trans) and a folded (cis) conformation, was used with the aim of opening ASIC1a by light (Fig. 1B). Secondly, bis-methane-thiosulfonate (MTS) cross-linkers of different length matching the distance between engineered Cys residue in ASIC1a mutants were administered with the aim of locking the channel in specific functional states. BMA and light activated the mutant I428C, as published previously, but no other tested mutant. We show that the activation of I428C occurred without cross-linking I428C of adjacent subunits. The MTS cross-linkers affected the pH dependence of many of the tested mutants, but in most cases without inducing a cross-link, providing thus not the expected structural information.

## RESULTS

### Light-activated current in ASIC1a

In a recent study it was shown that exposure of the mutants I428C and G430C of hASIC1a to BMA allowed the activation of the channel by light (Browne, Nunes et al. 2014). In the present study, we intended to use this approach at different positions of ASIC1a to probe for conformational changes involved in ASIC activation. As controls, activation of the two mutants I428C and G430C was investigated in the first set of experiments. The structural models indicated an intersubunit distance between Ile428 residues (measured between the  $\beta$ -carbon atoms, [ $\alpha$  for Gly]) of 21.3Å in the closed and 28.4Å in the open state; for Gly430 the corresponding distances were 9.5Å and 16.6Å, respectively (**Table S1**). These residues are located at the top of the TM2, in the extracellular pore entry, with Ile428 pointing towards the outside, and Gly430 towards the adjacent subunit in the open conformation (**Figure 1C**). The

end-to-end length of BMA is 13Å in the *cis*, and 22 Å in the *trans* configuration. Both the configuration is represented in **Figure 1B**. The I428C and G430C mutants were expressed separately in CHO cells, and cells were incubated with 10µM BMA for 12 min in the dark immediately before testing in whole-cell patch-clamp for two possible ways of activation, extracellular acidification and illumination with light of 440nm wavelength. The 440nm light induces the *trans* conformation of BMA. Changing the extracellular pH from 7.4 to 5.0 induced transient inward currents, as shown for I428C in Figure 1D (left trace). The pH of half-maximal activation (pH50) of I428C was  $6.46 \pm 0.03$  (n=7). Application of 440nm light for 5s to I428C induced inward currents containing a transient and a sustained component (**Figure 1D**, right), that had however smaller amplitudes than the pH5-induced currents (**Figure 1E**). Switching from 440nm to 360nm light for 0.1s brought the current back to the baseline (**Figure 1D**), due to induction of the *cis* conformation of BMA and likely subsequent deactivation. Channel activation occurred rapidly with both ways of activation, with time constants of  $\tau=48 \pm 16$ ms (440nm light) and  $\tau=106 \pm 24$ ms (pH5). In control experiments with cells expressing ASIC1a wild type (WT) that were exposed during 12min to 10µM BMA, 440 nm light did not induce any current (n=7), while the pH5-induced current amplitude was  $-4.2 \pm 1.1$ nA (n=7). In contrast to a previous study (Browne, Nunes et al. 2014), we were not able to induce current with 440nm light in the G430C mutant. The pH5-induced current amplitude in G430C-transfected cells was  $-5.2 \pm 1.1$ nA (n=7), indicating a normal expression of the mutant channels. Mutations homologous to ASIC1a-I428C and -G430C were also introduced in rat ASIC1b (I413C and G415C), human ASIC2a (V425C and A427C) and rat ASIC3 (V433C and E435C) and it was tested whether 440 nm light-induced currents after exposure to BMA. However, only pH-induced currents were observed in these mutants (data not shown).

### Characterization of light-activated current in ASIC1a I428C

It was then tested how the conditions of the BMA incubation affected the amplitude of the light-induced current of I428C. Varying the duration of the incubation with 10 $\mu$ M BMA between 12 and 20 min did not affect the current amplitude (**Figure 2A**). Also, there was no significant effect of the BMA concentration on the current amplitude when tested on an incubation duration of 20 min (**Figure 2B**), and in many experiments the amplitude of the light-induced current was very low (Figure 2A-B). Light-induced currents were generally only found in ~20-40% of the measured cells, if amplitudes >20pA were considered (**Figure 2C**). After incubation with 40 $\mu$ M BMA, the cells seemed in many cases to be stressed. The pH5-induced current amplitude was compared between the cells expressing light-induced currents and cells producing no light-induced current. The mean difference was significantly different only under 10 $\mu$ M BMA ( $-3.65 \pm 1.38$ nA, n=9-17,  $p < 0.05$ ) and not under 20 $\mu$ M ( $-1.32 \pm 1.45$ nA, n=8-16) and 40 $\mu$ M ( $-3.1 \pm 1.5$ nA, n=6-23) (Two-way ANOVA, Sidak's *post-hoc* test) (**Figure 2D**). The transient ASIC currents are Na<sup>+</sup>-selective, and ASICs are not permeable to the large cation NMDG. To further confirm that the light-induced current is mediated by the expressed ASIC1a channels, Na<sup>+</sup>, which is the main monovalent cation of the extracellular solution (*Methods*) was replaced with NMDG, resulting in a reversible loss of 440 nm light-induced current (**Figure 2E**, n=7, One-way ANOVA, Sidak's *post-hoc* test). If ASIC1a-I428C was repeatedly activated by 440 nm light, the current amplitude was increased at the second application relative to the first and showed then a rundown. This rundown did not depend on the interval between the applications of the light pulse (**Figure 2F and 2G**, n=3-6, Mixed effect One-way ANOVA, Dunnett *post-hoc* test).

### No BMA-mediated light-activated currents in mutants from different ASIC1a domains

Residues for mutations were chosen in domains that are known to be involved in activation or that seemed to be of interest based on the structure. To be able to react with BMA

on its both ends, the distance between two engineered Cys residues, either in the same or in adjacent subunits, were selected based on the end-to-end distances measured between the  $\beta$ -carbon atoms ( $\alpha$  for Gly residues), in order to match approximately the length of BMA in the *cis* or *trans* conformation. In pre-selected residues, this distance was compared in structural models of the closed, open and desensitized state, in order to select mutants in which it changed during activity. Selected double mutants are shown in **Figure 3A** and single mutants in **Figure 3B**. A list of these mutants, with indication of the distances, is shown in **Table S1**. All mutants were expressed in CHO cells and they produced normal current amplitudes. In the selected double mutants, the distances are compatible with cross-linking by BMA within the same subunit. Cross-linking with BMA was assessed by measuring the light-induced current. All mutants listed in **Table S1** were exposed to 440nm and 360nm light. However, none of the mutants except I428C produced detectable light-induced currents. Representative current traces of selected ASIC1a mutants, the double mutant E97C/V354C from the acidic pocket, and the single mutants T419C from lower palm and Y67C from TM1 are shown in **Figure 3C**.

### **Modulation of ASIC1a mutant currents by light**

Since light-induced currents were not observed in any mutant other than I428C, it was tested whether attaching of BMA to these engineered Cys residues, followed by applying 360 or 440nm light could modulate the pH-induced current of these channels. The ratio of  $I_{pH6.x}/I_{pH5}$  (with pH6.x being a pH that induced 30-60% of the maximal current amplitude in each mutant) was measured in the absence and presence of 440nm light to determine if the pH dependence of activation was affected by BMA binding and subsequent light application. Representative current traces of T419C in the absence and presence of 440nm light are shown in **Figure 4A**. The analysis indicates that this ratio was not affected by 440nm light in WT and any of the mutants (**Figure 4B and 4C**, Ordinary one-way ANOVA, Dunnett's *post-hoc* test). The mean difference in the ratio of  $I_{pH6.x}/I_{pH5}$  ratios obtained in the presence and absence of

440nm light are plotted and compared to that of the WT in **Figure 4D and 4E**, confirming the absence of a difference to the WT (One-way ANOVA, Dunnett's *post-hoc* test) in all mutants, except for E97C/D347C ( $-1.18 \pm 0.34$ ,  $n=4-7$ ,  $p < 0.05$ ). The ratio of the peak amplitudes  $I_{pH5_{440nm}}/I_{pH5_{ctrl}}$  indicated a decrease of the  $I_{pH5}$  amplitude in the WT and in many mutants, but no significant difference was observed between the WT and any mutant (**Figure 4F and 4G**, Ordinary one-way ANOVA, Dunnett's *post-hoc* test).

The same measurements as described above for 440nm light were then carried out with 360nm light. The application of 360nm light produced a modulatory effect by BMA on mutants G430C ( $0.23 \pm 0.04$ ,  $n=4$ ,  $p=0.01$ ), D237C/E315C ( $0.13 \pm 0.02$ ,  $n=4$ ,  $p < 0.006$ ), D237C/E355C ( $0.15 \pm 0.02$ ,  $n=4$ ,  $p=0.005$ ), and K246C/D347C ( $-0.11 \pm 0.03$ ,  $n=4$ ,  $p=0.05$ ). A significant difference was observed in the mean of  $I_{pH6.x}/I_{pH5}$  ratio under the presence and absence of light and indicated above for each mutant (**Figure 5A and 5B**, paired t-test (two-tailed)). The mean difference in the ratio of  $I_{pH6.x}/I_{pH5}$  ratios in the absence and presence of 360nm light showed some variability between mutants however, none was different from that of the WT (**Figure 5C and 5D**, Ordinary one-way ANOVA, Dunnett's *post-hoc* test). The ratio of the peak amplitude  $I_{pH5}$  under the presence and absence of 360nm indicated a significant difference in the WT ( $p < 0.5$ , paired t-test (two-tailed)) and a decrease of the  $I_{pH5_{360nm}}/I_{pH5_{ctrl}}$  amplitude in several mutants to the WT (**Figure 5E and 5F**, Ordinary one-way ANOVA, Dunnett's *post-hoc* test).

#### **No evidence for BMA cross-linking of the I428C mutant**

BMA is a cross-linker, and presumably it links in the I428C mutant the engineered Cys residues at position 428 of two adjacent subunits (Browne, Nunes et al. 2014). It has however also been shown in many studies that monovalent sulfhydryl reagents can change ASIC function (Tolino, Okumura et al. 2011, Roy, Boiteux et al. 2013, Bonifacio, Lelli et al. 2014, Gautschi, van Bemmelen et al. 2017). It was therefore tested biochemically in ASIC1a WT and

the two mutants I428C and G430C whether BMA cross-links two subunits. As in the patch-clamp experiments, cells expressing these ASICs were labeled with 20 $\mu$ M BMA for 20min in the dark. Cell surface proteins were labeled with biotin, and cells were lysed. The extracted biotinylated surface proteins were separated on SDS-PAGE and detected using an ASIC1 antibody on the western blot whose specificity had been demonstrated (Wemmie, Askwith et al. 2003). Monomeric ASIC1a WT or mutant bands were obtained at ~70kDa and dimer bands were obtained at ~130kDa (**Figure 6A**). Comparison of the dimer to monomer band intensity ratio under control and 20 $\mu$ M BMA treatment displayed no significant difference between control and treatment conditions (**Figure 6B**). The analysis was further extended to mutants in the TM2 domain and experiments were performed once in those mutants to detect cross-link. This indicative analysis shows that in all mutants tested; BMA did not form a cross-link (n=1) (**Figure S2**). For the mutants in the extracellular domain, western blot analysis to detect cross-link was not performed since the double mutations are introduced in the same domain, and thus a cross-linking would not link two subunits and double the apparent mass.

### **Modulation of H<sup>+</sup>-activated currents by MTS cross-linkers**

As an alternative approach to BMA, MTS cross-linkers were then used. MTS cross-linkers were selected based on their length (**Table S2**) to match the distance measured between the  $\beta$ -carbon atoms ( $\alpha$  for Gly) in one of the functional states of the mutants (**Table S1**), as indicated in Table 2. Successful cross-linking was expected to impose the distance of the cross-linker between the residue pair of the mutant and may therefore force the channel into the conformation that best matches the imposed distance between the two residues. Since many studies have shown that monovalent MTS reagents can affect ASIC function (Pfister, Gautschi et al. 2006, Tolino, Okumura et al. 2011, Frey, Pavlovicz et al. 2013, Gautschi, van Bemmelen et al. 2017), the effects of cross-linkers were compared of the effects of a monovalent MTS reagent of similar size.

The analysis with MTS cross-linkers was performed on the same mutants to which BMA had been applied, except for E63C, as its distances did not match the length of MTS-cross-linkers, I137C/K396C and I137C/E403C, because these mutants did not show any effect in experiments with BMA, and D237C/F257C, since no H<sup>+</sup>-induced current was detected after injection of D237C/F257C cRNA. Each mutant was tested with one or several MTS-cross-linkers that fit the distance between the two involved residues in the closed and the open state, and it was assumed that an effective cross-link would alter the channel function. For each mutant, the ASIC current was measured at two different pH values before and after modification by the cross-linker (3-min exposure at 1mM), pH6.x that induced 30-60% of the maximal current amplitude under control conditions, and pH5 for the maximal current amplitude. The current amplitude induced by pH5, and the I<sub>pH6.x</sub>/I<sub>pH5</sub> ratio was then compared between the control and the cross-link condition. If an MTS-cross-linker significantly affected the function of a given mutant, the same experiment was repeated with a monovalent MTS reagent of similar size (**Figure 7**). If the I<sub>pH6.x</sub>/I<sub>pH5</sub> ratio was smaller with the MTS-cross-linker when compared to the corresponding monovalent MTS reagent, and thus the effect of the cross-linker was greater than that of the monovalent compound, it suggested that the difference may be due to the cross-linking of two Cys residues. The (I<sub>pH6.x</sub><sub>MTS</sub>/I<sub>pH5</sub><sub>MTS</sub>)/(I<sub>pH6.x</sub><sub>Ctrl</sub>/I<sub>pH5</sub><sub>Ctrl</sub>) ratio with MTS cross-linkers for mutant D237C/I312C (MTS-17-MTS: 0.31±0.05, n=6), T236C/D351C (MTS-11-MTS:0.20±0.06, n=6) and D237C/E315C (MTS-14-MTS:0.21±0.04,n=4) was smaller than treatment with monovalent MTS reagent for D237C/I312C (MTS-PEO<sub>3</sub>-Biotin: 0.42±0.03, n=6), T236C/D351C (MTSEA-Biotin: 0.33±0.06, n=5) and D237C/E315C (MTS-PEO<sub>3</sub>-Biotin: 0.67±0.04, n=4) however, statistical test (unpaired t-test (two-tailed)) indicated no significant difference.

In control experiments, the ratio of the IpH6.4/IpH5 ratio after MTS exposure / control ( $\text{IpH6.4}_{\text{MTS}}/\text{IpH5}_{\text{MTS}}/ \text{IpH6.4}_{\text{Ctrl}}/\text{IpH5}_{\text{Ctrl}}$ ) was determined with ASIC1a WT for several compounds, showing no effect ( $\text{IpH6.4}_{\text{MTS}}/\text{IpH5}_{\text{MTS}}/ \text{IpH6.4}_{\text{Ctrl}}/\text{IpH5}_{\text{Ctrl}}$  ratios of  $1.09 \pm 0.1$ ,  $n=4$  (MTS-2-MTS),  $0.69 \pm 0.08$ ,  $n=3$  (MTS-4-MTS),  $0.85 \pm 0.06$ ,  $n=4$  (MTS-6-MTS),  $1.01 \pm 0.17$ ,  $n=4$  (MTS-11-MTS),  $1.03 \pm 0.08$ ,  $n=4$ , (MTS-14-MTS), and  $0.91 \pm 0.04$ ,  $n=4$ , (MTS-17-MTS); ordinary one-way ANOVA, Tukey *post-hoc* test).

In parallel, the effect of the MTS reagents on the IpH5 was analyzed. In many mutants, a significant decrease in IpH5 was observed. An increased IpH5 current was observed in H72C with MTS-PEO<sub>3</sub>-Biotin and E97C/E355C with MTSEA-Biotin (paired t-test) (**Figure 8**).

For the three promising double mutants and the corresponding single mutants, the IpH6.x/IpH5 ratio was determined, and the pH dependence of activation was measured under control conditions and after exposure to the MTS cross-linker, as illustrated in **Figures 9A-B** for I312C. The ratio of IpH6.x/IpH5 and the pH<sub>50</sub> of activation are plotted for each double mutant besides the corresponding values of the single mutants in **Figures 9C-H**. If cross-linking was responsible for the functional effect of a cross-linker, we would expect a small effect in each of the two single mutants, and a larger effect in the double mutant. Of the three double mutants, such a pattern is only observed for the mutant D237C/I312C. **Table 1** summarizes the shift in the pH dependence of activation and the change in maximal amplitude upon reagent exposure of the three double mutants and the corresponding single mutants. The pH<sub>50</sub> of activation was shifted by the reagent MTS-17-MTS to more acidic values in the double mutant D237C/I312C and the single mutant D237C, and to more alkaline values in I312C. The shift showed a tendency of being smaller in the single as compared to the double mutant. Therefore, it may be possible that the MTS-17-MTS-induced shift is due to a cross-link between D237C and I312C (**Figure 9I**).

## DISCUSSION

In this study we used cross-linking compounds on ASIC1a to detect conformational changes involved in channel activation. We show that hASIC1a-I428C that has reacted with the optical tweezer BMA can be activated by light, and that this does not involve a cross-linking between I428C of adjacent subunits. None of the other tested mutants containing single or double Cys mutations in the wrist or the acidic pocket was activated by light after exposure to BMA. In many of these mutants, MTS cross-linkers and monovalent MTS reagents changed the pH dependence. In three double mutants of the acidic pocket, cross-linkers induced stronger changes in pH dependence than the monovalent reagents. Analysis of the pH dependence of activation of these double mutants and the corresponding single mutants showed that MTS-17-MTS produced an acidic shift in D327C/I312C ( $0.25 \pm 0.15$ ,  $n=3$ ,  $p > 0.05$ ), and that this shift was smaller in the single mutant D237C ( $0.10 \pm 0.11$ ,  $n=5-6$ ,  $p > 0.05$ ), and absent in I312C ( $-0.05 \pm 0.11$ ,  $n=5-6$ ,  $p > 0.05$ ). The length of this compound corresponds to the distance between the two engineered Cys residues of D237C/I312C in the closed state and suggests therefore that constraining the distance between these two residues may hinder ASIC activation.

### **Light-dependent activation of ASIC1a after exposure to BMA**

To date, only a few studies have used optical tweezers to activate ion channels. This approach was in several studies successful with P2X (Browne, Nunes et al. 2014, Habermacher, Martz et al. 2016, Fryatt, Dayl et al. 2019). One of these studies also showed that two mutants of hASIC1a, I428C and G430C were opened by light after reaction with BMA (Browne, Nunes et al. 2014). In our hands, I428C, but not G430C produced light-induced channel activation after reaction with BMA. Comparison of the distances in the structures indicated intersubunit distances between the engineered Cys residues that appeared to be too high in the case of I428C and too low in the case of G430C for gating by BMA (**Table S1**). A biochemical analysis of cell surface expressed ASIC1a did not provide any evidence for a cross-linking of these two mutants by BMA. It may be possible that modification of I428C by

BMA occurs in a similar way as the modification of G430C by MTSET and MTSPTrEA that results in channel activation at pH7.4, producing a non-desensitizing, amiloride-sensitive current (Gautschi, van Bemmelen et al. 2017).

### **Modulatory effect of BMA by application of light on hASIC1a activity**

To assess the activation mechanism in ASIC1a, we have selected several mutants in the wrist domain and the acidic pocket, for which the distance between the engineered Cys residues in structural models of the closed, open or desensitized state matched the end-to-end distance of BMA in the *cis* or *trans* conformation (**Table S1**). In all the mutants shown in **Table S1**, application of 440nm and 360nm light after exposure to BMA did not induce any light-induced current. Comparison of the  $(I_{pH6.x440nm}/I_{pH5_{440nm}})/(I_{pH6.xCtrl}/I_{pH5_{Ctrl}})$  ratio showed a significant difference only between hASIC1a-E97C/D347C and WT. The ratios of  $I_{pH6.x}/I_{pH5}$  under control and 440nm light conditions were not significantly different in any of the mutants. It is possible that in the double mutants, 440nm light did not produce any significant modulatory effect. Analysis of the change in the  $I_{pH6.x}/I_{pH5}$  ratio under exposure to 360nm indicated a significant difference between control and light condition in D237C/E315C, D237C/E355C and K246C/D347C. These three mutants are part of the acidic pocket. Application of 360nm light should put BMA in the *cis* configuration, which for these mutants would correspond to open or desensitized state distances. In the two mutants D237C/E315C and D237C/E355C, 360nm light induced an alkaline shift of the pH dependence, which would be expected for a constraint that favors the open state, while an acidic shift was observed for K246C/D347C (**Figure 5B**). However, the ratio of  $I_{pH6.x}/I_{pH5}$  ratios between the three mutant and WT were not significantly different. Thus, it is not necessary to observe channel activation by light since a recent study mutated several acidic amino acids from the acidic pocket, and the channel was still functional concluding the role of acidic pocket in slower conformational changes associated with protonation even occurring

outside acidic pocket (Vullo, Bonifacio et al. 2017). There was some huge variability in the ratio of IpH6.x/IpH5 ratio for R64C and G433C under the presence and absence of 360nm light, which might be resulted from the experimental condition and considering more experiments can explain the effect. Similarly, variability was observed in E97C/D347C, which was not significantly different from WT under 360nm light application but was significant under 440nm light. In both cases, it is still possible that BMA can make cross-link at E97C/D347C and the shift in the ratio is result of it. But it remains unclear if the effects observed are due to cross-linking. These mutants were not assessed for cross-linking by BMA through western blot, since they are in the same subunit. Hence, it limits our speculation to know whether BMA can cross-link in these mutants and shift in the IpH6.x/IpH5 values through cross-linking.

#### **Functional analysis of hASIC1a mutants using MTS cross-linkers**

Thiol-specific MTS cross-linkers with various lengths of spacer arms were selected to match the distance between the C $\beta$  [C $\alpha$  for Gly] of residue pairs located in ASIC domains that have been associated with activation. Several studies have used previously the monovalent MTS to analyze the conformational changes associated with ASIC1a functional states (Pfister, Gautschi et al. 2006, Bargeton and Kellenberger 2010, Tolino, Okumura et al. 2011, Frey, Pavlovicz et al. 2013, Krauson, Rued et al. 2013, Gautschi, van Bemmelen et al. 2017). To date, only very few studies used MTS cross-linkers (Loo and Clarke 2001, Fryatt, Dayl et al. 2019). Loo et al used different thiol-specific MTS cross-linkers to assess the drug-binding domain of P-glycoprotein (P-gp) and the molecular mechanism associated to ATP-hydrolysis that causes drug transport. Cross-linked cysteine mutants of human P-gp by MTS cross-linker were visualized with western blot and cross-linking was observed in several mutants. Based on these results it was concluded that the drug-binding domain may form a funnel-like shape to accommodate several compounds of different size. Cross-linking in the TM domain inhibited

the ATPase activity due to hindered conformation changes. This approach with thiol-specific MTS cross-linkers of different length has not been reported before with ASIC1a.

Our analysis showed in some mutants a lower  $I_{pH6.x}/I_{pH5}$  value after exposure to MTS cross-linkers relative to the control condition in comparison to monovalent MTS reagents. Of these mutants, MTS-17-MTS, whose length matches the closed state distance in D237C/I312C, produced an acidic shift of the activation pH dependence, while it induced a smaller acidic shift in D237C, and had no effect on I312C. Our experiments do not prove that a cross-link is really formed between D237C and I312C. Since such a cross-link would occur within the same subunit, it would not significantly change the apparent mass in SDS-PAGE. There are however several other methods to analyze a possible cross-linking, and the most appropriate would be to use Mass spectrometry (MS)(Yakovlev 2009, Holding 2015).

### **Previous findings with MTS reagents in these domains**

For the mutant hASIC1-G430C, it was observed that MTSEA-biotin could produce an alkaline shift in the pH dependence of activation, indicating modification of the residue was more sensitive for activation (Gautschi, van Bemmelen et al. 2017). This residue was shown to be directly activated by MTSET and MTSPTrEA in the absence of extracellular acidification favoring a conducting state (**Table S3**) (Gautschi, van Bemmelen et al. 2017). The homologous mutation in mASIC1a was also shown to be involved in the pore opening mechanism (**Table S3**) (Tolino, Okumura et al. 2011). In our hand, MTS-4-MTS and MTS-10-MTS that approximately match to distance of the residues in the closed state produced a trend comparable to MTSEA-Biotin. It is possible that the mutant G430C is not cross-linked by both of these cross-linkers. Another study that used MTSET to modify engineered Cys residues showed that the pH<sub>50</sub> of activation was shifted to acidic value and peak amplitude was inhibited in hASIC1a-E315C and -D347C (Liechti, Berneche et al. 2010). Together, it was found that MTS-17-MTS shifted the pH dependence of activation in hASIC1a-D237C/I312C to an acidic

value. It is likely possible that MTS-17-MTS may form cross-link between D237C and I312C that need to be further validated to associate the conformational changes in these domains to the role in channel activation mechanism.

## **CONCLUSION**

In conclusion, two different cysteine-based cross-link approaches were applied in pursuit to identify the residues and associated conformational changes in the domains to understand the hASIC1a channel activation mechanism. The analysis revealed light-induced current in I428C without cross-link formation. Using MTS cross-linker, only a pair of residues, D237C/I312C was identified for possible cross-linking by MTS-17-MTS. Indeed, this functional analysis needs further validation to describe the conformational changes associated with the channel activity.

## **MATERIALS AND METHODS**

### **Optical tweezer labelling**

4, 4'-Bis (maleimido) azobenzene (BMA) was purchased from Toronto Research Chemicals (Canada). BMA was dissolved in DMSO to make a stock concentration of 10mM that was stored in the dark at -20°C. The stock solution was diluted at different concentrations 10, 20, and 40  $\mu$ M in the extracellular solution at pH7.3 and the cells were labelled at room temperature in the dark for 12, 20 or 40min. The cells were washed twice with the extracellular solution at pH 7.4 and were used immediately in the experiment. The light-induced current was measured at 10% intensity for 440nm and 100% intensity for 360nm. In all the cases, the given intensity of light was used to obtain light-induced current, unless stated.

### **Light-induced current in rP2X2-P329C and hASIC1a-I428C**

rP2X2 P329C was transfected in HEK cells and after 48h of protein expression, the cells were tethered to 10 $\mu$ M BMA for 12min under dark at extracellular pH7.3. The light-induced currents were measured by application of 440nm light and channel was closed by

application of 360nm light. In CHO cells, hASIC1a-I428C was transfected and after 48hr of channel expression, the cells were tethered to different concentration of BMA. In all experiments, using 440nm and 360nm light, the channel was activated by application of 440nm light at 10% intensity for 5s and 360nm light at 100% intensity for 0.1s. The measured output intensities for 440nm and 360nm light were, respectively, 6.3 and 2.9 mW/mm<sup>2</sup>.

### **Molecular biology**

Cysteine mutations were introduced in human ASIC1a, human ASIC2a, rat ASIC1bM3 and rat ASIC3 in the mammalian expression vector peak8 (Edge Biosystems, Gaithersburg, MD) using site-directed mutagenesis. Primers for the mutagenesis were designed using Quick-change site directed mutagenesis method in the PrimerX online tool and synthesized by Microsynth (Switzerland). Site-directed mutagenesis was performed using KAPA HiFi Hot-start PCR polymerase (Roche, Switzerland). All mutations were confirmed by sanger sequencing (Synergene and Microsynth, Switzerland). Human ASIC1a single mutant D237C and D351C in the background of D212 was used. The rat P2X2 P329C mutant in pcDNA3.1 was provided as a gift by Dr. Thomas Grutter (University of Strasbourg, France). Wild-type and mutant ASIC1a, ASIC2a, rASIC1bM3, rASIC3 were transiently co-transfected with EGFP or sfGFP in CHO cells using Rotifect (CarlRoth). The standard manufacturer protocol was followed for the transfection. For the expression rP2X2 P329C, HEK cells were transiently co-transfected with EGFP. The ratio of EGFP to ASIC or P2X2 was maintained at 0.2:1. CHO cells were cultured in DMEM/Nutrient Mixture F-12 with GlutaMAX<sup>TM</sup> medium, while HEK cells in GlutaMax<sup>TM</sup> medium supplemented with 10% fetal bovine serum (FBS, ThermoFischer Scientific) and 1% Penicillin/Streptomycin (5,000 U/mL, ThermoFischer Scientific) and the cells were grown at 37°C under 5% CO<sub>2</sub> atmosphere. Experiments were performed after 48h.

### **Patch-clamp electrophysiology**

Whole-cell patch-clamp recordings were carried out at -60mV at room temperature. After labelling the cells with BMA, whole-cell recordings were performed using an EPC-10 patch-clamp amplifier (HEKA Electronics, Germany). The solution exchange for the experiments was done using cFlow 8 channel flow controller connected to the MPRE8 perfusion head (Cell MicroControls, Virginia, USA). The sampling interval for all the experiments was set at 1ms and current filtering at 3 KHz. Patch pipettes of resistance between 3 - 4M $\Omega$  were filled with intracellular solution containing (in mM) 90 K-gluconate, 10 NaCl, 10 KCl, 60 HEPES, 10 EGTA, making a final osmolarity of 290 mOsm, adjusted to pH7.3 with KOH. The standard extracellular solution contained (in mM) 140 NaCl, 4 KCl, 2 CaCl<sub>2</sub>, 1 MgCl<sub>2</sub>, 10 MES, 10 HEPES, 10 Glucose to a final osmolarity of 320 mOsm, adjusted to pH7.4 with NaOH. For NMDG<sup>+</sup>-containing extracellular solution, NaCl was replaced by NMDG<sup>+</sup>. Illumination on cells was achieved by coupling high-power LEDs, 445nm (SOLIS, ThorLabs) and 365 nm (SOLIS, ThorLabs) to the microscope. Light was directed on cells using CFI S Fluor 40X Plan Fluorite 40X, 0.75 NA objective lens (Nikon). The intensity of the light output was measured using handheld optical meter (Newport). The measured output intensities for wavelengths for 360 and 440 nm were 2.8 and 6.3 mW/mm<sup>2</sup>. The relative light intensity in mW/mm<sup>2</sup> was measured as a function of voltage trigger, 0.1-2.5V for the 360nm LED and 0.1-4.5 V for the 440nm LED. The LEDs were controlled with external modulation option in the DC2200 LED driver device (Thor Labs, Germany) which was coupled with EPC10 patch-clamp amplifier and controlled by HEKA patch-master software.

### **Electrophysiological measurements using *Xenopus* oocytes**

Female South African clawed *Xenopus laevis* frogs were anaesthetized with 1.3g/L of MS-222 (Sigma-Aldrich, USA). A small incision of less than 1cm was performed on the abdominal wall for the extraction of oocytes. All procedures with *Xenopus laevis* were

approved by the local veterinary authority of Canton de Vaud, Switzerland. Healthy stage V and VI oocytes were isolated and treated with collagenase for isolation and defolliculation. Oocytes were injected with 50nl of cRNA (100 ng/ $\mu$ l to 500 ng/ $\mu$ l) of ASIC1a and mutants. Oocytes were stored in modified Barth's saline (MBS) containing (in mM) 85 NaCl, 1 KCl, 2.4 NaHCO<sub>3</sub>, 0.33 Ca (NO<sub>3</sub>)<sub>2</sub>, 0.82 MgSO<sub>4</sub>, 0.41 CaCl<sub>2</sub>, 10 HEPES, and 4.08 NaOH during protein expression phase. Electrophysiology experiments were performed 1-2 days after cRNA injection, and the currents were recorded with a Dagan TEV-200 amplifier (Minneapolis, MN) equipped with two bath electrodes at a holding potential of -60mV. Oocytes were placed in a recording chamber and perfused with experimental solutions by gravity at a rate of 10-12ml/min. Oocytes used for the experiments were conditioned with pH7.4 for 50s and peak currents were measured in ASICs by activation with two different acidic pH for 10s. After measuring peak currents, the oocytes were incubated for 3min with 1mM of monovalent or cross-linking MTS reagent in extracellular solution pH7.4. Following MTS reagent treatment, oocytes were washed for 1min with extracellular solution pH7.4 and peak currents were recorded by exposing the oocytes to conditioning pH7.4 for 50s, and ASICs were activated by two different acidic pH for 10s. Following MTS-reagent application, 10mM of DTT dissolved in extracellular solution pH7.4 was applied on the same oocyte and incubated for 3min. DTT was washed out before the measurement of peak currents in similar manner as MTS reagent treatment.

### **Cell surface cross-linking and biotinylation**

CHO cells were transiently transfected with 10 $\mu$ g of ASIC1a wild type and mutants cultured in 10cm cell culture plates. After 48hof transfection, the cells were washed twice with extracellular solution pH7.3. The cells were then labelled in the dark with 20 $\mu$ M of BMA for 20 min as described above. After the labelling, cells were washed once again with extracellular solution pH7.3, followed by two washing steps with ice-cold PBS-CM (in mM in mM, 137

NaCl, 2.7 KCl, 8 Na<sub>2</sub>HPO<sub>4</sub>, 2 KH<sub>2</sub>PO<sub>4</sub>, 0.1 CaCl<sub>2</sub>, 1 MgCl<sub>2</sub>) at pH7.4, followed by two wash steps with PBS-CM at pH8.0. Cells were incubated with EZ-link Sulfo-NHS-SS-Biotin (ThermoFischer Scientific) in PBS-CM (pH8) at a concentration of 1mg/ml for 15 min. Biotinylation was quenched by PBS-CM containing 100mM glycine for 10 min. The cells were washed twice with PBS-CM at pH7.4. The cell lysate was prepared by scrapping the cells in 1 ml of membrane isolation buffer containing (in mM) 100 NaCl, 5 EDTA, 20 HEPES, 1% Triton X-100 at pH 7.4, supplemented with 200mM cOmplete protease inhibitor (Roche). Lysed cells were centrifuged at 11000g, 4°C and a fraction of supernatant was stored as total protein extraction. All the steps were performed under ice-cold condition.

### **Molecular modelling**

The crystal structures of cASIC1a in open, desensitized and closed state (PDB ID: 4NTW, 4NYK and 5WKU) were used to generate homology models of human ASIC1a. The homology models were used as a template to identify the amino acid residues oriented towards each other from the adjacent subunits or within the same subunit. Amino acid residues were selected for introducing cysteine mutation by measuring the distance between C $\beta$  atom (C $\alpha$  for Gly) of the residues using UCSF chimera. It was predicted that BMA could bridge two cysteines in the *cis* conformation between the  $\beta$ -carbons of the cysteines at 13Å apart and 22Å in the *trans* conformation. These distances were used as selection criteria of residues, corresponding to *trans* and *cis* conformation of BMA.

### **Affinity purification and western blot**

The left-over fraction of lysed total protein was added to 50  $\mu$ l of Streptavidin Agarose resin beads (ThermoFischer Scientific) and samples were incubated overnight at 4°C in a rotating wheel. The next day, beads were washed thrice with ice-cold PBS-CM at pH7.4 and recovered by centrifugation at 4°C, 1000g. Recovered beads bound to the protein were added to 50  $\mu$ l of 2x sample loading buffer (20% glycerol, 6% SDS, 250mM Tris-HCl at pH6.7, 0.1%

(w/v) bromophenol blue, 50mM DTT), and 20 $\mu$ l of total protein with 5 $\mu$ l of 5x sample loading buffer (1.5M Sucrose, 10% SDS, 12.5mM EDTA, 312mM Tris pH8.8, 0.25% (w/v) bromophenol blue, 125 mM DTT). The total protein sample was treated at 95°C for 10min and surface protein was treated at 65°C for 15min. Total and surface protein samples of 25 $\mu$ l were loaded and resolved in Mini-protean TGX stain free 4-15% precast SDS-PAGE (BioRad) in running buffer containing 27.5mM Tris-base, 213mM Glycine and 1% SDS at 100V for 1.5h. Protein samples were transferred to Protran<sup>TM</sup> 0.2 $\mu$ M nitrocellulose membranes (Amersham Biosciences) at 4°C, 100V for 2.5h. After the transfer, the membrane was blocked by TBST (137mM NaCl, 2.7mM KCl, 19mM Tris-base, 0.1% Tween 20) containing 5% non-fat milk for 1h. Membranes were exposed overnight at 4°C to polyclonal anti-ASIC1 antibody MTY19 (1:1000)(John A. Wemmie 2003) present in 1% non-fat milk containing TBST buffer, washed three times, and were then exposed to Donkey anti-rabbit IgG horseradish peroxidase-linked secondary antibody (1:4000, GE healthcare, Switzerland). The antibody MTY19 is directed to the C-terminal 22 amino acid of mouse ASIC1a and it was used to detect ASIC1a with highly specificity in the hippocampus. To detect actin, the same blots were exposed overnight at 4°C to Anti-actin (1:1000, Sigma Aldrich) in TBST buffer containing 1% BSA, washed three times and detected with Donkey anti-rabbit IgG horseradish peroxidase linked secondary antibody (1:4000, GE healthcare). Blots were exposed to secondary antibodies for 1h at room temperature and washed three times with 1x TBST. The signals were detected using the Fusion SOLO chemiluminescence system (Vilber Lourmat, Marne-laVallée, France) using SuperSignal<sup>TM</sup> West Femto maximum sensitivity substrate (Thermo Scientific). The band intensities were quantified by the linear analysis method of the software, with the area of measurement kept constant for all samples of the same blot. Background noise was subtracted prior to determining the intensity occupied by individual bands.

### **Molecular cloning and cRNA synthesis for *Xenopus laevis***

Cysteine mutants present in ASIC1a peak8 vector were sub-cloned to the pSD5-derived vector containing 5' and 3' non-translated sequence of  $\beta$ -globin for improved protein expression in *Xenopus laevis* oocytes. Primers were designed using TaKaRa In-Fusion cloning primer designing tool. PCR was performed for ASIC1a mutants in peak8 vector using PrimeSTAR® Max DNA polymerase (TaKaRa, Switzerland). The psD5 vector was double digested by EcoRI and XbaI, and the PCR product was purified by gel extraction. The purified PCR product and double-digested vector were ligated by following the standard manufacturer protocol of the cloning kit In-Fusion HD (TaKaRa, Switzerland). From the ligation reaction, 2.5  $\mu$ l of the sample was transformed on LB agar containing ampicillin and single colonies were isolated for sub-culture. Plasmid DNA was extracted using Mini-prep Plasmid DNA purification kit (Machery-Nagel, Germany). cRNA was synthesized using the in vitro transcription kit mMMESSAGE mMACHINE™ SP6 (ThermoFisher, Switzerland). Integrity of the cRNA was verified by loading the synthesised cRNA on an agarose gel.

### **MTS reagents**

Several MTS (methanethiosulfonate) compounds were used in the electrophysiology experiments with *Xenopus laevis* oocytes expressing ASICs. These compounds, including MTS-2-MTS (1,2-Ethanediy l Bismethanethiosulfonate), MTS-4-MTS (1,4-Butanediy l Bismethanethiosulfonate), MTS-6-MTS (1,6-Hexanediy l Bismethanethiosulfonate), MTS-8-MTS (1,8-Octadiyl Bismethanethiosulfonate), MTS-10-MTS (1,10-Decadiyl Bismethanethiosulfonate), MTS-11-MTS (Undecane-1,11-diyl-bismethanethiosulfonate), MTS-14-PEO<sub>3</sub>-MTS (3,6,9,12-Tetraoxatetradecane-1,14-diyl bismethanethiosulfonate), MTS-17-PEO<sub>5</sub>-MTS (3,6,9,12,15-pentaoxaheptadecane-1,17-diyl bismethanethiosulfonate), MTSES (Sodium (2-Sulfonatoethyl)methanethiosulfonate)), MTSEA-Biotin (N-Biotinylaminoethyl Methanethiosulfonate), MTS-PEG<sub>4</sub>-Biotin (1-Biotinylamino-3,6,9-

trioxaundecane-11-yl-methanethiosulfonate) were purchased from Toronto Research Chemicals (Toronto, Canada). The MTS-2-MTS, MTS-4-MTS, MTS-6-MTS, MTS-8-MTS, MTS10-MTS, MTSES, MTSEA-Biotin, MTS-PEG4-Biotin were dissolved in dimethylsulphoxide (DMSO), while MTS-14-PEO<sub>3</sub>-MTS and MTS-17-PEO<sub>5</sub>-MTS in methanol, and MTS-11-MTS in chloroform at 100mM stock concentration and stored at -20°C. These compounds were thawed prior to experiment at 4°C and dissolved in extracellular solution pH7.4 just before the experiments.

### **Data analysis**

Electrophysiology recordings of current amplitudes were analyzed using Clampex 9.2 software (Molecular Devices) at a sampling rate of 10kHz. The pH of half maximal activation (pH<sub>50</sub>) was determined by fitting normalized activation curves to the Hill equation,  $I = I_{\max}/(1+(10^{-\text{pH}_{50}}/10^{-\text{pH}})^{nH})$ , where  $I_{\max}$  is the maximal current amplitude, pH<sub>50</sub> is the half-maximal current amplitude, and  $nH$  is the Hill-coefficient. Data are presented as mean  $\pm$  SEM. Differences between WT and mutant forms of ASIC1a and between different treatments were analyzed by ANOVA followed by indicated post hoc test, using GraphPad Prism.

## FIGURES

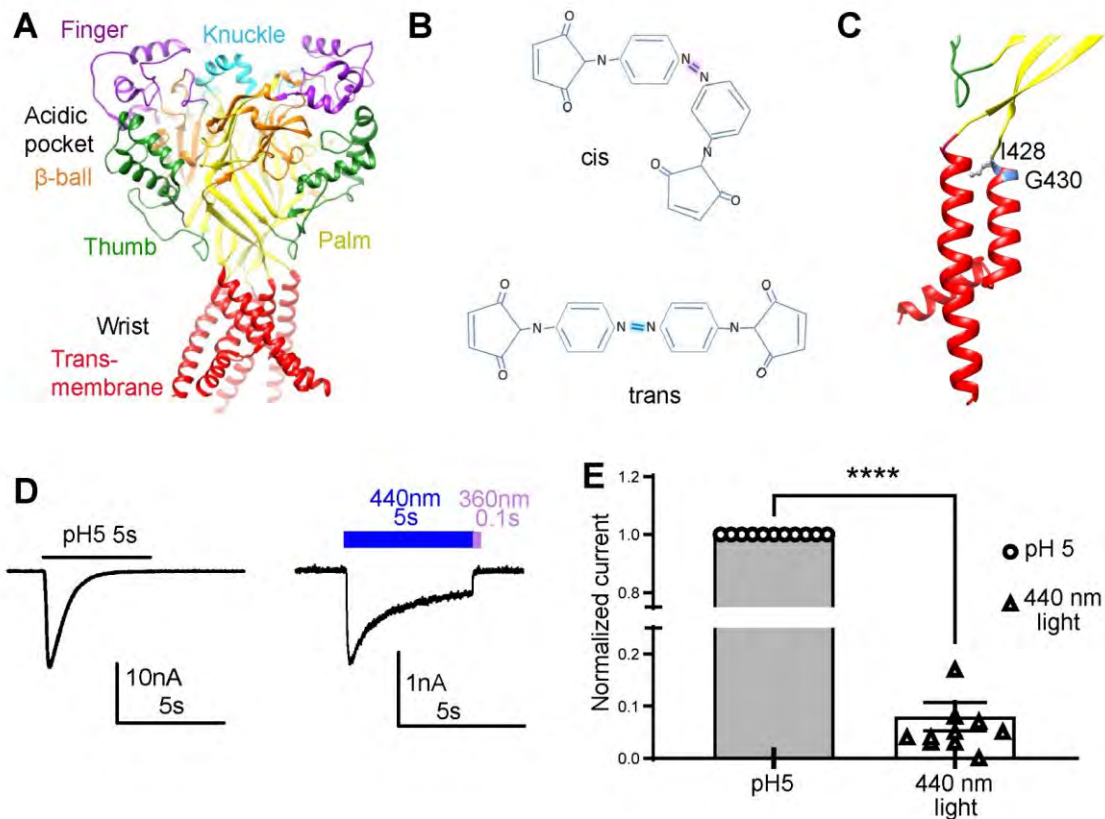


**Figure 1.** Light-dependent activation of ASIC1a channel. **A.** Structural image representation of ASIC1a trimer and its domain organization, transmembrane (red), thumb (green), palm (yellow),  $\beta$ -ball (orange), finger (purple), and knuckle (cyan) in human ASIC1a model based on chicken ASIC1a, **B.** BMA in *cis* state (top) and *trans* state (bottom), **C.** Location of I428 and G430 in the transmembrane 2 domain, **D.** pH5-induced (left) and 440nm light-induced current (right) in hASIC1a-I428C mutant. Blue bar over trace (right) represents 440nm light applied for 5s and 360nm light applied for 0.1s, **E.** Comparison of light-induced current in ASIC1a I428C to pH5-induced current. Statistical significance obtained by paired t-test (two-tailed) (n=11) \* $p < 0.05$ ; \*\* $p < 0.01$ , \*\*\*  $p < 0.001$ , \*\*\*\*  $p < 0.0001$ .

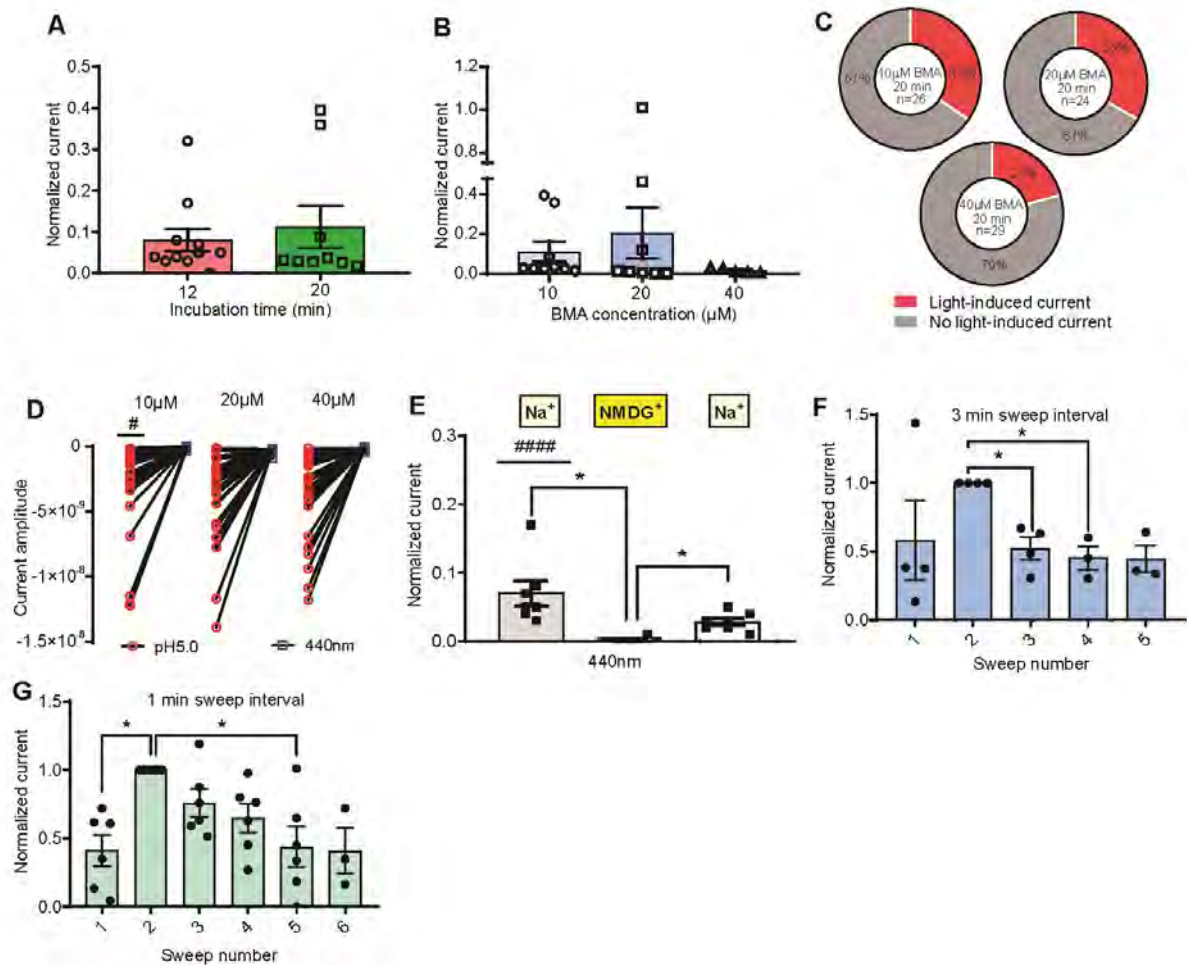


**Figure 2.** Characterization of light-activated current in ASIC1a I428C. **A.** Light-induced current normalized to  $I_{pH5}$  obtained in I428C by incubation of  $10\mu\text{M}$  BMA for 12 and 20 min, **B.** Light-induced current normalized to  $I_{pH5}$  obtained by incubation of I428C with different concentration of BMA for 20min, **C.** Frequency of light-induced current obtained (red) in comparison to no light-induced current (grey) normalized to  $I_{pH5}$  in I428C with different concentration of BMA incubated for 20 min, **D.** Current amplitude obtained under 440nm light and pH5 by incubation of hASIC1a-I428C with  $10\mu\text{M}$ ,  $20\mu\text{M}$  and  $40\mu\text{M}$ . The symbol # denotes the statistical significance between pH5 current in light-induced and no light-induced cells, **E.** Comparison of light-induced current normalized to  $I_{pH5}$  obtained with  $\text{Na}^+$  containing extracellular solution and loss of light-induced current with  $\text{NMDG}^+$  containing extracellular solution, Comparison of light-induced current normalized to sweep number 2 current between

each sweep at an interval of 3min (**F**) and 1min (**G**) between each 440nm light application (n=4). Statistical significance is denoted by \* $p < 0.05$ ; \*\* $p < 0.01$ , \*\*\*  $p < 0.001$ , \*\*\*\*  $p < 0.0001$ .

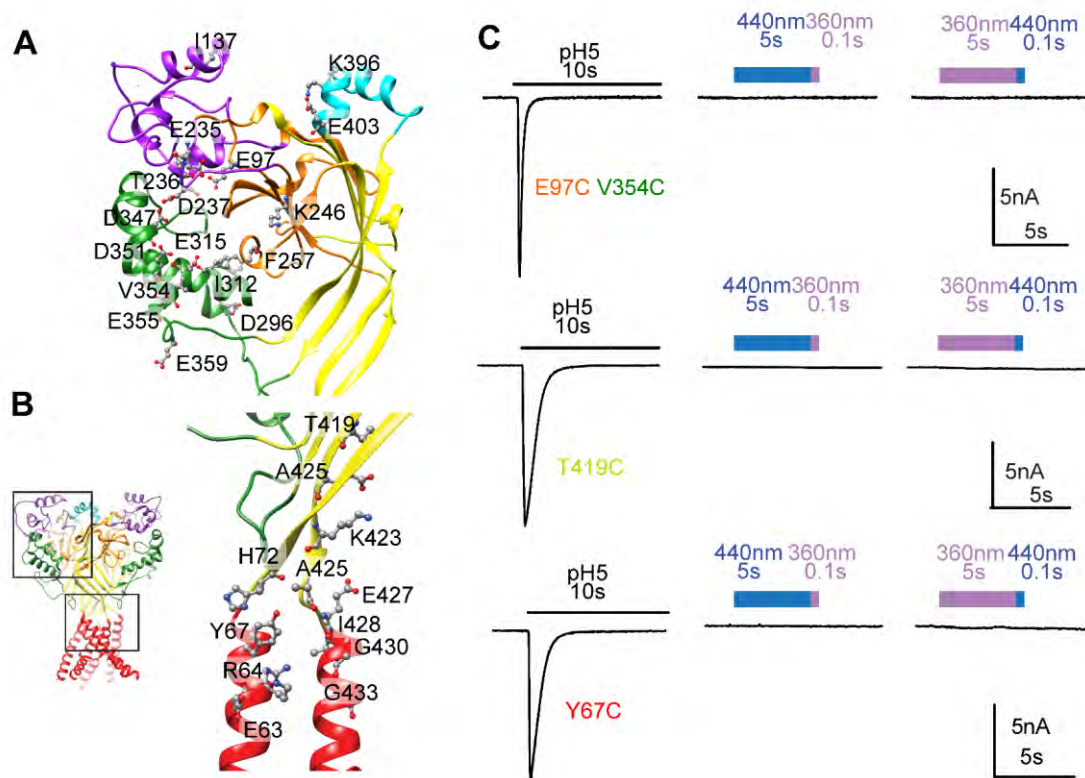


**Figure 3.** No light- and BMA-activated current in two series of new Cys mutants in ASIC1a. **A.** Cysteine mutation introduced in the thumb, finger, knuckle, palm and  $\beta$ -ball domains, **B.** Structural image representing the crystal structure of the channel highlighted (black box) with two regions in human ASIC1a closed state (left) and cysteine mutation introduced in the transmembrane domain (right), **C.** Trace representing pH5-induced current and absence of light-induced current for E97C/V354C (top), T419C (middle), Y67C (bottom). Blue bar represents light intensity of 440nm, and purple bar represents light intensity of 360nm. Both 440nm and 360 nm lights were applied either 5s or 0.1s. The mutants are labelled with color matching the domain organization.

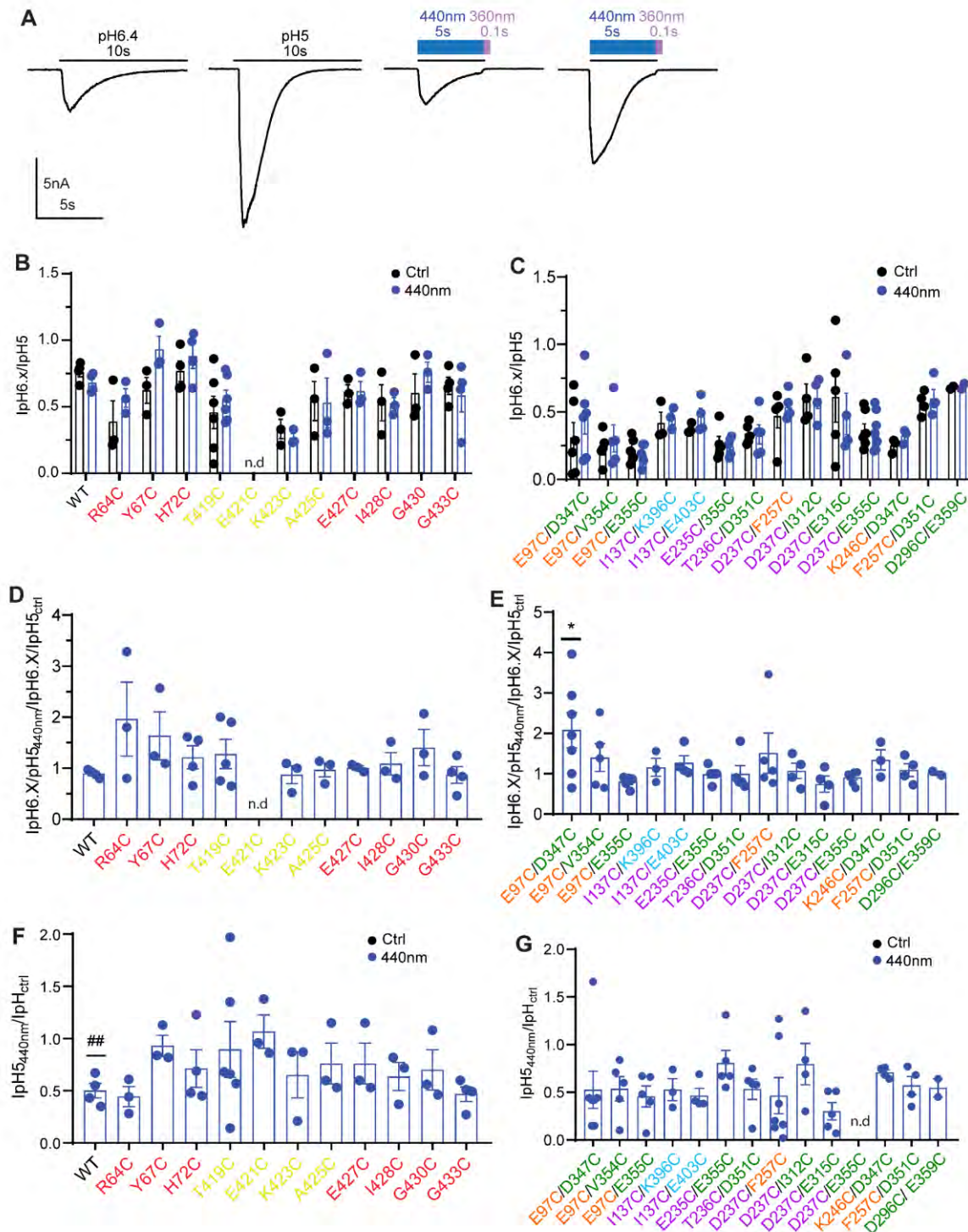


**Figure 4.** Modulatory effect of BMA assessed by the shift in the ratio of IpH6.x/IpH5 by 440nm light. **A.** Represented trace of T419C mutant under the presence and absence (control) of 440nm light. The ratio of IpH6.x/IpH5 measured before and after application of 440nm light (**B**) in the wild type and mutants of lower palm, TM1 and TM2 domain, and (**C**) in the double

mutants of ECM domain. The ratio of IpH6.x/IpH5 ratio under the presence and absence (control) of 440nm light (**D**) in the single mutants of lower palm, TM1 and TM2 domain, and (**E**) in the double mutants of ECM domain. The ratio of peak current amplitude IpH5 under the presence and absence (control) of 440nm light (**F**) in the single mutants of lower palm, TM1 and TM2 domain, and (**G**) in the double mutants of ECM domain. For all the mutants, the IpH6.x was measured at pH6.4, while for D237C/I312C- IpH6.0, K246C/D347C- IpH5.5, F257C/D351C- IpH6. The 440nm light was pre-applied 200ms before and 5s co-applied during the activation of channel by pH6.x and pH5. Statistical significance was determined by One-way ANOVA (Dunnett's *post-hoc* test) and indicated with \*p < 0.05; \*\*p < 0.01, \*\*\* p < 0.001, \*\*\*\* p < 0.0001 and mutants are labelled with color matching the domain organization. The symbol # indicates statistical significance in WT.

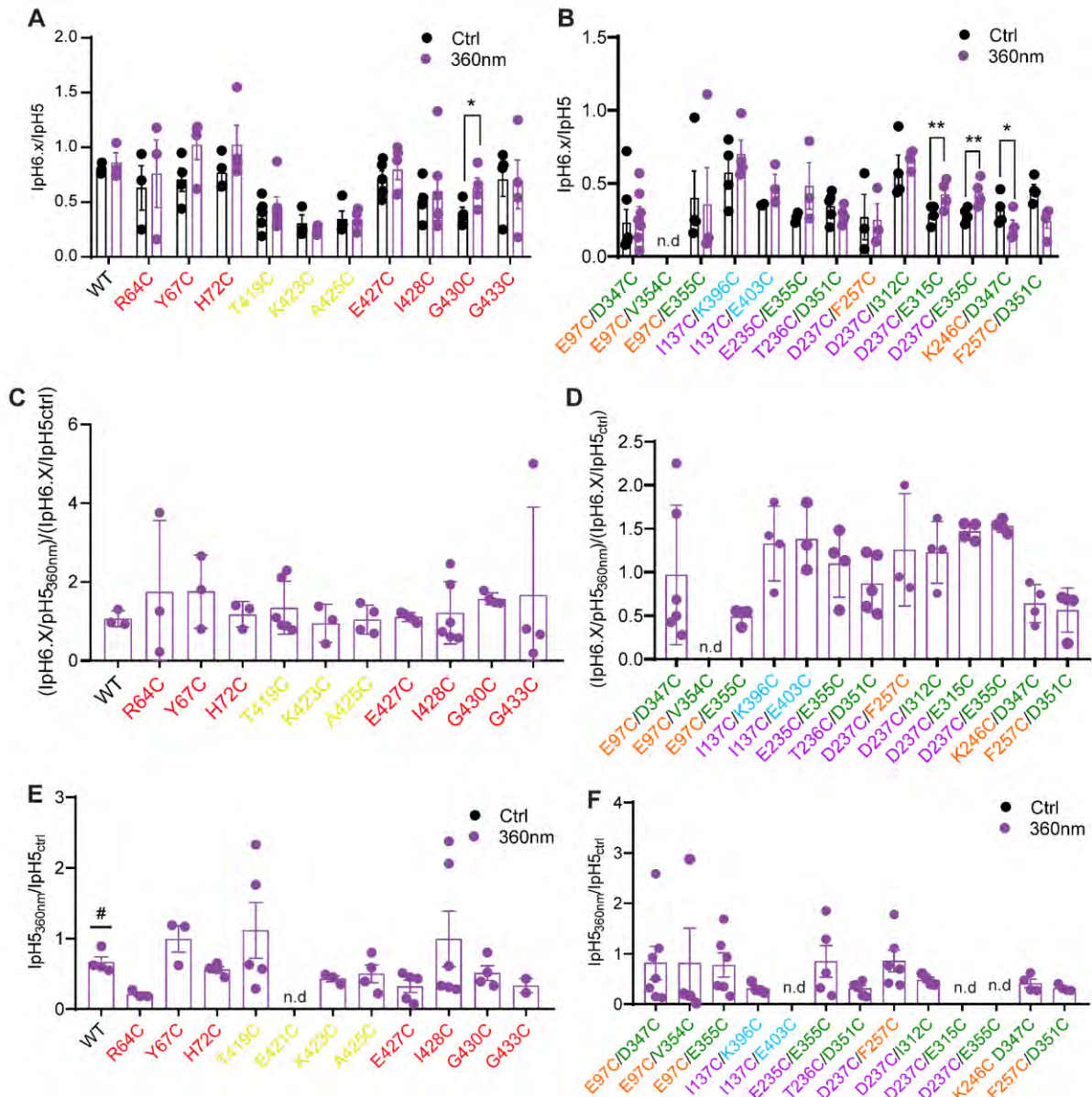


**Figure 5.** Modulatory effect of BMA assessed by the shift in the ratio of IpH6.x/IpH5 by 360nm light. The ratio of IpH6.x/IpH5 measured before and after application of 360nm light (A) in the wild type and mutants of lower palm, TM1 and TM2 domain, and (B) in the double mutants of ECM domain. The ratio of IpH6.x/IpH5 ratio under the presence and absence (control) of 360nm light (C) in the wild type and mutants of lower palm, TM1 and TM2 domain, and (D) in the double mutants of ECM domain. The ratio of peak current amplitude IpH5 under the presence and absence (control) of 360nm light (E) in the wild type and mutants of lower palm, TM1 and TM2 domain, and (F) in the double mutants of ECM domain. For all the

mutants, the IpH6.x was measured at pH6.4, while for D237C/I312C - IpH6.0, K246C/D347C - IpH5.5, F257C/D351C - IpH6. The 360nm light was pre-applied 200ms before and 5s co-applied during the activation of channel by pH6.x and pH5. Statistical significance was determined by One-way ANOVA (Dunnett's post-hoc test) and indicated with \* $p < 0.05$ ; \*\* $p < 0.01$ , \*\*\* $p < 0.001$ , \*\*\*\* $p < 0.0001$  and mutants are labelled with color matching the domain organization. The symbol # indicates statistical significance in WT.

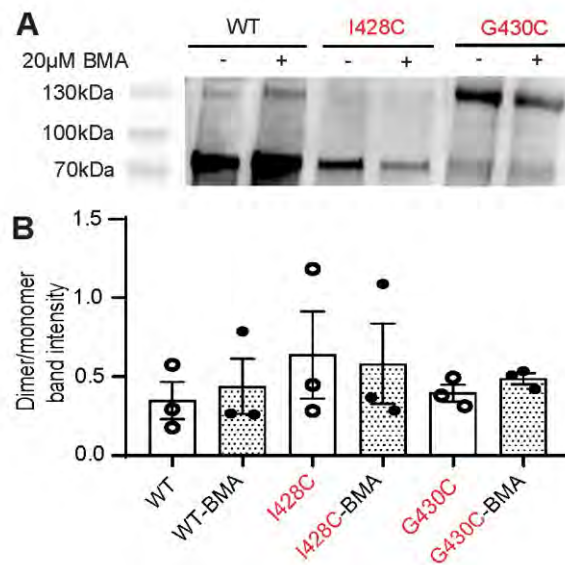


**Figure 6.** No evidence for cross-linking by BMA at engineered cysteine mutations in western blot analysis. **A.** CHO cells transfected with mutants were blotted by specific antibody against ASIC1a. Monomeric band obtained at 70kDa and dimeric band at 130KDa, **B.** Ratio between dimeric to monomeric band intensity,  $n=3$ .

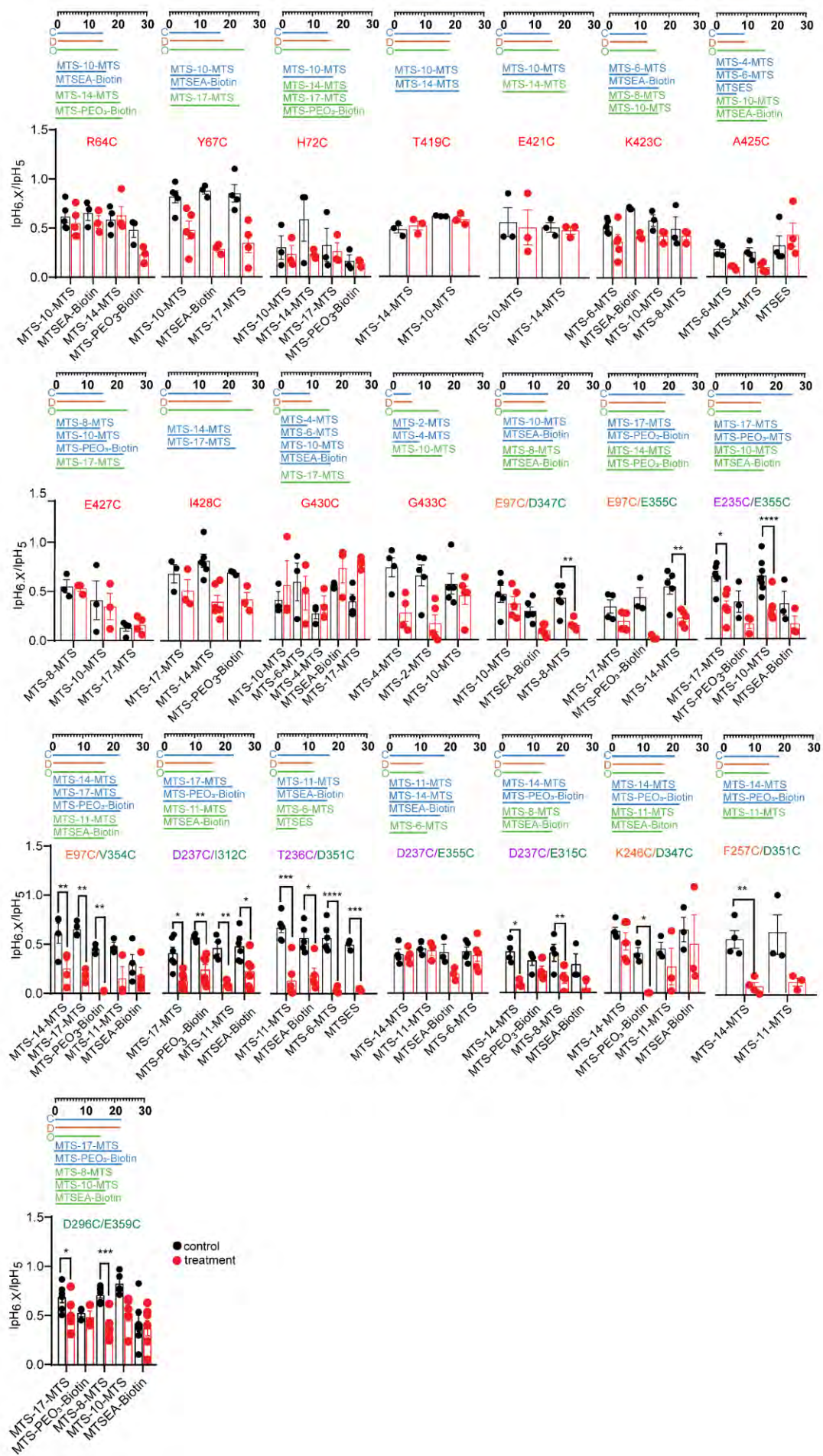


**Figure 7.** Analysis of the pH dependence of mutants before and after treatment with cross-linker and monovalent MTS reagents. The values of the  $pH_{6.x}$  were, for mutants Y67C, E427C, G430C, G433C, E97C-E355C –  $pH_{6.6}$ ; R64C, H72C, T419C, E421C, K423C, A425C, I428C, E235C/E355C, D237C/E315C, D296C/E359C, E97C/V354C, E237C/E355C –  $pH_{6.4}$ ; F257C/D351C, E97C/D347C –  $pH_6$ ; D237C/I312C, T236C/D351C –  $pH_{6.2}$ ; K246C/D347C –  $pH_{5.5}$ . In top of all mutants, a scale is indicated to match the distance between  $C\beta$ -atom of cysteine under the closed, open and desensitized state. Below the MTS cross-linker and MTS monovalent reagents with their distances matching the channel state is indicated. Differences between control and MTS condition are indicated for statistical significance from paired t-test (two-tailed) with \* $p < 0.05$ ; \*\* $p < 0.01$ , \*\*\*  $p < 0.001$ , \*\*\*\*  $p < 0.0001$ .

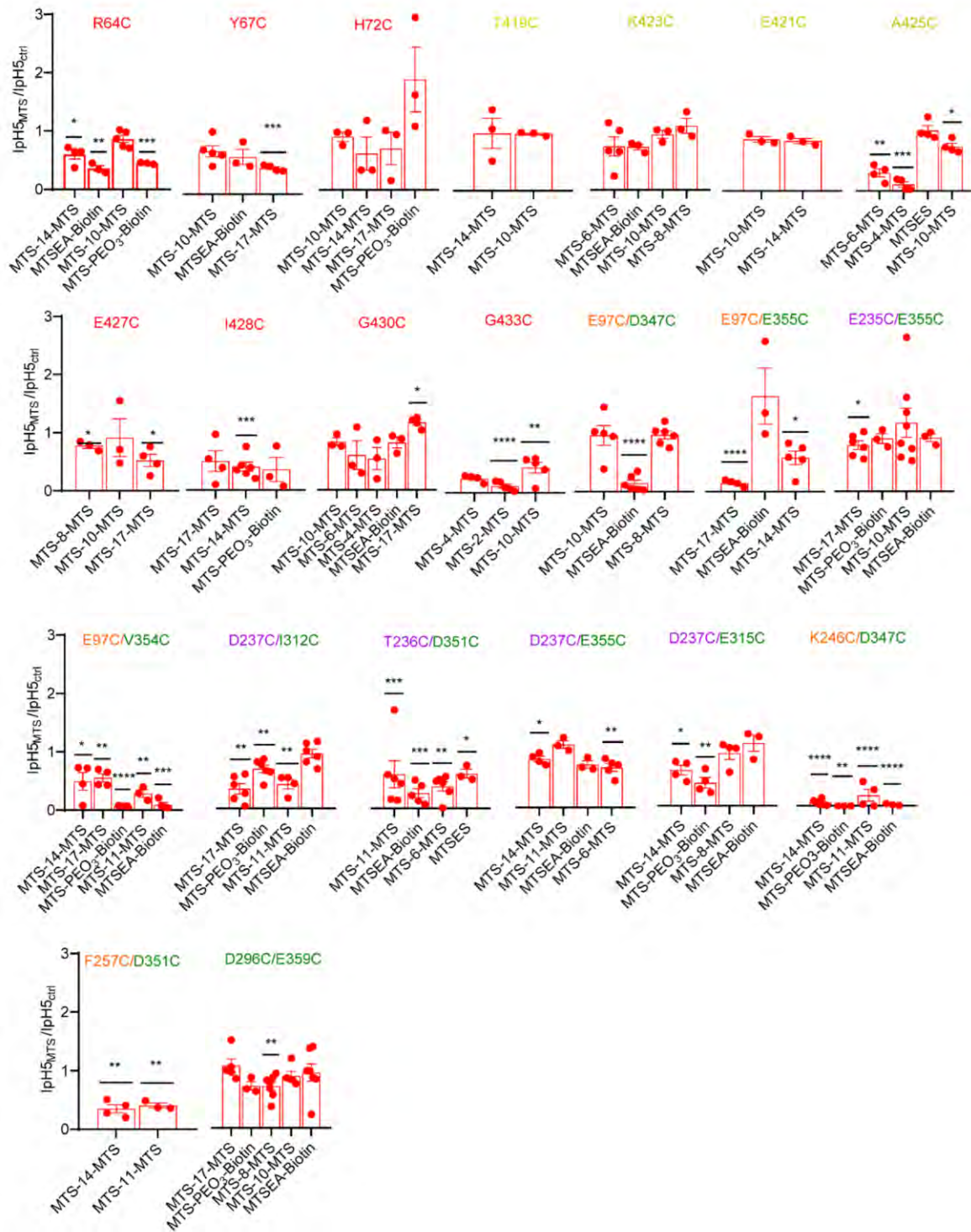


**Figure 8.** The ratio of peak maximal current obtained at IpH5 in mutants exposed to MTS cross-linker and monovalent MTS reagents. Difference between control and MTS condition are indicated with statistical significance from paired t-test (two-tailed) with \* $p < 0.05$ ; \*\* $p < 0.01$ , \*\*\*  $p < 0.001$ , \*\*\*\*  $p < 0.0001$  and mutants are labelled with color matching the domain organization.

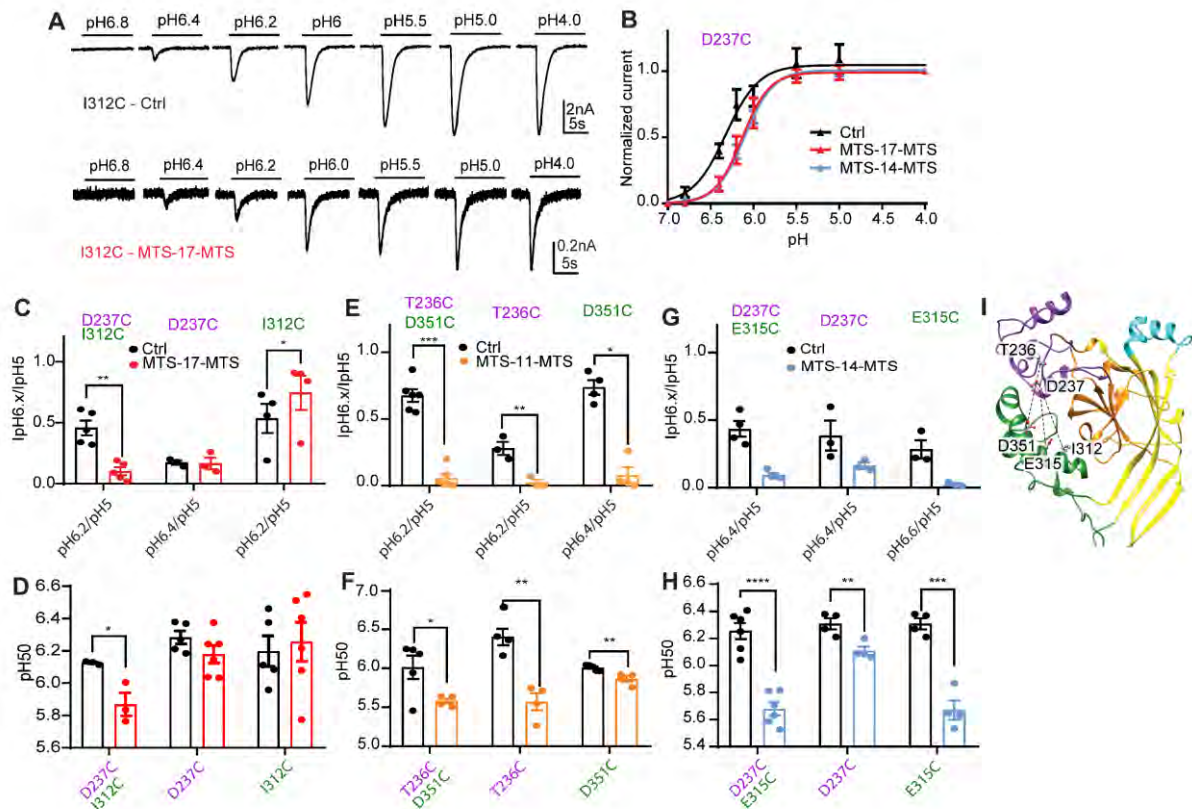


**Figure 9.** Effect of MTS-cross-linker on double mutant and their respective single mutants. **A.** Current trace of ASIC1a I312C under control (top) and treatment with MTS-17-MTS (bottom) condition. **B.** pH dependence of activation curve obtained as a function of pH activation with normalized current, ASIC1a D237C ctrl (black), MTS-17-MTS (red) and MTS-14-MTS (blue). **C.** Representation of  $I_{pH6.x}/I_{pH5}$  ratio for ASIC1a D237C/I312C, D237C and I312C (Ctrl-black; MTS-17-MTS -red). **D.** Shift in the pH dependence of activation under control and MTS-17-MTS treatment condition (Ctrl-black; MTS-17-MTS -red). **E.** Representation of  $I_{pH6.x}/I_{pH5}$  ratio for ASIC1a T236C/D351C, T236C and D351C (Ctrl-black; MTS-11-MTS -orange). **F.** Shift in the pH dependence of activation under control and MTS-11-MTS treatment condition (Ctrl-black; MTS-11-MTS -orange). **G.** Representation of  $I_{pH6.x}/I_{pH5}$  ratio for ASIC1a D237C/E315C, D237C and E315C (Ctrl-black; MTS-14-MTS -blue). **H.** Shift in the pH dependence of activation under control and MTS-14-MTS treatment condition (Ctrl-black; MTS-14-MTS -blue), **I.** Structural representation of double mutant in acidic pocket

of human ASIC1a structure in closed state. statistical significance represented by \* $p < 0.05$ ; \*\* $p < 0.01$ , \*\*\*  $p < 0.001$ , \*\*\*\*  $p < 0.0001$  and mutants are labelled with color matching the domain organization.

### SUPPLEMENTARY FIGURES LEGENDS

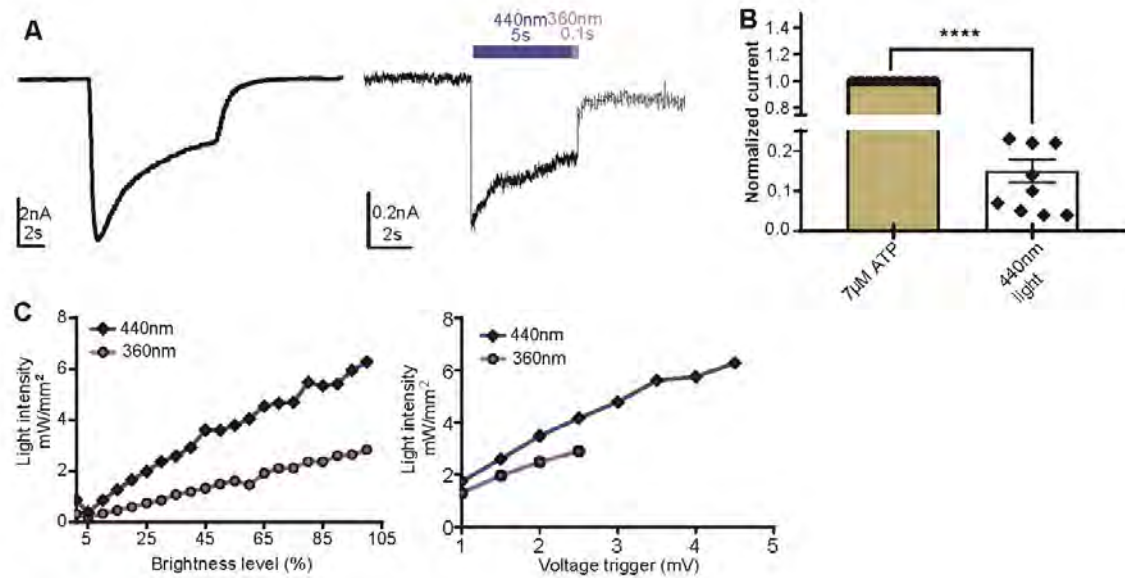


**Figure S1. Light-induced current in rP2X2.** **A.** Light-induced current obtained in rP2X2 P329C. 7 $\mu\text{M}$  ATP-induced (left) and 440nm light-activated current (right) in rP2X2 P329C. Blue bar over trace (right) represents 10% intensity of 440nm light applied for 5s and 100% intensity of 360nm light applied for 0.1s, **B.** Comparison of 7 $\mu\text{M}$  ATP-induced and light-induced current in rP2X2 P329C. Statistical significance obtained by paired t-test (two-tailed,  $n=11$ ) \* $p < 0.05$ ; \*\* $p < 0.01$ , \*\*\*  $p < 0.001$ , \*\*\*\*  $p < 0.0001$ . **C.** Different intensities of light obtained either by adjusting the brightness level value in DC2000 light controller device (left) or by adjusting the voltage trigger input in patch master software.

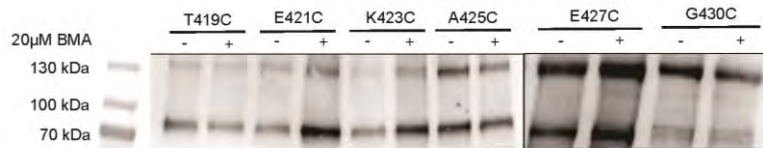


**Figure S2.** Cross-link reaction of BMA at engineered cysteine mutation analyzed by western blot. Cells transfected with mutants were blotted by specific antibody against ASIC1a. Monomeric band obtained at 70KDa and dimeric band at 130KDa.

**Table 1.** Summary of shift in pH50 of activation and change in IpH5 peak amplitude by MTS cross-linker in selected double mutants and the respective single mutants

| Mutant              | MTS cross-linker | pH50 shift          | IpH5 <sub>MTS/ctrl</sub> |
|---------------------|------------------|---------------------|--------------------------|
| hASIC1a-D237C I312C | MTS-17-MTS       | -0.26±0.07 (n=3)    | -0.71±0.08               |
| hASIC1a-D237C       | MTS-17-MTS       | -0.17±0.07 (n=3)    | -0.83±0.04               |
| hASIC1a-I312C       | MTS-17-MTS       | +0.07±0.16 (n=4)    | 0.02±0.18                |
| hASIC1a-D351C T236C | MTS-11-MTS       | -0.43±0.17 (n= 4-5) | -0.69±0.09               |
| hASIC1a-D351C       | MTS-11-MTS       | -0.14±0.03 (n=4-5)  | -0.41±0.05               |
| hASIC1a-T236C       | MTS-11-MTS       | -0.83±0.15 (n=4)    | -0.15±0.06               |
| hASIC1a-D237C E315C | MTS-14-MTS       | -0.57±0.07 (n=6)    | -0.38±0.08               |
| hASIC1a-D237C       | MTS-14-MTS       | -0.20±0.05 (n=4)    | 0.25±0.05                |
| hASIC1a-E315C       | MTS-14-MTS       | -0.64±0.08 (n=4)    | -0.33±0.05               |

The symbol ‘-’ indicates the decrease in current amplitude and ‘+’ indicates the increase in current amplitude.

**Table 2.** Selection of MTS cross-linker and MTS monovalent reagents based on their lengths matching to the distances between engineered Cys mutation in open (4NTW), desensitized (4NYK) and closed state (5WKU) models of human ASIC1a.

| Mutant    | Open state                |                              | Closed state                                      |                              |
|-----------|---------------------------|------------------------------|---|------------------------------|
|           | MTS Cross-linker          | MTS Monovalent               | MTS Cross-linker                                  | MTS Monovalent               |
| R64C      | MTS-14-MTS                | MTS-PEO <sub>3</sub> -Biotin | MTS-10-MTS <sup>#</sup>                           | MTSEA-Biotin                 |
| Y67C      | MTS-17-MTS                | -                            | MTS-10-MTS <sup>#</sup>                           | MTSEA-Biotin                 |
| H72C      | MTS-14-MTS,<br>MTS-17-MTS | MTS-PEO <sub>3</sub> -Biotin | MTS-10-MTS <sup>#</sup>                           | -                            |
| T419C     | -                         | -                            | MTS-10-MTS <sup>#</sup><br>MTS-14-MTS             | -                            |
| E421C     | MTS-14-MTS                | -                            | MTS-10-MTS <sup>#</sup>                           | -                            |
| K423C     | MTS-8-MTS<br>MTS-10-MTS   | -                            | MTS-6-MTS <sup>#</sup>                            | MTSEA-Biotin                 |
| A425C     | MTS-10-MTS                | MTSEA-Biotin                 | MTS-4-MTS <sup>#</sup><br>MTS-6-MTS <sup>#</sup>  | MTSES                        |
| E427C     | MTS-17-MTS                | -                            | MTS-8-MTS<br>MTS-10-MTS <sup>#</sup>              | MTS-PEO <sub>3</sub> -Biotin |
| I428C     | -                         | -                            | MTS-14-MTS <sup>#</sup><br>MTS-17-MTS             | -                            |
| G430C     | MTS-17-MTS                | -                            | MTS-4-MTS <sup>#</sup><br>MTS-6-MTS<br>MTS-10-MTS | MTSEA-Biotin                 |
| G433C     | MTS-10-MTS                | -                            | MTS-2-MTS <sup>#</sup><br>MTS-4-MTS               | -                            |
| E97/D347  | MTS-8-MTS <sup>#</sup>    | MTSEA-Biotin                 | MTS-10-MTS  | MTSEA-Biotin                 |
| E97/V354  | MTS-11-MTS <sup>#</sup>   | MTSEA-Biotin                 | MTS-14-MTS<br>MTS-17-MTS                          | MTS-PEO <sub>3</sub> -Biotin |
| E97/E355  | MTS-14-MTS <sup>#</sup>   | MTS-PEO <sub>3</sub> -Biotin | MTS-17-MTS  | MTS-PEO <sub>3</sub> -Biotin |
| E235/E355 | MTS-10-MTS <sup>#</sup>   | MTSEA-Biotin                 | MTS-17-MTS  | MTS-PEO <sub>3</sub> -Biotin |
| T236/D351 | MTS-6-MTS <sup>#</sup>    | MTSES                        | MTS-11-MTS  | MTSEA-Biotin                 |
| D237/I312 | MTS-11-MTS <sup>#</sup>   | MTSEA-Biotin                 | MTS-17-MTS  | MTS-PEO <sub>3</sub> -Biotin |
| D237/E315 | MTS-8-MTS <sup>#</sup>    | MTSEA-Biotin                 | MTS-14-MTS  | MTS-PEO <sub>3</sub> -Biotin |
| D237/E355 | MTS-6-MTS <sup>#</sup>    | -                            | MTS-11-MTS<br>MTS-14-MTS                          | MTSEA-Biotin                 |
| K246/D347 | MTS-11-MTS <sup>#</sup>   | MTSEA-Biotin                 | MTS-14-MTS  | MTS-PEO <sub>3</sub> -Biotin |
| F257/D351 | MTS-11-MTS <sup>#</sup>   | -                            | MTS-14-MTS  | MTS-PEO <sub>3</sub> -Biotin |
| D296/E359 | MTS-8-MTS<br>MTS-10-MTS   | MTSEA-Biotin                 | MTS-17-MTS <sup>#</sup>                           | MTS-PEO <sub>3</sub> -Biotin |

MTS reagent with symbol # denotes the length of the reagent matching to the desensitized state.

### SUPPLEMENTARY DATA

**Table S1.** Distances between residues that were mutated to Cys in this study, determined between C $\beta$ -atoms (C $\alpha$  for Gly) of open (4NTW), desensitized (4NYK) and closed state (5WKU) models of human ASIC1a.

| Residue | Open state<br>4NTW<br>(Å) | Desensitized state<br>4NYK (Å) | Closed state<br>5WKU<br>(Å) | Residue   | Open state<br>4NTW<br>(Å) | Desensitized state<br>4NYK (Å) | Closed state<br>5WKU<br>(Å) |
|---------|---------------------------|--------------------------------|-----------------------------|-----------|---------------------------|--------------------------------|-----------------------------|
| E63     | 27                        | 22.2                           | 22.2                        | E97/D347  | 12.5                      | 12.8                           | 14.8                        |
| R64     | 21                        | 15                             | 15.2                        | E97/V354  | 17.2                      | 17.2                           | 21.2                        |
| Y67     | 24.8                      | 18                             | 17.7                        | E97/E355  | 19.8                      | 19.7                           | 25.4                        |
| H72     | 22.2                      | 15.5                           | 15.2                        | I137/K396 | 20.7                      | 21                             | 21                          |
| T419    | 17.3                      | 17.9                           | 18.8                        | I137/E403 | 20.4                      | 20.3                           | 21.2                        |
| E421    | 17.6                      | 16.3                           | 15.9                        | E235/E355 | 15.3                      | 15.4                           | 25.9                        |
| K423    | 16.3                      | 12.1                           | 11.8                        | T236/D351 | 11.4                      | 11.4                           | 17.4                        |
| A425    | 16.2                      | 9.2                            | 9                           | D237/F257 | 15.5                      | 16.3                           | 22.3                        |
| E427    | 23.8                      | 15.6                           | 16                          | D237/I312 | 17.0                      | 17.0                           | 23.4                        |
| I428    | 28.4                      | 21                             | 21.3                        | D237/E315 | 13.7                      | 14.1                           | 20.6                        |
| G430    | 16.6                      | 9.4                            | 9.5                         | D237/E355 | 11.6                      | 11.6                           | 18.2                        |
| G433    | 14.4                      | 5.2                            | 5.7                         | K246/D347 | 17.6                      | 17.7                           | 20.7                        |
|         |                           |                                |                             | F257/D351 | 14.6                      | 14.3                           | 18.0                        |
|         |                           |                                |                             | D296/E359 | 14.4                      | 22.8                           | 23.6                        |

The indicated distances are measured in hASIC1a models between two subunits for single mutants and within the subunit for double mutants.

**Table S2.** Distances of MTS cross-linker and monovalent reagent

| MTS cross-linker | Length (Å) | MTS monovalent               | Length (Å) |
|------------------|------------|------------------------------|------------|
| MTS-2-MTS        | 6.28       | MTSES                        | 5.06       |
| MTS-4-MTS        | 9.18       | MTSEA-Biotin                 | 10.9       |
| MTS-6-MTS        | 12.3       | MTS-PEO <sub>3</sub> -Biotin | 24.7       |
| MTS-8-MTS        | 14.6       |                              |            |
| MTS-10-MTS       | 15.84      |                              |            |
| MTS-11-MTS       | 17.46      |                              |            |
| MTS-14-MTS       | 21.05      |                              |            |
| MTS-17-MTS       | 23         |                              |            |

The distances of MTS cross-linker and monovalent reagents are measured between the Sulphur atom on both ends after the release of sulfinic acid (SO<sub>2</sub>CH<sub>3</sub>).

**Table S3.** Summary of functional information obtained from previous studies using monovalent MTS reagent on ASIC1a mutants

| <b>MTS reagent</b>              | <b>Mutation</b>              | <b>Information</b>  |
|---------------------------------|------------------------------|---|
| MTSET, MTSMT and MTSPT          | mASIC1a-G428C                | Direct activation of the channel in the absence of extracellular acidification (Tolino, Okumura et al. 2011)        |
| MTSET                           | mASIC1a Y424C-G428C          |   |
| MTSET and MTSPT <sub>r</sub> EA | hASIC1a-G430C, hASIC2a-A427C | Direct activation of the channel in the absence of extracellular acidification (Gautschi, van Bemmelen et al. 2017) |
| MTSET                           | hASIC1a-E315C, -D347C        | Acidic shift in the pH <sub>50</sub> of activation and inhibition of peak amplitude (Liechti, Berneche et al. 2010) |
| MTSET                           | hASIC1a-E235C, -E355C        | No shift in the pH <sub>50</sub> of activation (Liechti, Berneche et al. 2010)                                      |

### Acknowledgement

We thank Sophie Roy for synthesis of some DNA constructs and Ivan Gautschi for performing some TEVC experiments. This work was supported by the Swiss National Science Foundation grant 31003A\_172968, and by a grant from the Novartis Foundation for Medical-Biological Research to S.K.

### Author contributions

The designated authors, A.V and S.K designed together the project and wrote the manuscript.

### Abbreviations

ASIC: Acid-Sensing Ion Channel; cASIC1: chicken ASIC; cDNA: complementary deoxyribonucleic acid; CHO: Chinese Hamster Ovary; ASIC1a: human ASIC1a; GMQ: 2-Guanidine-4-methylquinazoline; Mamb1: Mambalgin1; mASIC1a: mouse ASIC1a; MD: Molecular dynamics; pH<sub>50</sub>: pH of half-maximal activation; pHD<sub>50</sub>: pH of half-maximal desensitization; PcTx1: Psalmotoxin1; SSD: Steady-state desensitization; WT: wild-type, BMA-4,4'-Bis(maleimido)azobenzene; MTS- Methanethiosulfonate

## References

1. Baconguis, I., C. J. Bohlen, A. Goehring, D. Julius and E. Gouaux (2014). "X-ray structure of acid-sensing ion channel 1-snake toxin complex reveals open state of a Na<sup>+</sup>-selective channel." Cell **156**(4): 717-729.
2. Baconguis, I., C. J. Bohlen, A. Goehring, D. Julius and E. Gouaux (2014). "X-ray structure of Acid-sensing ion channel 1-snake toxin complex reveals open state of a Na<sup>+</sup>-selective channel." Cell **156**(4): 717-729.
3. Bargeton, B. and S. Kellenberger (2010). "The contact region between three domains of the extracellular loop of ASIC1a is critical for channel function." J Biol Chem **285**(18): 13816-13826.
4. Bonifacio, G., C. I. Lelli and S. Kellenberger (2014). "Protonation controls ASIC1a activity via coordinated movements in multiple domains." J Gen Physiol **143**(1): 105-118.
5. Browne, L. E., J. P. Nunes, J. A. Sim, V. Chudasama, L. Bragg, S. Caddick and R. A. North (2014). "Optical control of trimeric P2X receptors and acid-sensing ion channels." Proc Natl Acad Sci U S A **111**(1): 521-526.
6. Dawson, R. J., J. Benz, P. Stohler, T. Tetaz, C. Joseph, S. Huber, G. Schmid, D. Hugin, P. Pflimlin, G. Trube, M. G. Rudolph, M. Hennig and A. Ruf (2012). "Structure of the acid-sensing ion channel 1 in complex with the gating modifier Psalmotoxin 1." Nat Commun **3**: 936.
7. Deval, E., J. Noel, N. Lay, A. Alloui, S. Diochot, V. Friend, M. Jodar, M. Lazdunski and E. Lingueglia (2008). "ASIC3, a sensor of acidic and primary inflammatory pain." EMBO J **27**(22): 3047-3055.
8. Frey, E. N., R. E. Pavlovicz, C. J. Wegman, C. Li and C. C. Askwith (2013). "Conformational changes in the lower palm domain of ASIC1a contribute to desensitization and RFamide modulation." PLoS One **8**(8): e71733.
9. Fryatt, A. G., S. Dayl, A. Stavrou, R. Schmid and R. J. Evans (2019). "Organization of ATP-gated P2X1 receptor intracellular termini in apo and desensitized states." J Gen Physiol **151**(2): 146-155.
10. Gautschi, I., M. X. van Bemmelen and L. Schild (2017). "Proton and non-proton activation of ASIC channels." PloS one **12**(4): e0175293.
11. Gonzales, E. B., T. Kawate and E. Gouaux (2009). "Pore architecture and ion sites in acid-sensing ion channels and P2X receptors." Nature **460**(7255): 599-604.
12. Grunder, S. and M. Pusch (2015). "Biophysical properties of acid-sensing ion channels (ASICs)." Neuropharmacology **94**: 9-18.
13. Habermacher, C., A. Martz, N. Calimet, D. Lemoine, L. Peverini, A. Specht, M. Cecchini and T. Grutter (2016). "Photo-switchable tweezers illuminate pore-opening motions of an ATP-gated P2X ion channel." Elife **5**: e11050.
14. Hesselager, M., D. B. Timmermann and P. K. Ahring (2004). "pH Dependency and desensitization kinetics of heterologously expressed combinations of acid-sensing ion channel subunits." J Biol Chem **279**(12): 11006-11015.
15. Holding, A. N. (2015). "XL-MS: Protein cross-linking coupled with mass spectrometry." Methods **89**: 54-63.
16. Jasti, J., H. Furukawa, E. B. Gonzales and E. Gouaux (2007). "Structure of acid-sensing ion channel 1 at 1.9 Å resolution and low pH." Nature **449**(7160): 316-323.
17. John A. Wemmie, C. C. A., Ejvis Lamani, Martin D. Cassell, John H. Freeman Jr and Michael J. Welsh (2003). "Acid-sensing ion channel 1 is localized in brain regions with high synaptic density and contributes to fear conditioning." The Journal of Neuroscience **23**: 5469-5502.

18. Kellenberger, S. and L. Schild (2002). "Epithelial sodium channel/degenerin family of ion channels: a variety of functions for a shared structure." Physiol Rev **82**(3): 735-767.
19. Kellenberger, S. and L. Schild (2015). "International Union of Basic and Clinical Pharmacology. XCI. structure, function, and pharmacology of acid-sensing ion channels and the epithelial Na<sup>+</sup> channel." Pharmacol Rev **67**(1): 1-35.
20. Krauson, A. J., A. C. Rued and M. D. Carattino (2013). "Independent contribution of extracellular proton binding sites to ASIC1a activation." J Biol Chem **288**(48): 34375-34383.
21. Li, T., Y. Yang and C. M. Canessa (2010). "Two residues in the extracellular domain convert a nonfunctional ASIC1 into a proton-activated channel." Am J Physiol Cell Physiol **299**(1): C66-73.
22. Liechti, L. A., S. Berneche, B. Bargeton, J. Iwaszkiewicz, S. Roy, O. Michielin and S. Kellenberger (2010). "A combined computational and functional approach identifies new residues involved in pH-dependent gating of ASIC1a." Journal of biological chemistry **285**(21): 16315-16329.
23. Loo, T. W. and D. M. Clarke (2001). "Determining the dimensions of the drug-binding domain of human P-glycoprotein using thiol cross-linking compounds as molecular rulers." J Biol Chem **276**(40): 36877-36880.
24. Lynagh, T., Y. Mikhaleva, J. M. Colding, J. C. Glover and S. A. Pless (2018). "Acid-sensing ion channels emerged over 600 Mya and are conserved throughout the deuterostomes." Proceedings of the National Academy of Sciences **115**(33): 8430-8435.
25. Paukert, M., X. Chen, G. Polleichtner, H. Schindelin and S. Grunder (2008). "Candidate amino acids involved in H<sup>+</sup> gating of acid-sensing ion channel 1a." J Biol Chem **283**(1): 572-581.
26. Pfister, Y., I. Gautschi, A. N. Takeda, M. van Bemmelen, S. Kellenberger and L. Schild (2006). "A gating mutation in the internal pore of ASIC1a." J Biol Chem **281**(17): 11787-11791.
27. Price, M. P., S. L. McIlwrath, J. Xie, C. Cheng, J. Qiao, D. E. Tarr, K. A. Sluka, T. J. Brennan, G. R. Lewin and M. J. Welsh (2001). "The DRASIC cation channel contributes to the detection of cutaneous touch and acid stimuli in mice." Neuron **32**(6): 1071-1083.
28. Roy, S., C. Boiteux, O. Alijevic, C. Liang, S. Berneche and S. Kellenberger (2013). "Molecular determinants of desensitization in an ENaC/degenerin channel." FASEB J **27**(12): 5034-5045.
29. Schuhmacher, L. N., S. Srivats and E. S. Smith (2015). "Structural domains underlying the activation of acid-sensing ion channel 2a." Mol Pharmacol **87**(4): 561-571.
30. Smith, E. S., X. Zhang, H. Cadiou and P. A. McNaughton (2007). "Proton binding sites involved in the activation of acid-sensing ion channel ASIC2a." Neurosci Lett **426**(1): 12-17.
31. Sun, D., S. Liu, S. Li, M. Zhang, F. Yang, M. Wen, P. Shi, T. Wang, M. Pan, S. Chang, X. Zhang, L. Zhang, C. Tian and L. Liu (2020). "Structural Insights into Human Acid-sensing Ion Channel 1a Inhibition by Snake Toxin Mambalgin." eLife.
32. Tolino, L. A., S. Okumura, O. B. Kashlan and M. D. Carattino (2011). "Insights into the mechanism of pore opening of acid-sensing ion channel 1a." J Biol Chem **286**(18): 16297-16307.
33. Vullo, S., G. Bonifacio, S. Roy, N. Johner, S. Berneche and S. Kellenberger (2017). "Conformational dynamics and role of the acidic pocket in ASIC pH-dependent gating." Proc Natl Acad Sci U S A **114**(14): 3768-3773.

34. Wemmie, J. A., C. C. Askwith, E. Lamani, M. D. Cassell, J. H. Freeman and M. J. Welsh (2003). "Acid-sensing ion channel 1 is localized in brain regions with high synaptic density and contributes to fear conditioning." Journal of Neuroscience **23**(13): 5496-5502.
35. Wemmie, J. A., R. J. Taugher and C. J. Kreple (2013). "Acid-sensing ion channels in pain and disease." Nat Rev Neurosci **14**(7): 461-471.
36. Xiong, Z. G., X. M. Zhu, X. P. Chu, M. Minami, J. Hey, W. L. Wei, J. F. MacDonald, J. A. Wemmie, M. P. Price, M. J. Welsh and R. P. Simon (2004). "Neuroprotection in ischemia: blocking calcium-permeable acid-sensing ion channels." Cell **118**(6): 687-698.
37. Yakovlev, A. A. (2009). "Crosslinkers and their utilization for studies of intermolecular interactions." Neurochemical Journal **3**(2): 139-144.
38. Yoder, N. and E. Gouaux (2020). "The His-Gly motif of acid-sensing ion channels resides in a reentrant 'loop' implicated in gating and ion selectivity." Elife **9**.
39. Yoder, N., C. Yoshioka and E. Gouaux (2018). "Gating mechanisms of acid-sensing ion channels." Nature **555**(7696): 397-401.
40. Ziemann, A. E., M. K. Schnizler, G. W. Albert, M. A. Severson, M. A. Howard, 3rd, M. J. Welsh and J. A. Wemmie (2008). "Seizure termination by acidosis depends on ASIC1a." Nat Neurosci **11**(7): 816-822.

## 6. Discussion

### 6.1. Modulatory effect by non-proton ligand GMQ and its derivatives on ASIC1a

To date, protons are the known agonist of ASICs. Yu et al identified GMQ as a nonproton ligand, that can open ASIC3 at physiological pH7.4<sup>89</sup>. Two residues, E423 and E79 belonging to the lower palm domain of ASIC3 were identified crucial for the activation of the channel by GMQ<sup>89</sup>. GMQ is known to shift the pH dependence of activation to more alkaline value in ASIC3 and create a window current at pH7.4 leading to the channel activation<sup>106</sup>. However, the effect of GMQ on gating mechanism is different on other ASIC subtypes. GMQ shifts the pH dependence of activation in both ASIC1a and ASIC1b to acidic value, whereas in ASIC3 to alkaline value. In ASIC1a-E418C, an acidic shift in the pH dependence of activation was induced by GMQ and it was not observed in ASIC1a-E79C. In both these mutants an acidic shift was observed in the steady-state desensitization, suggesting a partial loss of GMQ effect on the activation of ASIC1a<sup>106</sup>. At a concentration >1mM, GMQ inhibited the maximal peak current in all ASIC subtypes, but with a lower effect in ASIC1b. Thus, it was clear from previous studies that GMQ is a gating modifier and pore blocker of ASIC subtypes. To gain insight into the role of GMQ *in vivo*, currents were measured in rat DRG neurons in response to the application of GMQ<sup>89</sup>. In most neurons, ASIC-like currents evoked by acidification were observed even by GMQ, suggesting GMQ may also activate the channel *in vivo*. Since studies have shown the role of ASIC3-mediated pain responses<sup>78,84,104</sup>, GMQ was injected into the right hind paw of ASIC3<sup>-/-</sup> and ASIC3<sup>+/+</sup> mice. Intraplanar injection of 100 $\mu$ M GMQ-containing 0.9% NaCl solution in the mice showed paw licking time was higher in ASIC3<sup>+/+</sup> mice compared to ASIC3<sup>-/-</sup> mice. Additionally, the paw licking time was slightly prolonged in ASIC1<sup>-/-</sup> mice compared to ASIC1<sup>+/+</sup> mice. Thus, GMQ was shown to activate sensory neurons and cause pain-related behavior. Hence, it was interesting to find analogues of GMQ with higher affinity. To identify a potent small molecule based on GMQ, the guanidium moiety of GMQ was used as scaffold generate the derivatives, since previously tested GMQ analogues, 2-guanidino-benzimidazole, -

benzothiazole, and -benzoxazole modulated ASIC3 poorly<sup>89</sup>.

### 6.1.1. Blocking and gating effect by GMQ derivatives on ASIC1a and ASIC3

To measure the potency of GMQ derivatives on ASIC1a and ASIC3, gating and blocking effects were measured. Gating effect refers to the measurement of current ratio at two pH values, at pH6.6 close to the p<sub>H50</sub> of the channel in the steep part of activation curve and at pH5 to maximal channel activation where pH dependence has saturated. A change of this amplitude by a compound indicates that the compound affects the maximal current amplitude. For the blocking effect, currents were measured at pH5, where the pH dependence curve has saturated. For ASIC1a and ASIC3, the gating effect was measured at pH6.6 ( $I_{GMQ}/I_{ctrl}$ ) induced-current close to the p<sub>H50</sub> of activation for both the channels. The blocking effect was measured by the inhibition of current-induced by pH5 ( $I_{GMQ}/I_{ctrl}$ ). Five different cluster of compounds were tested and the number mentioned in the parenthesis of clusters correspond to a specific molecule shown in the figure 1 of the article<sup>146</sup>. Cluster1 was derived with the conserved bicyclic structure of GMQ but with a replaced cyclohexane ring for a benzene ring to evaluate the role of aromatic ring on ASIC activity. To evaluate the role of methyl group at position 4 and nitrogen atom at position 3 that is important for the GMQ activity to form H-bond interaction with guanidine to the nitrogen atom at position 1, quinoxaline (2) and quinoline (3a, b) compounds were tested. Cluster2 (4a, b, c), cluster3 (5a, b, c, d, e) and cluster4 (6) were generated with disconnected benzene ring to produce 6-, -5-,4-phenyl-2-guanidinopyridines. Cluster5 (7, 8) was generated with disconnected guanidine moiety. For the gating effect, compounds in cluster 1 (1, 2, 3a, 3b), 2(4c), 3 (5b, 5c, 5e) and 5 (7) produced strong acidic shift, while cluster5 (8) produced strong alkaline shift in the pH dependence of activation similar to GMQ in ASIC1a. For the blocking effect, quinoline (3a) produced strong inhibition while quinoxaline (2) and quinoline (3b) produced moderated effect like GMQ (Figure 2)<sup>146</sup>. In ASIC3, the compounds from cluster1 (1,3a) and 5 (7,8) produced an alkaline shift in the pH dependence of activation, while the compounds from cluster 3 (5b,5c,5e) produced acidic shift, suggesting an importance of aromatic group of guanidinopyridine in the

modulatory effect. For the blocking effect, cluster 1 (3a,3b), cluster2, cluster3 and cluster4 showed significant blocking effect at  $I_{pH5}$  (Figure 3)<sup>146</sup>.

Taken together, it was found that the nitrogen atom at position 3 plays a role in altering the blocking effect on ASIC1a and ASIC3. The blocking effect is due to inhibition of the current at pH5 by pore block that decreases the unitary current<sup>106</sup>. For the gating effect, binding of GMQ to the palm domain and by mutation of palm domain residues, GMQ binding was suppressed by shift in the pH dependence of steady-state desensitization, but not of activation<sup>106</sup>.

### 6.1.2. Gating and blocking effect by GMQ derivatives on heteromeric channels

In the CNS, functional ASIC1a homomers, and ASIC1a/2a and ASIC1a/2b heteromers are expressed. In the PNS, functional ASIC homomer and many more possible ASIC heteromers are possible, except ASIC4. Therefore, we used ASIC1a/2a heteromers representing the CNS and ASIC3/2a representing the PNS to test the GMQ derivatives at  $I_{pH5.8}$  and  $I_{pH4.0}$ . Transfection of two subunit cDNAs can lead to channels with different stoichiometry<sup>30</sup>. Depending on this stoichiometry, the pH dependence of activation is changed, and the pH dependence is assayed with the two pH conditions, pH5,8 and pH4.0. The test resulted in the variability of  $I_{pH5.8}/I_{pH4.0}$  ratio in cells expressing heteromers before the application of any derivative. To reduce the variability in the  $I_{pH5.8}/I_{pH4.0}$  ratio, different ratio of ASIC1a/2a and ASIC3/2a DNA were transfected and in cells producing  $I_{pH5.8}/I_{pH4.0}$  ratio between 0.25 to 0.75 were considered for treatment with GMQ derivatives. Several compounds like cluster 2(4a), cluster 4(6) and including GMQ showed significant alkaline shift in the  $I_{cpd}/I_{ctrl}$  ratios at pH5.8/pH4 opposite to the shift observed in ASIC1a and ASIC2a<sup>106</sup>. In ASIC3/2a, a significant alkaline shift in the  $I_{cpd}/I_{ctrl}$  ratios at pH5.8/pH4 was observed by compound from cluster2(4a) and cluster 5(8). For blocking effect, most of the compound like cluster1(3a) and cluster 5(7,8) significantly affected the  $I_{pH4}$  in ASIC3/2a and no loss in  $I_{pH4}$  was observed in ASIC1a/2a. Due to the inclusion of ASIC2a in the heteromers, the effect of modulation on ASIC1a/2a and ASIC3/2a heteromeric channel activity was less pronounced by the GMQ derivatives. It is known that the G445 of ASIC3 and

G440 of ASIC1a located in the pore, and that correspond to the residue in ENaC that is important for amiloride inhibition is also important for the blocking effect by GMQ. Mutation of these residues to Ala results in loss of the blocking effect by GMQ<sup>106</sup>. Sequence comparison among hASIC1a, hASIC2a and rASIC3 showed that the TM2 is well conserved in the pore region while the lower palm domain residues are not completely conserved. Therefore, binding of GMQ might be affected due to the altered interaction with binding partner in the palm domain, and the stoichiometry of heteromeric channel assembly itself might result in the partial loss of the modulatory and the inhibitory effect. Induction of LTP, for instance, increases the synaptic transmission and producing strengthened signal transmission can be beneficial and important for learning and memory<sup>36</sup>. In this case, cluster2(4a) compound that produce a small blocking effect at IpH5 can be used in the induction of LTP. A recent study used GMQ-guided *in silico* screening of 5 Food and Drug Administration (FDA) approved compounds and evaluated their modulatory effect on rASIC3. Based on the surface electrostatic analysis, sephin1 resulted in higher resemblance to GMQ and sephin1 activates rASIC3 at pH7.4 and potentiate its response to acidic stimuli at pH7.4. Sephin1 is a novel modulator of ASIC3<sup>147</sup>. Using a similar approach, combining both *in silico* and electrophysiology experiments, other compounds can be identified and assessed. In fact, techniques like voltage-sensitive dye-based assays in parallel to patch-clamp electrophysiology can be used as an alternative technique to provide a faster assessment of compounds based on their ability to modify channel activity.

## **6.2. Difference in the biophysical properties between WT (G212) and mutant (D212)**

### **ASIC1a**

In many laboratories, including ours, a human ASIC1a clone that contained Asp at position 212 was used as wild type. Residue 212 is in the palm domain at the subunit interface, facing towards the thumb domain of the adjacent subunit. Since the time when this human ASIC1a clone was generated, it contains Asp at position 212<sup>3</sup>. The occurrence of this mutation in humans is very low. This mutation might likely have been generated by an error in the clone generation

process or the clone was obtained from a person carrying the mutation at 212. It is possible for errors since these clones were generated from the assembly of three different contigs and one of the contigs might contain this error. The sequence similarity between hASIC1a and hASIC2a shown in Figure 2<sup>3</sup> of the article that clearly shows the hASIC1a clone contains D at 212. The Asp at 212 is in close proximity to the proposed Cl<sup>-</sup> binding site<sup>144</sup>. By examination of the biophysical properties, we found some difference between the WT hASIC1a-G212 and mutant hASIC1a-D212. An acidic shift in the pH dependence of steady-state desensitization by 0.08 pH units, ~20-fold higher current amplitudes, ~2-fold increased surface expression and slower current decay kinetics were observed in the WT hASIC1a-G212. In the open and desensitized crystal structure of cASIC1a, a chloride ion was shown to bound per subunit at Lys212 (hASIC1a-L211) that deeply inserts into the adjacent subunit<sup>25,28,29</sup>, however, this was not found in the closed state<sup>24</sup>. The predicted chloride ion binding-site is located between the two helices,  $\alpha$ 4 and  $\alpha$ 5 of the thumb domain. The coordination of chloride ion in cASIC1a was shown by Arg310, Glu314 and Lys212 from an adjacent subunit, and van der Waals interaction from the side chain of Leu352, Val353 and Cys360. Disruption of Cl<sup>-</sup> binding site alters the pH-dependent gating, time course of desensitization and attenuates tachyphylaxis<sup>144</sup>. Kusama et al showed that chloride concentration can affect the ASIC current decay kinetics<sup>144,148</sup>. Mutation of the chloride binding residue in mASIC1a resulted in disrupted modulation of current decay kinetics<sup>144</sup>. Mutation of the conserved intersubunit chloride binding site in mASIC2a produced partial effect and no effect in rASIC3. In the closed state, it was found that the channel lacks bound Cl<sup>-</sup> within the thumb domain and this may be due to the conformational changes associated with high pH resulting in the expansion of acidic pocket<sup>145</sup>. It is assumed that mASIC1a-K211 is uncharged at the closed state and charged at the open or the desensitized state based on the pKa values of the lysine side chains that can be lower than 6.0<sup>149</sup>. Since the aim was to identify the differences in the biophysical properties between hASIC1a-D212 and -G212 and it is known that 212 is a site close in proximity to the chloride binding site<sup>145</sup>, extracellular chloride concentration was modified and

also replaced with  $\text{SCN}^-$  for  $\text{Cl}^-$ . An accelerated current decay kinetics was observed with  $\text{SCN}^-$  compared to  $\text{Cl}^-$  in both hASIC1a-D212 and -G212, but the binding of  $\text{SCN}^-$  and  $\text{Cl}^-$  occurs at the same site in ASIC1a as shown before<sup>144</sup>. The exchange of Asp with Gly at 212 produced a consequence on the current decay kinetics and may not affect the binding of  $\text{Cl}^-$  itself. Taken together, only a few differences were found in the biophysical properties of the channel and the studies done in other laboratories on hASIC1a-D212 mutant background remain valid even in hASIC1a-G212 WT. In a recent study, to understand the role of Gly212 in the activation and desensitization, Gly was replaced with A, D, E, F, Q, S and T. In Glu212, the pH dependence of activation was shifted to more alkaline values, while in other mutants to acidic value. In all mutants, functional analysis showed modulation of current decay kinetics by  $\text{Cl}^-$  were present, but the substitution with different amino acids at 212 did not affect the  $\text{Cl}^-$  binding, rather produced the consequence of its binding due to altered intra- and intersubunit interaction<sup>150</sup>.

### **6.3. Analysis on the structure-function relationship of ASIC1a channel activation**

#### **6.3.1. Light-induced channel activation in ASIC1a**

The wrist is a flexible region that connects the extracellular domains to the transmembrane domain in ASIC1a. In ratASIC1a, some residues like Glu, His and Asp were mutated, and this resulted in decreased  $\text{H}^+$ -sensitivity, suggesting this region to be critically involved in ASIC proton sensing<sup>151</sup>. In a study, two residues I428C and G430C of hASIC1a in the transmembrane domain tethered to BMA evoked light-induced current by application of 440nm light<sup>131</sup>. Similar light-induced channel activation was observed in rP2X2-P329C and rP2X3-P320C. ASICs and P2X receptors are two distinct ion channel families containing completely different amino acid sequence, however they share similar structural topology with two transmembrane domains linked to an agonist-binding extracellular domain rich in cysteine residues. With the crystal structures, structural parallels in the pore architecture were found in ASIC and P2X<sup>28,29,152</sup>. Structural and functional similarities in both these channels are well discussed in the review<sup>153</sup>. X-ray structures

revealed parallels in the structural architecture of the pore. In our analysis, we found with western blot analysis that residues Ile428C and Gly430C did not form cross-link at this position. In our hand, the light-induced current was only observed in Ile428C and not in Gly430C. From the structural information, the distance from the  $\alpha$  atom of Gly430 to Gly430 of the adjacent subunit is 9.5 Å in the closed state. The distance between adjacent Gly430 was smaller than the distance of BMA in the *cis* configuration. So, when BMA is incubated with the cells expressing hASIC1a-G430C, it is possible that BMA may bind to the channel at each G430C residue among the subunits but may not be possible to open the channel. On the other hand, the distance from the  $\beta$  atom of Ile to the adjacent Ile is 21.3 Å in the closed state. Also, our analysis in Ile428C and Gly430 shows BMA does not form a cross-link. Thus, the mechanism of activation by light may be due to the modification of Ile428C residue per subunit by BMA, but the exact mechanism behind light-dependent activation only at Ile428C is unknown. Studies have shown that positively charged MTS reagents can modify G430C due to their accessibility and thereby open the channel<sup>133,135</sup>. However, in our experiments hASIC1a-G430C did not produce a light-dependent activation and neither a shift in the baseline current at pH7.4. Hence, it was identified that BMA can modify only hASIC1a-I428C without cross-linking and result in light-dependent activation of ASIC1a at physiological pH7.4.

### **6.3.2. Light-induced shift in the pH dependence of activation**

It is known from various studies that the acidic pocket is an important region for ASIC1a function. Experiments with PcTx1 and mambalgin have shown that the acidic pocket regulates the pH dependence<sup>25-27</sup> and several studies have investigated the acidic pocket and associated conformational changes during channel activity. Using luminescence resonance energy transfer (LRET), the reduction in the distance between thumb and finger domains was observed in ASIC1a associated with proton gating<sup>154</sup>. In the acidic pocket, rapid and slow conformational changes were observed during activation and desensitization<sup>51</sup>. In our study, cross-linking by BMA in the double mutants was not assessed biochemically, as these mutants are located in the same subunit. We

applied both 440nm and 360nm light to identify any shift in the half-maximal pH. As studies show the correlation or requirement of acidic pocket collapse for ASIC activation, we observed application of 360nm light on BMA tethered to three double mutants, D237C/E315C, D237C/E355C and K246C/D347C of the acidic pocket shifted the pH dependence. However, it cannot be indicated whether a cross-linking has indeed occurred. Further analysis of cross-link in the pair of mutants is required to understand the conformation changes associated to channel function.

### **6.3.3. Shift in pH dependence of activation by MTS cross-linkers**

Different approaches have been applied to identify conformational changes during activation. To determine the structural changes, studies have measured the accessibility of Cys residue to specific MTS reagent. Structural changes during channel desensitization were observed in the lower palm<sup>138</sup>. We used a similar approach by introducing Cys mutation and modify them with MTS cross-linker. Such analysis was never done before in ASIC1a and we did an extensive analysis using selective MTS cross-linking reagents in which the distance between the two residues was different in the closed and the open state for pair of residues. Cross-linkers with the length that matches to the distance in either state was applied to the channel. The pH dependence of activation and maximal current amplitude was measured. It is expected that if a cross-link occurs, a compound can lock the channel in each functional state. Selected mutants, D237C/I312C, T236C/D351C and D237C/E315C alone showed a decrease in the ratio of  $I_{pH6.x}/I_{pH5_{MTS/ctrl}}$  with MTS cross-linker in comparison to the MTS monovalent reagent. The pH<sub>50</sub> of activation in the double mutants T236C/D351C and D237C/E315C, and its single mutant using MTS cross-linker showed an acidic shift. While in the mutant D237C/I312C, the pH<sub>50</sub> of activation under MTS cross-linker was shifted to acidic value. In D237C, the pH dependence of activation with MTS-17-MTS was shifted to acidic value and the shift was smaller than in the double mutant. In I312C, the pH dependence of activation with MTS-17-MTS was shifted to alkaline value. However, it was not confirmed if MTS-17-MTS can form cross-link at D237C/I312C and shift in

the pH dependence of activation is due to MTS-17-MTS cross-link. Since, both the mutant is in the same subunit, it limits the assessment of cross-link by MTS reagent.

There are some MTS crosslinking reagents that indicated a significant decrease in the pH dependence of activation compared to the control condition. For example, in hASIC1a-T236C/D351C, both MTSES and MTS-6-MTS indicated a strong acidic shift in the IpH6.2/IpH5.0 ratio. Similarly, in hASIC1a-E97C/V354C and -D237C/I312C, a strong shift in the IpH6.x/IpH5 was observed both in the treatment with MTS cross-linker and MTS monovalent reagent. In hASIC1a-E97C/V354C, the modification by MTS-17-MTS, MTS-14-MTS and MTS-PEO<sub>3</sub>-Biotin shifted the IpH6.4/IpH5 ratio. But in hASIC1a-D237C/I312C, the ratio of IpH6.0/IpH5 with MTS cross-linker was strongly decreased in comparison to the MTS monovalent reagent. Thus, in hASIC1a-T236C/D351C and -E97C/V354C, the shift in pH dependence may arise just by the modification of one of the cysteine mutations.

In comparison to voltage-clamp fluorometry (VCF) data, where the cysteine mutants were tethered to AlexaFluor488 C5 maleimide, the mutant D237W/D351C, D237C/D347C and E355C showed fast fluorescence signal change in correlation to the kinetics of current activation<sup>51</sup>. In an earlier study, using the same VCF approach, E355C was proposed to undergo first rapid movement associated with channel opening or an early preparation for desensitization. In the mutants E235C and V354, a backward movement was proposed during recovery from desensitized state<sup>155</sup>. Such studies have provided us with information on residues involved during channel activity and we can use that information to compare and correlate the results obtained using MTS cross-linkers with channel activity.

In our case, treatment of hASIC1a-D237C/I312C, -D237C/E315C and -T236C/D351C with MTS cross-linker matching to their distance in the close state produced a significant shift in the IpH6.x/IpH5 and inhibited peak maximal current. Though, these mutants are in pair with E355C and E97C, testing the single mutant with respective cross-linker may provide a better

understanding. As we know that E235C, D237C, D347C, D351C and E355C residues are required for the preparation of channel activation<sup>51,155</sup>, hence, it is likely possible that modification of these residues by MTS cross-linking reagent or MTS monovalent reagent may affect the movement of residue required for the channel activation. In the case of F257W/D351C, by VCF it was shown that fluorescence change kinetics were associated with current desensitization. In hASIC-D237C single mutant, both MTS-17-MTS and MTS-14-MTS whose length match with the closed state produced an acidic shift in the pH dependence of activation. We did not measure a monovalent MTS reagent on this mutant. Thus, in comparison, we can assume that one of the mutants is modified by MTS cross-link reagent and modification results in decreased activation. This is the first time an MTS cross-linker approach has been applied on ASIC1a to study the activation mechanism. We assume some limitations using this approach. First, it is possible that there may be some double mutant where cross-linking might have occurred and did not produce any effect on the channel, or the monovalent cross-linking reagent was a limit since its distances did not match exactly like a control for cross-linking MTS reagents. Secondly, it is possible that at least for one of the residues in the chosen pair from extracellular domain may not be accessible for cross-linking and this can be the case also in TM domain. Thirdly, it is possible that the structural distances between the two residues do not correspond to the distance of MTS cross-linking molecules. Considering these limitations, we assume that cross-linking may occur and it needs further validation to elucidate the conformation changes associated in this domain during the channel activation. Together, further analysis by mass spectrometry is required to identify the potential cross-linking in the double mutant. Overall, the cross-linking approach was not successful and the possible reasons could be 1) variation in the measured distances between the crystal structures and the physiological condition, 2) the length of compounds did not match exactly to the distances among the selected residues.

Using cysteine-based cross-linking approaches, BMA and MTS cross-linker did not cross-

link the same residues. Pair of residues found under both approaches were different from each other. With certain limitations using these two approaches to understand the channel activation mechanism, the results are only predictive to describe the conformational changes associated with the channel activity.

## 7. Conclusion and perspectives

Over recent years, ASICs have attracted the interest of researchers to investigate their role in physiological and pathological functions. Some research conducted on ASICs is focused on identifying potent modulators of channel activity and identifying proton binding sites. In ASICs, the exact mechanism of channel activation remains still unknown even with the availability of high-resolution structures. Several studies have identified possible protonation sites in ASIC1a, but the conformational changes associated with proton binding remain elusive. In my thesis, using the cysteine-based cross-linking approaches, few pairs of residues were to shift the pH dependence of activation by application of 360nm light and by MTS cross-linker. Only in hASIC1a-D237C/I312C the shift in the pH dependence of activation by MTS-17-MTS was stronger than its single mutants D237C and I312C. However, cross-linking of D237C/I312C by MTS-17-MTS needs further validation. To determine the cross-linking, purified peptide fragments of cross-linked hASIC1a-D237C/I312C can be used for mass spectrometry analysis. Studies have already used molecular dynamics simulation in parallel to the experimental approach to consolidate the structure-function findings in ASIC1a<sup>117,150,156</sup>. In the future, molecular simulation can also be applied to determine the pair of residues and the distance constraints required to obtain cross-linking using either BMA or MTS cross-linker reagents in different domains of hASIC1a.

## 8. References

- 1 Kellenberger, S. & Schild, L. International Union of Basic and Clinical Pharmacology. XCI. structure, function, and pharmacology of acid-sensing ion channels and the epithelial Na<sup>+</sup> channel. *Pharmacol Rev* **67**, 1-35, doi:10.1124/pr.114.009225 (2015).
- 2 Boscardin, E., Alijevic, O., Hummler, E., Frateschi, S. & Kellenberger, S. The function and regulation of acid-sensing ion channels (ASICs) and the epithelial Na<sup>(+)</sup> channel (ENaC): IUPHAR Review 19. *Br J Pharmacol* **173**, 2671-2701, doi:10.1111/bph.13533 (2016).
- 3 García-Añoveros, J., Derfler, B., Neville-Golden, J., Hyman, B. T. & Corey, D. P. BNaC1 and BNaC2 constitute a new family of human neuronal sodium channels related to degenerins and epithelial sodium channels. *Proceedings of the National Academy of Sciences* **94**, 1459-1464 (1997).
- 4 Jaime Garcia-Anoveros, B. D., Janine Neville-Golden, Bradley T.Hayman, and David P.Corey. BNaC1 and BNaC2 constitute a new family of human neuronal sodium channels related to degenerins and epithelial sodium channels. *Proceedings of the National Academy of Sciences* **94**, 1459-1464 (1997).
- 5 Margaret P. Price, P. M. S., and Michael J. Welsh. Cloning and Expression of a Novel Human Brain Na<sup>+</sup> Channel. *The Journal of Biological Chemistry* **14**, 7879-7882 (1996).
- 6 Rainer Waldmann‡, F. d. r. B., Jan de Weille‡, Guy Champigny, Catherine Heurteaux, and Michel Lazdunski. Molecular Cloning of a Non-inactivating Proton-gated Na<sup>+</sup> Channel Specific for Sensory Neurons. (1997).
- 7 Rainer Waldmann, G. C., Frédéric Bassilana, Catherine Heurteaux, and Michel Lazdunski. A proton-gated cation channel involved in acid-sensing. *Nature* **386**, 173–177 (1997).
- 8 Waldmann, R., Champigny, G., Voilley, N., Lauritzen, I. & Lazdunski, M. The mammalian degenerin MDEG, an amiloride-sensitive cation channel activated by mutations causing neurodegeneration in *Caenorhabditis elegans*. *J Biol Chem* **271**, 10433-10436, doi:10.1074/jbc.271.18.10433 (1996).
- 9 Eric Lingueglia, J. R. d. W., Frédéric Bassilana, Catherine Heurteaux, Hideki Sakai, Rainer Waldmann, and Michel Lazdunski. A modulatory subunit of acid sensing ion channels in brain and dorsal root ganglion cells. *The Journal of Biological Chemistry* **272**, 29778-29783 (1997).
- 10 Price, M. P., Snyder, P. M. & Welsh, M. J. Cloning and expression of a novel human brain Na<sup>+</sup> channel. *J Biol Chem* **271**, 7879-7882, doi:10.1074/jbc.271.14.7879 (1996).
- 11 Waldmann, R., Champigny, G., Voilley, N., Lauritzen, I. & Lazdunski, M. The mammalian degenerin MDEG, an amiloride-sensitive cation channel activated by mutations causing neurodegeneration in *Caenorhabditis elegans*. *Journal of Biological Chemistry* **271**, 10433-10436 (1996).
- 12 Waldmann, R., Champigny, G., Bassilana, F., Heurteaux, C. & Lazdunski, M. A proton-gated cation channel involved in acid-sensing. *Nature* **386**, 173-177, doi:10.1038/386173a0 (1997).
- 13 Waldmann, R. *et al.* Molecular cloning of a non-inactivating proton-gated Na<sup>+</sup> channel specific for sensory neurons. *J Biol Chem* **272**, 20975-20978, doi:10.1074/jbc.272.34.20975 (1997).
- 14 Lingueglia, E. *et al.* A modulatory subunit of acid sensing ion channels in brain and dorsal root ganglion cells. *Journal of Biological Chemistry* **272**, 29778-29783 (1997).
- 15 Hanukoglu, I. & Hanukoglu, A. Epithelial sodium channel (ENaC) family: Phylogeny, structure-function, tissue distribution, and associated inherited diseases. *Gene* **579**, 95-132, doi:10.1016/j.gene.2015.12.061 (2016).
- 16 Bassler, E. L., Ngo-Anh, T. J., Geisler, H. S., Ruppertsberg, J. P. & Grunder, S. Molecular and functional characterization of acid-sensing ion channel (ASIC) 1b. *J Biol Chem* **276**, 33782-33787, doi:10.1074/jbc.M104030200 (2001).
- 17 Chih-Cheng Chen, S. E., Armen N.Akopian, and John N. Wood. A sensory neuron-specific, proton gated ion channel. *Proceedings of the National Academy of Sciences* **95**, 10240-10245 (1998).
- 18 Kazimierz Babinski, K.-T. L., and Philippe Séguéla. Molecular cloning and regional distribution of a human proton receptor subunit with biphasic functional properties. *Journal of Neurochemistry* **72**, 51-57 (1999).
- 19 Grunder, S., Geissler, H. S., Bassler, E. L. & Ruppertsberg, J. P. A new member of acid-sensing ion channels from pituitary gland. *Neuroreport* **11**, 1607-1611, doi:10.1097/00001756-200006050-00003 (2000).
- 20 Akopian, A. N., Chen, C. C., Ding, Y., Cesare, P. & Wood, J. N. A new member of the acid-sensing ion channel family. *Neuroreport* **11**, 2217-2222, doi:10.1097/00001756-200007140-00031 (2000).
- 21 Marumo, K. I. a. F. Molecular cloning of a DEG ENaC sodium channel cDNA from human testis. *Biochemical and Biophysical Research Communication* **245**, 589-593 (1998).
- 22 Chen, S. G. a. X. Structure, function, and pharmacology of acid-sensing ion channels (ASICs) Focus on ASIC1a. *International Journal of Pathophysiology Pharmacology* **2** (2010).

- 23 Hesselager, M., Timmermann, D. B. & Ahring, P. K. pH Dependency and desensitization kinetics of heterologously expressed combinations of acid-sensing ion channel subunits. *J Biol Chem* **279**, 11006-11015, doi:10.1074/jbc.M313507200 (2004).
- 24 Yoder, N., Yoshioka, C. & Gouaux, E. Gating mechanisms of acid-sensing ion channels. *Nature* **555**, 397-401, doi:10.1038/nature25782 (2018).
- 25 Bacongus, I., Bohlen, C. J., Goehring, A., Julius, D. & Gouaux, E. X-ray structure of acid-sensing ion channel 1-snake toxin complex reveals open state of a Na(+)-selective channel. *Cell* **156**, 717-729, doi:10.1016/j.cell.2014.01.011 (2014).
- 26 Dawson, R. J. *et al.* Structure of the acid-sensing ion channel 1 in complex with the gating modifier Psalmotoxin 1. *Nat Commun* **3**, 936, doi:10.1038/ncomms1917 (2012).
- 27 Bacongus, I. & Gouaux, E. Structural plasticity and dynamic selectivity of acid-sensing ion channel-spider toxin complexes. *Nature* **489**, 400-405, doi:10.1038/nature11375 (2012).
- 28 Gonzales, E. B., Kawate, T. & Gouaux, E. Pore architecture and ion sites in acid-sensing ion channels and P2X receptors. *Nature* **460**, 599-604, doi:10.1038/nature08218 (2009).
- 29 Jasti, J., Furukawa, H., Gonzales, E. B. & Gouaux, E. Structure of acid-sensing ion channel 1 at 1.9 Å resolution and low pH. *Nature* **449**, 316-323, doi:10.1038/nature06163 (2007).
- 30 Bartoi, T., Augustinowski, K., Polleichtner, G., Grunder, S. & Ulbrich, M. H. Acid-sensing ion channel (ASIC) 1a/2a heteromers have a flexible 2:1/1:2 stoichiometry. *Proc Natl Acad Sci U S A* **111**, 8281-8286, doi:10.1073/pnas.1324060111 (2014).
- 31 Meltzer, R. H. *et al.* Heteromeric assembly of acid-sensitive ion channel and epithelial sodium channel subunits. *J Biol Chem* **282**, 25548-25559, doi:10.1074/jbc.M703825200 (2007).
- 32 Alvarez de la Rosa, D. *et al.* Distribution, subcellular localization and ontogeny of ASIC1 in the mammalian central nervous system. *J Physiol* **546**, 77-87, doi:10.1113/jphysiol.2002.030692 (2003).
- 33 Delaunay, A. *et al.* Human ASIC3 channel dynamically adapts its activity to sense the extracellular pH in both acidic and alkaline directions. *Proc Natl Acad Sci U S A* **109**, 13124-13129, doi:10.1073/pnas.1120350109 (2012).
- 34 Biagini, G., Babinski, K., Avoli, M., Marcinkiewicz, M. & Seguela, P. Regional and subunit-specific downregulation of acid-sensing ion channels in the pilocarpine model of epilepsy. *Neurobiol Dis* **8**, 45-58, doi:10.1006/nbdi.2000.0331 (2001).
- 35 John A. Wemmie, C. C. A., Ejvis Lamani, Martin D. Cassell, John H. Freeman Jr and Michael J. Welsh. Acid-sensing ion channel 1 is localized in brain regions with high synaptic density and contributes to fear conditioning. *The Journal of Neuroscience* **23**, 5469-5502 (2003).
- 36 Wemmie, J. A. *et al.* The acid-activated ion channel ASIC contributes to synaptic plasticity, learning, and memory. *Neuron* **34**, 463-477, doi:10.1016/s0896-6273(02)00661-x (2002).
- 37 Wenying Jin, C. S., Lan Jing, Xiang-ming Zha, Jun Xia. PICK1 regulates the trafficking of ASIC1a and acidotoxicity in a BAR domain lipid binding- dependent manner. *Molecular Brain* **3** (2010).
- 38 Gao, J. *et al.* Coupling between NMDA receptor and acid-sensing ion channel contributes to ischemic neuronal death. *Neuron* **48**, 635-646, doi:10.1016/j.neuron.2005.10.011 (2005).
- 39 Chai, S. *et al.* A kinase-anchoring protein 150 and calcineurin are involved in regulation of acid-sensing ion channels ASIC1a and ASIC2a. *J Biol Chem* **282**, 22668-22677, doi:10.1074/jbc.M703624200 (2007).
- 40 Harding, A. M. S., Kusama, N., Hattori, T., Gautam, M. & Benson, C. J. ASIC2 Subunits Facilitate Expression at the Cell Surface and Confer Regulation by PSD-95. *Plos One* **9**, doi:ARTN e93797  
10.1371/journal.pone.0093797 (2014).
- 41 Zha, X. M. *et al.* ASIC2 subunits target acid-sensing ion channels to the synapse via an association with PSD-95. *J Neurosci* **29**, 8438-8446, doi:10.1523/JNEUROSCI.1284-09.2009 (2009).
- 42 Voilley, N., de Weille, J., Mamet, J. & Lazdunski, M. Nonsteroid anti-inflammatory drugs inhibit both the activity and the inflammation-induced expression of acid-sensing ion channels in nociceptors. *Journal of Neuroscience* **21**, 8026-8033 (2001).
- 43 Olson, T. H., Riedl, M. S., Vulchanova, L., Ortiz-Gonzalez, X. R. & Elde, R. An acid sensing ion channel (ASIC) localizes to small primary afferent neurons in rats. *Neuroreport* **9**, 1109-1113, doi:10.1097/00001756-199804200-00028 (1998).
- 44 Wemmie, J. A., Taugher, R. J. & Kreple, C. J. Acid-sensing ion channels in pain and disease. *Nat Rev Neurosci* **14**, 461-471, doi:10.1038/nrn3529 (2013).
- 45 Song, X. L. *et al.* Postsynaptic Targeting and Mobility of Membrane Surface-Localized hASIC1a. *Neurosci Bull*, doi:10.1007/s12264-020-00581-9 (2020).
- 46 Huang, C. *et al.* Existence and distinction of acid-evoked currents in rat astrocytes. *Glia* **58**, 1415-1424,

- doi:10.1002/glia.21017 (2010).
- 47 Jahr, H., van Driel, M., van Osch, G. J., Weinans, H. & van Leeuwen, J. P. Identification of acid-sensing ion channels in bone. *Biochem Biophys Res Commun* **337**, 349-354, doi:10.1016/j.bbrc.2005.09.054 (2005).
- 48 Gitterman, D. P., Wilson, J. & Randall, A. D. Functional properties and pharmacological inhibition of ASIC channels in the human SJ-RH30 skeletal muscle cell line. *J Physiol* **562**, 759-769, doi:10.1113/jphysiol.2004.075069 (2005).
- 49 Chen, C. C., England, S., Akopian, A. N. & Wood, J. N. A sensory neuron-specific, proton-gated ion channel. *Proc Natl Acad Sci U S A* **95**, 10240-10245, doi:10.1073/pnas.95.17.10240 (1998).
- 50 Babinski, K., Le, K. T. & Seguela, P. Molecular cloning and regional distribution of a human proton receptor subunit with biphasic functional properties. *J Neurochem* **72**, 51-57, doi:10.1046/j.1471-4159.1999.0720051.x (1999).
- 51 Vullo, S. *et al.* Conformational dynamics and role of the acidic pocket in ASIC pH-dependent gating. *Proc Natl Acad Sci U S A* **114**, 3768-3773, doi:10.1073/pnas.1620560114 (2017).
- 52 Chen, X. & Grunder, S. Permeating protons contribute to tachyphylaxis of the acid-sensing ion channel (ASIC) 1a. *J Physiol* **579**, 657-670, doi:10.1113/jphysiol.2006.120733 (2007).
- 53 Aoi, W. & Marunaka, Y. Importance of pH homeostasis in metabolic health and diseases: crucial role of membrane proton transport. *Biomed Res Int* **2014**, 598986, doi:10.1155/2014/598986 (2014).
- 54 Morel, N. Neurotransmitter release: the dark side of the vacuolar-H<sup>+</sup>ATPase. *Biology of the Cell* **95**, 453-457, doi:10.1016/s0248-4900(03)00075-3 (2003).
- 55 Ziemann, A. E. *et al.* Seizure termination by acidosis depends on ASIC1a. *Nat Neurosci* **11**, 816-822, doi:10.1038/nn.2132 (2008).
- 56 Du, J. *et al.* Protons are a neurotransmitter that regulates synaptic plasticity in the lateral amygdala. *Proc Natl Acad Sci U S A* **111**, 8961-8966, doi:10.1073/pnas.1407018111 (2014).
- 57 Xiong, Z. G. *et al.* Neuroprotection in ischemia: blocking calcium-permeable acid-sensing ion channels. *Cell* **118**, 687-698, doi:10.1016/j.cell.2004.08.026 (2004).
- 58 Ferenczi, E. A. *et al.* Optogenetic approaches addressing extracellular modulation of neural excitability. *Sci Rep* **6**, 23947, doi:10.1038/srep23947 (2016).
- 59 Zeng, W. Z. *et al.* Activation of acid-sensing ion channels by localized proton transient reveals their role in proton signaling. *Sci Rep* **5**, 14125, doi:10.1038/srep14125 (2015).
- 60 Wu, P. Y. *et al.* Acid-sensing ion channel-1a is not required for normal hippocampal LTP and spatial memory. *J Neurosci* **33**, 1828-1832, doi:10.1523/JNEUROSCI.4132-12.2013 (2013).
- 61 Mango, D. *et al.* Acid-sensing ion channel 1a is required for mGlu receptor dependent long-term depression in the hippocampus. *Pharmacological Research* **119**, 12-19, doi:10.1016/j.phrs.2017.01.028 (2017).
- 62 Cho, J. H. & Askwith, C. C. Presynaptic release probability is increased in hippocampal neurons from ASIC1 knockout mice. *J Neurophysiol* **99**, 426-441, doi:10.1152/jn.00940.2007 (2008).
- 63 González-Inchauspe, C., Urbano, F. J., Di Guilmi, M. N. & Uchitel, O. D. Acid-Sensing Ion Channels Activated by Evoked Released Protons Modulate Synaptic Transmission at the Mouse Calyx of Held Synapse. *The Journal of Neuroscience* **37**, 2589-2599, doi:10.1523/jneurosci.2566-16.2017 (2017).
- 64 Coryell, M. W. *et al.* Targeting ASIC1a reduces innate fear and alters neuronal activity in the fear circuit. *Biol Psychiatry* **62**, 1140-1148, doi:10.1016/j.biopsych.2007.05.008 (2007).
- 65 Coryell, M. W. *et al.* Restoring Acid-sensing ion channel-1a in the amygdala of knock-out mice rescues fear memory but not unconditioned fear responses. *J Neurosci* **28**, 13738-13741, doi:10.1523/JNEUROSCI.3907-08.2008 (2008).
- 66 Wemmie, J. A. *et al.* Overexpression of acid-sensing ion channel 1a in transgenic mice increases acquired fear-related behavior. *Proc Natl Acad Sci U S A* **101**, 3621-3626, doi:10.1073/pnas.0308753101 (2004).
- 67 Chiang, P. H., Chien, T. C., Chen, C. C., Yanagawa, Y. & Lien, C. C. ASIC-dependent LTP at multiple glutamatergic synapses in amygdala network is required for fear memory. *Sci Rep* **5**, 10143, doi:10.1038/srep10143 (2015).
- 68 Olena Yermolaieva, A. S. L., Mikael K. Schnizler, Francois M. Abboud, and Michael J. Welsh. Extracellular acidosis increases neuronal cell calcium by activating acidsensing ion channel 1a. *Proceedings of the National Academy of Sciences* **101**, 6752-6757 (2003).
- 69 Pignataro, G., Simon, R. P. & Xiong, Z. G. Prolonged activation of ASIC1a and the time window for neuroprotection in cerebral ischaemia. *Brain* **130**, 151-158, doi:10.1093/brain/awl325 (2007).
- 70 Mari, Y., Katnik, C. & Cuevas, J. ASIC1a channels are activated by endogenous protons during ischemia and contribute to synergistic potentiation of intracellular Ca<sup>2+</sup> overload during ischemia and acidosis. *Cell Calcium* **48**, 70-82, doi:10.1016/j.ceca.2010.07.002 (2010).

- 71 Wang, Y. Z. *et al.* Tissue acidosis induces neuronal necroptosis via ASIC1a channel independent of its ionic  
conduction. *Elife* **4**, doi:10.7554/eLife.05682 (2015).
- 72 Zhang, H. *et al.* Glucose Deficiency Elevates Acid-Sensing Ion Channel 2a Expression and Increases Seizure  
Susceptibility in Temporal Lobe Epilepsy. *Sci Rep* **7**, 5870, doi:10.1038/s41598-017-05038-0 (2017).
- 73 Liang, J. H., L. Chen, X. Pan, S. Lu, Z. Xiao, Z. Amiloride suppresses pilocarpine-induced seizures via ASICs  
other than NHE in rats. *Int J Clin Exp Pathol* **8**, 14507-14513 (2015).
- 74 N'Gouemo, P. Amiloride delays the onset of pilocarpine-induced seizures in rats. *Brain Res* **1222**, 230-232,  
doi:10.1016/j.brainres.2008.05.010 (2008).
- 75 Ali, A. P., K K. Ahmad, FJ. Dua, Y. Vohora, D. Anticonvulsant effect of amiloride in pentetrazole-induced  
status epilepticus in mice. *Pharmacological reports* **58**, 242-245 (2006).
- 76 Luszczki, J. J., Sawicka, K. M., Kozinska, J., Dudra-Jastrzebska, M. & Czuczwar, S. J. Amiloride enhances  
the anticonvulsant action of various antiepileptic drugs in the mouse maximal electroshock seizure model. *J*  
*Neural Transm (Vienna)* **116**, 57-66, doi:10.1007/s00702-008-0152-2 (2009).
- 77 Julius, D. & Basbaum, A. I. Molecular mechanisms of nociception. *Nature* **413**, 203-210,  
doi:10.1038/35093019 (2001).
- 78 Chen, C. *et al.* A Role for ASIC3 in the Modulation of High-Intensity Pain Stimuli. *Proceedings of the*  
*National Academy of Sciences* **99**, 8992-8997 (2002).
- 79 Mogil, J. S. *et al.* Transgenic expression of a dominant-negative ASIC3 subunit leads to increased sensitivity  
to mechanical and inflammatory stimuli. *J Neurosci* **25**, 9893-9901, doi:10.1523/JNEUROSCI.2019-05.2005  
(2005).
- 80 Lee, C. H. & Chen, C. C. Roles of ASICs in Nociception and Proprioception. *Adv Exp Med Biol* **1099**, 37-47,  
doi:10.1007/978-981-13-1756-9\_4 (2018).
- 81 Pattison, L. A., Callejo, G. & St John Smith, E. Evolution of acid nociception: ion channels and receptors for  
detecting acid. *Philos Trans R Soc Lond B Biol Sci* **374**, 20190291, doi:10.1098/rstb.2019.0291 (2019).
- 82 Wu, J. *et al.* Sensitization of ASIC3 by proteinase-activated receptor 2 signaling contributes to acidosis-  
induced nociception. *J Neuroinflammation* **14**, 150, doi:10.1186/s12974-017-0916-4 (2017).
- 83 Deval, E. & Lingueglia, E. Acid-Sensing Ion Channels and nociception in the peripheral and central nervous  
systems. *Neuropharmacology* **94**, 49-57, doi:10.1016/j.neuropharm.2015.02.009 (2015).
- 84 Deval, E. *et al.* ASIC3, a sensor of acidic and primary inflammatory pain. *EMBO J* **27**, 3047-3055,  
doi:10.1038/emboj.2008.213 (2008).
- 85 Bohlen, C. J. *et al.* A heteromeric Texas coral snake toxin targets acid-sensing ion channels to produce pain.  
*Nature* **479**, 410-414, doi:10.1038/nature10607 (2011).
- 86 Diochot, S. *et al.* Black mamba venom peptides target acid-sensing ion channels to abolish pain. *Nature* **490**,  
552-555, doi:10.1038/nature11494 (2012).
- 87 Diochot, S. *et al.* Analgesic effects of mambalgin peptide inhibitors of acid-sensing ion channels in  
inflammatory and neuropathic pain. *Pain* **157**, 552-559, doi:10.1097/j.pain.0000000000000397 (2016).
- 88 Lee, J. Y. P. *et al.* Inhibition of acid-sensing ion channels by diminazene and APETx2 evoke partial and  
highly variable antihyperalgesia in a rat model of inflammatory pain. *Br J Pharmacol* **175**, 2204-2218,  
doi:10.1111/bph.14089 (2018).
- 89 Yu, Y. *et al.* A nonproton ligand sensor in the acid-sensing ion channel. *Neuron* **68**, 61-72,  
doi:10.1016/j.neuron.2010.09.001 (2010).
- 90 Marra, S. *et al.* Non-acidic activation of pain-related Acid-Sensing Ion Channel 3 by lipids. *EMBO J* **35**, 414-  
428, doi:10.15252/embj.201592335 (2016).
- 91 Mazzuca, M. *et al.* A tarantula peptide against pain via ASIC1a channels and opioid mechanisms. *Nat*  
*Neurosci* **10**, 943-945, doi:10.1038/nn1940 (2007).
- 92 Duan, B. *et al.* PI3-kinase/Akt pathway-regulated membrane insertion of acid-sensing ion channel 1a  
underlies BDNF-induced pain hypersensitivity. *J Neurosci* **32**, 6351-6363, doi:10.1523/JNEUROSCI.4479-  
11.2012 (2012).
- 93 Page, A. J. *et al.* The ion channel ASIC1 contributes to visceral but not cutaneous mechanoreceptor function.  
*Gastroenterology* **127**, 1739-1747, doi:10.1053/j.gastro.2004.08.061 (2004).
- 94 Lu, Y. *et al.* The ion channel ASIC2 is required for baroreceptor and autonomic control of the circulation.  
*Neuron* **64**, 885-897, doi:10.1016/j.neuron.2009.11.007 (2009).
- 95 Price, M. P. *et al.* The mammalian sodium channel BNC1 is required for normal touch sensation. *Nature* **407**,  
1007-1011 (2000).
- 96 Kang, S. *et al.* Simultaneous disruption of mouse ASIC1a, ASIC2 and ASIC3 genes enhances cutaneous  
mechanosensitivity. *PLoS One* **7**, e35225, doi:10.1371/journal.pone.0035225 (2012).

- 97 Chen, C. C. & Wong, C. W. Neurosensory mechanotransduction through acid-sensing ion channels. *J Cell Mol Med* **17**, 337-349, doi:10.1111/jcmm.12025 (2013).
- 98 Baron, A. *et al.* Venom toxins in the exploration of molecular, physiological and pathophysiological functions of acid-sensing ion channels. *Toxicon* **75**, 187-204, doi:10.1016/j.toxicon.2013.04.008 (2013).
- 99 Wu, Y., Chen, Z. & Canessa, C. M. A valve-like mechanism controls desensitization of functional mammalian isoforms of acid-sensing ion channels. *Elife* **8**, doi:10.7554/eLife.45851 (2019).
- 100 Vullo, S. & Kellenberger, S. A molecular view of the function and pharmacology of acid-sensing ion channels. *Pharmacol Res* **154**, 104166, doi:10.1016/j.phrs.2019.02.005 (2020).
- 101 Gwiazda, K., Bonifacio, G., Vullo, S. & Kellenberger, S. Extracellular Subunit Interactions Control Transitions between Functional States of Acid-sensing Ion Channel 1a. *J Biol Chem* **290**, 17956-17966, doi:10.1074/jbc.M115.641688 (2015).
- 102 Kleyman, T. R. & Cragoe Jr, E. J. Amiloride and its analogs as tools in the study of ion transport. *The Journal of membrane biology* **105**, 1-21 (1988).
- 103 Lingueglia, E. & Lazdunski, M. Pharmacology of ASIC channels. *Wiley Interdisciplinary Reviews: Membrane Transport and Signaling* **2**, 155-171, doi:10.1002/wmts.88 (2013).
- 104 Dube, G. R. *et al.* Electrophysiological and in vivo characterization of A-317567, a novel blocker of acid sensing ion channels. *Pain* **117**, 88-96, doi:10.1016/j.pain.2005.05.021 (2005).
- 105 Chen, X. *et al.* Diarylamidines: high potency inhibitors of acid-sensing ion channels. *Neuropharmacology* **58**, 1045-1053, doi:10.1016/j.neuropharm.2010.01.011 (2010).
- 106 Alijevic, O. & Kellenberger, S. Subtype-specific modulation of acid-sensing ion channel (ASIC) function by 2-guanidine-4-methylquinazoline. *J Biol Chem* **287**, 36059-36070, doi:10.1074/jbc.M112.360487 (2012).
- 107 Krauson, A. J., Rooney, J. G. & Carattino, M. D. Molecular basis of inhibition of acid sensing ion channel 1A by diminazene. *PLoS One* **13**, e0196894, doi:10.1371/journal.pone.0196894 (2018).
- 108 Munro, G. *et al.* NS383 Selectively Inhibits Acid-Sensing Ion Channels Containing 1a and 3 Subunits to Reverse Inflammatory and Neuropathic Hyperalgesia in Rats. *CNS Neurosci Ther* **22**, 135-145, doi:10.1111/cns.12487 (2016).
- 109 Li, W. G., Yu, Y., Zhang, Z. D., Cao, H. & Xu, T. L. ASIC3 channels integrate agmatine and multiple inflammatory signals through the nonproton ligand sensing domain. *Mol Pain* **6**, 88, doi:10.1186/1744-8069-6-88 (2010).
- 110 Besson, T., Lingueglia, E. & Salinas, M. Pharmacological modulation of Acid-Sensing Ion Channels 1a and 3 by amiloride and 2-guanidine-4-methylquinazoline (GMQ). *Neuropharmacology* **125**, 429-440, doi:10.1016/j.neuropharm.2017.08.004 (2017).
- 111 Chu, X. P. *et al.* Subunit-dependent high-affinity zinc inhibition of acid-sensing ion channels. *J Neurosci* **24**, 8678-8689, doi:10.1523/JNEUROSCI.2844-04.2004 (2004).
- 112 Baron, A., Schaefer, L., Lingueglia, E., Champigny, G. & Lazdunski, M. Zn<sup>2+</sup> and H<sup>+</sup> are coactivators of acid-sensing ion channels. *J Biol Chem* **276**, 35361-35367, doi:10.1074/jbc.M105208200 (2001).
- 113 Yang, X. N. *et al.* The nonproton ligand of acid-sensing ion channel 3 activates mollusk-specific FaNaC channels via a mechanism independent of the native FMRFamide peptide. *J Biol Chem* **292**, 21662-21675, doi:10.1074/jbc.M117.814707 (2017).
- 114 Askwith, C. C. *et al.* Neuropeptide FF and FMRFamide potentiate acid-evoked currents from sensory neurons and proton-gated DEG/ENaC channels. *Neuron* **26**, 133-141 (2000).
- 115 Frey, E. N., Pavlovicz, R. E., Wegman, C. J., Li, C. & Askwith, C. C. Conformational changes in the lower palm domain of ASIC1a contribute to desensitization and RFamide modulation. *PLoS One* **8**, e71733, doi:10.1371/journal.pone.0071733 (2013).
- 116 Lingueglia, E., Deval, E. & Lazdunski, M. FMRFamide-gated sodium channel and ASIC channels: a new class of ionotropic receptors for FMRFamide and related peptides. *Peptides* **27**, 1138-1152, doi:10.1016/j.peptides.2005.06.037 (2006).
- 117 Bargeton, B. *et al.* Mutations in the palm domain disrupt modulation of acid-sensing ion channel 1a currents by neuropeptides. *Sci Rep* **9**, 2599, doi:10.1038/s41598-018-37426-5 (2019).
- 118 Sherwood, T. W. & Askwith, C. C. Dynorphin opioid peptides enhance acid-sensing ion channel 1a activity and acidosis-induced neuronal death. *J Neurosci* **29**, 14371-14380, doi:10.1523/JNEUROSCI.2186-09.2009 (2009).
- 119 Borg, C. B. *et al.* Mechanism and site of action of big dynorphin on ASIC1a. *Proc Natl Acad Sci U S A* **117**, 7447-7454, doi:10.1073/pnas.1919323117 (2020).
- 120 Escoubas, P. *et al.* Isolation of a tarantula toxin specific for a class of proton-gated Na<sup>+</sup> channels. *J Biol Chem* **275**, 25116-25121, doi:10.1074/jbc.M003643200 (2000).

- 121 Escoubas, P., Bernard, C., Lambeau, G., Lazdunski, M. & Darbon, H. Recombinant production and solution structure of PcTx1, the specific peptide inhibitor of ASIC1a proton-gated cation channels. *Protein Sci* **12**, 1332-1343, doi:10.1110/ps.0307003 (2003).
- 122 Schroeder, C. I. *et al.* Chemical synthesis, 3D structure, and ASIC binding site of the toxin mambalgin-2. *Angew Chem Int Ed Engl* **53**, 1017-1020, doi:10.1002/anie.201308898 (2014).
- 123 Diochot, S. *et al.* A new sea anemone peptide, APETx2, inhibits ASIC3, a major acid-sensitive channel in sensory neurons. *The EMBO Journal* **23**, 1516-1525, doi:10.1038/sj.emboj.7600177 (2004).
- 124 Pham, E., Mills, E. & Truong, K. A synthetic photoactivated protein to generate local or global Ca(2+) signals. *Chem Biol* **18**, 880-890, doi:10.1016/j.chembiol.2011.04.014 (2011).
- 125 Rost, B. R., Schneider-Warme, F., Schmitz, D. & Hegemann, P. Optogenetic Tools for Subcellular Applications in Neuroscience. *Neuron* **96**, 572-603, doi:10.1016/j.neuron.2017.09.047 (2017).
- 126 Lynagh, T. *et al.* A selectivity filter at the intracellular end of the acid-sensing ion channel pore. *Elife* **6**, doi:10.7554/eLife.24630 (2017).
- 127 Bandara, H. M. & Burdette, S. C. Photoisomerization in different classes of azobenzene. *Chem Soc Rev* **41**, 1809-1825, doi:10.1039/c1cs15179g (2012).
- 128 Lemoine, D. *et al.* Optical control of an ion channel gate. *Proc Natl Acad Sci U S A* **110**, 20813-20818, doi:10.1073/pnas.1318715110 (2013).
- 129 Mourot, A., Herold, C., Kienzler, M. A. & Kramer, R. H. Understanding and improving photo-control of ion channels in nociceptors with azobenzene photo-switches. *Br J Pharmacol* **175**, 2296-2311, doi:10.1111/bph.13923 (2018).
- 130 Habermacher, C. *et al.* Photo-switchable tweezers illuminate pore-opening motions of an ATP-gated P2X ion channel. *Elife* **5**, e11050, doi:10.7554/eLife.11050 (2016).
- 131 Browne, L. E. *et al.* Optical control of trimeric P2X receptors and acid-sensing ion channels. *Proc Natl Acad Sci U S A* **111**, 521-526, doi:10.1073/pnas.1318582111 (2014).
- 132 Mourot, A. *et al.* Rapid optical control of nociception with an ion-channel photoswitch. *Nat Methods* **9**, 396-402, doi:10.1038/nmeth.1897 (2012).
- 133 Gautschi, I., van Bemmelen, M. X. & Schild, L. Proton and non-proton activation of ASIC channels. *PLoS one* **12**, e0175293 (2017).
- 134 Pfister, Y. *et al.* A gating mutation in the internal pore of ASIC1a. *J Biol Chem* **281**, 11787-11791, doi:10.1074/jbc.M513692200 (2006).
- 135 Tolino, L. A., Okumura, S., Kashlan, O. B. & Carattino, M. D. Insights into the mechanism of pore opening of acid-sensing ion channel 1a. *J Biol Chem* **286**, 16297-16307, doi:10.1074/jbc.M110.202366 (2011).
- 136 Bargeton, B. & Kellenberger, S. The contact region between three domains of the extracellular loop of ASIC1a is critical for channel function. *J Biol Chem* **285**, 13816-13826, doi:10.1074/jbc.M109.086843 (2010).
- 137 Krauson, A. J., Rued, A. C. & Carattino, M. D. Independent contribution of extracellular proton binding sites to ASIC1a activation. *J Biol Chem* **288**, 34375-34383, doi:10.1074/jbc.M113.504324 (2013).
- 138 Roy, S. *et al.* Molecular determinants of desensitization in an ENaC/degenerin channel. *FASEB J* **27**, 5034-5045, doi:10.1096/fj.13-230680 (2013).
- 139 Kellenberger, S., Gautschi, I. & Schild, L. An external site controls closing of the epithelial Na<sup>+</sup> channel ENaC. *J Physiol* **543**, 413-424, doi:10.1113/jphysiol.2002.022020 (2002).
- 140 Schmid, S. I. & Grissmer, S. Effect of verapamil on the action of methanethiosulfonate reagents on human voltage-gated K(v)1.3 channels: implications for the C-type inactivated state. *Br J Pharmacol* **163**, 662-674, doi:10.1111/j.1476-5381.2011.01258.x (2011).
- 141 O'Reilly, J. P. & Shockett, P. E. Time- and state-dependent effects of methanethiosulfonate ethylammonium (MTSEA) exposure differ between heart and skeletal muscle voltage-gated Na(+) channels. *Biochim Biophys Acta* **1818**, 443-447, doi:10.1016/j.bbame.2011.11.031 (2012).
- 142 Loo, T. W. & Clarke, D. M. Determining the dimensions of the drug-binding domain of human P-glycoprotein using thiol cross-linking compounds as molecular rulers. *J Biol Chem* **276**, 36877-36880, doi:10.1074/jbc.C100467200 (2001).
- 143 Fryatt, A. G., Dayl, S., Stavrou, A., Schmid, R. & Evans, R. J. Organization of ATP-gated P2X1 receptor intracellular termini in apo and desensitized states. *J Gen Physiol* **151**, 146-155, doi:10.1085/jgp.201812108 (2019).
- 144 Kusama, N., Harding, A. M. & Benson, C. J. Extracellular chloride modulates the desensitization kinetics of acid-sensing ion channel 1a (ASIC1a). *J Biol Chem* **285**, 17425-17431, doi:10.1074/jbc.M109.091561 (2010).
- 145 Yoder, N. & Gouaux, E. Divalent cation and chloride ion sites of chicken acid sensing ion channel 1a

- elucidated by x-ray crystallography. *PLoS One* **13**, e0202134, doi:10.1371/journal.pone.0202134 (2018).
- 146 Alijevic, O. *et al.* Heteroarylguanidines as Allosteric Modulators of ASIC1a and ASIC3 Channels. *ACS Chem*  
*Neurosci* **9**, 1357-1365, doi:10.1021/acscchemneuro.7b00529 (2018).
- 147 Callejo, G. *et al.* In silico screening of GMQ-like compounds reveals guanabenz and sephin1 as new allosteric  
modulators of acid-sensing ion channel 3. *Biochem Pharmacol* **174**, 113834, doi:10.1016/j.bcp.2020.113834  
(2020).
- 148 Kusama, N., Gautam, M., Harding, A. M., Snyder, P. M. & Benson, C. J. Acid-sensing ion channels (ASICs)  
are differentially modulated by anions dependent on their subunit composition. *Am J Physiol Cell Physiol*  
**304**, C89-101, doi:10.1152/ajpcell.00216.2012 (2013).
- 149 Lynagh, T., Mikhaleva, Y., Colding, J. M., Glover, J. C. & Pless, S. A. Acid-sensing ion channels emerged  
over 600 Mya and are conserved throughout the deuterostomes. *Proceedings of the National Academy of*  
*Sciences* **115**, 8430-8435 (2018).
- 150 Bignucolo, O., Vullo, S., Ambrosio, N., Gautschi, I. & Kellenberger, S. Structural and Functional Analysis  
of Gly212 Mutants Reveals the Importance of Intersubunit Interactions in ASIC1a Channel Function. *Front*  
*Mol Biosci* **7**, 58, doi:10.3389/fmolb.2020.00058 (2020).
- 151 Paukert, M., Chen, X., Polleichtner, G., Schindelin, H. & Grunder, S. Candidate amino acids involved in H<sup>+</sup>  
gating of acid-sensing ion channel 1a. *J Biol Chem* **283**, 572-581, doi:10.1074/jbc.M706811200 (2008).
- 152 Kawate, T., Michel, J. C., Birdsong, W. T. & Gouaux, E. Crystal structure of the ATP-gated P2X(4) ion  
channel in the closed state. *Nature* **460**, 592-598, doi:10.1038/nature08198 (2009).
- 153 Kellenberger, S. & Grutter, T. Architectural and functional similarities between trimeric ATP-gated P2X  
receptors and acid-sensing ion channels. *J Mol Biol* **427**, 54-66, doi:10.1016/j.jmb.2014.06.004 (2015).
- 154 Ramaswamy, S. S., MacLean, D. M., Gorfe, A. A. & Jayaraman, V. Proton-mediated conformational changes  
in an acid-sensing ion channel. *J Biol Chem* **288**, 35896-35903, doi:10.1074/jbc.M113.478982 (2013).
- 155 Bonifacio, G., Lelli, C. I. & Kellenberger, S. Protonation controls ASIC1a activity via coordinated movements  
in multiple domains. *J Gen Physiol* **143**, 105-118, doi:10.1085/jgp.201311053 (2014).
- 156 Liechti, L. A. *et al.* A combined computational and functional approach identifies new residues involved in  
pH-dependent gating of ASIC1a. *Journal of biological chemistry* **285**, 16315-16329 (2010).